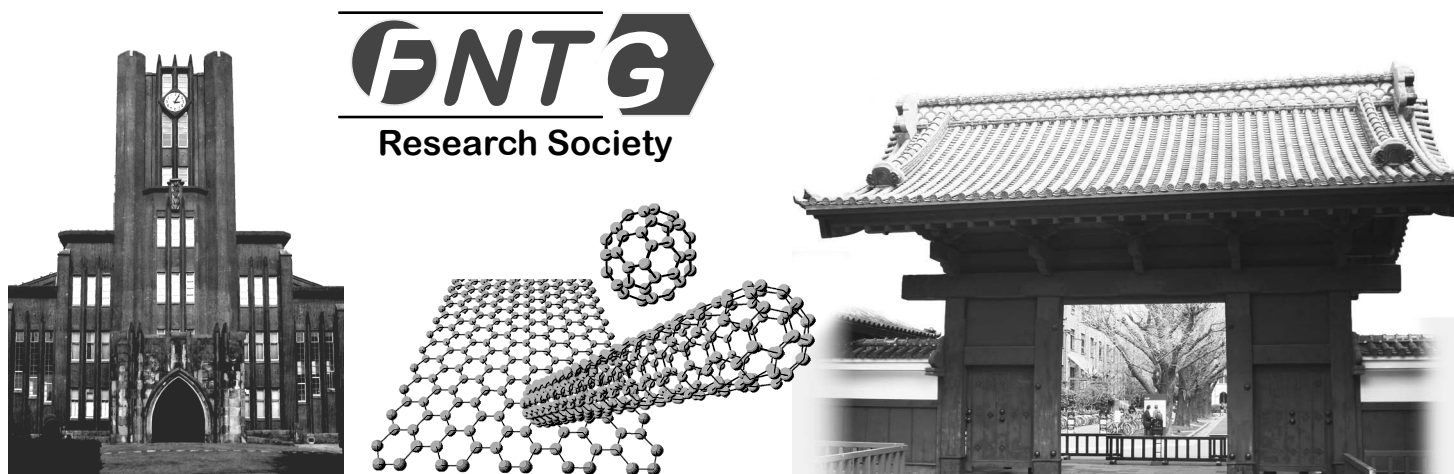


第44回 フラーレン・ナノチューブ・グラフェン 総合シンポジウム

The 44th Fullerenes-Nanotubes-Graphene General Symposium



講演要旨集 Abstracts

2013年3月11日(月)～13日(水)

東京大学 伊藤国際学術研究センター 伊藤謝恩ホール
The University of Tokyo, Ito International Research Center

主催 フラーレン・ナノチューブ・グラフェン学会
The Fullerenes, Nanotubes and Graphene Research Society

共催

日本化学会
東京大学GMSI

The Chemical Society of Japan
The University of Tokyo Global COE Program
"Global Center of Excellence for Mechanical Systems Innovation"

協賛

日本物理学会
応用物理学会
高分子学会
電気化学会

The Physical Society of Japan
The Japan Society of Applied Physics
The Society of Polymer Science, Japan
The Electrochemical Society of Japan

カーボンナノ材料新製品

酸化グラフェン **NEW!**

- 2 mg/mL, dispersion in H₂O

763705-25ML **¥26,100**
763705-100ML **¥59,500**

単層カーボンナノチューブ^{※1} **NEW!**

- single-walled (98% semiconducting SWNTs)
- single-walled (98% metallic SWNTs)
- single-walled (<1% catalyst content)
- single-walled (<3.5% catalyst content)

750522-1MG **¥65,700**
750530-1MG **¥99,500**
750514-25MG **¥43,100**
750492-100MG **¥46,500**

二層カーボンナノチューブ^{※2} **NEW!**

- double-walled, short, <10% Metal Oxide
- double-walled, <10% Metal Oxide

755141-1G **¥31,200**
755168-1G **¥31,200**

※1 NanoIntegris 社製 ※2 Nanocyl 社製

www.aldrich.com/nano-jp

SIGMA-ALDRICH®

シグマ アルドリッチ ジャパン

〒140-0002 東京都品川区東品川2-2-24
天王洲セントラルタワー4階

■製品に関するお問い合わせは、弊社テクニカルサポートへ
TEL : 03-5796-7330 FAX : 03-5796-7335
E-mail : sialjpts@sial.com

■在庫照会・ご注文方法に関するお問い合わせは、弊社カスタマーサービスへ
TEL : 03-5796-7320 FAX : 03-5796-7325
E-mail : sialjpcs@sial.com

<http://www.sigma-aldrich.com/japan>

Abstract

The 44th Fullerenes-Nanotubes-Graphene General Symposium

第44回フラーレン・ナノチューブ・グラフェン総合シンポジウム 講演要旨集

The Fullerenes, Nanotubes and Graphene Research Society
The Chemical Society of Japan
The Japan Society of Applied Physics
The Physical Society of Japan
The Electrochemical Society of Japan
The Society of Polymer Science, Japan
The University of Tokyo Global COE Program
Global center of Excellence for Mechanical Systems Innovation

主催：フラーレン・ナノチューブ・グラフェン学会

共催：日本化学会

東京大学グローバルCOEプログラム

機械システム・イノベーション国際拠点

協賛：日本物理学会・応用物理学会・電気化学会・高分子学会

Date: March 11th(Mon)–13th(Wed), 2013

Place: The University of Tokyo, ITO INTERNATIONAL RESEARCH CENTER
7-3-1 Hongo, Bunkyo-ku, Tokyo 113-8656

Presentation: Plenary Lecture (40 min presentation, 5min discussion)
Special Lecture (25 min presentation, 5min discussion)
General Lecture (10 min presentation, 5min discussion)
Poster Preview (1 min presentation, no discussion)

日時：平成25年3月11日(月)～13日(水)

場所：東京大学 伊藤国際学術研究センター 伊藤謝恩ホール
〒113-8656 東京都文京区本郷7-3-1

発表時間：基調講演	(発表 40分・質疑応答 5分)
特別講演	(発表 25分・質疑応答 5分)
一般講演	(発表 10分・質疑応答 5分)
ポスタープレビュー	(発表 1分・質疑応答 なし)

展示団体御芳名 (五十音順、敬称略)

アイクストロン(株)
 (株)ATR
QuantumWise Japan(株)
 コスモ・バイオ(株)
サーモフィッシャーサイエンティフィック(株)
 (株)島津製作所
 (株)スギノマシン
 (株)セントラル科学貿易
 ナカライテスク(株)
 ナノフォトン(株)
 日本電子(株)
(株)ニューメタルスエンドケミカルスコーポレーション
 日立工機(株)
 (株)堀場製作所
 (株)名城ナノカーボン

広告掲載団体御芳名 (五十音順、敬称略)

アイクストロン(株)
アイデア・インターナショナル(株)
 コスモ・バイオ(株)
 (株)コロナ
サーモフィッシャーサイエンティフィック(株)
シグマアルドリッチジャパン(株)
 (株)セントラル科学貿易
 ナカライテスク(株)
 ナノフォトン(株)
 日本電気(株)
 日本分析工業(株)
 フロンティアカーボン(株)
 和光純薬工業(株)

Contents

Time Table	• • • • •	i
Chairperson	• • • • •	iii
Program	Japanese • • • • •	iv
	English • • • • •	xvii
Abstracts	Plenary Lecture, Special Lecture • • •	1
	General Lecture • • • • •	11
	Poster Preview • • • • •	45
Author Index	• • • • •	185

目次

早見表	• • • • •	i
座長一覧	• • • • •	iii
プログラム	和文 • • • • •	iv
	英文 • • • • •	xvii
講演予稿	基調講演・特別講演 • • • • •	1
	一般講演 • • • • •	11
	ポスター発表 • • • • •	45
発表索引	• • • • •	185

プログラム早見表

3月11日 (月)	
	受付開始 8:30~ 講演開始 9:30~
9:30	特別講演 (赤阪健) 9:30-10:00
10:00	ポスタープレビュー (1P-1 ~ 1P-47) 10:00-10:45
10:45	ポスターセッション (多目的スペース) 10:45-12:30
12:30	昼食 (幹事会) 12:30-13:45
13:45	特別講演 (小松紘一) 13:45-14:15
14:15	一般講演 6件 (フラーレンの化学・ フラーレンの応用・ フラーレン) 14:15-15:45
15:45	休憩 15:45-16:00
16:00	特別講演 (江田剛輝) 16:00-16:30
16:30	一般講演 4件 (グラフェンの物性) 16:30-17:30
17:30	休憩 17:30-18:00
18:00	特別パネルセッション カーボンナノチューブの カイラリティ制御合成 に向けて 水谷・阿知波・斎藤(晋)・ 畠山・本間・篠原・野田・丸山 (伊藤ホール) 18:00-20:00

20:00

3月11日 (月)	
11:00	チュートリアル 講師: 中村栄一 東京大学 教授 (伊藤ホール) 11:00-12:30

12:30

3月12日 (火)	
	受付開始 8:30~ 講演開始 9:00~
9:00	基調講演 (Ming Zheng) 9:00-9:45
9:45	一般講演 3件 (ナノチューブの物性・ナノチュ ーブの生成と精製) 9:45-10:30
10:30	休憩 10:30-10:45
10:45	特別講演 (中嶋直敏) 10:45-11:15
11:15	一般講演 4件 (ナノチューブの物性・ ナノチューブの生成と精製・ ナノ炭素粒子) 11:15-12:15
12:15	昼食 12:15-13:30
13:30	授賞式 13:30-14:15
14:15	特別講演 (塚越一仁) 14:15-14:45
14:45	ポスタープレビュー (2P-1 ~ 2P-46) 14:45-15:30
15:30	ポスターセッション (多目的スペース) 15:30-17:00
17:00	休憩 17:00-17:15
17:15	一般講演 4件 (グラフェン生成・ グラフェンの物性) 17:15-18:15
18:15	
18:30	懇親会 (多目的スペース) 18:30-20:30

20:30

3月13日 (水)	
	受付開始 8:30~ 講演開始 9:00~
9:00	特別講演 (竹延大志) 9:00-9:30
9:30	一般講演 4件 (ナノチューブの物性・ ナノチューブの応用) 9:30-10:30
10:30	休憩 10:30-10:45
10:45	一般講演 5件 (ナノチューブの物性) 10:45-12:00
12:00	昼食 12:00-13:15
13:15	特別講演 (町田友樹) 13:15-13:45
13:45	ポスタープレビュー (3P-1 ~ 3P-46) 13:45-14:30
14:30	ポスターセッション (多目的スペース) 14:30-16:00
16:00	休憩 16:00-16:15
16:15	特別講演 (松尾豊) 16:15-16:45
16:45	一般講演 4件 (金属内包フラーレン) 16:45-17:45

17:45

基調講演 発表40分・質疑5分
特別講演 発表25分・質疑5分
一般講演 発表10分・質疑5分
ポスタープレビュー 発表1分・質疑なし

Time table

March 11 (Mon.)		March 12 (Tue.)		March 13 (Wed.)	
	Registration begins at 8:30 Lectures begin at 9:30		Registration begins at 8:30 Lectures begin at 9:00		Registration begins at 8:30 Lectures begin at 9:00
9:30	Special Lecture (T. Akasaka)	9:00	Plenary Lecture (Ming Zheng) 9:00-9:45	9:00	Special Lecture (T. Takenobu) 9:00-9:30
	9:30-10:00	9:45	General Lectures [3] (Properties of Nanotubes • Formation and Purification of Nanotubes) 9:45-10:30	9:30	General Lectures [4] (Properties of Nanotubes • Applications of Nanotubes) 9:30-10:30
10:00	Poster Preview (1P-1 through 1P-47) 10:00-10:45	10:30	Coffee Break 10:30-10:45	10:30	Coffee Break 10:30-10:45
10:45	Poster Session (Event Space) 10:45-12:30	10:45	Special Lecture (N. Nakashima) 10:45-11:15	10:45	General Lectures [5] (Properties of Nanotubes) 10:45-12:00
		11:15	General Lectures [4] (Properties of Nanotubes • Formation and Purification of Nanotubes • Carbon Nanoparticles) 11:15-12:15		
12:30	Lunch (Administrative meeting) 12:30-13:45	12:15	Lunch 12:15-13:30	12:00	Lunch 12:00-13:15
13:45	Special Lecture (K. Komatsu) 13:45-14:15	13:30	Award Ceremony 13:30-14:15	13:15	Special Lecture (T. Machida) 13:15-13:45
14:15	General Lectures [6] (Chemistry of Fullerenes • Applications of Fullerenes • Fullerenes) 14:15-15:45	14:15	Special Lecture (K. Tsukagoshi) 14:15-14:45	13:45	Poster Preview (3P-1 through 3P-46) 13:45-14:30
15:45	Coffee Break 15:45-16:00	14:45	Poster Preview (2P-1 through 2P-46) 14:45-15:30	14:30	Poster Session (Event Space) 14:30-16:00
16:00	Special Lecture (G. Eda) 16:00-16:30	15:30	Poster Session (Event Space) 15:30-17:00	16:00	Coffee Break 16:00-16:15
16:30	General Lectures [4] (Properties of Graphene) 16:30-17:30	17:00	Coffee Break 17:00-17:15	16:15	Special Lecture (Y. Matsuo) 16:15-16:45
17:30	Coffee Break 17:30-18:00	17:15	General Lectures [4] (Graphene Synthesis • Properties of Graphene) 17:15-18:15	16:45	General Lectures [4] (Endohedral Metallofullerenes) 16:45-17:45
18:00	Special Panel Session Toward the chirality controlled growth of carbon nanotubes (Mizutani • Achiba • S. Saito • Hatakeyama • Homma • Shinohara • Noda • Maruyama) (Ito Hall) 18:00-20:00	18:15		17:45	
20:00		18:30	Banquet (Event Space) 18:30-20:30		
	March 11 (Mon.)	20:30			
11:00	Tutorial Lecturer: Prof. E. Nakamura The University of Tokyo (Ito Hall) 11:00-12:30		Plenary Lecture: 40min (Presentation) + 5min (Discussion) Special Lecture: 25min (Presentation) + 5min (Discussion) General Lecture: 10min (Presentation) + 5min (Discussion) Poster Preview: 1min (Presentation)		
12:30					

座長一覽

3月11日(月)

(敬称略)

	時 間	座 長
特別講演(赤阪 健)	9:30 ~ 10:00	丸山 茂夫
ポスタープレビュー	10:00 ~ 10:45	高井 和之
ポスターセッション	10:45 ~ 12:30	千足 昇平
特別講演(小松 紘一)	13:45 ~ 14:15	篠原 久典
一般講演	14:15 ~ 15:45	宮田 耕充
特別講演(江田 剛輝)	16:00 ~ 16:30	吾郷 浩樹
一般講演	16:30 ~ 17:30	本間 芳和
特別パネルセッション	18:00 ~ 20:00	水谷 孝, 丸山 茂夫

3月12日(火)

	時 間	座 長
基調講演(Ming Zheng)	9:00 ~ 9:45	中嶋 直敏
一般講演	9:45 ~ 10:30	加藤 雄一郎
特別講演(中嶋 直敏)	10:45 ~ 11:15	片浦 弘道
一般講演	11:15 ~ 12:15	岡田 晋
特別講演(塚越 一仁)	14:15 ~ 14:45	長汐 晃輔
ポスタープレビュー	14:45 ~ 15:30	宮内 雄平
ポスターセッション	15:30 ~ 17:00	小鍋 哲
一般講演	17:15 ~ 18:15	塚越 一仁

3月13日(水)

	時 間	座 長
特別講演(竹延 大志)	9:00 ~ 9:30	齋藤 理一郎
一般講演	9:30 ~ 10:30	松田 一成
一般講演	10:45 ~ 12:00	竹延 大志
特別講演(町田 友樹)	13:15 ~ 13:45	山本 貴博
ポスタープレビュー	13:45 ~ 14:30	沖本 治哉
ポスターセッション	14:30 ~ 16:00	加藤 俊顕
特別講演(松尾 豊)	16:15 ~ 16:45	野田 優
一般講演	16:45 ~ 17:45	北浦 良

3月11日(月)

特別講演 発表25分・質疑応答5分
一般講演 発表10分・質疑応答5分
ポスタープレビュー 発表1分・質疑応答なし

特別講演 (9:30-10:00)

- 1S-1 金属内包フラーレンを鍵物質とする高次 π 空間の創発 1
赤阪 健

ポスタープレビュー (10:00-10:45)

ポスターセッション (10:45-12:30) (☆) 若手奨励賞候補

ナノチューブの物性

- 1P-1 Optical coupling of air-suspended carbon nanotubes to silicon microdisk resonators 45
☆ * Saneyuki Imamura, Ryosuke Watahiki, Ryohei Miura, Yuichiro K. Kato
- 1P-2 X-ray diffraction profile of highly purified (6,5) SWCNTs 46
* Tadera Shin, Haruka Kyakuno, Yusuke Nakai, Kazuhiro Yanagi, Yasumitsu Miyata, Hiromichi Kataura, Yutaka Maniwa
- 1P-3 Observation of circular dichroism in individual air-suspended single-walled carbon nanotubes 47
☆ * A. Yokoyama, A. Ishii, M. Yoshida, Y. K. Kato
- 1P-4 CNT分散溶液中の分散剤(Brij78)の定量 48
* 太田 一徳, 早川 由夫, 小野 泰蔵, 山脇 浩, 山本 和弘, 本田 一匡
- 1P-5 Effect of Impurity Scattering on AC Transport in Carbon Nanotubes 49
☆ * Daisuke Hirai, Takahiro Yamamoto, Satoshi Watanabe
- 1P-6 液相法によるカーボンナノチューブワイヤー 50
* 高木 勇樹, 大島 勇吾, 柳 和宏, 竹延 大志
- 1P-7 ラマン分光電気化学測定法によるSWCNTsの酸化開始電位の解析 51
☆ * 坂本 伸悟, 富永 昌人
- 1P-8 酸素ドーピングカーボンナノチューブにおける強い発光飽和 52
岩村 宗千代, * 宮内 雄平, 秋月 直人, 毛利 真一郎, 松田 一成
- 1P-9 走査ゲート顕微法によるSWNTネットワークFET中で観測される量子伝導現象の検討 53
☆ * 魏 小均, 松永 正広, 前田 賢治, 矢萩 達朗, 青木 伸之, J.P. バード, 石橋 幸治, 落合 勇一

ナノチューブの応用

- 1P-10 PEDOT:PSS/単層、多層カーボンナノチューブ複合膜を正孔輸送層に用いた有機薄膜太陽電池 54
* 岸 直希, 林 純輝, 斎藤 毅, 曾我 哲夫, 神保 孝志
- 1P-11 High efficiency carbon nanotube/silicon heterojunction solar cells fabricated using high quality carbon nanotube network film 55
☆ * 王 飛久, 小澤 大知, 宮内 雄平, 毛利 真一郎, 大野 雄高, 松田 一成
- 1P-12 カーボンナノチューブ電気二重層トランジスタにおけるp-n接合の形成 56
* Ryo Shimizu, Yijin Zhang, Kazuhiro Yanagi, Yoshihiro Iwasa, Taishi Takenobu
- 1P-13 High-mobility, flexible, n-type carbon nanotube thin-film transistors 57
☆ * Tomohiro Yasunishi, Yutaka Ohno, Shigeru Kishimoto, Takashi Mizutani
- 1P-14 免疫測定応用を目指したカーボンナノチューブの抗体による修飾 58
* 飯泉 陽子, 岡崎 俊也, 池原 譲, 小倉 睦郎, 湯田坂 雅子

ナノチューブの生成と精製

1P-15	ガス温度制御アーク放電によるナノチューブ合成 * 三重野 哲, 鈴木 崇	59
1P-16	重水・軽水混合液を用いた電界誘起層形成法による金属型/半導体型単層カーボンナノチューブ分離 ☆ * 佐々木 扶紗子, 沼田 秀昭, 斎藤 毅, 二瓶 史行	60
1P-17	高品質な単層カーボンナノチューブ成長におけるコールドウォール化学気相成長装置のヒーター部改良 * 津田 悠作, 土肥 智史, 石井 宏治, 岩田 展幸, 矢島 博史, 山本 寛	61
1P-18	Nitrogen-doped single-walled carbon nanotubes and their growth mechanism * Theerapol Thurakitseree, Christian Kramberger, Akihito Kumamoto, Shohei Chiashi, Erik Einarsson, Shigeo Maruyama	62
1P-19	パルスプラズマCVD法による(6, 5)単層カーボンナノチューブの選択的多量合成 ☆ * 村越 幸史, 加藤 俊顕, 畠山 力三, 金子 俊郎	63
1P-20	アルコールCVD法によるフラーレンを用いた単層CNTの合成 * 中村 謙太, 海野 貴徳, 千足 昇平, 丸山 茂夫	64
1P-21	走査型顕微鏡による水晶基板上の水平配向単層カーボンナノチューブの分析 * 長谷川 大祐, 井ノ上 泰輝, 大塚 慶吾, バダル サイフッラー, 千足 昇平, 丸山 茂夫	65
1P-22	String-like Aggregates of Aligned (6, 5) Single Wall Carbon Nanotubes ☆ * 河合 英輝, 長谷川 凱, 中津 亨, 内藤 泰久, 高木 勇樹, 竹延 大志, 柳 和宏	66
1P-23	スーパーグロース: 高濃度低活性炭素源を用いた高収量CNT合成法 * 木村 寛恵, 後藤 潤大, 保田 諭, 桜井 俊介, 湯村 守雄, 二葉 ドン, 畠 賢治	67
1P-24	高温パルスアーク放電の圧力依存性 * 菊池 隼人, 勝英 寺田, 菅井 俊樹	68

内包ナノチューブ

1P-25	溶液中で[10]Cycloparaphenyleneと共存するN@C ₆₀ のESR測定 * 岡本 光弘, 岩本 貴寛, 山子 茂, 加藤 立久	69
1P-26	高性能ラマンイメージングマーカーとしてのポリチオフェンを内包したカーボンナノチューブ ☆ * 宮浦 健志, 宮田 耕充, 若森 育也, ボアネルゲス テンディ, 北浦 良, 篠原 久典	70

ナノホーン

1P-27	カーボンナノホーンの生物分解 * 張 民芳, 揚 梅, プセイ シリル, アリーボセタ ハイネン, 飯島 澄男, コスタイラス コスタス, 湯田坂 雅子	71
1P-28	Carbon nanohorns induced RAW264.7 apoptosis: Lysosomal membrane destabilization caused reactive oxygen * Mei Yang, Minfang Zhang, Yoshio Tahara, Sumio Iijima, Masako Yudasaka	72
1P-29	酸素還元触媒能を有する窒素ドーパカーボンナノホーン集合体 * 弓削 亮太, 眞子 隆志, 坂東 俊治, 湯田坂 雅子, 當山 清彦, 山口 貴司, 飯島 澄男, 中野 嘉一郎	73

グラフェン生成

1P-30	ヘテロエピタキシャルCu(111)上でのBernal積層した二層グラフェンのCVD成長 ☆ * 田上 翔太, 河原 憲治, 辻 正治, 吾郷 浩樹	74
-------	--	----

3月11日(月)

1P-31	Scalable processing of crystallographic etching for graphite powder using supercritical fluid * 筈居 高明, 田村 直貴, 本間 格	75
1P-32	化学気相成長法によるグラフェン成長過程の反射高速電子回折その場観察 ☆ * 湊 拓郎, 中原 仁, 安坂 幸師, 齋藤 弥八	76
1P-33	Influence of applied potentials for electrochemical exfoliation of graphite * Haruya Okimoto, Syun Takabayashi, Yuhei Sobe, Masahito Sano	77
グラフェンの応用		
1P-34	形状制御されたグラフェン・窒化ホウ素複合シートのCVD合成 ☆ * 前田 枝里子, 宮田 耕充, 北浦 良, 篠原 久典	78
1P-35	CVDグラフェン上での方向制御されたNbS ₂ ナノシートの合成 Wanyin Ge, 河原 憲治, 辻 正治, * 吾郷 浩樹	79
1P-36	グラフェン修飾表面における有機半導体分子のナノ柱状結晶成長 ☆ * 岡田 賢, 古川 俊輔, 田中 秀幸, 原野 幸治, 中村 栄一	80
グラフェンの物性		
1P-37	Heイオン顕微鏡でグラフェンの格子像がみえるか? : 第一原理計算による予測 * 宮本 良之	81
1P-38	欠損のあるグラフェンナノリボンにおけるアンダーソン局在 ☆ * 高島 健悟, 高田 幸宏, 山本 貴博	82
1P-39	Gapped and gapless graphene and graphene-nanoribbon/nanotube complex * Shota Kizukuri, Takashi Koretsune, Susumu Saito	83
1P-40	SGM investigation of graphene nano structure * 古屋 惣平, 高井 和之, 佐藤 慶明, 榎 敏明	84
1P-41	Raman spectroscopy of mechanically strained chemically functionalized graphene ☆ * Mark Bissett, Masaharu Tsuji, Hiroki Ago	85
1P-42	ナノグラファイト-酸素分子間の磁氣的相互作用 * 高井 和之, Alexander. I Shames, Vladimir Yu Osipov, Alexander Ya Vul', 鏑木 裕, 林 卓也, 榎 敏明	86
ナノ炭素粒子		
1P-43	爆轟法ナノダイヤモンドの新展開 * 佐々木 修一, 山野井 亮子, 大澤 映二	87
1P-44	バイオメテック・アプローチによる高強度ナノダイヤモンド複合材料の合成 * 藤原 圭汰, 伊神 俊輝, 伊藤 正雅, 小澤 理樹	88
1P-45	光誘起反応によるポリイン-ヨウ素錯体の生成における速度論的考察 * 和田 資子, 若林 知成	89
その他		
1P-46	カーボンナノコイル添加によるバッキーペーパーの機械的特性の向上 * 丸山 皓司, 須田 善行, 滝川 浩史, 田上 英人, 植 仁志, 清水 一樹, 梅田 良人	90
1P-47	Measurement of electric resistance of a single carbon nanocoil * 國本 隆司, 米村 泰一郎, 須田 善行, 田上 英人, 滝川 浩史, 植 仁志, 清水 一樹, 梅田 良人	91

>>>>>>> 昼食 (12:30-13:45) <<<<<<<<

3月11日(月)

特別講演 (13:45-14:15)

- 1S-2 フラーレンの固体反応 --温故知新-- 2
小松 紘一

一般講演 (14:15-15:45)

フラーレンの化学・フラーレンの応用・フラーレン

- 1-1 ヘリウム内包フラーレンの有機合成ならびに 2つの異種原子を内包したフラーレンの発生 11
* 森中 裕太, 佐藤 悟, 若宮 淳志, 二川 秀史, 溝呂木 直美, 田邊 史行, 村田 理尚,
小松 紘一, 古川 貢, 加藤 立久, 永瀬 茂, 赤阪 健, 村田 靖次郎
- 1-2 Fullerene bis-carboxylic acid derivatives by Prato reaction 12
アロウア サフワン, * 山越 葉子
- 1-3 有限長カーボンナノチューブとフラーレンからなる分子ベアリングの構築と回転挙動 13
* 一杉 俊平, 山崎 孝史, 飯塚 亮介, 磯部 寛之
- 1-4 アルコキシフラーレン $C_{60}(OR)_5Br$ の選択的合成: アルコールによる $C_{60}Br_6$ の置換反応 14
* 内山 幸也, 森山 広思, 与座 健治
- 1-5 水酸化フラーレン固体の 1H -NMRによるプロトンダイナミクス 15
* 馬場 啓輔, 緒方 啓典
- 1-6 Kinetic Stability Governs Relative Fullerene Isomer Abundance 16
* イレ ステファン, 西村 好史, Alexander Fedorov, Henryk Witek

>>>>>>> 休憩 (15:45-16:00) <<<<<<<<

特別講演 (16:00-16:30)

- 1S-3 グラフェンおよびその他の2次元材料の蛍光特性 3
江田 剛輝

一般講演 (16:30-17:30)

グラフェンの物性

- 1-7 高速液体クロマトグラフィーにより分離したグラフェン量子ドットの光学特性 17
* 冬野 直人, 小澤 大知, 宮内 雄平, 毛利 真一郎, 北浦 良, 篠原 久典, 保田 徳, 小松 直樹,
松田 一成
- 1-8 化学ドーピングによる単原子層 MoS_2 の光学スペクトルの変調 18
* 毛利 真一郎, 宮内 雄平, 松田 一成
- 1-9 2層グラフェンにおけるクーロンドラッグと励起子絶縁体 19
* 小鍋 哲, 岡田 晋
- 1-10 Resonance and interference effect of Raman spectroscopy of graphene in the magnetic field 20
* Riichiro Saito, Qiu Caiyu, Yu Ting

>>>>>>> 休憩 (17:30-18:00) <<<<<<<<

特別パネルセッション (18:00-20:00)

カーボンナノチューブのカイラリティ制御合成に向けて
水谷 孝, 阿知波 洋次, 斎藤 晋, 畠山 力三, 本間 芳和, 篠原 久典, 野田 優, 丸山 茂夫

3月12日(火)

基調講演 発表40分・質疑応答5分
特別講演 発表25分・質疑応答5分
一般講演 発表10分・質疑応答5分
ポスタープレビュー 発表1分・質疑応答なし

基調講演 (9:00-9:45)

2S-4 Combining separation and synthesis to achieve structure control of carbon nanotubes 4
Ming Zheng

一般講演 (9:45-10:30)

ナノチューブの物性・ナノチューブの生成と精製

- 2-1 単層カーボンナノチューブの電子準位の経験的予測 21
* 平分 康彦, 宮内 雄平, 毛利 真一郎, 松田 一成, 中嶋 直敏
- 2-2 水蒸気雰囲気下でのSWNTのRBMに関する分子動力学計算 22
* 本間 直樹, 佐藤 慎太郎, 千足 昇平, 本間 芳和, 山本 貴博
- 2-3 フルオレン系ポリマーに包まれた単層カーボンナノチューブにおける発光ピークのエネルギーシフト 23
* 丹下 将克, 岡崎 俊也, 飯島 澄男

>>>>>>> 休憩 (10:30-10:45) <<<<<<<<

特別講演 (10:45-11:15)

2S-5 Fundamental and Advanced Materials Design of Soluble Carbon Nanotubes 5
中嶋 直敏

一般講演 (11:15-12:15)

ナノチューブの物性・ナノチューブの生成と精製・ナノ炭素粒子

- 2-4 Simultaneous Discrimination of Diameter, Handedness, and Metallicity of Single-Walled Carbon Nanotubes with Chiral Diporphyrin Nanocalipers 24
* 劉 剛, 汪 鋒, Chaunchaiyakul Songpol, 木村 隆英, 桑原 裕司, 小松 直樹
- 2-5 コール酸ナトリウムと様々な鎖長のオリゴDNAの単層カーボンナノチューブ表面での置換反応 25
* 井上 彩花, 加藤 雄一, 新留 康郎, 中嶋 直敏
- 2-6 紫外透過顕微鏡を用いたポリイン分散固体の光学特性の研究 26
* 若林 知成, 粕 和成, 柴田 宙延, 和田 資子
- 2-7 粘液状ナノダイヤモンドファイバーの形成 27
勝野 俊作, * 伊藤 正雅, 小澤 理樹

>>>>>>> 昼食 (12:15-13:30) <<<<<<<<

大澤賞・飯島賞・若手奨励賞の授賞式 (13:30-14:15)

特別講演 (14:15-14:45)

2S-6 Band engineering in bilayer graphene for future electron-devices 6
* K.Tsukagoshi, H.Miyazaki, S.-L.Li, A.A.Ferreira, M.Y.Chan, K. Komatsu, S.Nakaharai

ポスタープレビュー (14:45-15:30)

ポスターセッション (15:30-17:00) (☆) 若手奨励賞候補

フラーレンの化学

2P-1 [n]Cycloparaphenylene カチオンラジカルのESR測定 92
* 香山 貴彦, 茅原 栄一, 山子 茂, 加藤 立久

3月12日(火)

2P-2	リチウムイオン内包フラーレンのシクロペンタジエン付加体の単離と物性	93
☆	* 川上 裕貴, 岡田 洋史, 松尾 豊	
2P-3	FeCl ₃ を使った溶液相中でのC ₁₂₀ ダンベル型ダイマー合成	94
	橋口 昌彦, * 稲田 寛, 松尾 豊	
フラーレンの応用		
2P-4	Growth and Electric Properties of C ₆₀ Whiskers Directly Grown between Electrodes by Surface Treatment	95
	* 糰田 克矢, 岩田 展幸, 山本 寛	
金属内包フラーレン		
2P-5	La ₂ @C ₈₀ の環化付加反応と振電相互作用密度解析	96
	* 春田 直毅, 佐藤 徹, 田中 一義	
2P-6	新規non-IPR金属内包フラーレン: La ₂ @C _s (17490)-C ₇₆	97
☆	* 鈴木 光明, 溝呂木 直美, スラニナ ズデネク, ロウ シン, 永瀬 茂, 赤阪 健	
2P-7	水溶液中のGd@C ₈₂ -PEG-b-PAMA錯体パーティクルが示す磁性	98
	* 相澤 俊博, 堀口 諭吉, 長崎 幸夫, 篠原 久典, 加藤 立久	
フラーレン		
2P-8	液-液界面析出法によるC ₇₀ ナノシートの合成	99
	* 小菌江 佳菜, 鹿野 亮祐, 橋 勝	
2P-9	含硫黄開口部をもつC ₆₀ 誘導体の合成と窒素分子内包体のX線構造	100
☆	* 二子石 師, 村田 理尚, 村田 靖次郎	
2P-10	Polymerization in C ₆₀ thin films deposited under in situ UV light irradiation	101
	* Daijiro Arai, Hisanori Tanimoto, Manabu Ohtomo, Shiro Entani, Yoshihiro Matsumoto, Seiji Sakai	
ナノチューブの物性		
2P-11	Chirality dependence of exciton diffusion in air-suspended single-walled carbon nanotubes	102
☆	* A. Ishii, A. Yokoyama, M. Yoshida, T. Shimada, Y. K. Kato	
2P-12	Electric Double Layer Transistors using Thick Films in Single Chiral States of (6,5) and (11,10) Single-Wall Carbon Nanotubes	103
	* 工藤 光, 河合 将利, 船迫 友之, 野房 勇希, 竹延 大志, 柳 和宏	
2P-13	コール酸ナトリウムとDNA交換反応から見られる単層カーボンナノチューブ上のコール酸ナトリウムの異なる平衡状態	104
☆	* 加藤 雄一, 新留 康郎, 中嶋 直敏	
2P-14	電気二重層を用いたキャリア注入による単層カーボンナノチューブの光吸収制御	105
	* 五十嵐 透, 長谷川 凱, 船迫 友之, 小野 新平, 柳 和宏	
2P-15	コール酸ナトリウムと2本鎖DNAのナノチューブ表面での置換反応における熱力学	106
☆	* 續 明子, 井上 彩花, 加藤 雄一, 新留 康郎, 中嶋 直敏	
2P-16	後工程処理によるCNTの特性向上	107
	* 松本 尚之, 大島 あずさ, 湯村 守雄, 二葉 ドン, 畠 賢治	
2P-17	カーボンナノチューブ繊維を構成しているカーボンナノチューブ単体の引張強度	108
☆	* 鈴木 英彰, 佐藤 義倫, 山本 剛, 本宮 憲一, 橋田 俊之, 田路 和幸	

3月12日(火)

ナノチューブの応用

- 2P-18 Bending Properties of Single-Walled Carbon Nanotube Film Transistors 109
* Hiroki Hamahata, Yuki Nobusa, Yohei Yomogida, Kazuhiro Yanagi, Yoshihiro Iwasa, Taishi Takenobu
- 2P-19 High-performance, flexible carbon nanotube transparent conductive films of double layered structure 110
☆ * Norihiro Fukaya, Yusuke Kataoka, Dong Young Kim, Shigeru Kishimoto, Takashi Mizutani, Suguru Noda, Yutaka Ohno
- 2P-20 導電性AFMを用いたCNT/SiC界面の接触抵抗評価 111
* 渋谷 恵, 稲葉 優文, 大原 一慶, 落合 拓海, 増田 佳穂, 平岩 篤, 楠 美智子, 川原田 洋
- 2P-21 High-mobility carbon nanotube thin-film transistors fabricated on transparent plastic film by flexographic printing technique 112
☆ * Kentaro Higuchi, Yuta Nakajima, Takuya Tomura, Masafumi Takesue, Shigeru Kishimoto, Takashi Mizutani, Katsuhiko Hata, Yutaka Ohno
- 2P-22 ガス雰囲気半導体単層カーボンナノチューブ/Siヘテロ接合型光電変換デバイス特性に与える影響について 113
* 庄司 真雄, 中野 睦, 緒方 啓典

ナノチューブの生成と精製

- 2P-23 単層カーボンナノチューブ、ミリメートルスケール成長における酸化アルミニウム下地の影響 114
* 長谷川 馨, 野田 優
- 2P-24 炭素及びニッケルのダブルターゲットを用いたカーボンナノチューブの合成 115
* 石井 宏治, 岩田 展幸, 山本 寛, 矢島 博文
- 2P-25 フラビン誘導体を用いた単層カーボンナノチューブのカイラリティ選択的可溶化 116
☆ * 加藤 雄一, 新留 康郎, 中嶋 直敏
- 2P-26 高真空アルコールガスソース法による Al_2O_3 層上Pt触媒からの単層カーボンナノチューブ成長 117
* 福岡 直也, 近藤 弘基, 澤木 祐哉, Ranajit Ghosh, 成塚 重弥, 丸山 隆浩
- 2P-27 導電性下地上でのカーボンナノチューブ稠密配列の低温成長 118
☆ * 羅 ヌリ, 肖 英紀, 幾原 雄一, 野田 優
- 2P-28 分子ガラスの熱リソグラフィを用いた金属性単層カーボンナノチューブの選択的除去 119
* 大塚 慶吾, 井ノ上 泰輝, 長谷川 大祐, 千足 昇平, 丸山 茂夫
- 2P-29 Effects of discharge current direction and magnetic field for the production of single-walled carbon nanotubes in the arc discharge method 120
* Mohammad Jellur Rahman, Tetsu Mieno
- 2P-30 ゲルカラムクロマトグラフィーによる金属性単層カーボンナノチューブのカイラリティ分離 121
* 田中 丈士, 卜部 泰子, 片浦 弘道

内包ナノチューブ

- 2P-31 鋳型法による超伝導金属炭化物のカーボンナノチューブ内部への内包 122
* 小林 慶太, 斎藤 毅, 清宮 維春, 保田 英洋
- 2P-32 短いCNTに内包された C_{60} のエネルギー論と電子構造 123
☆ * 木暮 聖太, 岡田 晋

グラフェン生成

- 2P-33 Effect of inert gas on the growth of epitaxial graphene on Si-terminated SiC (0001) 124
* Akkawat Ruammaitree, Hitoshi Nakahara, Yahachi Saito

3月12日(火)

2P-34	暗視野透過型電子顕微鏡を用いたグラフェン端の構造評価	125
☆	* 藤原 美帆, 宮田 耕充, 北浦 良, 前田 枝里子, 篠原 久典	
2P-35	窒素置換構造が制御されたカーボン材料の合成	126
	* 保田 諭, 余力, 村越 敬	
2P-36	触媒カッティングを用いた高密度グラフェンナリボンの作製	127
☆	* 嘉陽 安理, ソリス フェルナンデス パブロ, 吉田 和真, 辻 正治, 吾郷 浩樹	

グラフェンの応用

2P-37	衝撃圧縮法によってカーボンナノウォールから生成された透明グラファイトフィルム	128
	* 中村 和貴, 阿藤 敏行, 庭瀬 敬右, 中村 一隆, 橘 勝	
2P-38	ポリグリセロール修飾によるグラフェンの水溶化	129
☆	* 保田 徳, 趙 利, 劉 剛, 青沼 秀児, 木村 隆英, 小松 直樹	
2P-39	マイクロ波プラズマCVD法によるカーボンナノシート薄膜の形態, 電子物性と電界放出特性の関係	130
	* 早瀬 勝平, 王 志朋, 緒方 啓典	

グラフェンの物性

2P-40	マイクロ波プラズマCVD法により堆積させたグラフェン膜の電気伝導特性評価	131
	* 沖川 侑揮, 津川 和夫, 山田 貴壽, 石原 正統, 長谷川 雅考	
2P-41	ナノグラフェンとガス分子のホスト-ゲスト相互作用	132
	* 高城 順一, 高井 和之, 木口 学, 榎 敏明, 山田 健郎, 畠 賢治, 石井 孝文, 京谷 隆	
2P-42	部分的に水素終端されたダイヤモンド構造(111)面における線形分散バンド	133
☆	* 曾根 準基, 岡田 晋	
2P-43	グラフェンの機械的変形が熱物性に与える影響	134
	* 船谷 宜嗣, 山本 貴博, 小川 真人, 相馬 聡文	
2P-44	エッジ修飾されたアームチェア型グラフェンナリボンの第一原理計算	135
	* 實宝 秀幸, 大淵 真理	

その他

2P-45	酸化鉄ナノチューブ・水酸化フラーレン複合体における光誘起電流の増大	136
	白木 勇喜, * 三品 雄基, 坂東 俊治	
2P-46	多段トラップ気相移動度測定システムの開発	137
	* 菅井 俊樹	

>>>>>>> 休憩 (17:00-17:15) <<<<<<<<

一般講演 (17:15-18:15)

グラフェン生成・グラフェンの物性

2-8	グラフェン-金属電極コンタクト特性に対する酸素吸着効果	28
	* 佐藤 慶明, 高井 和之, 榎 敏明	
2-9	Atomic structure determination of the graphene/sapphire interface by normal incident X-ray standing wave spectroscopy	29
	* Shiro Entani, Pavel Sorokin, Pavel Avramov, Manabu Ohtomo, Yoshihiro Matsumoto, Liubov Antipina, Ayumi Narita, Norie Hirao, Iwao Shimoyama, Tetsuhiro Sekiguchi, Hiroshi Naramoto, Yuji Baba, Seiji Sakai	
2-10	高性能グラフェンナリボントランジスタの集積化	30
	* 加藤 俊顕, 畠山 力三, 金子 俊郎	
2-11	CVDグラフェンにおけるドメイン間のキャリア輸送特性	31
	* 小川 友以, 河原 憲治, 宮下 雅大, 辻 正治, 小松 克伊, 塚越 一仁, 吾郷 浩樹	

3月13日(水)

特別講演 発表25分・質疑応答5分
一般講演 発表10分・質疑応答5分
ポスタープレビュー 発表1分・質疑応答なし

特別講演 (9:00-9:30)

- 3S-7 新しい機能性ナノチューブトランジスタ 7
竹延 大志

一般講演 (9:30-10:30)

ナノチューブの物性・ナノチューブの応用

- 3-1 n型およびp型ドーパント分子を内包した半導体型カーボンナノチューブを用いたCMOS
インバータの作製 32
* 伊藤 靖浩, 藤井 俊治郎, 清水 麻希, 田中 丈士, 片浦 弘道
- 3-2 Micro-Honeycomb Network Structure of Single-Walled Carbon Nanotube Film for
Solar Cells 33
* 崔 可航, 千葉 孝昭, 木下 英典, 趙 ペイ, Theerapol Thurakitseree, 井上 泰輝,
Erik Einarsson, 千足 昇平, 丸山 茂夫
- 3-3 垂直配向CNTの燃料電池電極への応用 34
* 村田 成亮, 今西 雅弘, 長谷川 茂樹, 難波 良一
- 3-4 Electromigration suppression in copper by carbon nanotubes : A mechanistic insight 35
* Chandramouli Subramaniam, Takeo Yamada, Don N. Futaba, Kenji Hata, Motoo Yumura

>>>>>>> 休憩 (10:30-10:45) <<<<<<<<<

一般講演 (10:45-12:00)

ナノチューブの物性

- 3-5 SWNT薄膜の熱起電力の第一原理シミュレーション 36
* 加藤 哲平, 臼井 信志, 山本 貴博
- 3-6 Influence of Carbon nano-inclusion dimensionality in the thermal conductivity
enhancement of aqueous and non-aqueous fluids 37
* Sivasankaran Harish, Kei Ishikawa, Erik Einarsson, Shohei Chiashi, Junichiro Shiomi,
Shigeo Maruyama
- 3-7 First Principles-Based Estimate of the Critical SWCNT Length for Raman D
and G Band Intensity Inversion 38
* 西村 好史, Henryk Witek, Stephan Irlle
- 3-8 Exciton effects on coherent phonon spectroscopy of carbon nanotubes 39
* アフマド ヌグラハ, ハスデオ エッドウィ, 齋藤 理一郎
- 3-9 High-temperature in-situ TEM Observation of Zipper-like Wall-to-Wall Coalescence
of Double-Wall Carbon Nanotubes 40
* 趙 思瀚, 北浦 良, 宮田 耕充, 篠原 久典

>>>>>>> 昼食 (12:00-13:15) <<<<<<<<<

特別講演 (13:15-13:45)

- 3S-8 Ballistic transport in graphene/h-BN 8
* Tomoki Machida, Satoru Masubuchi, Masahiro Onuki, Sei Morikawa,
Kazuyuki Iguchi, Takehiro Yamaguchi, Miho Arai, Kenji Watanabe, Takashi Taniguchi

3月13日(水)

ポスタープレビュー (13:45-14:30)

ポスターセッション (14:30-16:00) (☆) 若手奨励賞候補

フラーレンの化学

- 3P-1 C₆₀とシラシクロプロパンの熱反応:カルボシリル化フラーレンの生成 138
* 飯田 亮介, 高木 賢太郎, 加固 昌寛, 長谷川 正, 前田 優, 山田 道夫, 赤阪 健
- 3P-2 フラーレンC₇₀における開口部構築と水分子の内包 139
☆ * 張 鋭, 村田 理尚, 村田 靖次郎
- 3P-3 芳香族ジエナミンとC₆₀の熱[2+2]環化付加反応 140
* 伊熊 直彦, 山本 浩之, 三木江 翼, 小久保 研, 大島 巧

フラーレンの応用

- 3P-4 光渦照射によって作製したC₆₀光重合体の伝導特性評価 141
* Naoto Toriumi, Tatsuya Doi, Daiki Momiyama, Wataru Akiyama, Katsuhiko Miyamoto, Takashige Omatsu, Jonathan Bird, Yuichi Ochiai, Nobuyuki Aoki
- 3P-5 PCBMと混合ドナーを用いた有機薄膜太陽電池の作製 142
* 藤井 俊治郎, 段 宗範, 奥川 孝紀, 柳 雄一郎, 吉田 哲, 田中 丈士, 西岡 泰城, 片浦 弘道

金属内包フラーレン

- 3P-6 Trimetallic Nitride Template-Endohedral Metallofullerenes(TNT-EMFs)とアジリジンの反応 143
☆ * 木村 仁士, 上田 ちひろ, 山田 道夫, 前田 優, 長谷川 正, 赤阪 健
- 3P-7 トリエチルアミン-アセトン混合溶媒を用いた不安定複核金属内包フラーレンの抽出 144
* 富樫 愛美, 兒玉 健, 藤田 渉, 菊地 耕一, 阿知波 洋次

フラーレン

- 3P-8 ラジカルを有するフラーレンのスピンの状態 145
* 岡田 晋, 山本 貴博
- 3P-9 十重付加体フラーレンの磁性状態 146
☆ * 新夕 晴奈, 岡田 晋
- 3P-10 高強度フェムト秒レーザーを用いた溶液内反応によるC₆₀からのnon-IPRフラーレンの合成 147
* 兒玉 健, 藤野 竜也, 城丸 春夫, 阿知波 洋次

ナノ環境と安全評価

- 3P-11 カーボンナノチューブとホモポリペプチドの相互作用 148
* 平野 篤, 亀田 倫史, 田中 丈士, 片浦 弘道

ナノチューブの物性

- 3P-12 単層カーボンナノチューブバンドル界面における分子認識 149
☆ * 柳 鍾泰, 藤ヶ谷 剛彦, 中嶋 直敏
- 3P-13 Enhancement of photoluminescence from single-walled carbon nanotubes by photonic crystal nanocavities 150
Ryosuke Watahiki, * Takashi Shimada, Pei Zhao, Shohei Chiashi, Satoshi Iwamoto, Yasuhiko Arakawa, Shigeo Maruyama, Yuichiro K. Kato
- 3P-14 単層カーボンナノチューブの電気化学バンドギャップへの溶媒効果の検討 151
☆ * 宮崎 大悟, 平分 康彦, 新留 康郎, 中嶋 直敏
- 3P-15 単層・二層カーボンナノチューブの構造特性に対するOPOレーザー照射の影響 152
* 大藤 哲哉, 熊沢 陽, 長屋 祐香, 土屋 好司, 石井 忠浩, 矢島 博文

3月13日(水)

3P-16	Vernier spectrum in finite-length armchair carbon nanotubes	153
☆	* 辰巳 由樹, 泉田 渉, 齋藤 理一郎	
3P-17	細いナノチューブにおけるRBMの第一原理計算	154
	* 是常 隆, 齋藤 晋	
3P-18	平行電界によって電荷が蓄積されたキャップ付きカーボンナノチューブの電子物性	155
☆	* 山中 綾香, 岡田 晋	
3P-19	Electronic Raman scattering and origin of the Fano resonance in metallic carbon nanotubes	156
	* Eddwi Hasdeo, Ahmad Nugraha, Kentaro Sato, Riichiro Saito	

ナノチューブの応用

3P-20	Selective Dispersion of Single-Walled Carbon Nanotubes into Nano-Cage of Helical Conformation of Poly(m-phenylene-ethynylene) Derivatives	157
	Fumito Kobayashi, Yuki Moriyama, * Masahiro Takahashi, Masayoshi Tange, Toshiya Okazaki, Keiki Kishikawa, Shigeo Kohmoto	
3P-21	単層カーボンナノチューブのポリグリセロール修飾による可溶化と液体クロマトグラフィによるサイズ分離	158
☆	* 中村 圭祐, 趙 利, 青沼 秀児, 木村 隆英, 小松 直樹	
3P-22	Electric double layer transistors of aligned carbon nanotube thin film	159
	* Yoshifumi Wada, Jiang Pu, Yuki Takagi, Kazuhiro Yanagi, Taishi Takenobu	
3P-23	単層カーボンナノチューブ膜の光熱起電力特性	160
☆	* 榊原 甫, 佐藤 義倫, 伊野 浩介, 伊藤 暁彦, 末永 智一, 後藤 孝, 本宮 憲一, 田路 和幸	
3P-24	Specific biosensor based on biotin-labeled double-walled carbon nanotube FET	161
	* Akihiro Kuno, Yuka Nagaya, Koji Tsuchiya, Akira Hida, Koji Ishibashi, Hirofumi Yajima	

ナノチューブの生成と精製

3P-25	錯体ポリマーによる単層カーボンナノチューブの選択的可溶化	162
	* 利光 史行, 藤ヶ谷 剛彦, 中嶋 直敏	
3P-26	分子動力学シミュレーションにおける単層カーボンナノチューブ成長のカイラリティ解析	163
	* 川鈴木 智哉, 久間 馨, 高木 勇輝, 千足 昇平, 丸山 茂夫	
3P-27	Methane-assisted CVD yielding millimeter-tall single-wall carbon nanotubes of smaller diameters	164
☆	* 陳 忠明, 金 東榮, 長谷川 馨, 野田 優	
3P-28	ピレン分子ノギスによる金属単層カーボンナノチューブの選択的抽出	165
	劉 剛, * 小松 直樹, 木村 隆英	
3P-29	In situ Raman monitoring formation of SWNTs: process optimization and low temperature synthesis	166
	* Ming Liu, Yuquan Su, Rong Xiang, Zikang Tang	
3P-30	One-Step Catalyst-Free Mist Flow CVD Growth of Single-Wall Carbon Nanotubes using C ₆₀ Fullerenes	167
☆	* Yun Sun, Ryo Kitaura, Jinying Zhang, Yasumitsu Miyata, Hisanori Shinohara	
3P-31	単層CNTフォレスト成長制御に向けた触媒微粒子アレイ形成過程のモデル分析	168
	* 桜井 俊介, フタバドン, 湯村 守雄, 畠 賢治	

3月13日(水)

- 3P-32 コールドウォール化学気相成長法による単層カーボンナノチューブの位置、カイラリティ、
面内配向の同時制御 169
* 相良 拓実, 土肥 智史, 石井 宏治, 岩田 展幸, 矢島 博文, 山本 寛

内包ナノチューブ

- 3P-33 Diameter Dependent Interaction between Single-Walled Carbon Nanotubes and
Encapsulated Ferrocenes 170
* 鈴木 浩紀, 飯泉 陽子, 岡崎 俊也
- 3P-34 単層カーボンナノチューブ内部に作成した単層窒化ホウ素ナノチューブの分光分析 171
☆ * 中西 亮, 北浦 良, 山本 悠太, 荒井 重勇, Warner Jamie, 宮田 耕充, 篠原 久典

グラフェン生成

- 3P-35 触媒CVD法における多層グラフェン生成の分子動力学シミュレーション 172
* 高木 勇輝, 久間 馨, 川鈴木 智哉, 千足 昇平, 丸山 茂夫
- 3P-36 ラージグレイン単層BNドープグラフェンの合成と評価 173
☆ * 小林 佑, 宮田 耕充, 前田 枝里子, 北浦 良, 篠原 久典
- 3P-37 室温超伝導を実現するグラファイト/グラフェン層間化合物の生成と特性評価 174
* 佐藤 祥吾, 市川 博亮, 岩田 展幸, 山本 寛
- 3P-38 基板対向CVD法によるCu上でのグラフェンの指向性成長 175
☆ * 増田 竜也, 河原 憲治, 吾郷 浩樹, 野田 優

グラフェンの応用

- 3P-39 Monte Carlo Particle Simulations of Local Heating Properties in Graphene-channel
nano-FETs 176
* 大木 秀祐, 三澤 太一, 栗野 祐二
- 3P-40 グラフェンを用いた超高速黒体放射発光素子 177
☆ * 横井 智哉, 高山 雄介, 森 達也, 津谷 大樹, 牧 英之
- 3P-41 Few-layer Graphene/silicon Heterojunction Photovoltaic Cells by Microwave Plasma-
Enhanced Chemical Vapor Deposition 178
* Z. Wang, S. Hayase, M Shoji, H Hironori

グラフェンの物性

- 3P-42 遠心分離した酸化グラフェンの酸化度 179
* 横井 裕之, 鯉沼 陸央, 畠山 一翔, 谷口 貴章, 松本 泰道
- 3P-43 Spin polarization of hexagonal boron nitride/Ni(111) interface studied by spin-polarized
metastable de-excitation spectroscopy. 180
* 大伴 真名歩, 山内 泰,, 圓谷 志郎, 松本 吉弘, 檜本 洋, 境 誠司
- 3P-44 2次元金属炭素同素体の物性 181
☆ * 丸山 実那, 岡田 晋
- 3P-45 グラファイトのレーザーアブレーションにより生成したグラフェンナノ物質 182
* 中村 真紀, 河合 孝純, 入江 路子, 弓削 亮太, 飯島 澄男, 坂東 俊治, 湯田坂 雅子
- 3P-46 エッチング液と合成温度が窒素ドープしたグラフェン膜の表面抵抗率に及ぼす効果 183
水野 貴裕, * 坂東 俊治

>>>>>>> 休憩 (16:00-16:15) <<<<<<<<

3月13日（水）

特別講演（16:15-16:45）

- 3S-9 有機薄膜太陽電池に用いるフラーレン誘導体の設計と合成および物性 9
松尾 豊

一般講演（16:45-17:45）

金属内包フラーレン

- 3-10 金属内包フラーレンの成長機構 41
* 阿知波 洋次, 兒玉 健, 橋本 健朗, 城丸 春夫
- 3-11 単結晶X線回折による低対称性フラーレンに内包されたツリウム原子および炭素クラスターの構造解析 42
* 佐道 祐貴, 青柳 忍, 泉 乃里子, 北浦 良, Tim Kowalczyk, Jian Wang, Stephan Irle, 西堀 英治, 杉本 邦久, 篠原 久典
- 3-12 リチウム内包フラーレンとクロリン誘導体の超分子内光電子移動反応 43
* 大久保 敬, 川島 雄樹, 間瀬 謙太郎, 福住 俊一
- 3-13 $Gd_3N@C_{80}$ と $Er_3N@C_{80}$ の紫外光電子スペクトル 44
* 宮崎 隆文, 中西 勇介, 佐々木 祐生, 丹羽 宏之, 野田 祥子, 西 龍彦, 太田 知那, 篠原 久典, 日野 照純

March 11th, Mon.

Special Lecture: 25min (Presentation) + 5min (Discussion)

General Lecture: 10min (Presentation) + 5min (Discussion)

Poster Preview: 1min (Presentation)

Special Lecture (9:30–10:00)

- 1S-1 New Vistas in Chemistry of Endohedral Metallofullerenes 1
Takeshi Akasaka

Poster Preview (10:00–10:45)

Poster Session (10:45–12:30) (★) Candidates for the Young Scientist Poster Award

Properties of nanotubes

- 1P-1 Optical coupling of air-suspended carbon nanotubes to silicon microdisk resonators 45
★ * *Saneyuki Imamura, Ryosuke Watahiki, Ryohei Miura, Yuichiro K. Kato*
- 1P-2 X-ray diffraction profile of highly purified (6,5) SWCNTs 46
* *Shin Tadera, Haruka Kyakuno, Yusuke Nakai, Kazuhiro Yanagi, Yasumitsu Miyata, Hiromichi Kataura, Yutaka Maniwa*
- 1P-3 Observation of circular dichroism in individual air-suspended single-walled carbon nanotubes 47
★ * *A. Yokoyama, A. Ishii, M. Yoshida, Y. K. Kato*
- 1P-4 Determination of surfactant (Brij 78) in aquatic CNT dispersion 48
* *Kazutoku Ohta, Yoshio Hayakawa, Taizo Ono, Hiroshi Yamawaki, Kazuhiro Yamamoto, Kazumasa Honda*
- 1P-5 Effect of Impurity Scattering on AC Transport in Carbon Nanotubes 49
★ * *Daisuke Hirai, Takahiro Yamamoto, Satoshi Watanabe*
- 1P-6 Solution growth of carbon-nanotube wires 50
* *Yuki Takagi, Yugo Oshima, Kazuhiro Yanagi, Taishi Takenobu*
- 1P-7 In-situ Raman spectroelectrochemical investigation on diameter-dependent onset potential of oxygenation reaction of SWCNTs 51
★ * *Shingo Sakamoto, Masato Tominaga*
- 1P-8 Strong saturation of photoluminescence from local quantum states in oxygen-doped carbon nanotubes 52
*Munechiyo Iwamura, * Yuhei Miyauchi, Naoto Akizuki, Shinichiro Mouri, Kazunari Matsuda*
- 1P-9 Quantum Mechanical Transport in SWNTs Network FETs Studied via Scanning Gate Microscopy 53
★ * *Xiaojun Wei, Masahiro Matsunaga, Kenji Maeda, Tatsuro Yahagi, Nobuyuki Aoki, Jonathan P. Bird, Koji Ishibashi, Yuichi Ochiai*

Applications of nanotubes

- 1P-10 Polymer Solar Cells with PEDOT:PSS / SWCNTs and MWCNTs Composite as Hole Transport Layer 54
* *Naoki Kishi, Junki Hayashi, Takeshi Saito, Tetsuo Soga, Takashi Jimbo*
- 1P-11 High efficiency carbon nanotube/silicon heterojunction solar cells fabricated using high quality carbon nanotube network film 55
★ * *Feijiu Wang, Daichi Kozawa, Yuhei Miyauchi, Shinichiro Mouri, Yutaka Ohno, Kazunari Matsuda*
- 1P-12 P-N junction in Carbon Nanotube Electric Double Layer Transistor 56
* *Ryo Shimizu, Yijin Zhang, Kazuhiro Yanagi, Yoshihiro Iwasa, Taishi Takenobu*
- 1P-13 High-mobility, flexible, n-type carbon nanotube thin-film transistors 57
★ * *Tomohiro Yasunishi, Yutaka Ohno, Shigeru Kishimoto, Takashi Mizutani*
- 1P-14 Functionalization of Carbon Nanotubes with Antibody for Immunoassay 58
* *Yoko Iizumi, Toshiya Okazaki, Yuzuru Ikehara, Mutuo Ogura, Masako Yudasaka*

March 11th, Mon.

Formation and purification of nanotubes

- 1P-15 Arc Production of SWNTS under Controlled He Gas Temperature 59
* *Tetsu Mieno, Takashi Suzuki*
- 1P-16 Electric-field-induced layer formation of metallic and semiconducting single-wall carbon nanotubes in D₂O – H₂O mixtures 60
☆ * *Fusako Sasaki, Hideaki Numata, Takeshi Saito, Fumiyuki Nihey*
- 1P-17 Development of Substrate Heater System of Cold-Wall Chemical Vapor Deposition Equipment for Improvement of Single-Walled Carbon Nanotubes Quality 61
* *Yusaku Tsuda, Satoshi Doi, Koji Ishii, Nobuyuki Iwata, Hirihumi Yajima, Hiroshi Yamamoto*
- 1P-18 Nitrogen-doped single-walled carbon nanotubes and their growth mechanism 62
* *Theerapol Thurakitserree, Christian Kramberger, Akihito Kumamoto, Shohei Chiashi, Erik Einarsson, Shigeo Maruyama*
- 1P-19 Selective synthesis of large amount of (6, 5) single-walled carbon nanotubes using pulse plasma CVD 63
☆ * *Koshi Murakoshi, Toshiaki Kato, Rikizo Hatakeyama, Toshiro Kaneko*
- 1P-20 Alcohol Catalytic CVD Synthesis of Single-Walled Carbon Nanotubes Using C₆₀ as the Catalysts 64
* *Kenta Nakamura, Takanori Umino, Shohei Chiashi, Shigeo Maruyama*
- 1P-21 Characterization of Horizontally Aligned Single-Walled Carbon Nanotubes Grown on Crystal Quartz by Using Scanning Microscopy 65
* *Daisuke Hasegawa, Taiki Inoue, Keigo Otsuka, Saifullah Badar, Shohei Chiashi, Shigeo Maruyama*
- 1P-22 String-like Aggregates of Aligned (6, 5) Single Wall Carbon Nanotubes 66
☆ * *Hideki Kawai, Kai Hasegawa, Touru Nakatsu, Yasuhisa Naitou, Yuuki Takagi, Taishi Takenobu, Kazuhiro Yanagi*
- 1P-23 Super Growth: Unexpectedly High Yield Carbon Nanotube Synthesis from Low Activity Carbon Feedstocks at High Concentrations 67
* *Hiroe Kimura, Jundai Goto, Satoshi Yasuda, Shunsuke Sakurai, Motoo Yumura, Don Futaba, Kenji Hata*
- 1P-24 Pressure dependence of High-temperature Pulsed-arc Discharge 68
* *Hayato Kikuchi, Katsuhide Terada, Toshiki Sugai*

Endohedral nanotubes

- 1P-25 ESR Measurements of N@C₆₀ with [10]Cycloparaphenylene in Solution 69
* *Mitsuhiro Okamoto, Takahiro Iwamoto, Shigeru Yamago, Tatsuhisa Kato*
- 1P-26 Polythiophene encapsulated in carbon nanotubes as a high-throughput Raman imaging marker 70
☆ * *Kenshi Miyaura, Yasumitsu Miyata, Ikuya Wakamori, Boanerges Thendie, Ryo Kitaura, Hisanori Shinohara*

Nanohorns

- 1P-27 Biodegradation of Single-Wall Carbon Nanohorns 71
* *Minfang Zhang, Mei Yang, Cyrill Bussy, Hanene Ali-Boucetta, Sumio Iijima, Kostas Kostarelos, Masako Yudasaka*
- 1P-28 Carbon nanohorns induced RAW264.7 apoptosis: Lysosomal membrane destabilization caused reactive oxygen species generation, leading cell apoptosis 72
* *Mei Yang, Minfang Zhang, Yoshio Tahara, Sumio Iijima, Masako Yudasaka*
- 1P-29 Nitrogen-doped carbon nanohorn aggregates with electrocatalytic activity for oxygen reduction 73
* *Ryota Yuge, Takashi Manako, Shunji Bandow, Masako Yudasaka, Kiyohiko Toyama, Takashi Yamaguchi, Sumio Iijima, Kaichiro Nakano*

March 11th, Mon.

Graphene synthesis

1P-30	CVD Growth of Bernal Stacked Bilayer Graphene on Heteroepitaxial Cu(111) Film	74
☆	* <i>Shota Tanoue, Kenji Kawahara, Masaharu Tsuji, Hiroki Ago</i>	
1P-31	Scalable processing of crystallographic etching for graphite powder using supercritical fluid	75
	* <i>Takaaki Tomai, Naoki Tamura, Itaru Honma</i>	
1P-32	In situ RHEED Study on Growth Process of Graphene by Chemical Vapor Deposition	76
☆	* <i>Takuro Minato, Hitoshi Nakahara, Koji Asaka, Yahachi Saito</i>	
1P-33	Influence of applied potentials for electrochemical exfoliation of graphite	77
	* <i>Haruya Okimoto, Syun Takabayashi, Yuhei Sobe, Masahito Sano</i>	

Applications of graphene

1P-34	CVD synthesis of shape-controlled graphene and boron nitride heterostructures	78
☆	* <i>Eriko Maeda, Yasumitsu Miyata, Ryo Kitaura, Hisanori Shinohara</i>	
1P-35	Orientation Controlled Growth of NbS ₂ Nanosheets on CVD Graphene	79
	<i>Wanyin Ge, Kenji Kawahara, Masaharu Tsuji, * Hiroki Ago</i>	
1P-36	Nanocolumnar Crystal Growth of Organic Semiconductor Molecules on a Graphene-Modified Surface	80
☆	* <i>Satoshi Okada, Shunsuke Furukawa, Hideyuki Tanaka, Koji Harano, Eiichi Nakamura</i>	

Properties of graphene

1P-37	Imaging graphene lattice by the helium ion microscope: A prediction by ab initio simulations	81
	* <i>Yoshiyuki Miyamoto</i>	
1P-38	Anderson Localization of Edge-Disordered Graphene Nanoribbons	82
☆	* <i>Kengo Takashima, Yukihiro Takada, Takahiro Yamamoto</i>	
1P-39	Gapped and gapless graphene and graphene-nanoribbon/nanotube complex	83
	* <i>Shota Kizukuri, Takashi Koretsune, Susumu Saito</i>	
1P-40	SGM investigation of graphene nano structure	84
	* <i>Souhei Furuya, Kazuyuki Takai, Yoshiaki Sato, Toshiaki Enoki</i>	
1P-41	Raman spectroscopy of mechanically strained chemically functionalized graphene	85
☆	* <i>Mark Bissett, Masaharu Tsuji, Hiroki Ago</i>	
1P-42	Magnetic Interactions between Nanographite and Oxygen Molecule	86
	* <i>Kazuyuki Takai, Alexander. I Shames, Vladimir Yu Osipov, Alexander Ya Vul', Yutaka Kaburagi, Takuya Hayashi, Toshiaki Enoki</i>	

Carbon nanoparticles

1P-43	A New Stage in Detonation Nanodiamond Research	87
	* <i>Shuichi Sasaki, Ryoko Yamanoi, Eiji Osawa</i>	
1P-44	Biomimetic approach toward tough nanodiamond materials	88
	* <i>Keita Fujiwara, Toshiki Ikami, Tadamasato Ito, Masaki Ozawa</i>	
1P-45	Kinetic consideration on the formation of polyyn-iodine complex by photoinduced reaction	89
	* <i>Yoriko Wada, Tomonari Wakabayashi</i>	

Other topics

1P-46	Improved Mechanical Property of Bucky Paper by Adding Carbon Nanocil	90
	* <i>Koji Maruyama, Yosiyuki Suda, Hirohumi Takikawa, Hideto Tanoue, Hitosi Ue, Kazuki Shimizu, Yosito Umeda</i>	
1P-47	Measurement of electric resistance of a single carbon nanocoil	91
	* <i>Ryuji Kunitomo, Taiichiro Yonemura, Yoshiyuki Suda, Hideto Tanoue, Hirofumi Takikawa, Hitoshi Ue, Kazuki Shimizu, Yoshito Umeda</i>	

March 11th, Mon.

>>>>>>> Lunch Time (12:30–13:45) <<<<<<<<

Special Lecture (13:45–14:15)

- 1S-2 Solid-State Chemistry of Fullerenes --Learning the New, through Visiting the Old-- 2
Koichi Komatsu

General Lecture (14:15–15:45)

Chemistry of fullerenes ▪ Applications of fullerenes ▪ Fullerenes

- 1-1 Organic Synthesis of Helium-Containing Fullerenes and Generation of Endohedral Fullerenes 11
Encapsulating Two Different Atoms
** Yuta Morinaka, Satoru Sato, Atsushi Wakamiya, Hidefumi Nikawa, Naomi Mizorogi, Fumiyuki Tanabe, Michihisa Murata, Koichi Komatsu, Ko Furukawa, Tatsuhisa Kato, Shigeru Nagase, Takeshi Akasaka, Yasujiro Murata*
- 1-2 Fullerene bis-carboxylic acid derivatives by Prato reaction 12
*Safwan Aroua, * Yoko Yamakoshi*
- 1-3 Molecular Bearing of Finite Carbon Nanotube and Fullerene in Ensemble Rolling Motion 13
** Shunpei Hitosugi, Takashi Yamasaki, Ryosuke Iizuka, Hiroyuki Isobe*
- 1-4 Selective synthesis of alkoxyfullerenes $C_{60}(OR)_5Br$: Substitution reaction of $C_{60}Br_6$ with alcohol 14
** Kouya Uchiyama, Hiroshi Moriyama, Kenji Yoza*
- 1-5 Proton dynamics in Fullerenol solids studied by 1H -NMR 15
** Keisuke Baba, Hironori Ogata*
- 1-6 Kinetic Stability Governs Relative Fullerene Isomer Abundance 16
** Stephan Irle, Yoshifumi Nishimura, Alexander Fedorov, Henryk Witek*

>>>>>>> Coffee Break (15:45–16:00) <<<<<<<<

Special Lecture (16:00–16:30)

- 1S-3 Photoluminescence properties of some graphene-based and inorganic two-dimensional materials 3
Goki Eda

General Lecture (16:30–17:30)

Properties of graphene

- 1-7 Optical properties of graphene quantum dots separated by high performance liquid chromatography 17
** Naoto Fuyuno, Daichi Kozawa, Yuhei Miyachi, Shinichiro Mouri, Ryo Kitaura, Hisanori Shinohara, Toku Yasuda, Naoki Komatsu, Kazunari Matsuda*
- 1-8 Modulation of Optical Spectra of Monolayer MoS_2 by Chemical Doping 18
** Shinichiro Mouri, Yuhei Miyachi, Kazunari Matsuda*
- 1-9 Coulomb drag and excitonic insulator in double-layer graphene 19
** Satoru Konabe, Susumu Okada*
- 1-10 Resonance and interference effect of Raman spectroscopy of graphene in the magnetic field 20
** Riichiro Saito, Qiu Caiyu, Yu Ting*

>>>>>>> Coffee Break (17:30–18:00) <<<<<<<<

Special Panel Session (18:00–20:00)

Toward the chirality controlled growth of carbon nanotubes

Takashi Mizutani, Yohji Achiba, Susumu Saito, Rikizo Hatakeyama, Yoshikazu Homma, Hisanori Shinohara, Suguru Noda, Shigeo Maruyama

March 12th, Tue.

Plenary Lecture: 40min (Presentation) + 5min (Discussion)

Special Lecture: 25min (Presentation) + 5min (Discussion)

General Lecture: 10min (Presentation) + 5min (Discussion)

Poster Preview: 1min (Presentation)

Plenary Lecture (9:00–9:45)

- 2S-4 Combining separation and synthesis to achieve structure control of carbon nanotubes 4
Ming Zheng

General Lecture (9:45–10:30)

Properties of nanotubes ▪ Formation and purification of nanotubes

- 2-1 Empirical Prediction of Electronic Potentials of Single-Walled Carbon Nanotubes 21
** Yasuhiko Hirana, Yuhei Miyauchi, Shinichirou Mouri, Kazunari Matsuda, Naotoshi Nakashima*
- 2-2 Molecular Dynamics Simulation on RBM of Single-Walled Carbon Nanotubes in Water Vapor 22
** Naoki Homma, Shintaroh Sato, Shohei Chiashi, Yoshikazu Homma, Takahiro Yamamoto*
- 2-3 Energy shift of photoluminescence peaks of SWCNTs wrapped by fluorene-based polymers 23
** Masayoshi Tange, Toshiya Okazaki, Sumio Iijima*

>>>>>>> **Coffee Break (10:30–10:45)** <<<<<<<<<

Special Lecture (10:45–11:15)

- 2S-5 Fundamental and Advanced Materials Design of Soluble Carbon Nanotubes 5
Naotoshi Nakashima

General Lecture (11:15–12:15)

Properties of nanotubes ▪ Formation and purification of nanotubes ▪ Carbon nanoparticles

- 2-4 Simultaneous Discrimination of Diameter, Handedness, and Metallicity of Single-Walled Carbon Nanotubes with Chiral Diporphyrin Nanocalipers 24
** Gang Liu, Feng Wang, Songpol Chaunchaiyakul, Takahide Kimura, Yuji Kuwahara, Naoki Komatsu*
- 2-5 Exchanges of sodium cholate and oligo-DNAs with different chain length on single-walled carbon nanotubes 25
** Ayaka Inoue, Yuichi Kato, Yasuro Niidome, Naotoshi Nakashima*
- 2-6 Optical Properties of Polyynes Molecules Dispersed in Solids as Studied by An UV Transmission Microscope 26
** Tomonari Wakabayashi, Kazunari Koma, Okinaga Shibata, Yoriko Wada*
- 2-7 Slimy fibers of nanodiamonds assembled in polyacrylamide aqueous solutions 27
*Shunsaku Katsuno, * Tadamasa Ito, Masaki Ozawa*

>>>>>>> **Lunch Time (12:15–13:30)** <<<<<<<<<

Awards Ceremony (13:30–14:15)

Special Lecture (14:15–14:45)

- 2S-6 Band engineering in bilayer graphene for future electron-devices 6
** K.Tsukagoshi, H.Miyazaki, S.-L.Li, A.A.Ferreira, M.Y.Chan, K. Komatsu, S.Nakaharai*

March 12th, Tue.

Poster Preview (14:45–15:30)

Poster Session (15:30–17:00) (★) Candidates for the Young Scientist Poster Award

Chemistry of fullerenes

- 2P-1 ESR Measurements of Series of [n]Cycloparaphenylene Cation Radicals in Solution 92
* *Takahiko Kouyama, Eiichi Kayahara, Shigeru Yamago, Tatsuhisa Kato*
- 2P-2 Isolation and Properties of a Cyclopentadiene Adduct of Lithium-ion Encapsulated [60] Fullerene 93
★ * *Hiroki Kawakami, Hiroshi Okada, Yutaka Matsuo*
- 2P-3 Solution-phase Synthesis of Dumbbell-Shaped Dimer C₁₂₀ by the Use of FeCl₃ 94
*Masahiko Hashiguchi, * Hiroshi Inada, Yutaka Matsuo*

Applications of fullerenes

- 2P-4 Growth and Electric Properties of C₆₀ Whiskers Directly Grown between Electrodes 95
by Surface Treatment
* *Katsuya Uruchida, Nobuyuki Iwata, Hiroshi Yamamoto*

Endohedral metallofullerenes

- 2P-5 Cycloadditions to La₂@C₈₀ and vibronic coupling density analysis 96
* *Naoki Haruta, Tohru Sato, Kazuyoshi Tanaka*
- 2P-6 A Novel Non-IPR Endohedral Metallofullerene: La₂@C_s(17490)-C₇₆ 97
★ * *Mitsuaki Suzuki, Naomi Mizorogi, Zdenek Slanina, Xing Lu, Shigeru Nagase, Takeshi Akasaka*
- 2P-7 Magnetic Properties of Gd@C₈₂-PEG-b-PAMA-complexed Nanoparticle 98
* *Toshihiro Aizawa, Yukichi Horiguchi, Yukio Nagasaki, Hisanori Shinohara, Tatsuhisa Kato*

Fullerenes

- 2P-8 Synthesis of C₇₀ Nanosheets by Liquid-Liquid Interfacial Precipitation Method 99
* *Kana Osonoe, Ryosuke Kano, Masaru Tachibana*
- 2P-9 Synthesis of C₆₀ Derivatives Having a Sulfur-containing Opening and X-ray Structure of N₂ 100
Encapsulated Molecule
★ * *Tsukasa Futagoishi, Michihisa Murata, Yasujiro Murata*
- 2P-10 Polymerization in C₆₀ thin films deposited under in situ UV light irradiation 101
* *Daijiro Arai, Hisanori Tanimoto, Manabu Ohtomo, Shiro Entani, Yoshihiro Matsumoto, Seiji Sakai*

Properties of nanotubes

- 2P-11 Chirality dependence of exciton diffusion in air-suspended single-walled carbon nanotubes 102
★ * *A. Ishii, A. Yokoyama, M. Yoshida, T. Shimada, Y. K. Kato*
- 2P-12 Electric Double Layer Transistors using Thick Films in Single Chiral States of (6,5) and (11,10) 103
Single-Wall Carbon Nanotubes
* *Hikaru Kudo, Masatoshi Kawai, Tomoyuki Hunabasama, Yuki Nobusa, Taishi Takenobu, Kazuhiro Yanagi*
- 2P-13 Existence of two distinct equilibrium states in the exchange reaction of sodium cholate and oligo 104
DNA on single-walled carbon nanotubes
★ * *Yuichi Kato, Yasuro Niidome, Naotoshi Nakashima*
- 2P-14 Control of UV Optical Absorption of Single-Wall Carbon Nanotubes Using Electro-chemical 105
Doping Techniques
* *Toru Igarashi, Kai Hasegawa, Tomoyuki Funabasama, Shimpei Ono, Kazuhiro Yanagi*

March 12th, Tue.

2P-15	Thermodynamics for the exchange reaction of sodium cholate and double-stranded DNA on single-walled carbon nanotubes	106
☆	* Akiko Tsuzuki, Ayaka Inoue, Yuichi Kato, Yasuro Niidome, Naotoshi Nakashima	
2P-16	Improvement of CNT Properties through a Post Synthetic Treatment	107
	* Naoyuki Matsumoto, Azusa Oshima, Motoo Yumura, Don Futaba, Kenji Hata	
2P-17	Tensile strength of individual multi-walled carbon nanotube constituting MWCNT fiber	108
☆	* Hideaki Suzuki, Yoshinori Sato, Go Yamamoto, Kenichi Motomiya, Toshiyuki Hashida, Kazuyuki Tohji	
Applications of nanotubes		
2P-18	Bending Properties of Single-Walled Carbon Nanotube Film Transistors	109
	* Hiroki Hamahata, Yuki Nobusa, Yohei Yomogida, Kazuhiro Yanagi, Yoshihiro Iwasa, Taishi Takenobu	
2P-19	High-performance, flexible carbon nanotube transparent conductive films of double layered structure	110
☆	* Norihiro Fukaya, Yusuke Kataoka, Dong Young Kim, Shigeru Kishimoto, Takashi Mizutani, Suguru Noda, Yutaka Ohno	
2P-20	Evaluation of the contact resistivity at CNT/SiC interface using conductive AFM	111
	* Megumi Shibuya, Masafumi Inaba, Kazuyoshi Oohara, Takumi Ochiai, Yoshiho Masuda, Atsushi Hiraiwa, Michiko Kusunoki, Hiroshi Kawarada	
2P-21	High-mobility carbon nanotube thin-film transistors fabricated on transparent plastic film by flexographic printing technique	112
☆	* Kentaro Higuchi, Yuta Nakajima, Takuya Tomura, Masafumi Takesue, Shigeru Kishimoto, Takashi Mizutani, Katsuhiko Hata, Yutaka Ohno	
2P-22	Effect of gas atmosphere on the photovoltaic characteristics of semiconducting single-walled carbon nanotubes/Si heterojunction photovoltaic cells	113
	* Mao Shoji, Atsushi Nakano, Hironori Ogata	
Formation and purification of nanotubes		
2P-23	Effect of oxidized Al support property for millimeter-scale SWCNT growth	114
	* Kei Hasegawa, Suguru Noda	
2P-24	CNT Synthesis by Laser Ablation Method Using Carbon and Nickel Double Target	115
	* Koji Ishii, Nobuyuki Iwata, Hiroshi Yamamoto, Hirofumi Yajima	
2P-25	Solubilization of single-walled carbon nanotubes using a flavin derivative in organic solvents	116
☆	* Yuichi Kato, Yasuro Niidome, Naotoshi Nakashima	
2P-26	SWNT growth from Pt catalysts on Al ₂ O _x buffer layer by Alcohol Gas Source Method in High Vacuum	117
	* Naoya Fukuoka, Hiroki Kondo, Yuya Sawaki, Ranajit Ghosh, Shigeya Naritsuka, Takahiro Maruyama	
2P-27	Low temperature growth of dense carbon nanotube arrays on conductive underlayers	118
☆	* Nuri Na, Yeong-Gi So, Yuichi Ikuhara, Suguru Noda	
2P-28	Selective Removal of Metallic Single-Walled Carbon Nanotubes Utilizing Thermal Lithography of Molecular Glass Thin Films	119
	* Keigo Otsuka, Taiki Inoue, Daisuke Hasegawa, Shohei Chiashi, Shigeo Maruyama	
2P-29	Effects of discharge current direction and magnetic field for the production of single-walled carbon nanotubes in the arc discharge method	120
	* Mohammad Jellur Rahman, Tetsu Mieno	

March 12th, Tue.

- 2P-30 Chirality separation of metallic single-wall carbon nanotubes by gel column chromatography 121
* Takeshi Tanaka, Yasuko Urabe, Hiromichi Kataura

Endohedral nanotubes

- 2P-31 Encapsulation of superconductive metal carbide in the inner space of carbon nanotubes 122
by template method
* Keita Kobayashi, Takeshi Saito, Masaharu Kiyomiya, Hidehiro Yasuda
- 2P-32 Energetics and Electronic Structures of C₆₀ Rolled in the Shortest Zigzag Carbon Nanotubes 123
☆ * Shota Kigure, Susumu Okada

Graphene synthesis

- 2P-33 Effect of inert gas on the growth of epitaxial graphene on Si-terminated SiC (0001) 124
* Akkawat Ruammitree, Hitoshi Nakahara, Yahachi Saito
- 2P-34 Structural characterization of graphene edges using dark-field TEM 125
☆ * Miho Fujihara, Yasumitsu Miyata, Ryo Kitaura, Eriko Maeda, Hisanori Shinohara
- 2P-35 Synthesis of Nitrogen-doped Carbon Materials Controlled Nitrogen Bonding Configuration 126
* Satoshi Yasuda, Li Yu, Kei Murakoshi
- 2P-36 Preparation of High-Density Graphene Nanoribbons by Anisotropic Catalyst Cutting 127
☆ * Yasumichi Kayo, Pablo Solís-Fernández, Kazuma Yoshida, Masaharu Tsuji, Hiroki Ago

Applications of graphene

- 2P-37 Transparent graphitic tiles synthesized from carbon nanowalls by shock compression 128
* Kazutaka Nakamura, Toshiyuki Atou, Keisuke Niwase, Kazutaka Nakamura, Masaru Tachibana
- 2P-38 Water-Soluble Graphene through Polyglycerol Grafting 129
☆ * Toku Yasuda, Li Zhao, Gang Liu, Shuji Aonuma, Takahide Kimura, Naoki Komatsu
- 2P-39 Relationship between morphology, electric properties and field emission characteristics 130
of carbon nanosheets films by microwave plasma-enhanced chemical vapor deposition
* Shohei Hayase, Zhipeng Wang, Hironori Ogata

Properties of graphene

- 2P-40 Characterization of Electrical Properties for Graphene Film Deposited by Microwave Plasma CVD 131
* Yuki Okigawa, Kazuo Tsugawa, Takatoshi Yamada, Masatou Ishihara, Masataka Hasegawa
- 2P-41 Host-guest Interactions between Nanographene and Gas molecules 132
* Junichi Takashiro, Kazuyuki Takai, Manabu Kiguchi, Toshiaki Enoki, Takeo Yamada,
Kenji Hata, Takafumi Ishii, Takashi Kyotani
- 2P-42 Linear Dispersion Bands on Partially H-Terminated (111) Surface of Diamond Structure 133
☆ * Junki Sone, Susumu Okada
- 2P-43 Influence of mechanical deformation on thermal properties of graphene 134
* Takashi Funatani, Takahiro Yamamoto, Matsuto Ogawa, Satofumi Souma
- 2P-44 First-principles study of edge-modified armchair graphene nanoribbons 135
* Hideyuki Jippo, Mari Ohfuchi

Other topics

- 2P-45 Enhancement of photo-induced current in the complex of iron oxide nanotubes and fullerenols 136
Yuki Shiraki, * Yuki Mishina, Shunji Bandow
- 2P-46 Development of Multi-stage Ion Trap Mobility System 137
* Toshiki Sugai

March 12th, Tue.

>>>>>>> Coffee Break (17:00–17:15) <<<<<<<<<

General Lecture (17:15–18:15)

Graphene synthesis ▪ Properties of graphene

2–8	Oxygen Adsorption Effect on Graphene–Metal Contact Characteristics <i>* Yoshiaki Sato, Kazuyuki Takai, Toshiaki Enoki</i>	28
2–9	Atomic structure determination of the graphene/sapphire interface by normal incident X-ray standing wave spectroscopy <i>* Shiro Entani, Pavel Sorokin, Pavel Avramov, Manabu Ohtomo, Yoshihiro Matsumoto, Liubov Antipina, Ayumi Narita, Norie Hirao, Iwao Shimoyama, Tetsuhiro Sekiguchi, Hiroshi Naramoto, Yuji Baba, Seiji Sakai</i>	29
2–10	Integration of high performance graphene nanoribbon field effect transistors <i>* Toshiaki Kato, Rikizo Hatakeyama, Toshiro Kaneko</i>	30
2–11	Transport Property of CVD Graphene across Domain Boundary <i>* Yui Ogawa, Kenji Kawahara, Masahiro Miyashita, Masaharu Tsuji, Katsuyoshi Komatsu, Kazahito Tsukagoshi, Hiroki Ago</i>	31

March 13th, Wed.

Special Lecture: 25min (Presentation) + 5min (Discussion)

General Lecture: 10min (Presentation) + 5min (Discussion)

Poster Preview: 1min (Presentation)

Special Lecture (9:00–9:30)

- 3S-7 Novel Functional Carbon-Nanotube Transistors 7
Taishi Takenobu

General Lecture (9:30–10:30)

Properties of nanotubes ▪ Applications of nanotubes

- 3-1 Fabrication of CMOS inverters using semiconducting SWCNTs encapsulating n- and p-type dopant molecules 32
** Yasuhiro Ito, Shunjiro Fujii, Maki Shimizu, Takeshi Tanaka, Hiromichi Kataura*
- 3-2 Micro-Honeycomb Network Structure of Single-Walled Carbon Nanotube Film for Solar Cells 33
** Kehang Cui, Takaaki Chiba, Hidenori Kinoshita, Pei Zhao, Theerapol Thurakitserree, Taiki Inoue, Erik Einarsson, Shohei Chiashi, Shigeo Maruyama*
- 3-3 Application of Vertically Aligned CNTs for Electrodes of PEMFC 34
** Shigeaki Murata, Masahiro Imanishi, Shigeki Hasegawa, Ryoichi Namba*
- 3-4 Electromigration suppression in copper by carbon nanotubes : A mechanistic insight 35
** Chandramouli Subramaniam, Takeo Yamada, Don N. Futaba, Kenji Hata, Motoo Yumura*

>>>>>>> **Coffee Break (10:30–10:45)** <<<<<<<<<

General Lecture (10:45–12:00)

Properties of nanotubes

- 3-5 First-Principles Simulation on Thermoelectric Power of SWNT Buckypapers 36
** Teppei Kato, Shinji Usui, Takahiro Yamamoto*
- 3-6 Influence of Carbon nano-inclusion dimensionality in the thermal conductivity enhancement of aqueous and non-aqueous fluids 37
** Sivasankaran Harish, Kei Ishikawa, Erik Einarsson, Shohei Chiashi, Junichiro Shiomi, Shigeo Maruyama*
- 3-7 First Principles-Based Estimate of the Critical SWCNT Length for Raman D and G Band Intensity Inversion 38
** Yoshifumi Nishimura, Henryk Witek, Stephan Irle*
- 3-8 Exciton effects on coherent phonon spectroscopy of carbon nanotubes 39
** Ahmad Nugraha, Eddwi Hasdeo, Riichiro Saito*
- 3-9 High-temperature in-situ TEM Observation of Zipper-like Wall-to-Wall Coalescence of Double-Wall Carbon Nanotubes 40
** Sihan Zhao, Ryo Kitaura, Yasumitsu Miyata, Hisanori Shinohara*

>>>>>>> **Lunch Time (12:00–13:15)** <<<<<<<<<

Special Lecture (13:15–13:45)

- 3S-8 Ballistic transport in graphene/h-BN 8
** Tomoki Machida, Satoru Masubuchi, Masahiro Onuki, Sei Morikawa, Kazuyuki Iguchi, Takehiro Yamaguchi, Miho Arai, Kenji Watanabe, Takashi Taniguchi*

March 13th, Wed.

Poster Preview (13:45–14:30)

Poster Session (14:30–16:00) (☆) Candidates for the Young Scientist Poster Award

Chemistry of fullerenes

- 3P-1 Thermal Reactions of C₆₀ with Siliranes: Formation of Carbosilylated Fullerenes 138
* *Ryosuke Iida, Kentaro Takagi, Masahiro Kako, Tadashi Hasegawa, Yutaka Maeda, Michio Yamada, Takeshi Akasaka*
- 3P-2 Construction of an Opening on Fullerene C₇₀ and Encapsulation of a Water Molecule 139
☆ * *Rui Zhang, Michihisa Murata, Yasujiro Murata*
- 3P-3 Thermal [2+2] cycloaddition of C₆₀ with aryl dienamines 140
* *Naohiko Ikuma, Hiroyuki Yamamoto, Tsubasa Mikie, Ken Kokubo, Takumi Oshima*

Applications of fullerenes

- 3P-4 Transport Characteristics of C₆₀ Photo-Polymers Fabricated by Focused Optical Vortex Irradiation 141
* *Naoto Toriumi, Tatsuya Doi, Daiki Momiyama, Wataru Akiyama, Katsuhiko Miyamoto, Takashige Omatsu, Jonathan Bird, Yuichi Ochiai, Nobuyuki Aoki*
- 3P-5 Fabrication of bulk-heterojunction organic solar cells using PCBM and mixed donors of P3HT and phenylene–thiophene oligomer 142
* *Shunjiro Fujii, Zongfan Duan, Takanori Okukawa, Yuichiro Yanagi, Akira Yoshida, Takeshi Tanaka, Yasuhiro Nishioka, Hiromichi Kataura*

Endohedral metallofullerenes

- 3P-6 Reaction of Trimetallic Nitride Template-Endohedral Metallofullerenes(TNT-EMFs) with Aziridine 143
☆ * *Masato Kimura, Chihiro Ueda, Michio Yamada, Yutaka Maeda, Tadashi Hasegawa, Takeshi Akasaka*
- 3P-7 Extraction of unstable di-metallofullerenes using a mixed solvent of triethylamine and acetone 144
* *Aimi Togashi, Takeshi Kodama, Wataru Fujita, Koichi Kikuchi, Yohji Achiba*

Fullerenes

- 3P-8 Spin Configurations of Three Radicals on Fullerenes 145
* *Susumu Okada, Takahiro Yamamoto*
- 3P-9 Magnetic Properties of Deca-Methyl Fullerenes 146
☆ * *Haruna Nitta, Susumu Okada*
- 3P-10 Synthesis of non-IPR fullerenes from C₆₀ in liquid phase by irradiation of intense femtosecond laser pulses 147
* *Takeshi Kodama, Tatsuya Fujino, Haruo Shiromaru, Yohji Achiba*

Environmental/Safety characterization of nanomaterials

- 3P-11 Interaction of carbon nanotubes with homopolypeptides 148
* *Atsushi Hirano, Tomoshi Kameda, Takeshi Tanaka, Hiromichi Kataura*

Properties of nanotubes

- 3P-12 Molecular recognition of external grooves on bundled surfaces of single-walled carbon nanotubes 149
☆ * *JongTae Yoo, Tsuyohiko Fujigaya, Naotoshi Nakashima*
- 3P-13 Enhancement of photoluminescence from single-walled carbon nanotubes by photonic crystal nanocavities 150
*Ryosuke Watahiki, * Takashi Shimada, Pei Zhao, Shohei Chiashi, Satoshi Iwamoto, Yasuhiko Arakawa, Shigeo Maruyama, Yuichiro K. Kato*
- 3P-14 Effect of Solvents on Electrochemical Band Gaps of Single-Walled Carbon Nanotubes 151
☆ * *Daigo Miyazaki, Yasuhiko Hirana, Yasuro Niidome, Naotoshi Nakashima*

March 13th, Wed.

3P-15	Effects of OPO Laser Irradiation on the Structural Characteristics of Single- and Double-Walled Carbon Nanotubes <i>* Tetsuya Oto, Akira Kumazawa, Yuka Nagaya, Koji Tsuchiya, Tadahiro Ishii, Hirofumi Yajima</i>	152
3P-16	Vernier spectrum in finite-length armchair carbon nanotubes ☆ <i>* Yuki Tatsumi, Wataru Izumida, Riichiro Saito</i>	153
3P-17	First-principles study of radial breathing modes in small-diameter carbon nanotubes <i>* Takashi Koretsune, Susumu Saito</i>	154
3P-18	Electronic Properties of Capped Carbon Nanotubes with Accumulated Electrons by a Parallel Electric Field ☆ <i>* Ayaka Yamanaka, Susumu Okada</i>	155
3P-19	Electronic Raman scattering and origin of the Fano resonance in metallic carbon nanotubes <i>* Eddwi Hasdeo, Ahmad Nugraha, Kentaro Sato, Riichiro Saito</i>	156
Applications of nanotubes		
3P-20	Selective Dispersion of Single-Walled Carbon Nanotubes into Nano-Cage of Helical Conformation of Poly(m-phenylene-ethynylene) Derivatives <i>Fumito Kobayashi, Yuki Moriyama, * Masahiro Takahashi, Masayoshi Tange, Toshiya Okazaki, Keiki Kishikawa, Shigeo Kohmoto</i>	157
3P-21	Chromatographic Separation of Highly Soluble SWNTs Prepared by Polyglycerol Grafting ☆ <i>* Keisuke Nakamura, Li Zhao, Shuji Aonuma, Takahide Kimura, Naoki Komatsu</i>	158
3P-22	Electric double layer transistors of aligned carbon nanotube thin film <i>* Yoshifumi Wada, Jiang Pu, Yuki Takagi, Kazuhiro Yanagi, Taishi Takenobu</i>	159
3P-23	Photo-thermoelectric power of single-walled carbon nanotube films ☆ <i>* Hajime Sakakibara, Yoshinori Sato, Kosuke Ino, Akihiko Ito, Tomokazu Matsue, Takashi Goto, Kenichi Motomiya, Kazuyuki Tohji</i>	160
3P-24	Specific biosensor based on biotin-labeled double-walled carbon nanotube FET <i>* Akihiro Kuno, Yuka Nagaya, Koji Tsuchiya, Akira Hida, Koji Ishibashi, Hirofumi Yajima</i>	161
Formation and purification of nanotubes		
3P-25	Selective Solubilization of Semiconducting-Carbon Nanotubes by Using Weak-Bond Connecting Fluorene-Based Polymers <i>* Toshimitsu Fumiyuki, Tsuyohiko Fujigaya, Naotoshi Nakashima</i>	162
3P-26	Chirality Analysis of Single-walled Carbon Nanotubes Growth in Molecular Dynamics Simulation <i>* Tomoya Kawasuzuki, Kaoru Hisama, Yuki Takaki, Shohei Chiashi, Shigeo Maruyama</i>	163
3P-27	Methane-assisted CVD yielding millimeter-tall single-wall carbon nanotubes of smaller diameters ☆ <i>* Zhongming Chen, Dong Young Kim, Kei Hasegawa, Suguru Noda</i>	164
3P-28	Pyrene-based nanocalipers for selective extraction of metallic SWNTs <i>Gang Liu, * Naoki Komatsu, Takahide Kimura</i>	165
3P-29	In situ Raman monitoring formation of SWNTs: process optimization and low temperature synthesis <i>* Ming Liu, Yuquan Su, Rong Xiang, Zikang Tang</i>	166
3P-30	One-Step Catalyst-Free Mist Flow CVD Growth of Single-Wall Carbon Nanotubes using C ₆₀ Fullerenes ☆ <i>* Yun Sun, Ryo Kitaura, Jinying Zhang, Yasumitsu Miyata, Hisanori Shinohara</i>	167
3P-31	Modeling the catalyst formation process to achieve diameter and density control of single-wall carbon nanotube forests <i>* Shunsuke Sakurai, Don Futaba, Motoo Yumura, Kenji Hata</i>	168

March 13th, Wed.

- 3P-32 Simultaneous Growth Control of Position, Chirality, and in-plane Orientation of Single-Walled Carbon Nanotubes by Cold-Wall Chemical Vapor Deposition Method 169
** Takumi Sagara, Satoshi Doi, Koji Ishii, Nobuyuki Iwata, Hirofumi Yajima, Hiroshi Yamamoto*

Endohedral nanotubes

- 3P-33 Diameter Dependent Interaction between Single-Walled Carbon Nanotubes and Encapsulated Ferrocenes 170
** Hironori Suzuki, Yoko Iizumi, Toshiya Okazaki*
- 3P-34 Spectroscopic studies of single-wall boron nitride nanotubes synthesized in single-wall carbon nanotubes 171
☆ ** Ryo Nakanishi, Ryo Kitaura, Yuta Yamamoto, Shigeo Arai, Jamie Warner, Yasumitsu Miyata, Hisanori Shinohara*

Graphene synthesis

- 3P-35 Molecular Dynamics Simulation of Multi-layer Graphene Growth by Catalytic CVD Method 172
** Yuki Takaki, Kaoru Hisama, Tomoya Kawasuzuki, Shohei Chiashi, Shigeo Maruyama*
- 3P-36 Synthesis and characterization of large sized-grain, single-layer BN-doped graphene 173
☆ ** Yu Kobayashi, Yasumitsu Miyata, Eriko Maeda, Ryo Kitaura, Hisanori Shinohara*
- 3P-37 Synthesis and Characterization of Intercalated Graphite and Graphene for Room Temperature Superconductivity 174
** Shogo Sato, Hiroaki Ichikawa, Nobuyuki Iwata, Hiroshi Yamamoto*
- 3P-38 Directional growth of graphene over Cu catalyst by face-to-face configuration CVD 175
☆ ** Tatsuya Masuda, Kenji Kawahara, Hiroki Ago, Noda Suguru*

Applications of graphene

- 3P-39 Monte Carlo Particle Simulations of Local Heating Properties in Graphene-channel nano-FETs 176
** Shusuke Oki, Taichi Misawa, Yuji Awano*
- 3P-40 Electrically driven ultra-high-speed black body emitters based on graphene 177
☆ ** Tomoya Yokoi, Yusuke Takayama, Tatsuya Mori, Daiju Tsuya, Hideyuki Maki*
- 3P-41 Few-layer Graphene/silicon Heterojunction Photovoltaic Cells by Microwave Plasma-Enhanced Chemical Vapor Deposition 178
** Z. Wang, S. Hayase, M Shoji, H Ogata*

Properties of graphene

- 3P-42 Degree of oxidation of centrifuged graphene oxide 179
** Hiroyuki Yokoi, Michio Koinuma, Kazuto Hatakeyama, Takaaki Taniguchi, Yasumichi Matsumoto*
- 3P-43 Spin polarization of hexagonal boron nitride/Ni(111) interface studied by spin-polarized metastable de-excitation spectroscopy 180
** Manabu Ohtomo, Yasushi Yamauchi, Pavel Avramov, Shiro Entani, Yoshihiro Matsumoto, Hiroshi Naramoto, Seiji Sakai*
- 3P-44 Tetragonal C₄ Polymer: A Two-dimensional Metallic sp² Carbon Allotrope 181
☆ ** Mina Maruyama, Susumu Okada*
- 3P-45 Graphene-based nanomaterials prepared by laser ablation of graphite 182
** Maki Nakamura, Takazumi Kawai, Michiko Irie, Ryota Yuge, Sumio Iijima, Shunji Bandow, Masako Yudasaka*
- 3P-46 Effects of etchant and synthesis temperature on the sheet-resistivity of nitrogen doped graphene film 183
*Takahiro Mizuno, * Shunji Bandow*

March 13th, Wed.

>>>>>>> Coffee Break (16:00–16:15) <<<<<<<<<

Special Lecture (16:15–16:45)

- 3S-9 Design, Synthesis, and Properties of Fullerene Derivatives for Organic Thin Film Solar Cells 9
Yutaka Matsuo

General Lecture (16:45–17:45)

Endohedral metallofullerenes

- 3-10 A hypothetical intermediate structure in growth of metallofullerenes 41
* *Yohji Achiba, Takeshi Kodama, Kenro Hashimoto, Haruo Shiromaru*
- 3-11 Structure of Thulium and Carbon Cluster Encapsulated in Low-Symmetry C₈₂(C_s(6)) Fullerene Cage by Single Crystal X-ray Diffraction 42
* *Yuki Sado, Shinobu Aoyagi, Noriko Izumi, Ryo Kitaura, Tim Kowalczyk, Jian Wang, Stephan Irle, Eiji Nishibori, Kunihisa Sugimoto, Hisanori Shinohara*
- 3-12 Photoinduced electron transfer in supramolecules between Li⁺@C₆₀ and chlorin derivatives 43
* *Kei Ohkubo, Yuki Kawashima, Kentaro Mase, Shunichi Fukuzumi*
- 3-13 Ultraviolet Photoelectron Spectra of Gd₃N@C₈₀ and Er₃N@C₈₀ 44
* *Takafumi Miyazaki, Yusuke Nakanishi, Yuki Sasaki, Hiroyuki Niwa, Shoko Noda, Tatsuhiko Nishi, Tomona Ohta, Hisanori Shinohara, Shojun Hino*

基調講演
Plenary Lecture

特別講演
Special Lecture

1S – 1 ~ 1S – 3

2S – 4 ~ 2S – 6

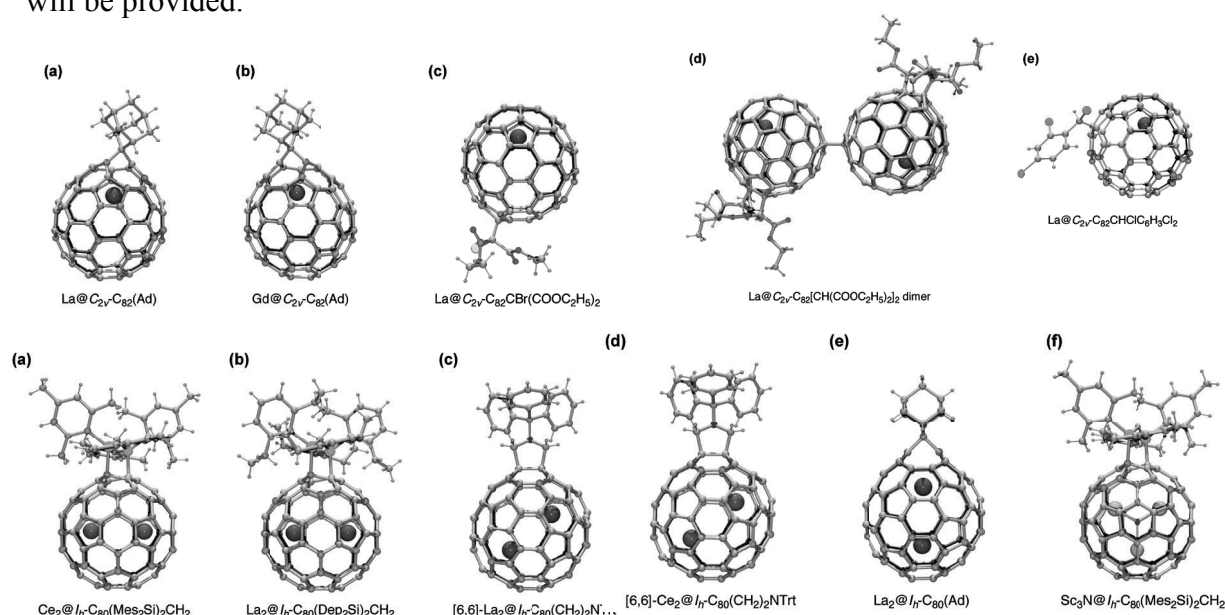
3S – 7 ~ 3S – 9

New Vistas in Chemistry of Endohedral Metallofullerenes

Takeshi Akasaka

*Life Science Center of Tsukuba Advanced Research Alliance, University of Tsukuba,
Tsukuba 305-8577, Japan*

The paper will present a description of recent advances in fundamental aspects of the chemistry of endohedral metallofullerenes for future applications as organic carbon nanomaterials.¹⁻³ Synthesis and characterization of endohedral metallofullerenes and their derivatives are particularly addressed. Throughout this presentation, guidelines for understanding structural, electronic and chemical properties of endohedral metallofullerenes will be provided.



[1] *Chemistry of Nanocarbons*; T. Akasaka, F. Wudl, S. Nagase, Eds.; Wiley-Blackwell: London, 2010; *Endofullerenes: A New Family of Carbon Cluster*; T. Akasaka, S. Nagase, Eds.; Kluwer Academic Publisher: Dordrecht, 2002.

[2] See recent book chapters: *"Handbook of Carbon Nano Materials"* F. D'Souza and K. M. Kadish, Eds.; World Scientific, 2011; Vol. 1, pp. 145-184; *"Chemistry of Nanocarbons"*, T. Akasaka, F. Wudl, and S. Nagase Eds.; John Wiley & Sons, Chichester, 2010; pp 261-286; *"Carbon Nanotubes and Related Structures"*, D. Guldi and N. Martin Eds.; Wiley-VCH, Verlag GmbH & Co. KGaA, Weinheim, 2010; pp 455-490; *"Rare Earth Coordination Chemistry - Fundamentals and Applications"*, C. H. Huang Ed.; John Wiley & Sons, Singapore, 2010; pp 269-304.

[3] See recent reviews: *Chem. Soc. Rev.* **41**, 7723-7760 (2012) (Critical Review); *Chem. Rec.* **12**, 256-259 (2012); *Polyhedron*, in press. [DOI: 10.1016/j.poly.2012.06.072]; *Chem. Eur. J. (Concept article)* **18**, 5136-5148 (2012); *Chem. Commun.* **47**, 5942-5957 (2011) (Feature Article); *Nanoscale*, **3**, 2421 (2011); *Acc. Chem. Res.*, **43**, 92-102 (2010).

Corresponding Author: T. Akasaka

Tel: +81-29-853-6409, Fax: +81-29-853-6409,

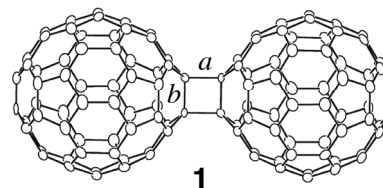
E-mail: akasaka@tara.tsukuba.ac.jp, takasaka04@yahoo.co.jp

Solid-State Chemistry of Fullerenes
— Learning the New, through Visiting the Old —

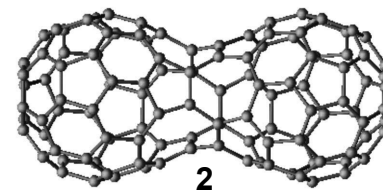
Koichi Komatsu

Professor Emeritus, Kyoto University, Uji 611-0011, Kyoto, Japan

It is now well recognized that fullerene C_{60} undergoes various types of liquid-phase reactions, affording a whole variety of its derivatives. Yet, there are still some reactions, which can take place only under the solid-state reaction conditions. The typical example is [2+2] dimerization, giving dumbbell-shaped C_{120} (**1**). [1]



The X-ray crystallography on **1** indicates that the two kinds of single bonds *a* and *b* in the central four-membered ring are of comparable length suggesting that the energies for bond cleavage of *a* and *b* are nearly the same. Here, if the intra-cage bond *b* could be selectively cleaved, the shape of C_{120} would be transformed into a peanuts-type such as **2** after rearrangements. However, simply upon heating, dumbbell-shaped C_{120} **1** only dissociates into the starting C_{60} quantitatively. [1]



Then, is the formation of peanuts type dimer **2** impossible? Previously, Onoe and coworkers inferred the formation of such a dimer by irradiation of electron beam on a thin layer of C_{60} , based on IR studies.[2] The clearer evidence of the formation of peanuts-shaped C_{120} is the direct TEM-observation of coalescence of two molecules of C_{60} inside of a single-walled carbon nanotube (SWNT) upon the electron-beam irradiation.[3] This clearly indicates that the inside of the SWNT provides a highly activated space for reactions to afford molecules of novel structures.

[1] G-W. Wang, K. Komatsu, Y. Murata, M. Shiro, *Nature* **387**, 583 (1997).

[2] A. Takashima, J. Onoe, T. Nishii, *J. Appl. Phys.* **108**, 033514 (2010).

[3] M. Koshino, Y. Niimi, E. Nakamura, H. Kataura, T. Okazaki, K. Suenaga, S. Iijima, *Nature Chemistry* **2**, 117 (2010).

Corresponding Author: K. Komatsu

Tel: +81-75-761-8039, Fax: +81-75-761-8089

E-mail: komatsu@scl.kyoto-u.ac.jp

Photoluminescence properties of some graphene-based and inorganic two-dimensional materials

○Goki Eda^{1,2,3}

¹ Department of Physics, National University of Singapore, Singapore 117542

² Department of Chemistry, National University of Singapore, Singapore 117543

³ Graphene Research Centre, National University of Singapore, Singapore 117546

Two-dimensional (2D) crystals derived from layered structures exhibit a unique set of properties as strikingly demonstrated for graphene. Semiconducting 2D structures are attractive building blocks for novel electronic and optoelectronic devices. In this talk, we will report photoluminescence properties of two distinct classes of 2D semiconductors, graphene oxide and transition metal dichalcogenides, and discuss how their spectral features provide insight into the evolution of chemical, structural, and electronic properties of these materials.

Graphene oxide (GO) is a localized insulator consisting of sp^2 carbon clusters embedded inside a sp^3 carbon matrix. Due to chemical inhomogeneity and spatial confinement of π electrons, GO exhibits heterogeneous electronic structure with locally varying energy gaps. We demonstrate that GO exhibits tunable photoluminescence over the visible spectrum during controlled reduction [1,2]. We show that blue photoluminescence can be attributed to electron-hole recombination within small sp^2 clusters.

A single layer molybdenum disulfide (MoS_2) is a direct gap semiconductor in striking contrast to its indirect gap bulk counterpart [3]. We report differential reflectance and photoluminescence spectra of mono- to few-layer WS_2 and WSe_2 that indicate that the band structure of these materials undergoes similar indirect-to-direct gap transition when thinned to a single monolayer (Fig. 1) [4]. The transition is evidenced by distinctly enhanced PL peak centered at 630 and 750 nm in monolayer WS_2 and WSe_2 , respectively. We demonstrate that indirect gap emission and direct gap hot electron emission is pronounced in few-layer WSe_2 due to small energy difference between the two transitions. Temperature dependence of their photoluminescence spectra indicate crossover of these band edges similar to the case of $MoSe_2$ [5].

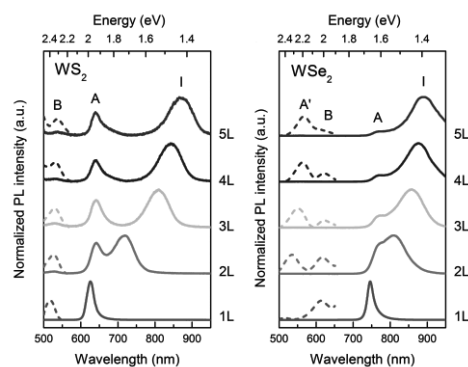


Fig.1 Photoluminescence spectra of 1 to 5 layer WS_2 and WSe_2 .

[1] Eda et al. Adv. Mater. 22, 505 (2010) .

[2] Chien et al. Angew Chem. Int. Ed. 51, 6662 (2012).

[3] K. F. Mak et al. Phys. Rev. Lett. 105, 136805 (2010).

[4] Zhao et al. ACS nano. DOI: 10.1021/nm305275h

[5] Tongay et al. Nano Lett. 12, 5576 (2012).

Corresponding Author: G. Eda

Tel: +65- 6516-2970, Fax: +65- 6777 - 6126,

E-mail: g.eda@nus.edu.sg

**Combining separation and synthesis to achieve structure control
of carbon nanotubes**

○Ming Zheng

*Materials Science and Engineering Division, National Institute of Standards and Technology
Gaithersburg, Maryland 20899, United States*

Carbon nanotubes (CNTs) possess a unique set of physical properties that may enable many technologies ranging from ultrahigh capacity, ultralow dissipation power transmission lines to CNT-based digital electronics as the replacement of the current CMOS technology. Making CNTs of defined structure has been a fundamental challenge hampering the science and technology of CNTs for many years. Recent works coming from my lab and that of our collaborators are aimed at providing a route to solve the CNT structure control problem:

1. We have developed [1] a DNA-based method to purify single-chirality CNTs from synthetic mixtures.
2. Using DNA-purified single-chirality CNTs as seeds, we have shown [2] that new CNTs of identical chirality can be grown without the aid of metal catalyst.

In this presentation, I will discuss these results and report our latest findings in achieving chirality control via combined separation and synthesis approach.

[1] Tu *et al.*, *Nature* 460, 250(2009)

[2] Liu *et al.*, *Nature Communications* 3, 1199 (2012)

Corresponding Author: Ming Zheng

Tel: 301-975-8995, Fax: 301-975-4924

E-mail: ming.zheng@nist.gov

Fundamental and Advanced Materials Design of Soluble Carbon Nanotubes

○Naotoshi Nakashima^{1,2,3}

¹*Department of Applied Chemistry, Kyushu University, Fukuoka 819-0395, Japan*

²*WPI-I2CNER, Kyushu University, Fukuoka 819-0395, Japan*

³*JST-CREST*

One of the key issues in the utilization of carbon nanotubes (CNTs) for basic researches together with their potential applications in many areas is to develop a methodology to solubilize/disperse them in solvents.[1]

After brief introduction about the strategy to solubilize CNTs in solution, we report our recent study on the following five topics.

- i) Determination of precise electronic states of individually dissolved (n,m)single-walled carbon nanotubes (SWNTs), and SWNT trions [2-5]
- ii) SWNT chirality recognition/extraction by polymers and its application[6-10]
- iii) High conductive transparent SWNT ultrathin films[11]
- iv) CNTs/polymer gel-near IR responsive materials [12-14]
- v) Electrocatalyst for fuel cell using soluble CNTs[15-19]

Topic (i): Electronic structures of SWNTs, one of the fundamental features of nanotubes, strongly depend on the chirality of the nanotubes. We have discovered that we can determine the precise electronic states of isolated SWNTs having their own chirality indices by *in situ* near-IR photoluminescence spectroelectrochemistry at the fabricated modified ITO electrode.

Topic (ii): The facile separation of a mixture of SWNTs into specific chirality components has recently attracted great attention. We report that certain chiral polyfluorene copolymers can well recognize SWNTs with certain chirality preferentially, leading to solubilization of specific chiral SWNTs. This is the first example showing the rational design and synthesis of novel fluorene-based copolymers toward the recognition/extraction of targeted (n,m)-chirality of the SWNTs.

Topic (v): We report new electrocatalysts composed of CNTs, polybenzimidazole (PBI) and platinum nanoparticles that act as in which CNTs are efficient catalysts for fuel cells. The design and synthesis of a nitrogen-containing calcined PBI/CNT hybrid that acts as an oxygen reduction catalyst will be also reported.

References (authors: N. Nakashima et al.)

- [1](Review) *J. Nanoscience Nanotechnol.*, **2012**, *12*, 1739-1747. [2] *Angew. Chem. Int. Ed.* **2009**, *48*, 7655-7659. [3] *J. Am. Chem. Soc.* **2010**, *132*, 13072–13077. [4] *Bull. Chem. Soc. Jpn.*, **2012**, *85*, 1262-1267. [5] *J. Am. Chem. Soc.* **2012**, *134*, 14461-14466. [6] *Angew. Chem. Int. Ed.*, **2009**, *48*, 5435-5438. [7] *J. Am. Chem. Soc.* **2011**, *133*, 2651–2657. [8] *Chem. Eur. J.* **2011**, *17*, 13438-13444. [9] *J. Am. Chem. Soc.* **2011**, *133*, 14771–14777. [10] *J. Am. Chem. Soc.* **2012**, *134*, 12700-12707. [11] *Scientific Reports*, **2012**, *2*, doi:10.1038/srep00733. [12] *J. Am. Chem. Soc.*, **2010**, *132*, 16581–16586. [13] *Soft Matter*, **2011**, *7*, 2647-2652. [14] *ACS Nano*, **2011**, *5*, 4414-4421. [15] *Small*, **2009**, *5*, 735-740. [16] *Adv. Functional Mater.*, **2011**, *21*, 1089–1094. [17] *J. Mater. Chem.*, **2011**, *21*, 1187-1190. [18] *Chem. Commun.* **2011**, *47*, 6843-6845. [19] *Adv. Mater.*, in press.

Corresponding Author: N. Nakashima; Tel/FAX: +81-92-802-2840

E-mail: e-mail: nakashima-tcm@mail.cstm.kyushu-u.ac.jp

Band engineering in bilayer graphene for future electron-devices

○K.Tsukagoshi¹, H.Miyazaki¹, S.-L.Li¹, A.A.Ferreira¹, M.Y.Chan¹, K. Komatsu¹,
S.Nakaharai²,

¹WPI-MANA, NIMS, Tsukuba, 305-0047, Japan

²GNC, AIST, Tsukuba, 305-8569, Japan

We present a review of our experiments on graphene transistors in its potential use as atomic film switching devices.

We found that large transport energy gaps (>100 meV) can be fulfilled in dualgated bilayer graphene underneath a simple alumina passivation top gate stack, which directly contacts the graphene channels without an inserted buffer layer. With the presence of energy gaps, the electrical properties of the graphene transistors are significantly enhanced, as manifested by enhanced on/off current ratio, subthreshold slope, and current saturation. For the first time, complementary-like semiconducting logic graphene inverters are demonstrated that show a large improvement over their metallic counterparts.

We also demonstrated a tunneling (Fig.1) and rectification behavior in bilayer graphene with bandgap. A stepped dielectric top gate creates a spatially modulated electric field, which opened the band gap in the graphene and produced an insulating region at the p-n interface. Furthermore, series of tunneling junctions enabled unipolar graphene transistors.

This result may open the way for logic applications of gap-engineered graphene.

Acknowledgments: This work was supported in part by a FIRST Program from the Japan Society for the Promotion of Science.

References

1. H.Miyazaki, K.Tsukagoshi, A.Kanda, M.Otani, S.Okada, Nano Letters 10, 3888 (2010)
2. S.-L.Li, H.Miyazaki, A.Kumatani, A.Kanda, K.Tsukagoshi, Nano Letters 10 (7) 2357-2362 (2010).
3. H.Miyazaki, S.-L.Li, H.Hiura, K.Tsukagoshi, A.Kanda, Journal of Physical Society of Japan 81, 014708 (2012).
4. A.A.Ferreira, H.Miyazaki, S.-L.Li, K.Komatsu, S.Nakaharai, K.Tsukagoshi, Nanoscale 4 (24) 7842 (2012).

Corresponding Author: K. Tsukagoshi

TEL:+81-29-860-4894, FAX:+81-29-860-4706

E-mail: TSUKAGOSHI.Kazuhito@nims.go.jp

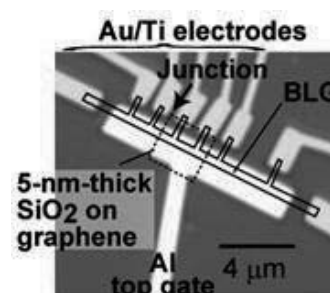


Fig.1 Optical-microscope image of gate-tunable bilayer graphene transistor.

Novel Functional Carbon-Nanotube Transistors

Taishi Takenobu

Department of Applied Physics, Waseda University, Shinjuku 169-8555, Japan

Flexible, printed, and stretchable electronics are attracting considerable attention as the next-generation functional electronics because it is believed that in future many electronic assemblies on rigid substrates will be replaced by mechanically flexible or even stretchable alternatives. This is a consequence of the ambient intelligence vision where the citizen carries along more and more electronics systems, near the body, on or even inside the body. These systems must be light weighted, must preferably take the shape of the object in which they are integrated, and must even follow all complex movements of these objects, explaining the need for stretchability. Although organic materials have been playing the main role in these research fields, in this study, we would like to show you the considerable potential in single-walled carbon-nanotube (SWCNT) films.

High-performance SWCNT transistors: As the first step for carbon-nanotube flexible, printed, and stretchable electronics, we found the simple method to fabricate high-performance SWCNT film transistors using the enriched semiconductor SWCNT [1,2] and one of the solid electrolyte dielectric materials, ion gel [3,4]. These semiconducting SWCNT transistors hold carrier mobility of more than $100 \text{ cm}^2/\text{Vs}$ and on/off ratio of 10^4 - 10^5 .

Flexible SWCNT transistors: Based on this method, we fabricated SWCNT transistors on flexible plastic substrates. The flexible SWCNT transistors also show high performance with carrier mobility of more than $100 \text{ cm}^2/\text{Vs}$ and on/off ratio of 10^4 . Moreover, we have tested bending durability of devices on flexible substrates down to curvature radius of $300 \mu\text{m}$. During the bending test, both on- and off-current of SWCNT transistor was almost constant, and transistor kept high performance without degradation. To the best of our knowledge, this curvature radius of less than $300 \mu\text{m}$ is minimum champion record among SWCNT flexible transistors [5].

Printed SWCNT transistors: Because we have already performed the ink-jet printing of SWCNT transistors [6,7], the fully ink-jet printed all-carbon SWCNT transistors were fabricated on flexible plastic films. We ink-jet printed the enriched metallic SWCNT, enriched semiconducting SWCNT, and ion gel as electrodes, active layer, and dielectric layer, respectively. These printed SWCNT transistors also revealed high performance and excellent flexibility.

Stretchable SWCNT transistors: We applied our SWCNT films into a stretchable poly(dimethylsiloxane) (PDMS) substrates and successfully fabricated stretchable SWCNT transistors. We have preliminary tested expanding durability of devices on PDMS substrates up to strain of 10% and, during expanding test, both carrier mobility and on/off ratio were approximately constant, which is better stretchability than the recent graphene transistors [8].



Picture of SWCNT transistor

- [1] K. Yanagi, *T.T et al.*, *ACS NANO* 4 (2010) 4027.
- [2] K. Yanagi, *T.T et al.*, *Adv. Mater.* 23 (2011) 2811.
- [3] Y. Yomogida, *T.T et al.*, *Adv. Mater.* 24 (2012) 4392.
- [4] J. Pu, *T.T et al.*, *Nano Lett.* 12 (2012) 4013.
- [5] S. Aikawa, *et al.*, *Appl. Phys. Lett.* 100 (2012) 063502.
- [6] H. Okimoto, *T.T et al.*, *Adv. Mater.* 22 (2010) 3981.
- [7] D. Fu, *T.T et al.*, *Adv. Mater.* 22 (2010) 4867.
- [8] S. K. Lee, *et al.*, *Nano Lett.* 11 (2011) 4642.

Tel/Fax: +81-3-5286-2981, E-mail: takenobu@waseda.jp

Ballistic transport in graphene/h-BN

○Tomoki Machida^{1,2,3}, Satoru Masubuchi^{1,2}, Masahiro Onuki¹, Sei Morikawa¹, Kazuyuki Iguchi¹, Takehiro Yamaguchi¹, Miho Arai¹, Kenji Watanabe⁴, Takashi Taniguchi⁴

¹ *Institute of Industrial Science, University of Tokyo, Tokyo 153-8505, Japan*

² *INQIE, University of Tokyo, Tokyo 153-8505, Japan*

³ *PRESTO, Japan Science and Technology Agency, Saitama 332-0012, Japan*

⁴ *National Institute for Materials Science, Tsukuba, 305-0044, Japan*

The presence of unique relativistic charge carriers, massless Dirac fermions, in monolayer graphene has led to the emergence of novel transport phenomena. When the mean free path of the Dirac fermions exceeds the size of conductor, the charge carriers in a ballistic transport regime exhibit more intriguing transport phenomena.

In this work, we study magnetotransport in ballistic graphene mesoscopic wires on hexagonal boron nitride (h-BN). We observed anomalous magnetoresistance curves with characteristic peak structures where the peak field scales with the ratio of cyclotron radius R_C and wire width W [1]. The obtained commensurability ratio $\alpha \equiv W / R_C = 0.95 \pm 0.1$ contrasts with $\alpha = 0.55$ in semiconductor two-dimensional electron gas systems.

The graphene mesoscopic wire/h-BN was fabricated using the mechanical exfoliation and transfer technique. A monolayer graphene deposited on a spin-coated PMMA was transferred on the h-BN crystal using an alignment technique under an optical microscope. A wire-shaped geometry was defined using the standard electron-beam lithography and subsequent oxygen plasma etching technique. The carrier mobility is $70,000 \text{ cm}^2/\text{Vs}$ at 4 K, and the carrier mean free path exceeds $1 \text{ }\mu\text{m}$ at high carrier density of $3 \times 10^{12} \text{ cm}^{-2}$.

Two-terminal resistance shows an anomalous peak structure indicating that the carriers are transmitted ballistically in an inner region of the conduction channel and scattered diffusively at the boundary. The resistance peak occurs at a magnetic field which scales with the ratio of R_C and W as $W / R_C = 0.95 \pm 0.1$ independently from W . The result suggests the characteristic commensurability ratio and unique boundary scattering in graphene.

The carrier focusing effect in a ballistic transport regime and the photovoltaic effect due to the cyclotron resonance in graphene/h-BN will also be presented.

[1] S. Masubuchi *et al.* Phys. Rev. Lett. **109**, 036601 (2012).

Corresponding Author: Tomoki Machida

Tel: +81-3-5452-6742, Fax: +81-3-5452-6743,

E-mail: tmachida@iis.u-tokyo.ac.jp

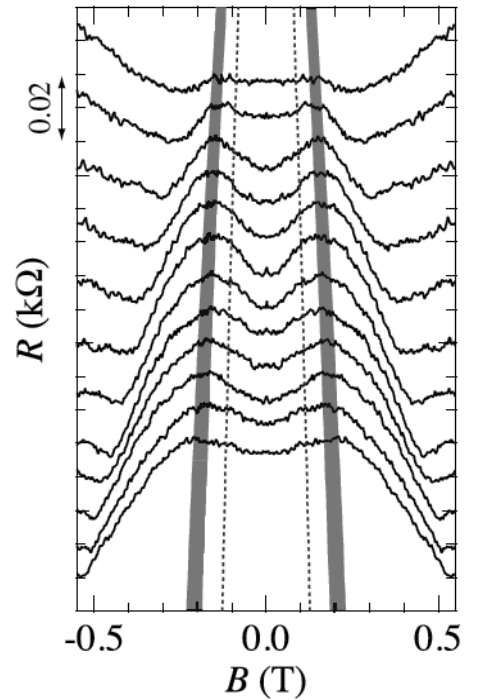


Fig.1 Two-terminal resistance R as a function of magnetic field B at $T = 4 \text{ K}$ for the device with $L = 2.3 \text{ }\mu\text{m}$ and $W = 1.0 \text{ }\mu\text{m}$ with back-gate voltage $V_{\text{BG}} = -50, -48, \dots, -28 \text{ V}$ (bottom to top). Each curve was offset vertically. The dotted line and colored area indicate the expected peak

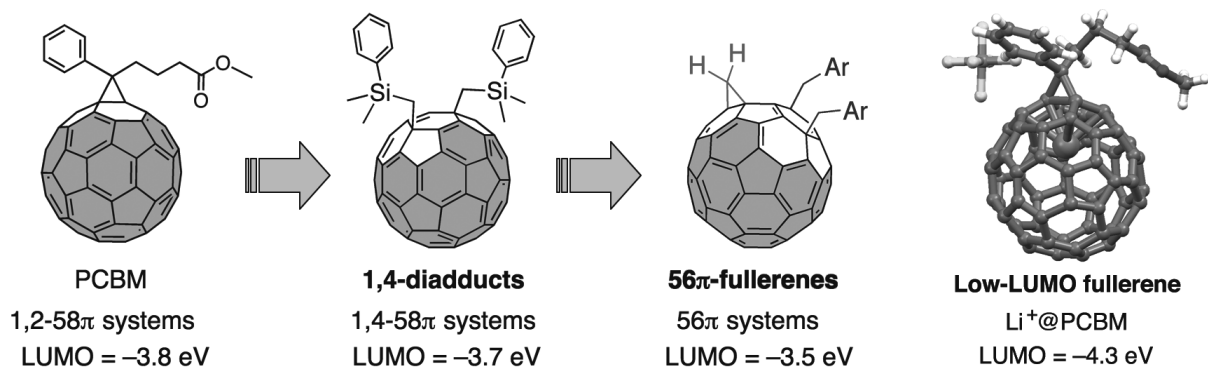
Design, Synthesis, and Properties of Fullerene Derivatives for Organic Thin Film Solar Cells

○Yutaka Matsuo

Department of Chemistry, School of Science, The University of Tokyo, 7-3-1 Hongo, Bunkyo-ku, Tokyo 113-0033, Japan

Development of organic thin-film photovoltaic cells have become important subjects because those devices are expected to provide renewable energy technology. Fullerenes are commonly used as photoelectrochemically active materials in organic photovoltaics due to their high electron affinity that enables efficient photoinduced electron transfer and charge separation. To achieve efficient and mechanistically well-defined photo-energy conversion, rational design of fullerene derivatives and construction of their ordered supramolecular structures in solid states as well as on surface are of importance. Herein we report design of new fullerene derivatives and their application to organic photovoltaic devices.

Photoelectronic functions of fullerene derivatives mainly depend on the size and shape of their π -electron conjugated systems, which can be modified by the change of number and position of organic addends on the fullerene core. In this presentation, we focus on development of new fullerene derivatives that have suitable LUMO levels for high open-circuit voltage, high electron mobility, and self-assembling ability to achieve high-performance organic photovoltaic cells.



[1] Y. Matsuo *et al.* *J. Am. Chem. Soc.* **2009**, *131*, 16048.

[2] Y. Zhang *et al.* *J. Am. Chem. Soc.* **2011**, *133*, 6890.

[3] Y. Matsuo *et al.* *Appl. Phys. Lett.* **2012**, *100*, 063303.

[4] Y. Matsuo *et al.* *Chem. Commun.* **2012**, *48*, 3878.

[5] Y. Matsuo *et al.* *Org. Lett.* **2012**, *14*, 3784.

Corresponding Author: Y. Matsuo

Tel: +81-3-5841-1476, Fax: +81-3-5841-1476

E-mail: matsuo@chem.s.u-tokyo.ac.jp

一般講演
General Lecture

1-1 ~ 1-10

2-1 ~ 2-11

3-1 ~ 3-13

Organic Synthesis of Helium-Containing Fullerenes and Generation of Endohedral Fullerenes Encapsulating Two Different Atoms

○Yuta Morinaka¹, Satoru Sato², Atsushi Wakamiya¹, Hidefumi Nikawa², Naomi Mizorogi², Fumiyuki Tanabe¹, Michihisa Murata¹, Koichi Komatsu¹, Ko Furukawa³, Tatsuhisa Kato⁴, Shigeru Nagase⁵, Takeshi Akasaka², Yasujiro Murata^{1,6}

¹ Institute for Chemical Research, Kyoto University, Uji, Kyoto 611-0011, Japan

² Life Science Center of Tsukuba Advanced Research Alliance, University of Tsukuba, Tsukuba, Ibaraki 305-8577, Japan

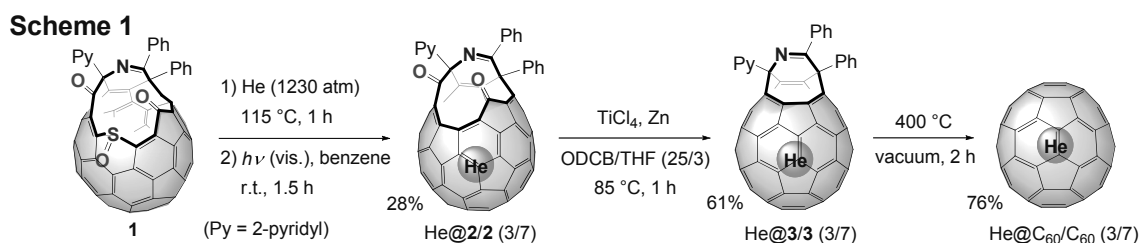
³ Institute for Molecular Science, Okazaki, Aichi 444-8585, Japan

⁴ Institute for the Promotion of Excellence in Higher Education, Kyoto University, Kyoto 606-8501, Japan

⁵ Fukui Institute for Fundamental Chemistry, Kyoto University, Kyoto 606-8103, Japan

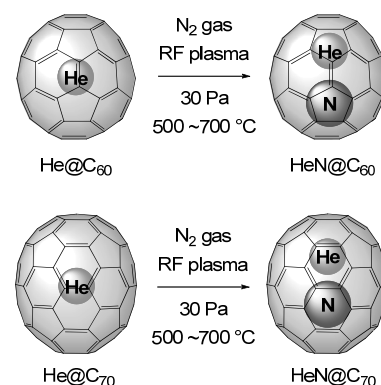
⁶ JST, PRESTO

Previously, we have synthesized open-cage fullerenes and introduced hydrogen molecule(s) into the fullerene cages through the opening [1]. Under the similar conditions, a helium atom was incorporated inside the open-cage C₆₀ derivative **1** followed by the irradiation with a high-pressure mercury lamp to give He@**2** at occupation level of 30% (Scheme 1) [2]. After the restoration of the openings, synthesis of the He@C₆₀ was achieved at occupation level of 30%. He@C₇₀ was also synthesized by applying this synthetic technique. The encapsulated helium atom inside C₆₀ was confirmed by the single crystal X-ray analysis of He@C₆₀ as the first report on X-ray diffraction data containing helium [3].



It is well known that a nitrogen atom can be encapsulated into C₆₀ and C₇₀ under nitrogen radio-frequency (RF) plasma conditions. In this study, we tried insertion of a nitrogen atom into He@C₆₀ and He@C₇₀ under plasma conditions [3]. The ESR analyses of the products demonstrated that novel endohedral fullerenes encapsulating both helium and nitrogen atoms were generated (Scheme 2). This is the first achievement for the production of endohedral fullerenes by combining two individual insertion techniques.

Scheme 2



[1] M. Murata, Y. Murata, K. Komatsu, *Chem. Commun.* 6083 (2008).

[2] Y. Morinaka, F. Tanabe, M. Murata, Y. Murata, K. Komatsu, *Chem. Commun.* **46**, 4532 (2010).

[3] Y. Morinaka, S. Sato, A. Wakamiya, F. Nikawa, N. Mizorogi, F. Tanabe, M. Murata, K. Komatsu, K. Furukawa, T. Kato, S. Nagase, T. Akasaka, Y. Murata, *submitted*.

Corresponding Author: Yasujiro Murata

Tel: +81-774-38-3172, Fax: +81-774-38-3178

E-mail: yasujiro@scl.kyoto-u.ac.jp

Fullerene bis-carboxylic acid derivatives by Prato reaction

○Safwan Aroua and Yoko Yamakoshi

¹ *Laboratorium für Organische Chemie, ETH-Zürich, Wolfgang-Pauli-Strasse 10 CH8093 Zürich, Switzerland*

In order to prepare water-soluble fullerene materials, bis-carboxylic acid derivatives of C₆₀ and M₃N@C₈₀ (M = Sc, Y, Lu, Gd) were synthesized by Prato reaction with a glycine derivative **1** and formaldehyde. The subsequent addition of PEG chains by amide formation successfully leads to water-soluble fullerene materials.

The glycine derivative **1** was prepared from di-*tert*-butyl 3-oxopentanedioate and subjected to the reaction with fullerenes in the presence of formaldehyde (Figure 1). In the reaction of C₆₀, mono [6,6]-adduct was observed as a major product (Figure 2). In the reactions of M₃N@C₈₀, the initial adducts were [6,6]-adducts, which were converted to [5,6]-adducts by heating (Figure 3). The reaction rate of the isomerization step was dependent on the metal cluster size inside of the C₈₀ cage, with smaller sizes leading to slower rates. Interestingly, in the case of larger metal cluster (Y and Gd), the isomerization occurred in equilibrium (Figure 4). By addition of PEG moieties via amide formation using HPTU as a coupling reagent, water-soluble materials of C₆₀ and Gd₃N@C₈₀ were successfully prepared. These materials appear to form micelle-like small particles in aqueous solution.

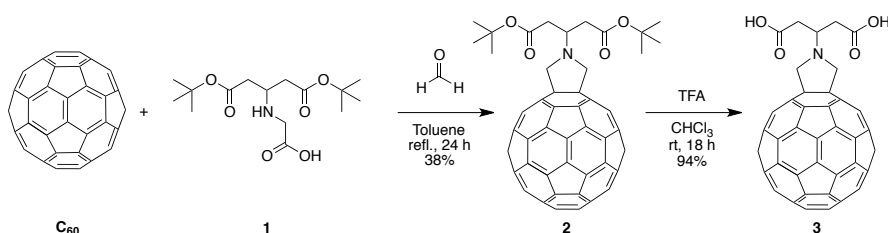


Figure 1. Prato reaction of C₆₀.

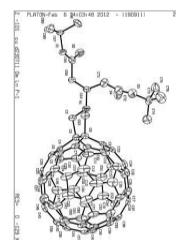


Figure 2. Perspective view of **2**.

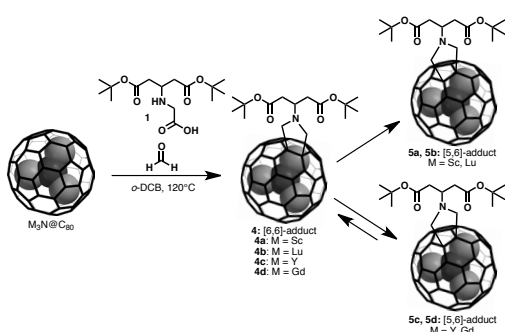


Figure 3. Prato reaction of M₃N@C₈₀.

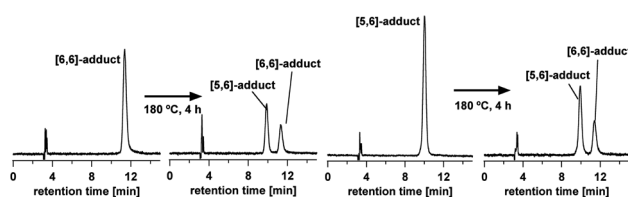


Figure 4. Thermal conversion of Gd₃N@C₈₀ [6,6]-adduct to [5,6]-adduct (upper) and [5,6]-adduct to [6,6]-adduct (lower) upon heating (HPLC: Buckyprep, toluene, 1 mL/min, 390 nm).

[1] A. Safwan *et al.* *J. Am. Chem. Soc.* **134**, 20242 (2012).

Corresponding Author: Y. Yamakoshi

Tel: +41-44-633-6420, Fax: +41-44-633-1235,

E-mail: yamakoshi@org.chem.ethz.ch, website: <http://www.yamakoshi.ethz.ch/>

Molecular Bearing of Finite Carbon Nanotube and Fullerene in Ensemble Rolling Motion

○Shunpei Hitosugi, Yamasaki Takashi, Ryosuke Iizuka, Hiroyuki Isobe

Department of Chemistry, Tohoku University, Sendai, 980-8578, Japan

The combination of convex and concave surfaces of carbonaceous entities provides an interesting element of nanoscale machines because of its ultralow friction originates from the smoothness and the non-directional van der Waals nature of the attractive forces at the complementary interface. Although the multi-wall carbon nanotube based prototype machine has attracted an immediate interest, the advancement in the chemical production of such carbonaceous machinery is much slower than expected. The major obstacle to advancement is the lack of discrete carbon nanotubes that can be handled as a molecular entity: Inhomogeneous molecular structures of available carbon nanotubes allow for handling only as a mixture of various structures and hamper the rational molecular design of the machinery. We report a minimal carbonaceous bearing composed of finite single-wall carbon nanotube (SWNT) and fullerene molecules.

The finite SWNT bearing in our study is [4]cyclochrysenylene ([4]CC), a belt-persistent variant of tubular cycloarylene molecules from bottom-up synthesis.^[1] We determined the association constant between (*P*)-(12,8)-[4]CC and C₆₀ by using the fluorescence quenching titration to obtain the value, $\log K_a = 12.3$ in benzene, which surpassed that of the previously tightest complex with C₆₀ (Fig. 1a). The introduction of a "shaft" moiety into the C₆₀ journal allowed us to realize the anisotropic ensemble rolling motion in the peapod bearing. The functionalized journal is a protonated form of *N*-methyl fulleropyrrolidine **1** that possesses a five-membered ring as the shaft on the spherical journal. The results of VT-NMR analysis demonstrate that the journal in the bore rolls rapidly on the NMR timescale and acts as a "symmetry top" from 25 °C to -60 °C (Fig. 1b).^[2]

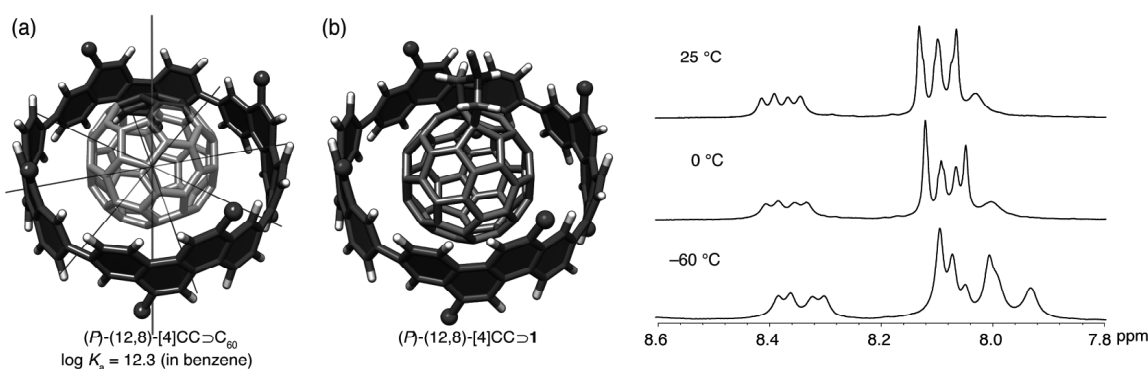


Fig. 1 (a) A molecular model of (*P*)-(12,8)-[4]CC⊃C₆₀. Hexyl groups of [4]CC are represented as balls for clarity. (b) A molecular model of a protonated form of *N*-methyl fulleropyrrolidine **1** encapsulated in (*P*)-(12,8)-[4]CC and the aromatic resonances in ¹H NMR spectra in CD₂Cl₂.

[1] Hitosugi, S.; Nakanishi, W.; Yamasaki, T.; Isobe, H. *Nat. Commun.* **2**, doi: 10.1038/ncomms1505 (2011). Hitosugi, S.; Yamasaki, T.; Isobe, H. *J. Am. Chem. Soc.* **134**, 12442 (2012).

[2] Isobe, H.; Hitosugi, S.; Yamasaki, T.; Iizuka, R. *Chem. Sci.* published online (doi: 10.1039/C3SC22181D).

Corresponding Author: H. Isobe

Tel: +81-22-795-6585, Fax: +81-22-795-6586,

E-mail: isobe@m.tohoku.ac.jp

Selective synthesis of alkoxyfullerenes $C_{60}(OR)_5Br$: Substitution reaction of $C_{60}Br_6$ with alcohol

○Kouya Uchiyama ¹, Hiroshi Moriyama ^{*1}, Kenji Yoza ²

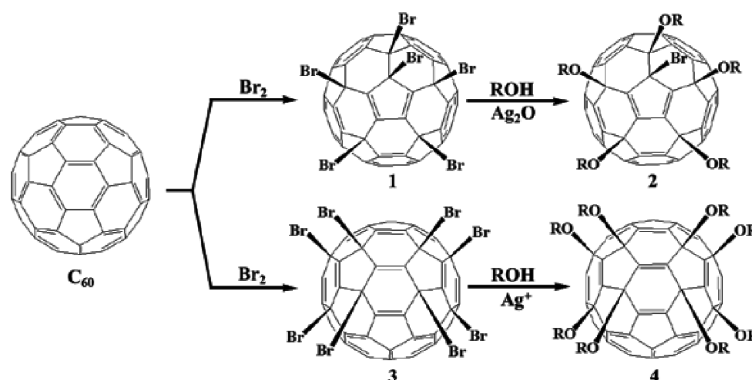
¹ Department of Chemistry, Toho University, Funabashi, 274-8510, Japan

² Bruker AXS, Yokohama, 221-0022, Japan

Halofullerenes, $C_{60}X_n$, such as chlorofullerene and bromofullerene, are recognized as suitable starting materials for further synthesis of fullerene derivatives, because they have relatively weak C–X bonds; therefore, substitution reactions with various nucleophiles can easily occur to give multifunctionalized fullerene derivatives regioselectively. However, compared with chlorofullerenes, bromofullerenes have not so far been studied intensively because of their low solubility in organic solvents.

We have reported a selective substitution reaction of octabromofullerene $C_{60}Br_8$ [1] with methanol and ethanol in the presence of a silver salt, which facilitates the substitution reaction of all bromine atoms to give novel alkoxyfullerenes $C_{60}(OR)_8$ ($R = CH_3, C_2H_5$) [2], as the result of total substitution of the bromines of $C_{60}Br_8$. We characterized the products by ¹H and ¹³C NMR spectroscopy, and single-crystal X-ray crystal structure analysis. The molecular structure of these alkoxyfullerenes, C_{2v} , was found to be retained, which is completely consistent with the addition pattern.

Here we report another type of reaction, hexabromofullerene $C_{60}Br_6$ [1] with alcohols, in which novel pentakisalkoxyfullerenes $C_{60}(OR)_5Br$ ($R = Me, Et, ^nPr, ^nBu, ^iBu, ^nPn, 2-MeEt$) were newly obtained and characterized by ¹H and ¹³C NMR spectroscopy. The substitution reaction proceeds efficiently in the presence of Ag_2O , which facilitates bromine elimination.



Scheme

The pentakisalkoxyfullerenes $C_{60}(OR)_5Cl$ ($R = Me, Et$) have been reported [3]; however, no pentakisalkoxyfullerenes with a longer alkyl chain such as Pr, Bu, Pn, have been reported in the case of $C_{60}(OR)_5Cl$. The substitution of bromine seems rather easier than is the case for chlorine. However, it was found that the unique bromine atom at the center of the fullerene molecule was not substituted under these reaction conditions, as was observed for $C_{60}(OR)_5Cl$. A new oxygen-bridged tetrakisalkoxyfullerene compound, $C_{60}(OR)_4O$, was also obtained, depending on the bulkiness of the alkyl group. These alkoxyfullerene derivatives, $C_{60}(OR)_5Br$, seem to have potential use as unique starting compounds for the synthesis of other fullerene derivatives.

[1] P. R. Birkett, P. B. Hitchcock, H. W. Kroto, R. Taylor, D. R. M. Walton, *Nature*, **357**, 479–481 (1992).

[2] K. Uchiyama, H. Moriyama, K. Yoza, The 43rd FNTG Symposium Abstract, 1P-14 (2012); JP2012–194209.

[3] A. G. Avent, P. R. Birkett, A. D. Darwish, S. Houlton, R. Taylor, K. S. T. Thomson, X.-W. Wei, *J. Chem. Soc., Perkin Trans. 2*, **5**, 782–786 (2001).

Corresponding Author: Hiroshi Moriyama

TEL: +81-47-472-1211, FAX: +81-47-476-9449, E-mail: moriyama@chem.sci.toho-u.ac.jp

Proton dynamics in Fullerenol solids studied by $^1\text{H-NMR}$

○Keisuke Baba¹ and Hironori Ogata^{1,2}

¹ *Department of Chemical Science and Technology, Hosei University, Koganei 184-8584, Japan*

² *Research Center for Micro-Nano Technology, Hosei University, Koganei 184-0003, Japan*

Fullerenols (Polyhydroxylated Fullerene: $\text{C}_{60}(\text{OH})_x$) have been a subject of intense research in many fields with the claim of possible applications in a variety of areas, including optoelectronics, medical therapeutics, biotechnology, chemical mechanical polishing, and fuel cells, owing to their high solubility in a large variety of solvents (depending on the number of hydroxyl groups, x). It is reported that $\text{C}_{60}(\text{OH})_n$ ($n \sim 12$) show proton conductivity and their applications for the proton conducting membrane of a polymer electrolyte fuel cell (PEFC) is proposed. However, their proton conduction mechanism has not been thoroughly studied yet. We previously reported the fabrication of both nanosheets and nanocrystals consist of the two types of fullerenols ($\text{C}_{60}(\text{OH})_{13.5}$ and $\text{C}_{60}(\text{OH})_{38.7}(\text{O})_{1.6}$) by the liquid phase growth method using both good and poor solvents.

We have studied proton dynamics in both $\text{C}_{60}(\text{OH})_{13.5}$ and $\text{C}_{60}(\text{OH})_{38.7}(\text{O})_{1.6}$ solids by means of ^1H -solid-state NMR. Figure 1 shows the temperature dependence of $^1\text{H-NMR}$ spectra in (a) $\text{C}_{60}(\text{OH})_{13.5}$ and (b) $\text{C}_{60}(\text{OH})_{38.7}(\text{O})_{1.6}$. The detailed results about their proton dynamics will be reported.

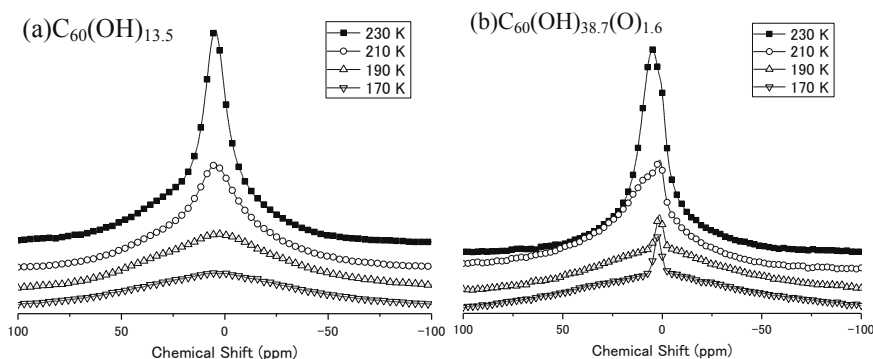


Fig.1. Temperature dependence of $^1\text{H-NMR}$ line shapes in (a) $\text{C}_{60}(\text{OH})_{13.5}$ and (b) $\text{C}_{60}(\text{OH})_{38.7}(\text{O})_{1.6}$.

[1] K. Hinokuma *et al.*, Chem. Phys. Lett., **341**, 442 (2001)

[2] Chiang *et al.* J. Org. Chem., **59**, 3960 (1994)

[3] K. Kokubo, *et al.*, ACS Nano, **2**, 327 (2008)

[4] K. Baba, *et al.*, The 43rd Fullerenes-Nanotubes-Graphene General Symposium, 1P-24 (2012)

Corresponding Author: Hironori Ogata

Tel: +81-42-387-6229, Fax: +81-42-387-6229,

E-mail: hogata@hosei.ac.jp

Kinetic Stability Governs Relative Fullerene Isomer Abundance

○ Stephan Irle¹, Yoshifumi Nishimura¹, Alexander S. Fedorov², Henryk A. Witek³

¹*Department of Chemistry and WPI-Institute of Transformative Bio-Molecules, Nagoya University, Nagoya 464-8602, Japan*

²*Kirensky Institute of Physics, Akademgorodok 50, Krasnoyarsk, 660036, Russia*

³*Department of Applied Chemistry and Institute of Molecular Science, National Chiao Tung University, Hsinchu 30010, Taiwan*

A methodology to evaluate the kinetic stability of molecular nanostructures is presented based on the assumption of the independent and random nature of thermal vibrations, calculated at the density functional theory (DFT) level of theory using the harmonic approximation [1]. The kinetic stability (KS) is directly correlated to the cleavage probability for the weakest bond of a given molecular geometry. The application of the presented method to a selection of fullerenes (see Fig. 1) and carbon nanotubes yields clear correlation to their experimentally observed relative isomer abundances.

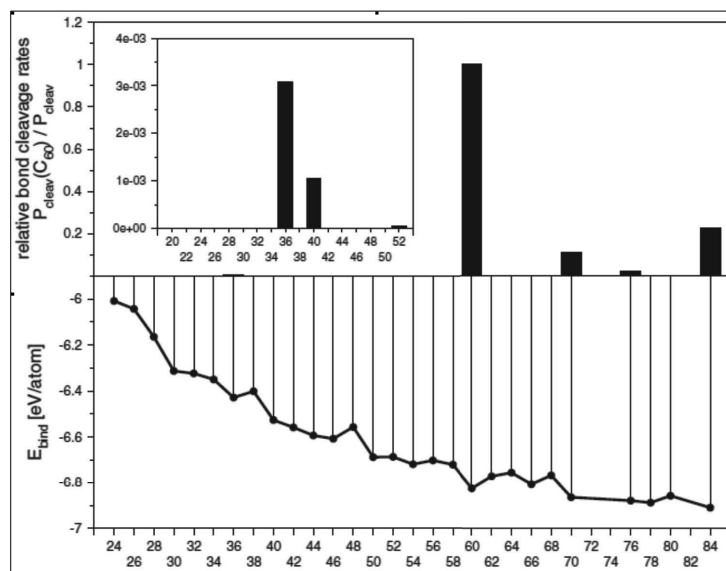


Fig.1 Calculated relative kinetic stability (upper part) and cohesion energy (bottom part) for different fullerenes.

Moreover, we present good agreement of harmonic vibrational eigenmodes between DFT and the computationally more efficient density-functional tight-binding (DFTB) method [2-4]. Thus, DFTB-based KS calculations allow the estimation of kinetic stability for more than 100,000 isomers of the fullerenes $\text{C}_{20}\text{-C}_{100}$. We found that the experimentally observed isomer abundances, as recorded for instance by mass spectroscopic investigations, are reasonably well reproduced by the Boltzmann-weighted kinetic stabilities of the cage isomers. This result suggests a mechanism of fullerene formation involving cage destruction, such as recently predicted by quantum chemical molecular dynamics (QM/MD) simulations [5-6].

[1] A. S. Fedorov *et al.*, *Phys. Rev. Lett.*, **107**, 175506 (2011).

[2] H. A. Witek *et al.*, *J. Chem. Phys.*, **121**, 5163 (2004).

[3] E. Małolepsza *et al.*, *Chem. Phys. Lett.*, **412**, 237 (2005).

[4] H. A. Witek *et al.*, *J. Chem. Phys.*, **125**, 214706 (2006).

[5] S. Irle *et al.*, *J. Phys. Chem. B*, **110**, 14531 (2006).

[6] B. Saha *et al.*, *J. Phys. Chem. A*, **115**, 22707 (2011).

Corresponding Author: S. Irle

Tel: +81-52-747-6397, Fax: +81-52-747-6397

E-mail: sirle@chem.nagoya-u.ac.jp

Optical properties of graphene quantum dots separated by high performance liquid chromatography

oNaoto Fuyuno¹, Daichi Kozawa¹, Yuhei Miyauchi^{1,2}, Shinichiro Mouri¹, Ryo Kitaura³, Hisanori Shinohara³, Toku Yasuda⁴, Naoki Komatsu⁴, and Kazunari Matsuda¹

¹*Institute of Advanced Energy, Kyoto University, Uji, Kyoto 611-0011, Japan*

²*Japan Science and Technology Agency, PRESTO, 4-1-8 Honcho Kawaguchi, Saitama 332-0012, Japan*

³*Department of Chemistry and Institute for Advanced Research, Nagoya University, Nagoya 464-8602, Japan*

⁴*Department of Chemistry, Shiga University of Medical Science, Otsu 520-2192, Japan*

Graphene quantum dots (GQDs), which are nanometer-size graphene pieces, have attracted a great deal of interest from the viewpoints of fundamental physics and optoelectronics. Although the optical properties of GQDs could be controlled by changing size due to the quantum confinement effect, accurate control of their size has not been achieved and thus their luminescence mechanism is not well understood. Therefore, achievement of size separation of GQDs, which would lead to narrower emission peaks, is important for both understanding their size-dependent optical properties and future optical applications.

In the present study, we conducted optical measurements on the GQDs separated by high performance liquid chromatography (HPLC) to explore the possibility of size separation and clarify their size-dependent optical properties. The GQDs were fabricated by the acid treatment of pitch-based carbon fibers [1] and then collected separately by HPLC (HPLC-GQDs). Figure 1 shows the photoluminescence excitation spectroscopy (PLE) maps of the HPLC-GQDs where the numbers in the maps indicate the fractions of the collection (larger numbers correspond to the longer retention times). Several luminescence features indicated by white ellipses (A, B, C and D) are observed in the PLE maps. These features could originate from different species since their patterns vary depending on the fractions. These results suggest that GQDs with various optical characteristics could be separated by HPLC, probably caused by the size variation of GQDs.

[1] J. Peng *et al.*, *Nano lett.* **12**, 844 (2012).
Corresponding Author: N. Fuyuno
Tel: +81-774-38-3465, Fax: +81-774-38-3467
E-mail: fuyuno.naoto.67n@st.kyoto-u.ac.jp

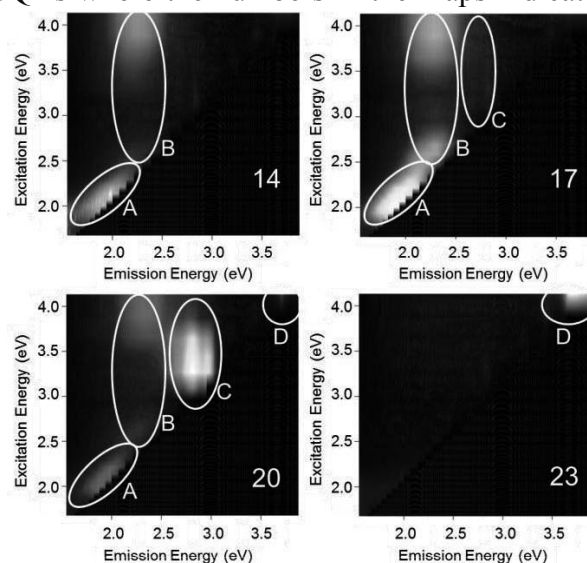


Fig. 1 PLE maps of the GQDs after the separation by HPLC. The numbers shown in the maps correspond to the fractions of the collection.

Modulation of Optical Spectra of Monolayer MoS₂ by Chemical Doping

○Shinichiro Mouri¹, Yuhei Miyauchi^{1,2}, Kazunari Matsuda¹

¹*Institute of Advanced Energy, Kyoto University, Uji, Kyoto 611-0011, Japan*

²*Japan Science and Technology Agency, PRESTO, 4-1-8 Honcho Kawaguchi, Saitama 332-0012, Japan*

Monolayer molybdenum disulfide (MoS₂) has attracted much attention as a novel two-dimensional direct band gap semiconductor [1], and also is a promising candidate to realize the ‘valleytronic’ devices since the valley selective optical excitation is possible [2]. The control of fundamental optical properties including excitonic effects is necessary to open up such applications. Charge-carrier doping is one of the effective methods to modify the excitonic behavior of ultrathin nanostructures, such as carbon nanotubes [3]. Recently, tightly bound trion, a quasi-particle composed of two electrons and a hole, has been observed in a monolayer MoS₂ FET device using the electro-static doping [4]. In this study, we investigated the chemical doping effects on the photoluminescence (PL) spectra of monolayer MoS₂.

Monolayer MoS₂ was prepared by the mechanical exfoliation and deposited on SiO₂/Si substrate. Excitation light source for the PL experiments was the cw solid-state laser (2.33 eV: 20 μW). We drop-casted a typical *p*-type dopant (F₄TCNQ) dissolved in toluene solution (1 μg/ml) on the surface of the monolayer MoS₂. Figure 1 shows the normalized PL spectra of as-prepared and hole-doped monolayer MoS₂ at room temperature. The PL peak around 1.8–1.9 eV can be decomposed into two components corresponding to the exciton (Peak A) and trion (Peak A⁻) PL [4]. In the as-prepared monolayer MoS₂, the trion PL (A⁻, ~1.85 eV) is dominant, because excitons can be easily bound by spontaneously doped negative charge-carriers (electrons) [4]. On the other hand, we found that exciton PL (A, ~1.89 eV) becomes dominant in the hole-doped monolayer MoS₂ presumably because the doped-holes compensate the Fermi energy shift induced by spontaneously doped negative charges. These results suggest that the optical properties of monolayer MoS₂ can be controlled by the chemical doping method.

- [1] A. Splendiani *et.al.* *Nano Lett.* **10**, 1271 (2010).
 [2] T. Cao *et.al.* *Nature Commu.* **3**, 1882 (2012).
 [3] S. Mouri *et.al.*, *Phys. Rev.* **B 87**, 045408 (2013).
 [4] K. Fai. Mak *et.al.* *Nature. Material.* **7**, 494 (2012).

Corresponding Author: Shinichiro Mouri
 Tel: +81-774-38-3463,
 Fax: +81-774-38-3467,
 E-mail: iguchan@iae.kyoto-u.ac.jp

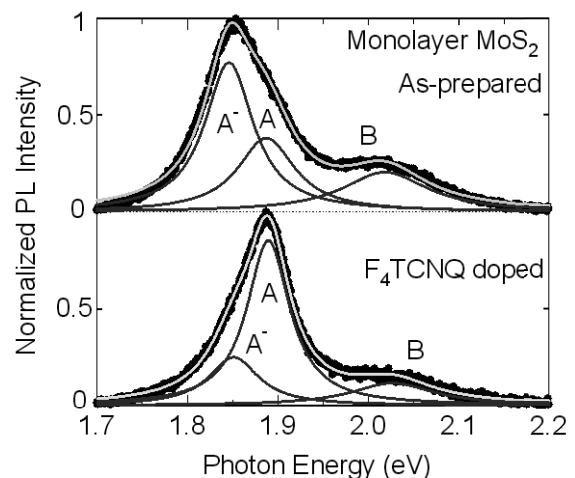


Figure 1 PL spectra of as-prepared (above) and F₄TCNQ doped (below) monolayer MoS₂.

Coulomb drag and excitonic insulator in double-layer graphene

○Satoru Konabe^{1,2} and Susumu Okada^{1,2}

¹*Graduate School of Pure and Applied Sciences, University of Tsukuba, Tsukuba, Ibaraki
305-8571, Japan*

²*Japan Science and Technology Agency, CREST, 5 Sanbancho, Chiyoda, Tokyo 102-0075,
Japan*

The Coulomb interaction among Dirac electrons leads to peculiar phenomena in graphene related systems [1]. For example, it has been theoretically proposed that an excitonic insulator phase could appear in two-monolayer graphene (double-layer graphene) [2]. The excitonic insulator is a phase where excitons are spontaneously generated at thermodynamic equilibrium even in the absence of an optical excitation. Such phase arises by the instability of the normal ground state of semiconductor or semimetal against the spontaneous formation and its condensation of bound electron-hole pairs. In the graphene double-layer system, electrons are distributed in one of two layers and holes are in the other layer, those of which form bound pairs through the interlayer Coulomb interaction. However, it is still unclear whether such state exist or not [3]. It is thus crucial to identify physical quantities that directly measure the excitonic insulator phase. To meet such demand, the Coulomb drag resistivity is the most favorable, which measures the ratio of a current passed through one of the layer and the induced voltage drop of the other layer [4].

In this work, we theoretically investigate transport properties of double-layer graphene, focusing on interlayer Coulomb interaction. For this purpose, we develop a theory of Coulomb drag in this system, which covers from the strongly fluctuated normal phase to the excitonic insulator phase. Using the theory, we calculate the drag resistivity that evaluate how the drag resistivity captures the phase transition to the excitonic insulator phase.

References:

- [1] V. N. Kotov *et al.* *Rev. Mod. Phys.* **84**, 1067 (2012).
- [2] H. Min *et al.* *Phys. Rev. B* **78**, 121401(R) (2008).
- [3] M. Y. Kharitonov *et al.* *Phys. Rev. B* **78**, 241401 (2008), Y. E. Lozovik *et al.* *JETP Lett.* **87**, 61 (2008), R. B. Bistritzer *et al.* *Phys. Rev. Lett.* **101**, 256406 (2008), D. K. Efimkin *et al.* *JETP Lett.* **93**, 238 (2011), M. P. Mink *et al.* *Phys. Rev. B* **84**, 155409 (2011), I. Sodemann *et al.* *Phys. Rev. B* **85**, 195136 (2012).
- [4] A. Kamenev *et al.* *Phys. Rev. B* **52**, 7516 (1995).

Corresponding Author: Satoru Konabe

E-mail: konabe@comas.frsc.tsukuba.ac.jp

Tel: +81-2-9853-5600 ext.8233

Resonance and interference effect of Raman spectroscopy of graphene in the magnetic field

○Riichiro Saito¹, Qiu Caiyu², Yu Ting²

¹ *Department of Physics, Tohoku University, Sendai, 980-8578, Japan*

² *Division of Physics and Applied Physics, School of Physical and Mathematical Sciences, Nanyang Technological University, 637371, Singapore*

In the Raman spectroscopy of graphene, some recent experiments show the resonance and interference effects on the Raman intensity and on the spectra shape. When the excitation energies of two elementary excitations such as (1) phonon, (2) optical absorption or (3) phonon of other molecule on graphene etc. are the same to each other, the resonance enhancement of Raman intensity may occur. Further if the initial and the final states of the optical processes for Raman spectra is the same, the scattering amplitudes of light can be interfered to each other which make can change the spectral shape [1]. Here we discuss these effects by recent measurement of Raman spectra of graphene in the presence of the magnetic field.

In the magnetic field, the electronic structure of graphene forms the Landau levels (LLs). The optical dipole transition energies between two LLs are observed as a function of the magnetic fields [2,3]. When the transition energy is close to the G band phonon energy, we expect an interference effect which is reported by several groups. In this case, G and LLs transition are coupled together and split into two peaks denoted by G+ and G-. Further if we use graphite as the substrate for graphene sample, the G band of graphite (Gi) can be resonance to the optical transition between LLs. In this case, we can see three peaks G-, Gi and G+ from a lower energy for a magnetic field (4.65T) of the crossing the LLs transition energy and G band phonon energy.

Here we discuss how to explain the experimental results by a model of graphene and what kind of physics are there in this system.

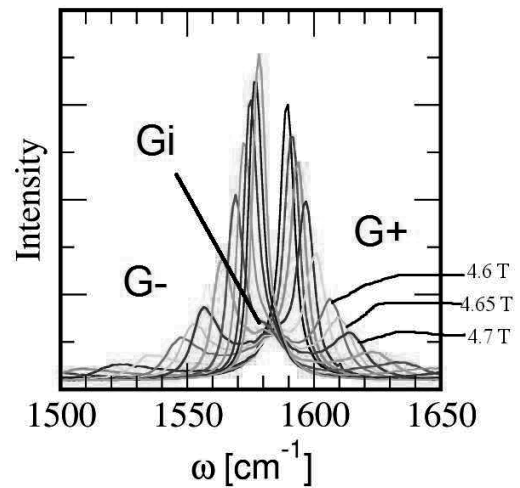


Fig. 1. Raman spectra of graphene around G band for different magnetic fields. We can see three peaks G-, Gi and G+ from lower energies for each magnetic field. The magnetic field for optical transition energy which is the same as G band energy is around 4.65T.

References:

- [1] A. Jorio et al. "Raman Spectroscopy of graphene related systems" Wiley (2011).
- [2] Q. Caiyu et al. unpublished.
- [3] J. Yang et al., Phys. Rev. Lett., 105, 22 (2010).

Corresponding Author: R. Saito

Tel: +81-22-795-7754, Fax: +81-22-795-6447,

E-mail: rsaito@flex.phys.tohoku.ac.jp

Empirical Prediction of Electronic Potentials of Single-Walled Carbon Nanotubes

○Yasuhiko Hirana,¹ Yuhei Miyauchi,^{2,3} Shinichirou Mouri,² Kazunari Matsuda,²
Naotoshi Nakashima^{1,4,5}

¹ *Department of Applied Chemistry, Graduate School of Engineering, Kyushu University,
Motooka 744, Fukuoka 819-0395, Japan*

² *Institute of Advanced Energy, Kyoto University, Uji, Kyoto 611-0011, Japan*

³ *PRESTO, Japan Science and Technology Agency (JST), 4-1-8 Honcho Kawaguchi, Saitama
332-0012, Japan*

⁴ *International Institute for Carbon-Neutral Energy Research (WPI-I2CNER), Kyushu
University, 744 Moto-oka, Nishi-ku, Fukuoka 819-0395, Japan*

⁵ *CREST, Japan Science and Technology Agency (JST), 5 Sanbancho, Chiyoda-ku, Tokyo,
102-0075, Japan*

The redox properties (i.e. electronic densities, the Fermi levels, redox potentials) of single-walled carbon nanotubes (SWNTs) are related to the structures of SWNTs that have a specified diameter and chiral angle uniquely related to a pair of integers (n,m); the so-called chiral index. We have previously reported a PL spectroelectrochemical method that determines the redox potentials of individual (n,m)SWNTs ($d = 0.75\text{-}1.10$ nm).^{1,2,3} For a deeper understanding of the electronic properties, the determination of the redox potentials of SWNTs with a wide range of diameters is very important.

At the meeting, we will provide empirical equations that predict the reduction and oxidation potentials of (n,m)SWNTs for a wide range of diameters and chiral angles. The study also revealed that the reduction and oxidation potentials of (n,m)SWNTs show somewhat different nanotube diameter dependence.

[1] Y. Tanaka, Y. Hirana, Y. Niidome, K. Kato, S. Saito, N. Nakashima, *Angew. Chem. Int. Ed.* **2009**, *48*, 7655.

[2] Y. Hirana, Y. Tanaka, Y. Niidome, N. Nakashima, *J. Am. Chem. Soc.* **2010**, *132*, 13072.

[3] Y. Hirana, Y. Tanaka, Y. Niidome, N. Nakashima, *Bull. Chem. Soc. Jpn.* **2012**, *85*, 1262.

Corresponding Author: Naotoshi Nakashima
Tel: +81-92-802-2842, Fax: +81-92-802-2842
E-mail: nakashima-tcm@mail.cstm.kyushu-u.ac.jp

Molecular Dynamics Simulation on RBM of Single-Walled Carbon Nanotubes in Water Vapor

○Naoki Homma¹, Shintaroh Sato¹, Shohei Chiashi², Yoshikazu Homma¹, and Takahiro Yamamoto³

¹*Dept. of Physics, Tokyo University of Science, Shinjuku, Tokyo 162-8601, Japan*

²*Dept. of Mechanical Engineering, The University of Tokyo, Bunkyo, Tokyo 113-8656, Japan*

³*Dept. of Liberal Arts, Tokyo University of Science, Chiyoda, Tokyo 102-0073, Japan*

Radial breathing mode (RBM) is one of the most important vibrational modes of SWNTs, because the measurement of RBM frequency ω_{RBM} enables us to uniquely assign the chirality of an individual SWNT by combining it with the theory of resonant transitions. The diameter dependence of ω_{RBM} can be phenomenologically written as $\omega_{\text{RBM}} = A/d_t + B$, where d_t is a tube diameter, and A and B are constant parameters with d_t . In particular, B gives the frequency shift by environmental effects.

Figure 1 shows our experimental results on d_t dependence of ω_{RBM} in vacuum (4.0Pa) and in saturated water vapor (630Pa). The experimental data well fit the form $\omega_{\text{RBM}} = A/d_t + B$, where $B \approx 0$ in vacuum or $B = 7.5 \pm 2.5 \text{ cm}^{-1}$ in vapor. It is noted that the value of B in air ($\approx 1 \text{ atm}$) is similar to that in vapor (630Pa).

To reveal underlying physics of this experiment, we theoretically investigated configuration of water molecules around an SWNT and effects of water vapor on ω_{RBM} using the classical molecular-dynamics simulation in the NVT ensemble. As shown in Fig. 2, our simulation results on d_t dependence of ω_{RBM} are in excellent agreement with the experimental results in Fig. 1. Water molecules are condensed around an SWNT surface due to the Van der Waals interactions between water molecules and an SWNT (left inset in Fig. 2). The condensed water molecules formed the hydrogen-bond network parallel to the SWNT surface and eventually they construct a few-layer structure. The first layer is physically bound to the SWNT, whereas the other layers are weakly bound. In consequence, only the first layer gives a significant contribution to the frequency shift B , and the value is almost independent of the number of water layers. This is a reason that experimental values of B in both air and vapor cases are similar each other.

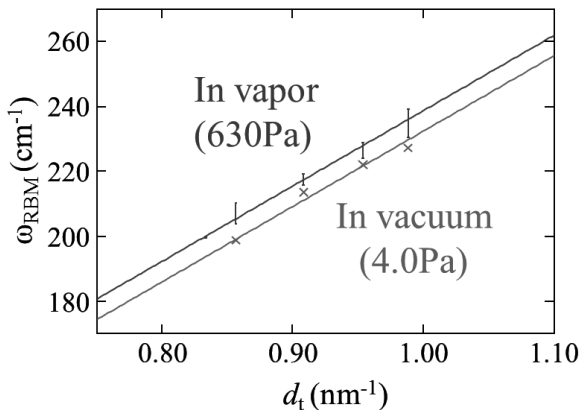


Fig.1 RBM frequency (experiment)

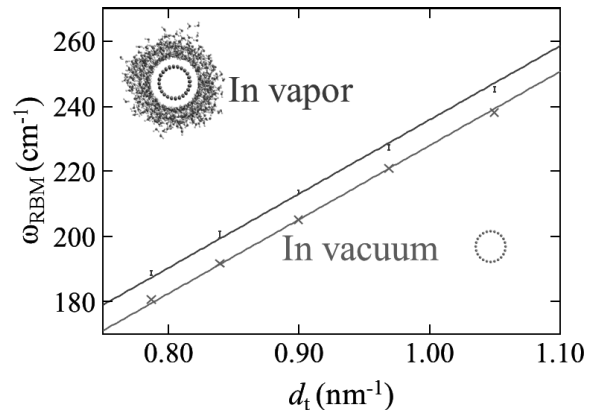


Fig.2 RBM frequency (calculation)

Corresponding Author: Takahiro Yamamoto,

Tel&FAX: +81-3-5213-0990,

E-mail: takahiro@rs.tus.ac.jp

Energy shift of photoluminescence peaks of SWCNTs wrapped by fluorene-based polymers

○Masayoshi Tange, Toshiya Okazaki, and Sumio Iijima

Nanotube Research Center, AIST, Tsukuba, 305-8565, Japan

The structures, i.e., tube diameter and chiral angle identified by chiral indices (n,m), of semiconducting single-walled carbon nanotubes (SWCNTs) can be investigated with photoluminescence excitation (PLE) spectroscopy because the optical transitions of SWCNTs are dependent on the tube structures. In general, photoluminescence (PL) peak positions predicted from empirical functions by Weisman and Bachilo^[1] are used for the assignment of each PL peak in the PLE map to different (n,m). However, when organic solvents are used for SWCNT solutions, a noticeable discrepancy between observed and predicted PL peaks will appear because the predicted peaks are proper for SWCNT aqueous solutions with surfactants such as sodium dodecyl sulfate (SDS). In particular, when only specific (n,m) species of semiconducting SWCNTs are selectively extracted via polymer wrapping sensitive to tube structures, the discrepancy disturbs the assignment of the PL peaks to (n,m). To avoid the noticeable discrepancy due to different solvents, we can use the PL peak positions of poly(9,9-di-*n*-dodecylfluorene) (PFD)-extracted SWCNTs, which show the geometrical patterns for SWCNT family “ $2n+m$ ” because PFD disperses various semiconducting SWCNTs in organic solvents, regardless of the structures of semiconducting SWCNTs.^[2] Moreover, the comparison between PFD and selective polymers will reveal the influence of wrapping polymers on the optical transitions of SWCNTs in organic solvents.

Recently, we reported poly(9,9-dioctylfluorene-*alt*-pridine) (PFOPy) to selectively extract specific semiconducting SWCNTs showing 1500 nm emissions in toluene.^[3] For the study, SWCNTs synthesized by pulsed-laser vaporization (PLV) were used as initial materials. In this work, to investigate the influence of PFOPy wrapping on the optical transitions, we have compared PL peak positions of PFOPy-wrapped SWCNTs with those of PFD-wrapped semiconducting SWCNTs, which were extracted from the same PLV-SWCNTs to exclude an influence due to differences in the product processes of SWCNTs. As a result, emissions of a few (n,m) species in PFOPy-wrapped SWCNTs are found to be blue-shifted relative to those of PFD-wrapped SWCNTs as shown in Figure 1. On the other hand, the excitation wavelengths for the PL peaks were inversely shifted, i.e., red-shifted. On the basis of the energy shift of optical transitions due to a strain effect,^[4] we can interpret the energy shifts of optical transitions to be partially governed by strains of SWCNTs due to the PFOPy wrapping. In addition, when *p*-xylene, which has a similar dielectric constant to toluene, was used as the organic solvent for the PFOPy-wrapped SWCNT solution, remarkable changes in emission energies of PFOPy-wrapped SWCNTs occurred in (14,3) and (15,4) tubes, being consistent with the interpretation that wrapping PFOPy imposes stress on the specific SWCNTs in toluene.

[1] R.B. Weisman and S.M. Bachilo, *Nano Lett.* **3**, 1235 (2003).

[2] M. Tange *et al.*, *J. Am. Chem. Soc.* **133**, 11908 (2011).

[3] M. Tange *et al.*, *ACS Appl. Mater. Interfaces* **4**, 6458 (2012).

[4] L. Yang and J. Han, *Phys. Rev. Lett.* **85**, 154 (2000).

Corresponding Author: T. Okazaki and M. Tange

E-mail: toshi.okazaki@aist.go.jp and masa-tange@aist.go.jp

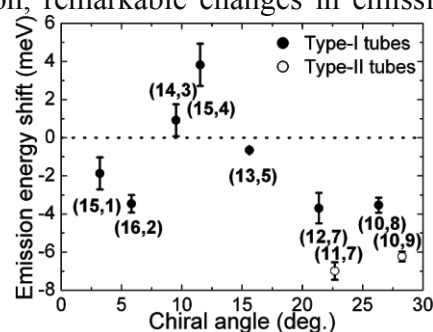


Fig. 1. Emission energy shift of PFOPy-wrapped SWCNTs relative to PFD-wrapped ones.

Simultaneous Discrimination of Diameter, Handedness, and Metallicity of Single-Walled Carbon Nanotubes with Chiral Diporphyrin Nanocalipers

○Gang Liu¹, Feng Wang¹, Songpol Chaunchaiyakul², Takahide Kimura¹, Yuji Kuwahara², Naoki Komatsu¹

¹ Department of Chemistry, Shiga University of Medical Science, Otsu 520-2192, Japan.

² Department of Precision Science and Technology, Osaka University, Osaka 565-0871, Japan

We have been developing the methodology to discriminate the handedness and diameter of SWNTs through molecular recognition using chiral diporphyrin nanotweezers such as **1** and **2** shown in Fig. 1a and 1b, respectively [1-4]. Although relatively small diameters of SWNTs (less than 1.0 nm) were recognized well [4], nanotweezers were not able to form stable complexes with the SWNTs with the diameters larger than 1.0 nm. In this context, we designed chiral diporphyrin **3** with much larger cavity; namely “nanocalipers” (Fig. 1c) [5]. The feature of the newly designed host molecule is 1) long spacer with more than 1.4 nm consisting of three aromatic moieties, 2) nearly parallel orientation of the two porphyrins, 3) restricted conformation by biaryl linkages, 4) strong interaction of two porphyrins and anthracene with the surface of a SWNT through π - π stacking, and 5) stereogenic centers at the periphery of porphyrins discriminating helicity of SWNTs.

As expected, we obtained optically active SWNTs with more than 1.0 nm in diameter (Fig. 2) and, unexpectedly, enriched metallic SWNTs over semiconducting ones. The optically active metallic SWNTs are identified for the first time, in addition to the optically active semiconducting SWNTs with such large diameters (Fig. 2). The nanocalipers are found to recognize the diameter, handedness, and metallicity of SWNTs simultaneously [5].

References

[1] G. Liu, N. Komatsu, in *Handbook of carbon nano materials*, World Scientific, **2012**; Vol. 3, p 203; [2] X. Peng, N. Komatsu, *Chem. Lett.* **2010**, 39, 1022. [3] G. Liu, N. Komatsu, *Org. Biomol. Chem.* **2012**, 10, 5830; [4] F. Wang, K. Matsuda, N. Komatsu, *J. Am. Chem. Soc.* **2010**, 132, 10876. [5] G. Liu, F. Wang, S. Chaunchaiyakul, Y. Saito, A. K. Bauri, T. Kimura, Y. Kuwahara, N. Komatsu, submitted.

Corresponding Author: Gang Liu
Tel: +81-77-548-2102, Fax: +81-77-548-2405,
E-mail: gliu@belle.shiga-med.ac.jp

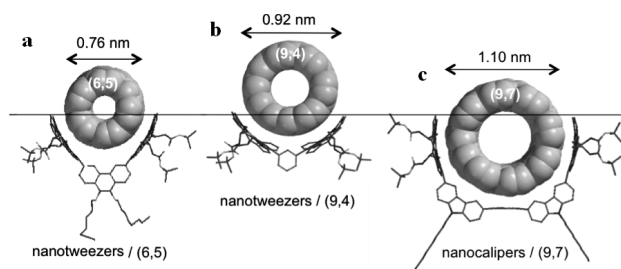


Fig. 1 Complex structures of (6,5)-, (9,4)-, and (9,7)-SWNTs with chiral diporphyrin nanotweezers **1** (a) and **2** (b), and nanocalipers **3** (c), respectively.

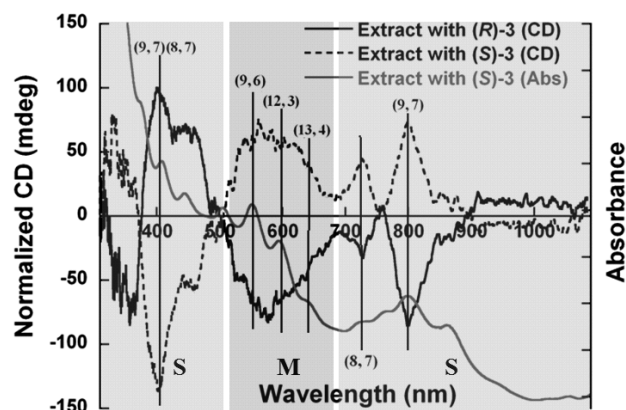


Fig. 2 CD spectra of SWNTs extracted with (R)- and (S)-**3**, and absorption spectra of SWNTs extracted with (S)-**3**.

Exchanges of sodium cholate and oligo-DNAs with different chain length on single-walled carbon nanotubes

○Ayaka Inoue¹, Yuichi Kato¹, Yasuro Niidome^{1,2}, Naotoshi Nakashima^{1,2,3}

¹ Department of Applied Chemistry, Graduate School of Engineering, Kyushu University, Fukuoka 819-0395, Japan

² WPI I2CNER, Fukuoka 819-0395, Japan

³ JST-CREST, Tokyo 102-0075, Japan

Single-walled carbon nanotubes (SWNTs) are rolled-up graphene sheets with rigid one-dimensional structures. The diameter and optical band gap of SWNTs are uniquely related to their chiral indices (n,m), which represent how the graphene sheets are rolled up. Evaluation of the interactions between solubilizing molecules and SWNTs has attracted much research. Fluorescence and Raman spectroscopies provide important information about the molecules on the SWNTs. However, such studies are not very powerful to understand the interaction between solubilizing molecules and SWNTs quantitatively.

In this work, we quantitatively evaluated exchanges of solubilizers (here sodium cholate (SC) and DNA) on SWNTs. In this method, sonication procedure is not contained, thus, denaturation of the DNA does not need to consider. The exchanges were monitored with near-IR absorption spectral changes of the solubilized SWNTs that were caused from the change in microscopic environments around the SWNTs.

We examined the exchange of SC on SWNTs using oligo-DNAs (dCn (n = 4, 5, 6, 7, 8, 10, 15, and 20)). The fractions of the DNA-solubilized SWNTs were quantitatively evaluated from the analysis of absorption spectral change of the SWNTs [1, 2]. The spectral changes of the SWNTs were fitted with Hill equation, from which K_a , ΔH and ΔS of the exchange reactions were evaluated. It was found that the exchanges of SC for dCn (n = 8-20) were endothermic, while for dCn (n = 4, 5), they were exothermic. For dC6 and dC7, the exchanges were switched from endothermic to exothermic depending on the chiralities. Notably, the thermodynamic parameters have indicated that the exchanges depend on the chiralities of the SWNTs as well as the chain length of the DNAs.

[1] Y. Kato, Y. Niidome, N. Nakashima, *Chem. Lett.* **40**, 730 (2011).

[2] Y. Kato, A. Inoue, Y. Niidome, N. Nakashima, *Scientific Reports* **2**, 733 (2012).

Corresponding Author: N. Nakashima

Tel: +81-3-802-2841, Fax: +81-3-802-2841,

E-mail: nakashima-tcm@mail.cstm.kyushu-u.ac.jp

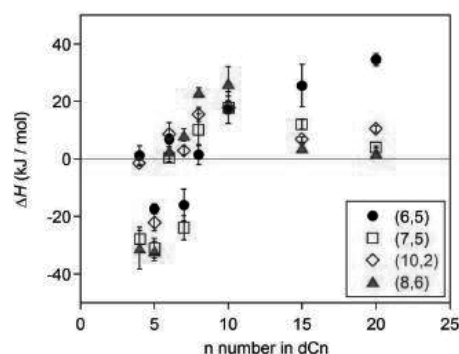


Fig. 1. Thermodynamic parameters of enthalpy changes (ΔH) for the exchanges of SC with dCn on SWNTs with different chiral indices.

Optical Properties of Polyynes Molecules Dispersed in Solids as Studied by An Ultraviolet Transmission Microscope

○Tomonari Wakabayashi, Kazunari Koma, Okinaga Shibata, Yoriko Wada

Department of Chemistry, Kinki University, Higashi-Osaka 577-8502, Japan

Linear carbon chain molecules, C_n ($n=3-15$), are highly reactive even under the cryogenic condition [1]. As they are terminated at each end by a hydrogen or a cyanide group, cyanopolynes $H(C\equiv C)_n C\equiv N$ ($n=3-6$), known as interstellar molecules ($n=3-5$), are stable enough to be isolated in organic solvents under the laboratory condition [2]. For a stable solid material, hydrogen-end-capped polyynes, $H(C\equiv C)_n H$ ($n=4-6$), are readily encapsulated inside SWNT [3], as extended to $H(C\equiv C)_n H@SWNT$ at $n=8$ [4].

Polyynes are characteristic in their optical properties related to molecular symmetry. Besides the conspicuous absorption bands in the UV, there are some weak absorption features in the near UV to visible wavelength regions [5]. The mechanism for the weak transition is suggested to be activation of an electric dipole by symmetry lowering due to nuclear displacements along a specific normal coordinate of the molecular vibration. According to the difference in the mechanisms between the allowed and forbidden transitions, directions in the transition dipole can be different [6]. The difference should be reflected on the optical spectra.

In this work, polyyne molecules are dispersed in solid materials, e.g., a transparent film with PVA (poly-vinyl alcohols), and their absorption spectra were measured in the UV-vis region. For the study on the direction of transition dipoles for polyyne molecules dispersed in the solid material, we have developed a new transmission microscope using an UV light source. The principle of the microscope, the aim of our research concerning the mechanism in optical transitions in the polyyne molecule, and some preliminary results will be introduced.

- [1] T. Wakabayashi and W. Krätschmer, "Carbon Chain Molecules in Cryogenic Matrices", Chapter 1 in *Polyynes: Synthesis, Properties, and Applications*, F. Cataldo ed., Taylor&Francis-CRC, pp.1-13 (2006).
- [2] T. Wakabayashi, M. Saikawa, Y. Wada, T. Minematsu, *Carbon* **50**, 47 (2012).
- [3] D. Nishide, T. Wakabayashi, T. Sugai, R. Kitaura, H. Kataura, Y. Achiba, H. Shinohara, *J. Phys. Chem. C* **111**, 5178 (2007).
- [4] T. Wakabayashi, T. Murakami, H. Nagayama, D. Nishide, H. Hataura, Y. Achiba, H. Tabata, S. Hayashi, H. Shinohara, *Eur. Phys. J. D* **52**, 79 (2009).
- [5] T. Wakabayashi, H. Nagayama, K. Daigoku, Y. Kiyooka, K. Hashimoto, *Chem. Phys. Lett.* **446**, 65 (2007).
- [6] T. Wakabayashi, Y. Wada, N. Iwahara, T. Sato, *J. Phys. Conf. Ser.* (2013) in press.

Corresponding Author: T. Wakabayashi

Tel: +81-6-6721-2332, Fax: +81-6-6723-2728,

E-mail: wakaba@chem.kindai.ac.jp

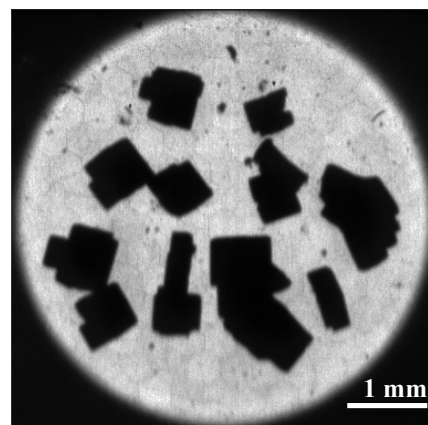


Fig. 1. UV-microscope images of crystalline α -cyclodextrin/hexane inclusion compounds containing an impurity amount of polyyne $C_{10}H_2$.

Slimy fibers of nanodiamonds assembled in polyacrylamide aqueous solutions

Shunsaku Katsuno, ◯Tadamasa Ito, Masaki Ozawa

Department of Materials Science and Engineering, Meijo University, Aichi 468-8502, Japan

Nanodiamond is a material of chemical interest. Functionalization of diamond surfaces causes no fundamental modification on the interior diamond lattices, unlike sp^2 -based materials. The outstanding chemical resistivity and hardness also facilitate chemical surface decorations. Only the problem is that such nanoparticles often form aggregates spontaneously upon addition of reactants or pH variations [1]. We had disclosed a facile method to break up those aggregates mechanically by sonication in the presence of hard ceramic beads, which in addition, can be readily incorporated in conventional glass systems for organic chemistry [2]. By using this technique, functionalization of primary nanodiamond particles can be performed even under an aggregating condition. Nanodiamonds thus functionalized are found assembled into slimy fibers, when a colloid is added into polyacrylamide aqueous solution. In this study, the assembling conditions, properties of the products, and the mechanisms were investigated.

Surface graphitized detonation nanodiamonds at 900 °C were allowed to react with diazonium salts of aryl derivatives having carboxyl or sulfo groups in aqueous media [3]. Slight amount of the resultant nanodiamond derivatives dispersed in water as well as non-functionalized nanodiamond colloids were then gave into polyacrylamide aqueous solutions. When mixed in solutions by tweezers, the dark brownish diamond colloids turned to look as sticky aggregates of fine fibers. Fig. 1(a) shows a colloid viscous enough to be pulled out from the solutions. It stretched like algae on chopsticks, but didn't shrink like elastic cords. Formation of fibrous aggregates was observed also by an optical microscope as demonstrated in Fig. 1(b). The viscosity highly depended on the surface groups of nanodiamonds as well as on the polymerization degrees of polyacrylamides. The trends indicated hydrogen bonds between amino groups of polyacrylamides and diamond surfaces playing a crucial role in the formation of those fibrous aggregates.

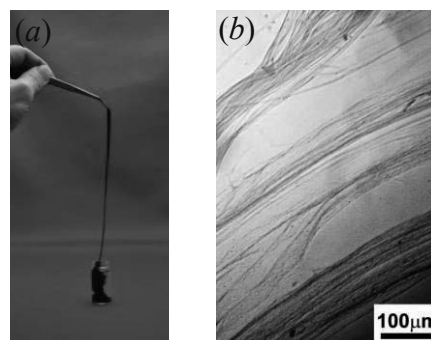


Fig.1 Slimy nanodiamond fibers assembled with polyacrylamides. (a) The sticky aggregates of nanodiamonds in a polyacrylamide aqueous solution can be pulled out from the solution. (b) Optical microscopy demonstrates formation of fibers.

[1] M. Ozawa *et al.* *Adv. Mater.* **19**, 1201 (2007).

[2] Y. Liang *et al.* *ACS Nano* **3**, 2288 (2009).

[3] Y. Liang *et al.* *J. Colloid Interface Sci.* **354**, 23 (2011).

Corresponding Author: T. Ito

Tel: +81-52-838-2410, Fax: +81-52-831-1170,

E-mail: 123434005@c alumni.meijo-u.ac.jp

Oxygen Adsorption Effect on Graphene–Metal Contact Characteristics

○Yoshiaki Sato, Kazuyuki Takai, Toshiaki Enoki

Department of Chemistry, Tokyo Institute of Technology, Tokyo 152-8551, Japan

Understanding the electron transport properties through the graphene–metal contact is crucial to realize high-performance graphene-based electronic devices. Recent studies have revealed that the long-range band bending [1] and the resistive carrier injection [2] at the contact region result in modification of carrier transport properties in graphene device, which are attributed to the small density of state of graphene and the charge transfer interactions at graphene–metal interface. Though these contact properties are inevitably affected by ambient through the various interactions with gas species, details still remain unclear. In the present study, we investigate the oxygen adsorption effect on the graphene–metal contact junction properties comparing various kinds of metals for contact materials.

Graphene flakes were obtained by “sticky-tape” method on SiO₂ (90 nm)/n⁺⁺-Si substrate. Attaching Cr (3 nm)/Au (30 nm) or Pd (25 nm) contacts to graphene, typical back-gated field-effect transistor (FET) structure was fabricated by means of photolithography. To enhance the electron transport characteristics in the vicinity of the contact region, we used short-channel devices with graphene channel length of $\lesssim 1 \mu\text{m}$. Conductivity measurements were performed under high vacuum ($< 10^{-5}$ Pa) at room temperature after fully eliminating surface contamination by vacuum annealing of graphene device (200 °C, over 10 h).

The top panels of Fig. 1 show resistance (R) of graphene FETs as a function of gate-bias voltage (V_g). Irrespective of contact materials, the gate-bias voltage giving resistance peak ($V_{g,\text{CNP}}$) gradually shifts towards $V_g > 0$ direction from its original position ($V_{g,\text{CNP}} \sim 0$ V) with increasing time of O₂ gas exposure, which indicates that the adsorbed oxygen species bring hole doping on graphene channel [3]. In contrast, asymmetric components in R vs V_g curves, $R_{\text{odd}} = R(\Delta V_g) - R(-\Delta V_g)$ with $\Delta V_g = V_g - V_{g,\text{CNP}}$, strongly depends on contact materials (the bottom panels of Fig. 1). The positive (negative) R_{odd} in $\Delta V_g > 0$ region was observed for devices with Pd (Cr/Au) contacts before exposure to O₂ gas, which is explained by p -type (n -type) feature of pristine Pd (Cr/Au) contacts. However, the exposure to O₂ gas drastically changes all the metal contacts to p -type, at much shorter time scale (< 1 min) than progress of hole doping to the graphene channel. These results suggest the extreme sensitivity of graphene–metal contact to oxygen adsorption.

[1] R. Nouchi & K. Tanigaki *Jpn. J. Appl. Phys.* **50**, 070109 (2011) [2] F. Xia *et al.*, *Nat. Nanotechnol.* **6**, 179 (2011) [3] Y. Sato, K. Takai & T. Enoki *Nano Lett.* **11**, 3468 (2011)

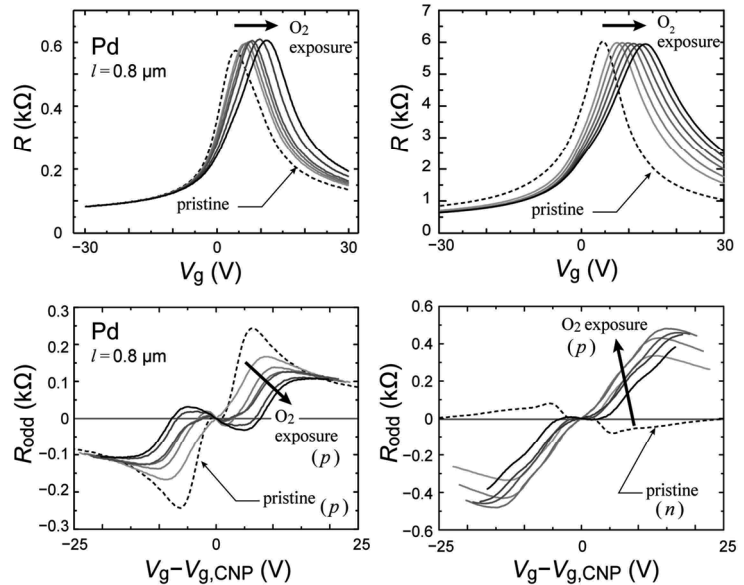


Fig.1 The R vs V_g characteristics (top panels) and their odd parts (bottom panels) for pristine and for O₂-exposed ($t = 0.5, 1, 2, 4, 8, 16$ min) devices attached with Pd or Cr/Au contacts.

Corresponding Author: T. Enoki
Tel: +81-3-5734-2242
E-mail: enoki.t.aa@m.titech.ac.jp

Atomic structure determination of the graphene/sapphire interface by normal incident X-ray standing wave spectroscopy

○Shiro Entani¹, Pavel B. Sorokin², Pavel V. Avramov¹, Manabu Ohtomo¹, Yoshihiro Matsumoto¹, Liubov Yu. Antipina², Ayumi Narita³, Norie Hirao³, Iwao Shimoyama³, Tetsuhiro Sekiguchi³, Hiroshi Naramoto¹, Yuji Baba³, and Seiji Sakai¹

¹Advanced Science Research Center, Japan Atomic Energy Agency, Tokai, 319-1195, Japan

²Technological Institute for Superhard and Novel Carbon Materials, Moscow, 142190, Russian Federation

³Quantum Beam Science Directorate, Japan Atomic Energy Agency, Tokai, 319-1195, Japan

Direct growth of graphene films on insulating substrates is one of the most important subjects for graphene-based nanoelectronics and spintronics. Despite such interest, the atomic structure and interactions at the graphene/insulator interface have not been studied extensively. Normal incident X-ray standing wave (NIXSW) spectroscopy is a powerful tool for investigating heterointerfaces, because the vertical arrangement of atoms on the single-crystal surface can be determined precisely and element-specifically [1]. The vertical atomic arrangement at the interface could be also a criterion for the interface interactions. In this study, the interface between *c*-plane sapphire (α -Al₂O₃(0001)) and single-layer graphene (SLG) directly grown on the surface has been studied by NIXSW spectroscopy.

The graphene growth on α -Al₂O₃(0001) was performed in a vacuum quartz tube furnace with a base pressure of 2×10^{-6} Pa. The SLG film was grown by exposing the α -Al₂O₃(0001) surface to methanol vapor in a pressure of 1000 Pa at the substrate temperature of 1273 K. The NIXSW measurements were conducted at the BL-27A station (the details of the measurement method are described in Ref. 2). The NIXSW profiles were obtained by recording the intensities of the Al 1s, O 1s and C 1s photoelectrons as a function of the photon energy, respectively.

Figure 1 shows the C 1s NIXSW profile for the C atoms in SLG/ α -Al₂O₃(0001) and the vertical atomic arrangement at the interface obtained by the NIXSW measurements. The vertical location of the SLG layer is estimated to be 2.6 Å from the top of the α -Al₂O₃(0001) surface. This value lies between the interlayer distance in graphite (3.35 Å) and the distance between SLG and the Ni(111) surface (2.12 Å) [3], suggesting rather strong interaction at the SLG/ α -Al₂O₃(0001) interface. The details and origins of the strong interface interaction will be discussed with results of *ab initio* calculations.

[1] D.P. Woodfuff *et al.* Phys. Rev. Lett. **58**, 1460 (1987).

[2] S. Baba *et al.* e-J. Surf. Sci. Nanotech. **10**, 69 (2012)

[3] Y. Gamo *et al.* Surf. Sci. **374**, 61 (1997)

Corresponding Author: S. Entani

Tel: +81-29-284-3802, Fax: +81-29-282-5939,

E-mail: entani.shiro@jaea.go.jp

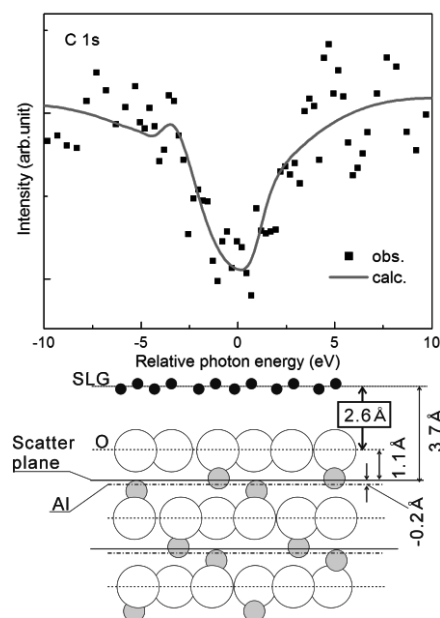


Fig. 1 C 1s NIXSW profile. The solid line represents the best-fit result(top), and the schematic representation of the atomic structure at SLG/ α -Al₂O₃(0001) interface (bottom).

Integration of high performance graphene nanoribbon field effect transistors

○Toshiaki Kato, Rikizo Hatakeyama, and Toshiro Kaneko

Department of Electronic Engineering, Tohoku University, Sendai 980-8579, Japan

Graphene nanoribbons combine the unique electronic and spin properties of graphene with a transport gap that arises from quantum confinement and edge effects. This makes them an attractive candidate material for the channels of next-generation transistors. Although nanoribbons can be made in a variety of ways, the reliable site and alignment control of nanoribbons with high on/off current ratios remains a challenge. Plasma chemical vapor deposition (CVD) is known as a fruitful method for the structural-controlled growth and damage-free functionalization of nano carbon materials such as carbon nanotubes (CNTs) [1-3] and graphene [4,5]. We have developed a new, simple, scalable method based on the advanced plasma CVD method for directly fabricating narrow (~23 nm) graphene nanoribbon devices with a clear transport gap (58.5 meV) and a high on/off ratio ($>10^4$) (Fig.1). Since the establishment of our novel graphene nanoribbon fabrication method, direct conversion of a Ni nanobar to a graphene nanoribbon is now possible. Indeed, graphene nanoribbons can be grown at any desired position on an insulating substrate without any post-growth treatment, and large-scale, two- and three dimensional integration of graphene nanoribbon devices should be realizable [6].

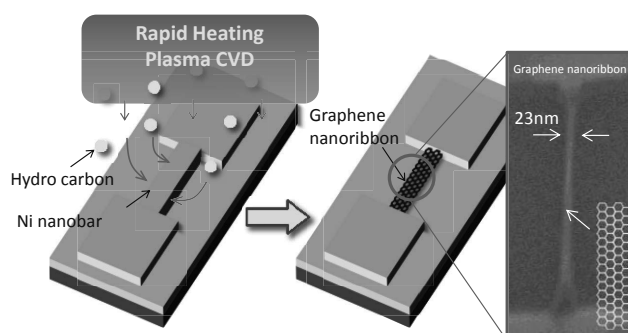


Fig. 1: Schematic illustration of graphene nanoribbon growth process.

- [1] T. Kato and R. Hatakeyama, *J. Am. Chem. Soc.* **130**, 8101 (2008).
- [2] T. Kato and R. Hatakeyama, *ACS Nano* **4**, 7395 (2010).
- [3] Z. Ghorannevis, T. Kato, T. Kaneko, and R. Hatakeyama, *J. Am. Chem. Soc.* **132**, 9570 (2010).
- [4] T. Kato, L. Jiao, X. Wang, H. Wang, X. Li, L. Zhang, R. Hatakeyama, and H. Dai, *Small* **7**, 574 (2011).
- [5] T. Kato and R. Hatakeyama, *ACS Nano* **6**, 8508 (2012).
- [6] T. Kato and R. Hatakeyama, *Nature Nanotechnology* **7**, 651 (2012).

Corresponding Author: T. Kato

Tel: +81-22-795-7046, Fax: +81-22-263-9225,

E-mail: kato12@ecei.tohoku.ac.jp

Transport Property of CVD Graphene across Domain Boundary

◦Yui Ogawa,¹ Kenji Kawahara,² Masahiro Miyashita,¹ Masaharu Tsuji^{1,2}
Katsuyoshi Komastu,³ Kazuhito Tsukagoshi,^{3,*} and Hiroki Ago^{1,2,*}

¹*Graduate School of Engineering Sciences, Kyushu University, Fukuoka 816-8580, Japan*

²*Institute for Materials Chemistry and Engineering, Kyushu University, Fukuoka 816-8580, Japan*

³*International Center for Materials Nanoarchitectonics (WPI-MANA),
National Institute for Materials Science (NIMS) Ibaraki 305-0044, Japan*

Chemical vapor deposition (CVD) growth of graphene on Cu catalyst has attracted an interest for large area and low cost synthesis. The CVD graphene has multi domain structure with a number of domain boundaries [1] which limit the physical properties [2,3]. Therefore, it is important to investigate and control the domain structure of CVD graphene [4,5]. We previously reported the orientation-controlled graphene produced by epitaxial CVD growth using single-crystalline Cu and Co films [5-7]. And, we found that two neighboring graphene domains merged with a different angle always give the Raman D-band at its domain boundary. On the other hand, two merged domains with the identical angle sometimes gave no D-band at the domain boundary [8].

In this study, we investigated the transport properties of two merged domains in terms of the effect of the domain boundary by fabricating graphene field effect transistor (FET). Large hexagonal graphene domains with three main relative orientations, 0, 30, and -10 degrees were synthesized by CVD at 1075 °C on the hetero-epitaxial Cu(100) film. We measured the carrier transport within a hexagonal domain (intra-domain) and over two merged domains (inter-domain) for two types of merged domains; merged with the identical angle and different angles. The inter-domain region showed higher resistivity than the intra-domain region irrespective of merged angle. This phenomenon was observed not only for the domains with different angles but also for those with the identical angle. Our results suggest that defects formed at the domain boundary cause electron scattering and reduce carrier mobility. We will also discuss a relationship between Raman D-band and the transport property.

References:

[1] P. Y. Huang *et al.*, *Nature* **469**, 389 (2011). [2] H. S. Song *et al.*, *Sci. Rep.* **2**, 1 (2012). [3] C. M. Orofeo *et al.*, *Carbon* **50**, 2189 (2012). [4] Q. Yu *et al.*, *Nat. Mater.* **10**, 443 (2011). [5] Y. Ogawa *et al.*, *J. Phys. Chem. Lett.* **3**, 2 (2012). [6] H. Ago *et al.*, *ACS Nano* **4**, 1414 (2010). [7] B. Hu *et al.*, *Carbon* **50**, 57 (2012). [8] Y. Ogawa *et al.*, The 43rd Fullerenes-Nanotubes-Graphene General Symposium, 3P-8

Corresponding Authors (H. Ago : ago@cm.kyushu-u.ac.jp, K. Tsukagoshi : TSUKAGOSHI.Kazuhito@nims.go.jp)

Fabrication of CMOS inverters using semiconducting SWCNTs encapsulating n- and p-type dopant molecules

○Yasuhiro Ito^{1,2}, Shunjiro Fujii^{1,2}, Maki Shimizu^{1,2}, Takeshi Tanaka¹, Hiromichi Kataura^{1,2}

¹ *Nanosystem Research Institute, National Institute of Advanced Industrial Science and Technology (AIST), Tsukuba, Ibaraki, 305-8562, Japan*

² *Japan Science and Technology Agency, CREST, Kawaguchi, Saitama, 330-0012, Japan*

A thin film transistor (TFT) using semiconducting single-wall carbon nanotube (s-SWCNTs) is promising for low-cost and high-performance printed electronics applications. For the practical applications to logic circuits such as a complementary metal-oxide semiconductor (CMOS) type operation, n- and p-type s-SWCNTs are both necessary. It is known that a chemical doping can fabricate n- and p-type s-SWCNT TFTs. However, the external doping requires additional patterning process that is not suitable to the printed electronics. In this work, we tried carrier control of TFT channel by an internal chemical doping using molecular encapsulation into s-SWCNTs.

Semiconducting APJ-type SWCNTs ($\phi = \sim 1.4$ nm) were purified by a gel column chromatography method [1]. N- and p-type s-SWCNT inks using aqueous sodium deoxycholate suspensions were prepared by inserting cobaltocene and F₄TCNQ (2,3,5,6-tetrafluoro-7,7,8,8-tetracyanoquinodimethane) molecules into the s-SWCNTs, respectively. Then n- and p-type TFTs were successfully prepared on SiO₂/Si substrates with Ti/Au electrode [2]. Figure 1a and b show the transfer characteristics of cobaltocene and F₄TCNQ encapsulated s-SWCNT-TFTs measured under vacuum, respectively. These TFTs showed almost n- and p-type transfer characteristics. These results suggest that electron and hole carrier densities in s-SWCNTs can be controlled by molecular encapsulation. Furthermore, the CMOS inverter operation was confirmed (figure 2). Typical voltage gain was 10. To our knowledge, this result is the world-first demonstration of CMOS inverter operation fabricated simply using molecular encapsulating s-SWCNTs.

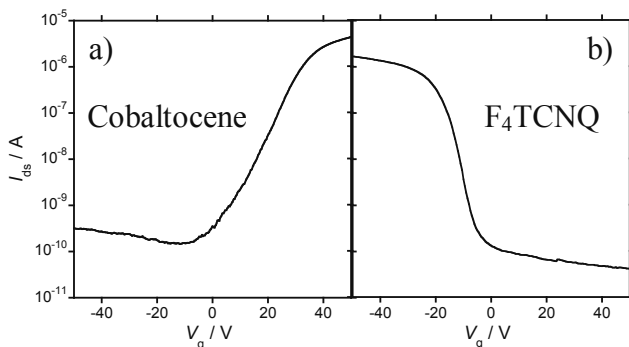


Fig.1 Transfer characteristics of the (a) cobaltocene and (b) F₄TCNQ encapsulated s-SWCNT-TFTs under vacuum (7.4×10^{-6} Torr). The channel length and width are 100 and 200 μm , respectively. The

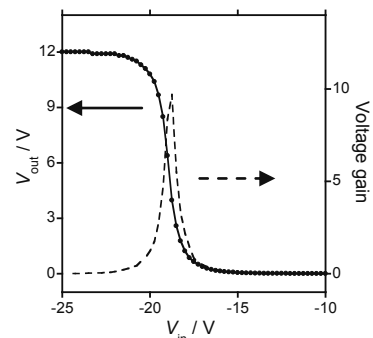


Fig.2 Output characteristics of the CMOS inverter constructed with molecular encapsulated s-SWCNT-TFTs. The power supply voltage (V_{dd}) was 12 V. Voltage gain of the devices was around 10.

[1] Y. Miyata *et al.*, *Nano Res.*, **4**, 963 (2011). [2] S. Fujii *et al.*, *Phys. Stat. Sol. B* **248**, 2692 (2011).

Corresponding Author: Hiromichi Kataura

E-mail: h-kataura@aist.go.jp **Tel:** +81-29-861-2551, **Fax:** +81-29-861-2786

Micro-Honeycomb Network Structure of Single-Walled Carbon Nanotube Film for Solar Cells

○Kehang Cui¹, Takaaki Chiba¹, Hidenori Kinoshita¹, Pei Zhao¹, Theerapol Thurakitserree¹, Taiki Inoue¹, Erik Einarsson², Shohei Chiashi¹, Shigeo Maruyama¹

¹Department of Mechanical Engineering, The University of Tokyo, Tokyo 113-8656, Japan

²Global Center of Excellence for Mechanical Systems Innovation, The University of Tokyo, Tokyo 113-8656, Japan

To bridge the superior nanoscale electrical, optical, thermal and mechanical properties of single-walled carbon nanotubes (SWNTs) with corresponding device-level performance, the micro/macroscale morphologies of SWNTs are of great importance. We propose here a self-organized micro-honeycomb network structure of single-walled carbon nanotubes (SWNTs) obtained by water vapor treatment of as-synthesized vertically aligned SWNTs (VA-SWNTs) [1] for a SWNT/n-Si heterojunction solar cell [2-6]. Dependence of photovoltaic conversion efficiency (PCE) on the nanotube network structure was examined.

The VA-SWNTs were synthesized by the standard alcohol-catalytic CVD method with Co/Mo dip-coated on Si/SiO₂ substrate [1]. The micro-honeycomb structured film was obtained by exposing the VA-SWNT film to water vapor. Changing the exposure conditions resulted in different morphologies (Fig. 1).

Figure 2 shows current density and voltage (J-V) characteristics of the SWNT-Si heterojunction solar cells. The optimal photovoltaic conversion efficiency (PCE) under AM1.5 is 5.04%, with a fill factor of 59.2%. The open-circuit voltage and short-circuit current are 0.53V and 16.06 mA/cm², respectively. This showed a substantial improvement compared with previously reported results [3-6]. We attribute the improvement to the self-organizing micro-honeycomb network, in which the random SWNTs in good contact with the Si serve as the charge carrier separation interface, and the artery-like condensed SWNTs serve as hole collector and transport highway.

Part of this work was financially supported by Grant-in-Aid for Scientific Research (22226006, 19054003), JSPS Core-to-Core Program, and Global COE Program 'Global Center for Excellence for Mechanical Systems Innovation'.

[1] Y. Murakami et al., Chem. Phys. Lett., 385 (2004) 298.

[2] Y. Jia et al., Adv. Mat., 20 (2008) 4594.

[3] P. Wadhwa et al., Nano Lett., 10 (2010) 5001.

[4] D. Kozawa et al., Appl. Phys. Express, 5 (2012) 042304.

[5] P. Ong et al., Nanotechnology, 21 (2010) 105203.

[6] Y. Jia et al., Mater. Res. Bull., 45 (2010) 1401.

Corresponding Author: S. Maruyama

Tel: +81-3- 5841-6421, Fax: +81-3-5800-6983,

E-mail: maruyama@photon.t.u-tokyo.ac.jp

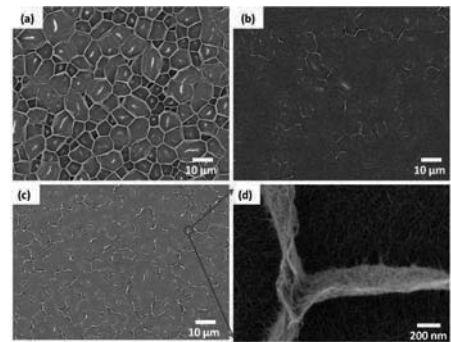


Figure 1 (a, b, c) SEM morphologies of self-organizing micro-honeycomb networks of SWNTs; (d) enlarged image of condensed SWNTs bundles from c.

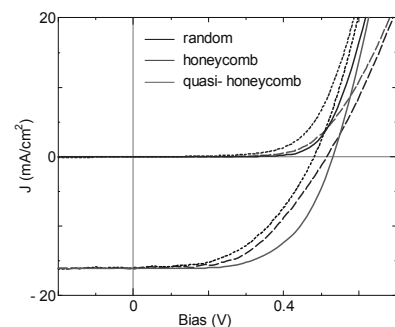


Figure 2 J-V characteristics of SWNT devices with random, honeycomb and quasi-honeycomb morphologies under dark and AM1.5

Application of Vertically Aligned CNTs for Electrodes of PEMFC

○Shigeaki Murata, Masahiro Imanishi, Shigeaki Hasegawa, Ryoichi Namba

Fuel Cell System Development Division, Toyota Motor Corporation, Susono 410-1193, Japan

The fabrication process of the conventional fuel cell electrode is basically not changed from the beginning of 1990s [1]. It is ink-based process and the structure of the electrodes, such as thickness, porosity or pore size, is fixed through the process condition. An alternative structure and process is desired in which the structure can be designed and controlled. We successfully developed an electrode of polymer electrolyte membrane fuel cells making high current density operation possible using vertically aligned carbon nanotubes (CNTs) as the catalyst support, and also prepared membrane electrodes assemblies (MEAs) applicable size for vehicle use. Fig. 1 shows the concept of the electrodes. The structure of the electrodes improved the mass transport of the reactance in electrodes and made it possible to perform $2.6\text{A}/\text{cm}^2$ @ 0.6V with $0.1\text{mgPt}/\text{cm}^2$ @Cathode. The mechanism to improve the mass transport was concluded that the continuity of the pore, no agglomeration of catalyst supports by SEM observation (Fig.2) and better contact between catalyst layer and micro porous layer by evaluation tests of the elasticity of the CNTs.

CNTs were grown on stainless steel substrate by CVD method developed by Hitachi Zosen Corporation [2]. The specification of the CNTs is listed in Table 1. Platinum was deposited on the CNTs by conventional impregnation/H₂-reduction method. The solution of the Pt salt was converted from water base acid to ethanol. After the platinum deposition, the Pt/CNTs was coated with ionomer by applying an ethanol-diluted ionomer solution and drying it. The water content of the ionomer solution should be decreased lower than 2%. MEAs were fabricated by hot-pressing the ionomer coated Pt/CNTs electrodes to electrolyte membrane at 140 deg.C and peeling off the substrate. It was the key point to apply the wavy CNTs having resistance against agglomeration and to change the solutions to lower surface tension ones. The CNTs compressed in the cells were no more vertically aligned (Fig.2). It was concluded that the property vertically aligned served an important function in MEA fabrication process but was not critical for the cell performance.

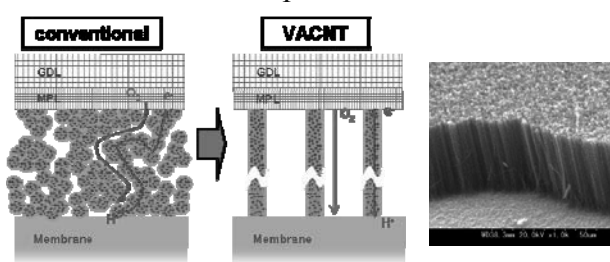


Fig. 1. Concept of VACNT Electrodes.

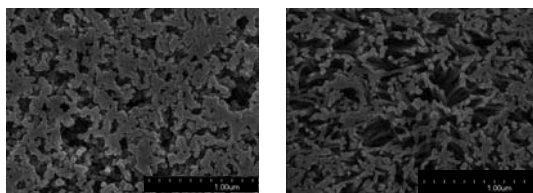


Fig. 2. Cross Section of Electrodes.
Left: Conventional, Right: CNTs.

Table 1. Specification of CNTs.

Length	40-60 μm
Tortuosity	2
Diameter	20nm
Number Density	$3 \times 10^9/\text{cm}^2$
Average Distance	200nm
Weight	0.3mg/cm ²
SSA	200m ² /g

[1] M. S. Wilson and S. Gottesfeld, *J. Appl. Electrochem.*, 22 (1992) 1-7.

[2] H. Shioyama, Y. Yamada, Y. Sairyō: *TANSO*, 209 (2003), 171-173 (in Japanese).

Corresponding Author: S. Murata

Tel: +81-55-997-7987, Fax: +81-55-997-7120,

E-mail: shigeaki@murata.tec.toyota.co.jp

Electromigration suppression in copper by carbon nanotubes : A mechanistic insight

○Chandramouli Subramaniam¹, Takeo Yamada^{1,2}, Don N. Futaba^{1,2}, Kenji Hata^{1,2} and Motoo Yumura^{1,2}

¹ *Technology Research Association for Single Wall Carbon Nanotubes (TASC), Central 5, 1-1-1 Higashi, Tsukuba 305-0046, Japan.*

² *National Institute of Advanced Industrial Science and Technology (AIST), Central 5, 1-1-1 Higashi, Tsukuba 305-0046, Japan.*

Recently, we reported a 100 times enhancement in the current-carrying-capacity of copper by using super-growth carbon nanotubes (CNT). Such high current-carrying-capacity offers diverse areas of applications ranging from miniaturized electronics components to heavy duty transmission cables. Here, we present mechanistic insights to explain the higher current-carrying-capacity of CNT-Cu composite compared to any metal.

First, we experimentally estimate the activation energy for Cu diffusion in CNT-Cu composite, from Black's theory of electromigration. The value estimated thus for CNT-Cu composite (2.1 eV) corresponds with the activation energy of Cu lattice/bulk diffusion in pure Cu (2.0 – 2.3 eV). This is also higher than Cu diffusion value at surface (~1.0 eV) and grain-boundaries (~1.2 eV) in pure Cu. Thus, we interpret that the CNT present in CNT-Cu composite suppresses the diffusion of Cu at surface and grain boundaries (easiest failure pathways). Cu bulk diffusion being the most difficult pathway (requiring the highest activation energy) provides the CNT-Cu composite with higher stability against electromigration and consequently higher current-carrying-capacity.

Second, from the activation energy analysis, we estimate the diffusion coefficient, D^* which is related to the ease of electromigration.

$$D^* = D_0 \exp\left(\frac{-E_a}{kT}\right)$$

where, D_0 is the diffusion coefficient at infinity ($\sim 10^{-8}$ cm²/s), E_a is the activation energy, k the Boltzmann constant and T the temperature. The estimated D^* of Cu in the CNT-Cu composite (3.7×10^{-31} cm²/s) by bulk diffusion was 10^4 times lower than that of copper (2.2×10^{-27} cm²/s), which should significantly contribute to the observed high current-carrying-capacity.

Finally, we numerically estimate the maximum-allowable current through the CNT-Cu composite before material-failure from Joule-heating. The current-carrying-capacity estimated thus (1200 MA/cm²) is in good agreement with the experimentally observed value (600 MA/cm²), validating our understanding.

In conclusion, we understand that the CNT in CNT-Cu composite plays a significant role in suppressing Cu diffusion and providing it with superior electrical properties than metals. This effect is analogous to the well-known practice alloying steel with carbon for strengthening.

Corresponding Author: Kenji Hata

Tel: +81-298614654, Fax: +81-298614851,

E-mail: kenji-hata@aist.go.jp

First-Principles Simulation on Thermoelectric Power of SWNT Buckypapers

○Tepei Kato¹, Shinji Usui², Takahiro Yamamoto^{1,3}

¹Dept. of Electrical Engineering, Tokyo Univ. of Science, Chiyoda-ku, Tokyo 102-0073, Japan

²QuantumWise Japan KK, Shinjuku-ku, Tokyo 160-0023, Japan

³Dept. of Liberal Arts, Tokyo Univ. of Science, Chiyoda-ku, Tokyo 102-0073, Japan

An SWNT buckypaper is expected to be a ubiquitous thermoelectric material with large thermoelectric power factor. Recent experiments reported that the temperature dependence and doping dependence of Seebeck coefficient (thermoelectric power) of SWNT buckypapers are essentially different from those of an individual SWNT [1,2]. However, such unusual behaviors of Seebeck coefficient of SWNT buckypapers have not been understood yet. In this study, we clarify the Seebeck coefficient of SWNT buckypapers by performing the first-principles simulation based on density-functional theory and the none-equilibrium Green's function method [3]. We consider that the above unusual behaviors originate from the contacts between SWNTs, and we set a simulation model consisting of the laterally-contacted SWNTs as shown in Fig.(a). The obtained results are as follows.

- (1) Seebeck coefficients exhibit larger value of the order of $100\mu\text{V/K}$ at the room temperature.
- (2) The sign of Seebeck coefficient can change at the low temperature.
- (3) The temperature dependence of Seebeck coefficient is sensitive to small changes of the chemical potential.

These simulation results are in good agreements with experimental results and can be understood in terms of Mott's formula.

References

- [1] Hone *et al.*, Phys. Rev. Lett. **80**, 1042 (1998).
 [2] Bradley *et al.*, Phys. Rev. Lett. **85**, 4361 (2000).
 [2] <http://quantumwise.co.jp/>

Corresponding Authors: Takahiro Yamamoto

TEL&FAX: +81-3-5213-0990

E-mail: takahiro@rs.tus.ac.jp

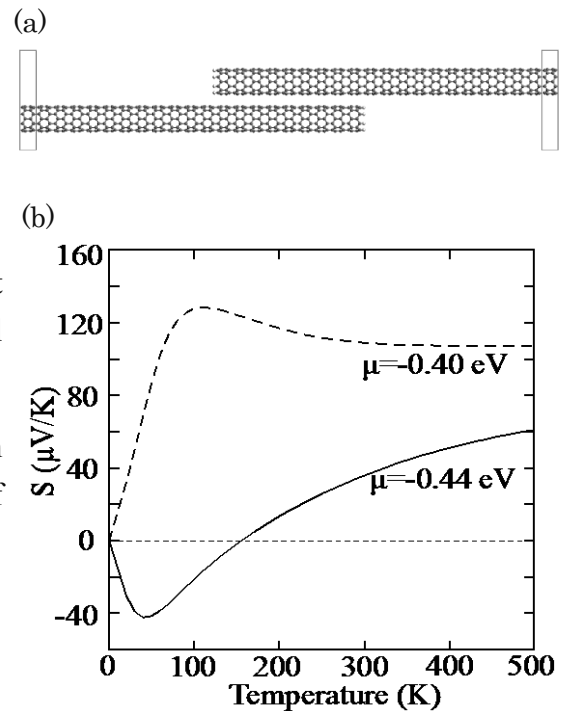


Fig.: (a) (8,0)/(8,0)SWNT contact,
 (b) T -dependence of Seebeck coefficient.

Influence of Carbon nano-inclusion dimensionality in the thermal conductivity enhancement of aqueous and non-aqueous fluids

○ Sivasankaran Harish¹, Kei Ishikawa¹, Erik Einarsson^{1,2}, Shohei Chiashi¹,
Junichiro Shiomi¹, Shigeo Maruyama¹

¹*Department of Mechanical Engineering, The University of Tokyo, 7-3-1 Hongo, Bunkyo-ku,
Tokyo 113-8656, Japan.*

²*Global Center of Excellence for Mechanical Systems Innovation, The University of Tokyo,*

7-3-1 Hongo, Bunkyo-ku, Tokyo 113-8656, Japan.

In the present work we systematically investigate the thermal conductivity enhancement of water, ethylene glycol and phase change alkane *n*-Octadecane in the presence of spherical, one-dimensional and two-dimensional carbon nano inclusions. Single-walled carbon nanohorns, single-walled carbon nanotubes and exfoliated graphite nanoplatelets were used as the nano inclusions. Thermal conductivity measurements were carried out using a transient hot-wire technique for different temperature and loadings of nano inclusions. It was found that two-dimensional inclusions lead to higher thermal conductivity improvement followed by one-dimensional and spherical inclusions. Solidification of *n*-Octadecane resulted in higher thermal conductivity enhancement in the solid state compared to the liquid state irrespective of the dimensionality of the nano inclusion. In the solidified state carbon nanotubes outperformed graphite nanoplatelets and carbon nanohorns due to their ability to form percolating networks at low loading. Viscosity measurements show that the viscosity of suspensions increases linearly with increasing nano-inclusion loading. The potential mechanism behind the thermal conductivity enhancement and the critical yet detrimental role of thermal boundary resistance in limiting the heat conduction is discussed, and the experimental results are compared with classical heat conduction models and other results in the literature.

[1] S. Harish *et al.* Int. J. Heat Mass Transfer, **55**, 3885 (2012)

[2] S. Harish *et al.* Int. Mater. Express, **2**, 213 (2012)

Corresponding Author: Prof. Shigeo Maruyama

Tel: +81-3-5874-6421

E-mail: maruyama@photon.t.u-tokyo.ac.jp

First Principles-Based Estimate of the Critical SWCNT Length for Raman D and G Band Intensity Inversion

○Yoshifumi Nishimura¹, Henryk A. Witek², Stephan Irle¹

¹ Department of Chemistry and Institute of Transformative Bio-Molecules, Nagoya University, Nagoya 464-8602, Japan

² Department of Applied Chemistry and Institute of Molecular Science, National Chiao Tung University, Hsinchu 30010, Taiwan

We present theoretical prediction of physical and spectroscopic properties of hydrogen-terminated single-walled carbon nanotube (SWCNTs) model systems containing up to ~1000 atoms on the basis of the self-consistent-charge density-functional tight-binding (SCC-DFTB) [1] method. Employing our implementation of analytical second-order geometrical derivatives [2] and specifically developed parameter sets [3], this approximate density functional theory (DFT) method has already demonstrated the accurate calculations of vibrational frequencies and infrared (IR) and Raman intensities for fullerenes [4] and nanodiamonds [5] in excellent agreement with standard DFT for the smaller model systems. Here, evolution of SWCNT molecular models with respect to elongation of tube length and different diameter size is focused on.

For example, simulations of Raman spectra for armchair (n, n) SWCNTs with $n = 3$ to 7 at a fixed length of 8 nm (largest model: C₉₂₄H₂₈) confirm the previously found quantitative inverse relationship between tube diameter and radial breathing mode (RBM) frequency [6] (See Fig. 1). Fig. 2 shows the length dependence of Raman intensities for hydrogen-terminated (5,4) SWCNTs with lengths ranging from 1 to 10 nm, i.e. C₈₀H₁₈ to C₇₄₀H₁₈, indicating the critical SWCNT length for Raman D to G band intensity inversion is already observed around 1 nm.

In our presentation, other properties – IR spectra, electronic and vibrational density of states, and HOMO-LUMO gaps of the various SWCNT finite systems will be discussed together with the comparison of corresponding bulk quantities.

- [1] M. Elstner *et al.*, *Phys. Rev. B*, **58**, 7260 (1998).
 [2] H. A. Witek *et al.*, *J. Chem. Phys.*, **121**, 5163, (2004).
 [3] E. Małolepsza *et al.*, *Chem. Phys. Lett.*, **412**, 237, (2005).
 [4] H. A. Witek *et al.*, *J. Chem. Phys.*, **125**, 214706, (2006).
 [5] W. Li *et al.*, *ACS Nano*, **4**, 447, (2010).
 [6] A. Jorio *et al.*, *Phys. Rev. Lett.*, **86**, 1118, (2001).

Corresponding Author: S. Irle

Tel: +81-52-747-6397, Fax: +81-52-747-6397

E-mail: sirle@chem.nagoya-u.ac.jp

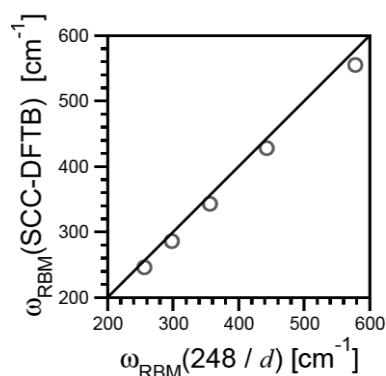


Fig.1 Correlation between SCC-DFTB harmonic frequency and inverse relationship of diameter [6] for RBM mode.

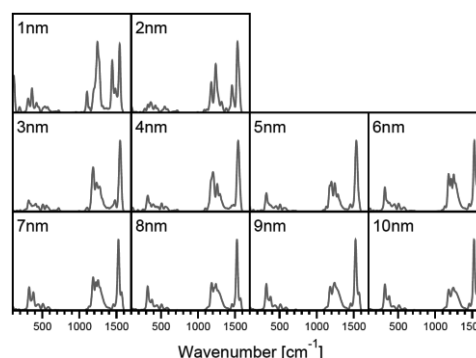


Fig.2 SCC-DFTB simulated Raman spectra of hydrogen-terminated (5,4) SWCNTs with increasing tube length from 1 to 10 nm.

Exciton effects on coherent phonon spectroscopy of carbon nanotubes

○ Ahmad R.T. Nugraha, Eddwi H. Hasdeo, Riichiro Saito
Department of Physics, Tohoku University, Sendai 980-8578, Japan

In this work, we consider ultrafast carrier dynamics and coherent phonons in carbon nanotubes by taking into account exciton effects. In an ultrafast pump-probe spectroscopy, femtosecond laser pump pulses applied to a SWNT sample induce photo-excited electron-hole pairs bound by the Coulomb interaction, called as excitons [1]. Shortly after the exciton relaxations to the lowest exciton states (~ 10 fs), the coherent lattice vibrations are generated by the exciton-phonon interactions. The coherent phonon motions can be observed as oscillations of either the differential transmittance or reflectivity of the probed light as a function of delay time between pump and probe pulses. By taking a Fourier transformation of the oscillations in the light transmission or reflection with respect to time, we obtain coherent phonon spectra as a function of phonon frequencies. The most easily observed coherent phonon modes in SWNTs are the so-called radial breathing mode, in which the tube diameter can initially expand or contract depending on the family classification and excitation energies [2]. Previously, we developed a microscopic theory for the generation and detection of coherent phonons in SWNTs within an extended tight binding model and effective mass theory [3]. We found that such expansion and contraction simply originate from k -dependent electron-phonon interaction in SWNTs.

However, we neglected the presence of excitons in SWNTs which have a strong binding energy even at room temperature [1]. Exciton effects should give the Gaussian-like driving force in the real space instead of the constant driving force considered previously. Therefore, we modify the coherent phonon equation motion by including the spatial dependence based on a periodic Gaussian structure. The equation of motion for the coherent phonons is modeled phenomenologically in terms of the Klein-Gordon equation, from which we can solve for the oscillations amplitudes as a function of space and time. By taking an average of the calculated amplitudes per nanotube length, we obtain time-dependent coherent phonon amplitudes that resemble homogeneous oscillations observed in the pump-probe experiments. This leads to a hypothesis that the pump-probe measurements are only able to see a spatial average of coherent phonon oscillations over the wavelength of light in carbon nanotubes. We then calculate the time-dependent absorption spectra as a result of macroscopic atomic displacements induced by the coherent phonon oscillations and thus reproduce the oscillation feature of the transmission or reflectance in the pump-probe spectroscopy experiments.

[1] J. Jiang et al., *Phys. Rev. B* **75**, 035405 (2007).

[2] J.-H. Kim et al., *PRL* **102**, 037402 (2009); Y.-S. Lim et al., *ACS Nano* **4**, 3222-3226 (2010).

[3] G. D. Sanders et al., *PRB* **79**, 205434 (2009); A. R. T. Nugraha et al., *PRB* **84**, 174302 (2011).

Corresponding Author: A. R. T. Nugraha

TEL: +81-22-795-6442, FAX: +81-22-795-6447, E-mail: nugraha@flex.phys.tohoku.ac.jp

High-temperature *in-situ* TEM Observation of Zipper-like Wall-to-Wall Coalescence of Double-Wall Carbon Nanotubes

○ Sihan Zhao, Ryo Kitaura, Yasumitsu Miyata and Hisanori Shinohara
Department of Chemistry & Institute for Advanced Research, Nagoya University, Nagoya
464-8602, Japan

We report, for the first time, the detailed *in-situ* TEM observation of wall to wall coalescence[1,2] of double-wall carbon nanotubes (DWCNTs) at very high temperature (>2000°C). The present observation is achieved by developing a high-temperature compatible TEM sample heating holder equipped with a micro-sized carbon nanotubes (CNTs) network heater (Figure 1). This micro-sized CNT network can heat a sample up to extremely high temperature (up to 3000°C) while minimizing spatial drift of the nanotube samples induced by the heating.

Figure 2 shows a time sequence on TEM images of a bundle of DWCNTs observed at 2,000 °C. A single larger-diameter DWCNT is formed at the final stage through a zipper-like mechanism of wall-to-wall coalescence between two individual outer shells and two individual inner shells. The time sequential TEM images obtained throughout the reaction suggests the presence of the Stone-Wales type transformation, which provides insight on thermal reconstruction process of the nanocarbon materials.

[1] M. Terrones et al. *Science* **2000**, 288, (5469), 1226-1229

[2] M. Endo et al. *Nano Letters* **2004**, 4, (8), 1451-1454.

Corresponding Author: R. Kitaura

Tel: +81-52-789-2477

E-mail: r.kitaura@nagoya-u.jp

&

H. Shinohara

Tel: +81-52-789-2482

E-mail: noris@cc.nagoya-u.ac.jp

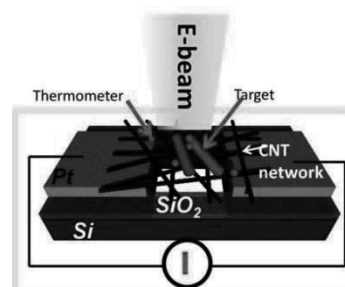


Figure 1. working principle of newly developed technique for *in-situ* heating TEM observation

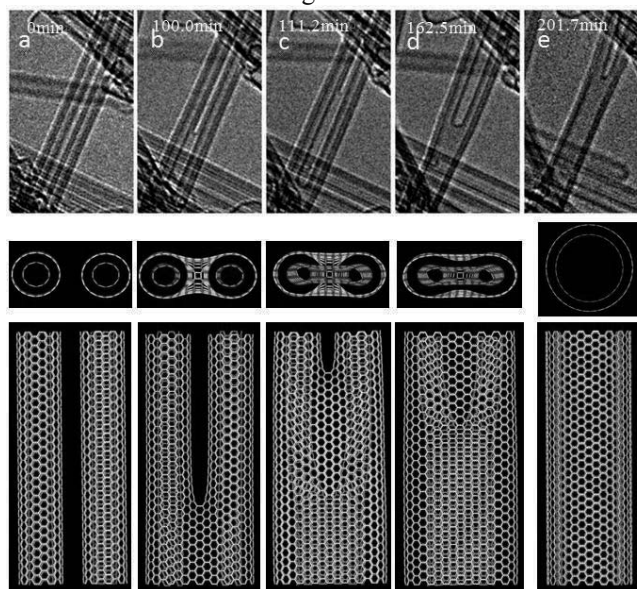


Figure 2. selective time sequential TEM images (with structural models) showing the main reaction stages of wall to wall coalescence of DWNTs

A hypothetical intermediate structure in growth of metallofullerenes

○Yohji Achiba, Takeshi Kodama, Kenro Hashimoto and Haruo Shiromaru

Department of Chemistry, Tokyo Metropolitan University, Hachioji, 192-0397, Japan

The isolation and characterization of metallofullerenes has been one of the biggest issues in the fullerene science and technology soon after the discovery of C₆₀ in 1985. Actually, after the first isolation and purification work of La@C₈₂ with a bulk quantity in 1993¹⁾, a lot of isolation works on metallofullerenes have been appeared in the literatures. Some of their cage structures have been well characterized by ¹³C NMR in solution. Furthermore, during the last 10 years, a single crystal X-ray diffraction method has been successfully introduced to carry out the crystallographic identification of a particular isomer with a particular size of metallofullerenes, and so far, over 36 different cage structures have been examined and identified²⁾. On the basis of these experimental progresses in determining cage structures, in the present work, we are intended to clarify “*what causes the selection of a particular cage structure in the metallofullerene growth process*”.

In order to construct a growth model for such a selective formation of a particular isomer structure, first, we have to consider the reason why a particular isomer structure is experimentally isolated and stabilized. There might be at least four key-factors by which some of metallofullerene isomers formed in the soot are actually experimentally isolated and identified: 1) Energetics (stability of “a particular charged state” of the π cage network with a particular size), 2) chemical stability of the particular charged state (large HOMO-LUMO gap is better, preventing from polymerization or other reactions), 3) 5/6 network structure superiority (closely related to network growth rate and stability), and 4) cage size (non IPR cage structure becomes to be much more important in the smaller size range). These four factors are definitely more or less related with each other even on the way of network forming process, but in the present work we will emphasize the important role of specific network structures of the intermediate precursors for the “*really*” isolated fullerenes.

Figure 1 shows one of the typical 5/6 network consisting of 4 pentagons and 15 hexagons with 48 carbons. An interesting aspect of this particular 5/6 network should be described by the fact that among 18 structurally determined M@C_{2n}, 12 kinds of M@C_{2n}, metallofullerenes with different sizes and structures commonly possess this patch in their 5/6 networks. Furthermore, our recent semi-empirical calculations (AM1) on over ten different kinds of C₄₈ molecules suggest that the structure shown in Fig.1 is one of the most energetically stable species as a di-anion among them. We will discuss in more detail on the plausible intermediate structures for the “*real*” growth of metallofullerenes in terms of both theoretical and experimental points.

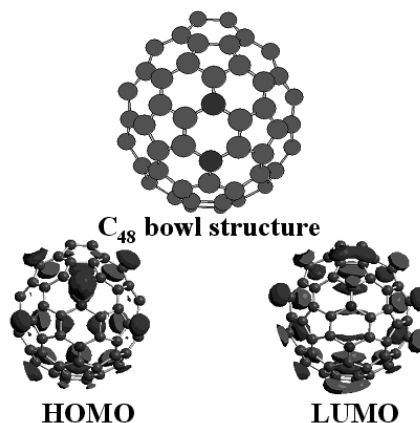


Fig.1 A hypothetical intermediate structure

[1] K. Kikuchi et al., Chem. Phys. Lett., 216, 67 (1993).

[2] see recent published literatures by Prof. T. Akasaka and Prof. A. Balch research group.

Corresponding Author: Y. Achiba

Tel: +81-42-677-2534, Fax: +81-42-677-2525,

E-mail: achiba-yohji@tmu.ac.jp

Structure of Thulium and Carbon Cluster Encapsulated in Low-Symmetry $C_{82}(C_5(6))$ Fullerene Cage by Single Crystal X-ray Diffraction

○Yuki Sado¹, Shinobu Aoyagi², Noriko Izumi¹, Ryo Kitaura¹, Tim Kowalczyk¹, Jian Wang¹, Stephan Irle¹, Eiji Nishibori³, Kunihisa Sugimoto⁴, and Hisanori Shinohara¹

¹ *Department of Chemistry & Institute for Advanced Research, Nagoya University, Nagoya 464-8602, Japan*

² *Department of Information and Biological Science, Nagoya City University, 467-8501, Japan*

³ *RIKEN RSC-RIGAKU Collaboration Center, RIKEN SPring-8 Center, RIKEN 1-1-1 Kouto, Sayo-cho, Sayo-gun, Hyogo 679-5148, Japan*

⁴ *Spring-8/JASRI, Kouto, Sayo, Hyogo 679-5198, Japan*

Endohedral metallofullerenes are among the most attractive molecules because of their unique structural and electronic properties¹. These properties have been found to depend strongly on the encapsulated species and carbon cage structure. Detailed structural analyses of endohedral metal atoms and clusters are essential to understand the properties of endohedral metallofullerenes.

For a deep understanding of the endohedral structure of metal atom(s) encapsulated, systematic structural studies with the same cage structure but with different number of endohedral atoms provide crucial knowledge. C_{82} based endohedral fullerenes, $M_x@C_{82}$ (M: metal), are the most feasible metallofullerenes for this purpose since many C_{82} based metallofullerenes, including mono-, di-, tri-metal and the corresponding metal-carbide endohedral fullerenes, have been synthesized and structurally characterized during the past a couple of decades. Recently, a structure of divalent mono-metallofullerene $Sm@C_{82}(C_5(6))$ has been synthesized and structurally characterized². The cage structure of $Sm@C_{82}(C_5(6))$ is the same as that of $Er_2@C_{82}(C_5(6))$ reported by Olmstead et al³. Therefore, the systematic production and structural characterizations of a series of C_{82} based metallofullerenes with the same fullerene cage is a promising route toward a deep understanding of the structural stability of endohedral metallofullerenes.

Here, we report single-crystal synchrotron X-ray structure analyses of $Tm_2@C_{82}(I)$ and $Tm_2C_2@C_{82}(I)$, both of which have a low-symmetry $C_{82}(C_5(6))$ cage. The single-crystal X-ray diffraction (XRD) experiments utilizing the third-generation synchrotron radiation with high counting statistics were performed at BL02B1 in SPring-8 (Hyogo, Japan). The structure analysis involving disorder of carbon cage orientation reveals that the Tm atoms and C_2 unit statically occupy specific positions inside the low-symmetry $C_{82}(C_5(6))$ cage. The resultant molecular structure is also energetically stable according to quantum chemical calculations. The determined structure can also be compared to that of the mono-metallofullerene, $Tm@C_{82}(C_5(6))$.

1. H. Shinohara, *Rep. Prog. Phys.*, 2000, **63**, 843-892.
2. H. Yang, H. Jin, X. Wang, Z. Liu, M. Yu, F. Zhao, B. Q. Mercado, M. M. Olmstead and A. L. Balch, *J. Am. Chem. Soc.*, 2012, **134**, 14127-14136.
3. M. M. Olmstead, A. de Bettencourt-Dias, S. Stevenson, H. C. Dorn and A. L. Balch, *J. Am. Chem. Soc.*, 2002, **124**, 4172-4173.

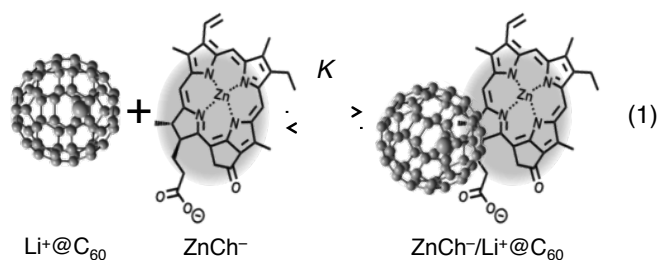
Photoinduced electron transfer in supramolecules between $\text{Li}^+@C_{60}$ and chlorin derivatives

○Kei Ohkubo, Yuki Kawashima, Kentaro Mase, Shunichi Fukuzumi

*Department of Material and Life Science, Graduate School of Engineering, Osaka University,
ALCA, Japan Science and Technology Agency, Suita, Osaka 565-0871, Japan*

Fullerenes and porphyrinoids that have highly delocalized π systems are suitable for efficient electron transfer because the uptake or release of electrons results in minimal structural and solvation changes upon electron transfer.^[1] Thus, they are suitable electron donor and acceptor for formation of the long-lived charge separated states. Therefore, there have been many reports of photoinduced charge separation in porphyrin-fullerene linked- and supramolecular systems. In natural systems, however, reduced porphyrins, namely chlorins are the electron donor pigments of the electron transfer processes. It is of great interest to examine the use of chlorophyll-like molecules such as chlorins. We report herein construction of chlorin/fullerene supramolecular system and photoinduced charge separation in a polar benzonitrile (PhCN) solution.

UV-vis absorption spectrum of an anionic zinc chlorin ($\text{ZnCh}^- \text{Bu}_4\text{N}^+$) in PhCN was changed upon addition of a cationic lithium encapsulated C_{60} ($\text{Li}^+@C_{60} \text{PF}_6^-$). The formation constant (K) was determined from the titration to



be $1.9 \times 10^4 \text{ M}^{-1}$. This result exhibits that strong supramolecular binding between ZnCh^- and $\text{Li}^+@C_{60}$ occurs by ionic interaction in PhCN (eq 1). The transient absorption spectra of $\text{ZnCh}^-/\text{Li}^+@C_{60}$ supramolecular complex were measured by nanosecond laser flash photolysis. The absorption band of the excited state of ZnCh^- ($^3[\text{ZnCh}^-]^*$) decays with increasing the absorbances at 790 and 1035 nm, which can be assigned to $[\text{ZnCh}^-]^+$ and $\text{Li}^+@C_{60}^-$, respectively.^[2-4] It clearly indicating the formation of the CS state by photoinduced electron transfer from $^3[\text{ZnCh}^-]^*$ to $\text{Li}^+@C_{60}$. The lifetimes of the triplet CS state in the supramolecular complex is determined to be 170 μs at 298 K. The quantum yield of the CS state is determined to be 0.62.

[1] S. Fukuzumi and K. Ohkubo *et al. Chem. Eur. J.* **9**, 1585 (2003).

[2] S. Fukuzumi and K. Ohkubo *et al. J. Am. Chem. Soc.* **133**, 15938 (2011).

[3] K. Ohkubo, Y. Kawashima, S. Fukuzumi *Chem. Commun.* **48**, 4314 (2012).

[4] Y. Kawashima, K. Ohkubo, S. Fukuzumi *J. Phys. Chem. A* **116**, 5942 (2012).

Corresponding Author: K. Ohkubo

Tel: +81-6-6879-7369, Fax: +81-6-6879-7370,

E-mail: ookubo@chem.eng.osaka-u.ac.jp

Ultraviolet Photoelectron Spectra of $\text{Gd}_3\text{N}@C_{80}$ and $\text{Er}_3\text{N}@C_{80}$

○Takafumi Miyazaki¹, Yusuke Nakanishi³, Yuki Sasaki³, Hiroyuki Niwa³, Shoko Noda³,
Tatsuhiko Nishi², Tomona Ohta¹, Hisanori Shinohara³ and Shojun Hino¹

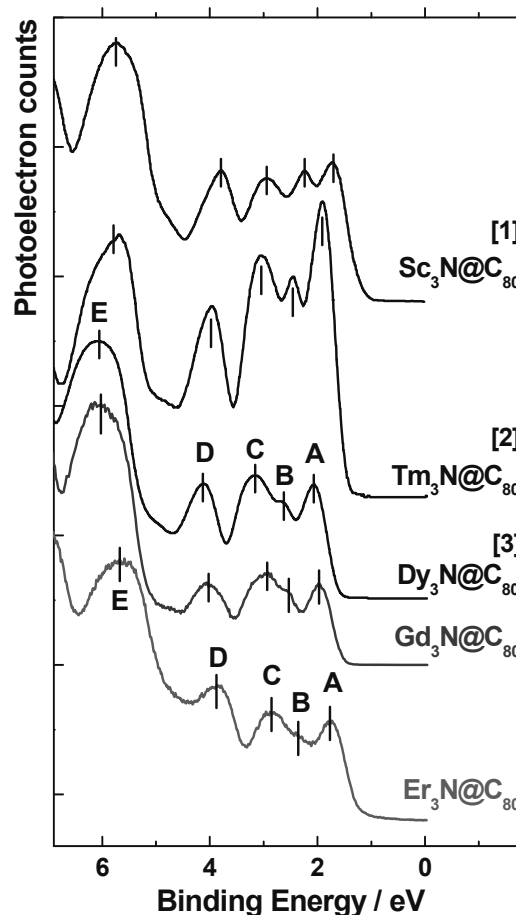
¹Graduate School of Science and Engineering, Ehime University, Matsuyama 790-8577, Japan

²Institute for Molecular Science, Okazaki, 444-8585, Japan

³Graduate School of Science, Nagoya University, Nagoya 464-8602, Japan

We have been measuring ultraviolet photoelectron spectra (UPS) of endohedral fullerenes to elucidate their electronic structure. Here, we present the UPS of $\text{Gd}_3\text{N}@C_{80}$ and $\text{Er}_3\text{N}@C_{80}$ and compare them with those of $\text{M}_3\text{N}@C_{80}$ ($\text{M}=\text{Sc}, \text{Tm}, \text{Dy}$) [1-3].

The UPS of $\text{Gd}_3\text{N}@C_{80}$ and $\text{Er}_3\text{N}@C_{80}$ are shown in Figure 1. These spectra were measured using a synchrotron radiation light source. The UPS of $\text{Sc}_3\text{N}@C_{80}$, $\text{Tm}_3\text{N}@C_{80}$ and $\text{Dy}_3\text{N}@C_{80}$ were also shown in the figure. The UPS onset energy of $\text{Er}_3\text{N}@C_{80}$ is 1.2 eV, which is the smallest among them. The UPS of deeper valence band region ($\text{BE}>5\text{eV}$) of these endohedral fullerenes shows fairly good correspondence. The upper valence band UPS ($\text{BE}<5\text{eV}$) of $\text{Er}_3\text{N}@C_{80}$, $\text{Gd}_3\text{N}@C_{80}$ and $\text{Dy}_3\text{N}@C_{80}$ resemble each other, but they are slightly different from those of $\text{Tm}_3\text{N}@C_{80}$ and $\text{Sc}_3\text{N}@C_{80}$ particularly in their peak positions and relative intensity. Comparison of the UPS with DFT calculated simulation spectra indicates that the structure of entrapped Sc_3N and Tm_3N is flat as was reported [1, 2] and that of $\text{Dy}_3\text{N}@C_{80}$ is triangular [3]. From the analogy of the UPS features the structure of the entrapped Gd_3N and Er_3N cluster might be triangular.



[1] L. Alvarez et al., Phys. Rev. B, 66, 035107 (2002). [2] X. Liu. et al., ibid. 72, 085407 (2005), [3] H. Shiozawa et al., ibid. 72, 195409 (2005),

Figure 1. The UPS of $\text{M}_3\text{N}@C_{80}$ ($\text{M}=\text{Er}, \text{Gd}, \text{Dy}, \text{Tm}, \text{Sc}$) endohedral fullerenes.

Corresponding Authors: T. Miyazaki, E-mail: miyazaki@eng.ehime-u.ac.jp, phone: 089-927-9930; S. Hino, E-mail: hino@eng.ehime-u.ac.jp, phone: 089-927-9924.

ポスター発表
Poster Preview

1P-1 ~ 1P-47

2P-1 ~ 2P-46

3P-1 ~ 3P-46

Optical coupling of air-suspended carbon nanotubes to silicon microdisk

○Saneyuki Imamura, Ryosuke Watahiki, Ryohei Miura, Yuichiro K. Kato

Institute of Engineering Innovation, The University of Tokyo, Tokyo 113-8656, Japan

Optical coupling of individual air-suspended single-walled carbon nanotubes to whispering-gallery modes in silicon microdisk resonators is studied. We fabricate silicon microdisks with diameters of $\sim 3 \mu\text{m}$ on SiO_2 supporting posts from silicon-on-insulator substrates, and synthesize carbon nanotubes from patterned catalysts by alcohol chemical vapor deposition to suspend them onto the microdisks. Interactions between carbon nanotubes and evanescent fields of microdisk modes are investigated by microspectroscopy at room temperature. We observe microdisk modes with quality factors of ~ 3000 at wavelengths longer than those of silicon emission, even at positions that are a few micrometers from the suspended carbon nanotubes. In addition, as microdisk modes also exist at excitation laser wavelengths, the photoluminescence intensity can be resonantly enhanced by tuning the laser wavelength to those modes.

This work is supported by SCOPE, KAKENHI, The Asahi Glass Foundation, and Photon Frontier Network Programs of MEXT, Japan. The devices were fabricated at the Center for Nano Lithography & Analysis at The University of Tokyo.

Corresponding Author: Y. K. Kato

Tel: +81-3-5841-7702, Fax: +81-3-5841-7772,

E-mail: ykato@sogo.t.u-tokyo.ac.jp

X-ray diffraction profile of highly purified (6, 5) SWCNTs

○Shin Tadera¹, Haruka Kyakuno¹, Yusuke Nakai¹, Kazuhiro Yanagi¹, Yasumitsu Miyata²,
Hiromichi Kataura^{2,3}, Yutaka Maniwa^{1,3}

¹ *Department of Physics, Faculty of Science, Tokyo Metropolitan University, 1-1
Minami-Osawa Hachioji, Tokyo 192-0397, Japan*

² *Nanosystem Research Institute (NRI), National Institute of Advanced Industrial Science and
Technology (AIST), Central 4, Higashi 1-1-1, Tsukuba, Ibaraki 305-8562, Japan*

³ *JST, CREST, Kawaguchi, 332-0012, Japan*

Single-walled carbon nanotubes (SWCNTs) have a cylindrical structure that consists of a rolled graphene sheet. Physical properties of SWCNT are highly dependent on its diameter and chiral index. A diameter of SWCNT is geometrically determined by its chiral index and C-C bond length. The C-C bond length of SWCNT is usually considered to be equal to that in graphene sheet, 1.42 Å which was experimentally determined in bulk graphite. However, no one reports a precise experimental value of the C-C bond length of SWCNTs.

We prepared highly purified (6,5) SWCNTs sample (see Fig. 1) with gel column separation method [2] and density gradient ultracentrifugation. We performed powder X-ray diffraction (XRD) measurements at KEK-PF, BL-8B, and found well-defined peaks near $Q = 5 \text{ \AA}^{-1}$, whose structures were not observed in low purity samples. We determined the C-C bond length by comparing with simulation patterns. Besides it was found that the XRD profiles can be used for fingerprinting of the chiral index of SWCNTs.

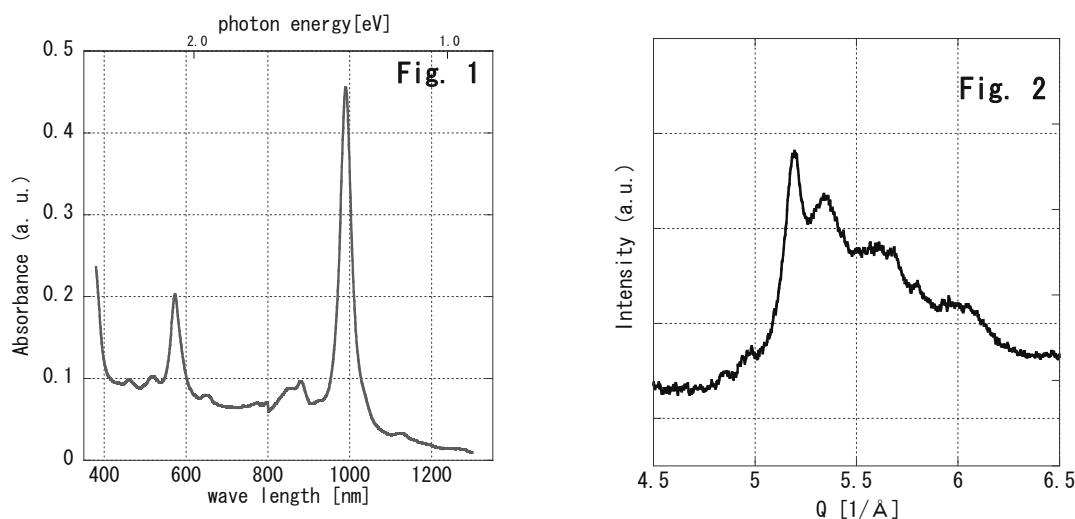


Fig. 1 Optical absorbance spectra of the SWCNT sample studied.

Fig. 2 Observed X-ray diffraction profile.

[1] Gmelin Handbuch Der Anorganischen Chemie, eighth ed., Handbuch der Anorganischen Chemie, vol. 14B/2 Verlag Chemie, Weinheim, 1968, p. 143.

[2] H. Liu, *et al.*, Nature Commun. 2 (2011) 309.

Corresponding Author: Yutaka Maniwa

Tel: +81-42-677-2490, E-mail: maniwa@phys.se.tmu.ac.jp

Observation of circular dichroism in individual air-suspended single-walled carbon nanotubes

○A.Yokoyama, A. Ishii, M. Yoshida, Y. K. Kato

Institute of Engineering Innovation, The University of Tokyo, Tokyo 113-8656, Japan

We have performed circular dichroism measurements on individual air-suspended single-walled carbon nanotubes, using photoluminescence intensity for detection. Inspection of photoluminescence spectra for right and left circularly polarized excitation reveals modulation of nanotube photoluminescence, while emission from silicon substrate shows negligible changes. Comparison of photoluminescence and polarization images shows that circular dichroism signal is spatially localized on nanotubes. The spectral and spatial localization of the signal supports the interpretation that circular dichroism originates from nanotubes. In addition, utilizing automated rotation and translation stages, we have performed measurements as a function of angle between optical axis and the nanotube. We find that the signal has large angle dependence and even changes its sign.

This work is supported by SCOPE, KAKENHI and the Photon Frontier Network Program of MEXT, Japan. Samples were fabricated at the Center for Nano Lithography & Analysis at The University of Tokyo.

Corresponding Author: Y. K. Kato
Tel: +81-3-5841-7702, Fax: +81-3-5841-7772,
E-mail: ykato@sogo.t.u-tokyo.ac.jp

Determination of surfactant (Brij 78) in aqueous CNT dispersion

○Kazutoku Ohta¹, Yoshio Hayakawa¹, Taizo Ono¹, Hiroshi Yamawaki²,
Kazuhiro Yamamoto², Kazumasa Honda³

¹ *Research Institute of Instrumentation Frontier, Nagoya 463-8560, Japan*

² *Research Institute of Instrumentation Frontier, Tsukuba 305-8565, Japan*

³ *Research Institute of Science for Safety and Sustainability, Tsukuba 305-8565, Japan*

Introduction Aqueous carbon nanotube (CNT) dispersion is commonly prepared by ultrasonication of aqueous surfactant solution including CNT. Following ultrasonication, ultracentrifugation is utilized for the removal of aggregated CNT in order to enhance the stability of the dispersion. The ultracentrifugation causes the difficulty for the accurate determination of CNT in the dispersion due to the uncertainty on the amount of the removed CNT. Therefore, it is much more difficult to determine free and adsorbed surfactant.

In this presentation, we propose a simple and useful way for the determination of CNT and surfactant (polyoxyethylene(20)stearyl ether, Brij 78) in high concentrated CNT dispersion.

CNT dispersion A 20-ml of aqueous 1-% (W/V) Brij 78 solution including 40-mg single-walled CNT (DIPS) was ultrasonicated using Branson S-450D with 1/2" tapped horn (amplitude 35%) at 20 °C for 1-6 h. After the ultrasonication, the solution was ultracentrifuged using Hitachi CS-100GXL with S52ST swing rotor (20,000 rpm) for 1 h.

Weighing of CNT A 45-ml tetrahydrofuran (THF) was added to 5-ml of CNT dispersion to remove Brij 78 adsorbed on CNT. A 50-ml water was added to the solution to agglutinate CNT. The solution was filtrated with 0.5- μ m PTFE filter. The resultant CNT was washed thoroughly with THF and weighed after drying at 140 °C for 2 h.

Determination of Brij 78 Determination of Brij 78 was carried out by reversed-phase HPLC. In-line filter equipment (filter pore size: 0.45- μ m) was inserted between injector and separation column. Total Brij 78 was determined using CNT dispersion itself as a sample. Free Brij 78 was determined using the filtrate obtained by removing CNT with 0.20- μ m PTFE filter. The amount of adsorbed Brij 78 was calculated by subtracting the amount of free Brij 78 from that of total Brij 78.

Result Table 1 shows analytical results of CNT and Brij 78 in dispersions. The weight of dispersing CNT increased with increasing time of sonication. The amount reached 1.0 mg (per 1-ml dispersion) at 6 h sonication. In contrast, the amount of adsorbed Brij 78 (per 1-mg CNT) was almost the same and the values were ca. 5 (mg/1-mg-CNT) under the dispersion conditions.

Table 1. Analytical results of CNT and Brij 78 in CNT dispersions.

Sonication time (h)	CNT (mg/ml)	Free Brij 78 (mg/ml)	Adsorbed Brij 78 (mg/mg-CNT)
1	0.64	5.0	4.8
2	0.77	4.1	5.4
4	0.93	4.0	5.4
6	1.0	3.2	5.2

Corresponding Author: K. Ohta,

Tel: +81-52-736-7363, Fax: +81-52-736-7224,

E-mail: kazu.ohta@aist.go.jp

Effect of Impurity Scattering on AC Transport in Carbon Nanotubes

○Daisuke Hirai¹, Takahiro Yamamoto², Satoshi Watanabe¹

¹*Department of Materials Engineering, The University of Tokyo*

²*Department of Electrical Engineering and Liberal Arts, Tokyo University of Science*

Due to peculiar structures of carbon nanotubes (CNTs), the electronic transport properties of metallic CNTs are sensitive to the range of impurity potential, d : in the case where the potential range is larger than the lattice constant, a , electron back-scatterings are suppressed; in the case of a short-range potential ($d < a$), the electron back-scatterings occur, which lead to the decrease of the DC conductance [1]. The back-scatterings must also affect the AC transport properties, but this issue has not been clarified yet.

In this study, we simulated the AC response of metallic CNTs with randomly distributed impurities to clarify the effect of impurity scatterings on the AC response. For calculating admittance, we used nonequilibrium Green's function method within the nearest-neighbor π -orbital tight-binding approximation and wide-band limit approximation [2-4]. We found that the behavior of the phase difference between the current and bias voltage drastically changes with the impurity-potential range: In the case of the short-range potential, the phase difference is smaller than that of pristine metallic CNTs and becomes smaller with an increase of the potential amplitude (Fig. 1(a)), while it is larger than that of the pristine ones and the relation between the phase difference and potential amplitude is opposite in the case of the long-range potential (Fig. 1(b)). This can be understood from the competition between the capacitive response due to electron back-scatterings [3,4] and inductive response due to the kinetic inductance [2]. As mentioned previously, the back-scatterings occur in the case of the short-range potential while they are suppressed in the case of the long-range potential. On the other hand, even if the electron back-scatterings are suppressed, the dwell time of the electrons increases, which increases the kinetic inductance [2] as well as the cases having the back-scatterings. Therefore, the difference in the back-scatterings between the short-range and long-range potentials causes the different AC response behaviors.

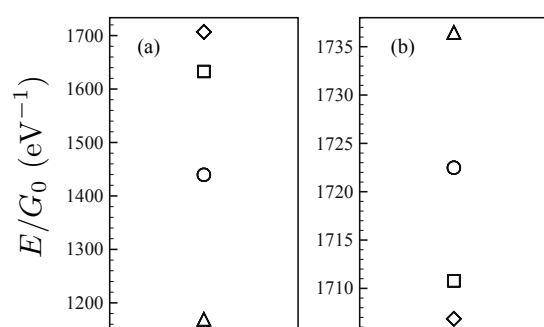


Fig. 1. Phase difference between the current and bias voltage (emittance: E) of a $1\mu\text{m}$ -long (10,10) CNT with impurity potentials of (a) $d = 0.1a$ and (b) $d = 1.5a$, for several potential amplitudes: \diamond is the emittance of the pristine CNT and \square , \circ , and \triangle are those of CNTs with impurity potentials of the amplitudes of 0.25, 0.5, and 0.75 eV, respectively.

[1] T. Ando *et al.*, J. Phys. Soc. Jpn. **67**, 1704 (1998).

[2] T. Yamamoto *et al.*, Phys. Rev. B **81**, 115448 (2010).

[3] D. Hirai *et al.*, Appl. Phys. Express, **4**, 075103 (2011).

[4] D. Hirai *et al.*, Jpn. J. Appl. Phys., **51**, 04DN01 (2012).

Corresponding Author: Daisuke Hirai

Tel: +81-3-5841-7136, Fax: +81-3-5841-1286,

E-mail: daisuke.hirai@cello.t.u-tokyo.ac.jp

Solution growth of carbon-nanotube wires

○Yuki Takagi¹, Yugo Oshima², Kazuhiro Yanagi³, Taishi Takenobu¹

¹ *Department of Applied Physics, Waseda University, Shinjuku 169-8555, Japan*

² *RIKEN, Wako 351-0198, Japan*

³ *Department of Physics, Tokyo Metropolitan University, Hachioji 192-0397, Japan*

Carbon nanotube (CNT) is known as excellent material which has nano-scale one dimensional structure and great transport properties. In particular, macro-scale thin-film devices consisting of networks of CNTs are of interest due to their applicability to flexible and printed electronics. In networks of CNTs, junctions between CNTs prevent the efficient charge transport and their reduction by making aligned CNT films or wires is crucially important for macro-scale CNT applications. Therefore, it is strongly required to establish fabrication method of such wire-like CNT thin films. Very recently, solution based crystallization method for one of nano-carbon materials, C₆₀, has been developed [1]. Here, we applied this method to another nano-carbon material, CNT, and tried to grow the high-density CNT aggregations.

Figure 1 shows a schematic illustration of fabrication process. CNTs were dispersed in *N*-methylpyrrolidone and the dispersion was dropped on substrate. Small hydrophilic substrate was put on large hydrophobic substrate to pin the droplet. Then, as shown in Fig. 1, CNT wires were self-assembly fabricated. We used small piece of Si substrate as hydrophilic pinning center and Si substrate modified with self-assembled monolayers (SAMs) as hydrophobic substrate. Because substrate surface energy and drying rate are important for growth of CNT wire, we optimized condition of fabrication process by preparing some types of SAMs and changing the drying condition. As a result, we achieved fabricating macro-scale wire-like CNT thin films (Figure 2).

In summary, we performed fabrication of wire-like CNT thin films via solution based growing method. This result enables us to fabricate separated and purified CNT wire which is expected to be used for physical properties research and high performance thin film device.

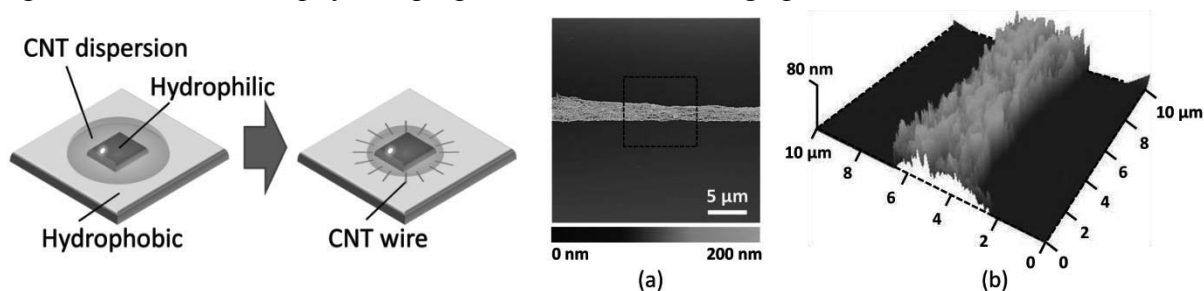


Fig. 1 The schematic of fabrication process

Fig. 2 (a); Atomic Force Microscope (AFM) image of fabricated semiconducting CNT thin film
(b); 3D image of dashed square region in (a)

[1] H. Y. Li *et al.* *J. Am. Chem. Soc.* **134**, 2760 (2012).

Corresponding Author: Taishi Takenobu, Tel and Fax: +03-5286-2981, E-mail: takenobu@waseda.jp

***In-situ* Raman spectroelectrochemical investigation on diameter-dependent onset potential of oxygenation reaction of SWCNTs**

○Shingo Sakamoto¹, Masato Tominaga^{1,2}

¹*Graduate School of Science and Technology, Kumamoto University, Kumamoto 860-8555, Japan*

²*Kumamoto Institute for Photo-Electro Organics (Phoenixes), Higashimachi, Kumamoto 862-0901, Japan*

The oxygenation reaction of single-walled carbon nanotubes (SWCNTs) is an important issue because chemical and physical properties, such as chemical reactivity, electronic conductance and optical characteristics, would be changed [1-4]. In this study, the onset oxygenation potential of SWCNTs in neutral aqueous solution was investigated by using *in-situ* Raman spectroelectrochemical measurements.

Fig. 1 shows the *in-situ* Raman spectra of SWCNTs/Au in the RBM band region. The peak intensity of the RBM at 0.4 V using 2.41 eV decreased in comparison with the initial peak intensity. However, the peak intensity returned to its initial value when the potential was applied at -0.2 V. This reversible intensity change between these potentials was likely due to the fact that electron depletion from the valence band of the SWCNTs would occur during potential application at 0.4 V, and electrons re-filling to the band would occur during -0.2 V. This intensity reversibility was observed at potentials up to 0.5 V. On the other hand, after the potential was applied up to 0.6 V, the peak intensity did not return to its initial intensity, even if a potential of -0.2 V was applied. This irreversible change was caused by the oxygenation of the SWCNTs. A similar tendency was also observed at 1.58 eV using an exciting laser. Further discussion on diameter dependence of oxygenation reaction will be presented.

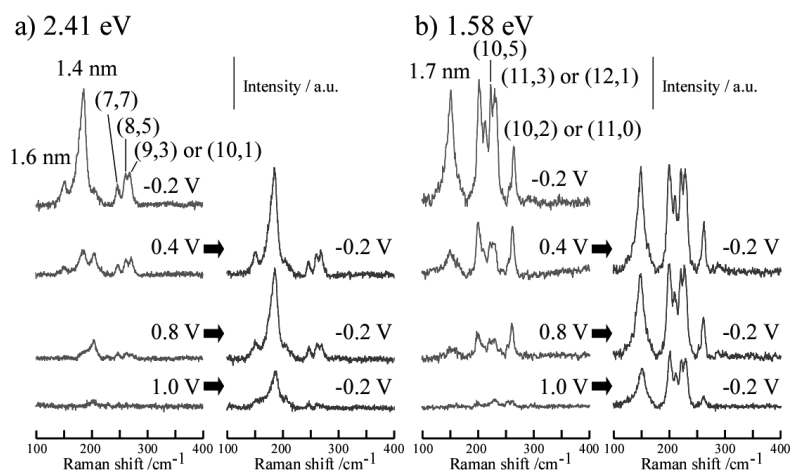


Fig. 1. *In-situ* Raman spectra of SWCNTs at various potentials excited by two laser energies of 2.41 (a) and 1.58 eV (b).

[1] P. G. Collins, K. Bradley, M. Ishigami and A. Zettl, *Science*, 2000, **287**, 1801-1804.

[2] S. Ghosh, S. M. Bachilo, R. A. Simonette, K. M. Beckingham and R. B. Weisman, *Science*, 2010, **330**, 1656-1659.

[3] M. Pumera, T. Sasaki and H. Iwai, *Chem. Asian J.*, 2008, **3**, 2046-2055.

[4] M. Tominaga, S. Sakamoto and H. Yamaguchi, *J. Phys. Chem. C*, 2012, **116**, 9498-9506.

Corresponding Author: M. Tominaga

Tel/ Fax: +81-96-342-3655, E-mail: masato@gpo.kumamoto-u.ac.jp

Strong saturation of photoluminescence from local quantum states in oxygen-doped carbon nanotubes

Munehiyo Iwamura¹, Yuhei Miyauchi^{1,2}, Naoto Akizuki¹,
Shinichiro Mouri¹ and Kazunari Matsuda¹

¹ Institute of Advanced Energy, Kyoto University, Uji, Kyoto, 611-0011, Japan

² PRESTO, Japan Science and Technology Agency, Kawaguchi, Saitama, 332-0012, Japan

Optically excited electrons and holes in single-walled carbon nanotubes (SWNTs) form two-particle bound states called as excitons. In contrast to intensive studies over the past decade on the intrinsic one-dimensional (1D) exciton photophysics in SWNTs [1,2], there have been only limited number of reports [3,4] on the impact of local quantum states on excitonic properties of SWNTs. If a well-organized 0D-like local luminescent state is generated in an intrinsic 1D SWNT, such a complex nanostructure can be viewed as an unprecedented, nearly ideal 1D-0D hybrid low dimensional system where novel exciton photophysics may emerge. Moreover, the modifications originating from the additional local states may exert changes on the intrinsic optical properties of SWNTs that are favorable for their optoelectronics applications.

In this study, we explore novel exciton photophysics in 1D-0D hybrid nanostructures through the observations of excitation power dependence of photoluminescence (PL) from 0D-like local luminescent states generated by atomic oxygen doping [4] in 1D SWNTs. We observed extraordinary rapid saturation behavior of PL intensity from the local states at E_{11}^* with increasing continuous-wave (cw) excitation power density as shown in Fig. 1. Based on the Monte Carlo simulation of the exciton dynamics where diffusion, trapping, and recombination of excitons at the local states are taken into account, the strong saturation behavior is attributed to the state filling in the local states that originates from the efficient accumulation of the excitons photogenerated in the intrinsic 1D segments into the small number of the local states. Our findings indicate that the excited state population of the local states can exceed the ground state population even under relatively low power cw optical excitation regime, namely, population inversion necessary for lasing, which has been hampered by the rapid exciton-exciton annihilation processes in intrinsic SWNTs [5], is readily achievable for the local states in SWNTs.

Acknowledgements: The authors thank Prof. B. Lounis, Dr. L. Cagnet and Dr. J. Shaver (Université de Bordeaux) for helpful discussions.

- [1] R. Matsunaga *et al.*, Phys. Rev. Lett. **101**, 147404 (2008).
- [2] Y. Miyauchi *et al.*, Phys. Rev. B **80**, 081410(R) (2009).
- [3] K. Iakoubovskii *et al.*, Appl. Phys. Lett. **89**, 173108 (2006).
- [4] S. Ghosh *et al.*, Science **330**, 1656 (2010).
- [5] Y. Murakami and J. Kono, Phys. Rev. Lett. **102**, 037401 (2009).

Corresponding Author: Y. Miyauchi

Tel: +81-774-38-3463, E-mail: miyauchi@iae.kyoto-u.ac.jp

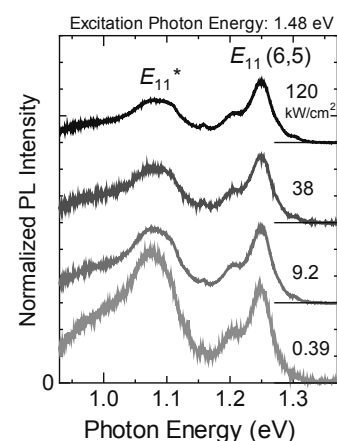


Fig.1. PL spectra of pristine and oxygen doped SWNTs measured at various excitation power density. Each spectrum is normalized by the corresponding excitation power density.

Quantum Mechanical Transport in SWNTs Network FETs Studied via Scanning Gate Microscopy

○Xiaojun Wei¹, Masahiro Matsunaga¹, Kenji Maeda¹, Taturou Yahagi¹, Nobuyuki Aoki¹, Jonathan P. Bird², Koji Ishibashi³ and Yuichi Ochiai¹

¹ Graduate School of Advanced Integration Science, Chiba University
1-33 Yayoi-cho, Inage-ku, Chiba 263-8522, Japan

² Department of Electrical Engineering, University at Buffalo,
SUNY, Buffalo, New York 14260-1920, USA

³ Advanced Device Laboratory, RIKEN, 2-1 Hirosawa, Wako, Saitama 351-0198, Japan

Carbon nanotubes (CNTs) have recently received extensive attention due to their nanoscale dimensions and outstanding materials properties such as ballistic electronic conduction, immunity from electromigration effects at high current densities, and transparent conduction. However, the local operation mechanism of field effect transistor (FET) composed of single wall carbon nanotubes (SWNTs) network has not been well evaluated yet. Scanning gate microscopy (SGM) is one of such techniques to establish a spatially resolved local gate study in semiconductor nano-structures. It has also been applied to investigate FET structures consisting of a SWNT. SGM responses related to a modulation of defects in a SWNT [1], Schottky barrier formed between the metallic electrode and a SWNT [2], and quantum states related to Coulomb blockade [3], have been visualized directly as the images in comparison to topographic scans.

In this paper, ring-shape response was observed at intra-tube positions corresponding semiconducting enriched by density gradient ultracentrifuge (DGU) process showed in Fig. 1. This is different from the former experiments using CoMoCAT SWNTs, SGM response was observed at specific inter-tube junctions suggesting a Schottky junction formed with semiconducting and metallic SWNTs in the network [4]. When the carrier density is enough by applying a negative back gate voltage, the response appears as one bright spot. However, it becomes multiple concentric rings near the sub-threshold region. The diameter of the rings depends on the back gate voltage and increases with increasing the voltage. Multiple concentric rings response would be related to a kind of quantum mechanical transports due to a formation of discrete energy levels by close defects in the SWNT at room temperature. Although the origin has not been clarified yet, resonant tunneling effect could be expected due to a confinement effect from close defects in the SWNT introduced during the DGU process.

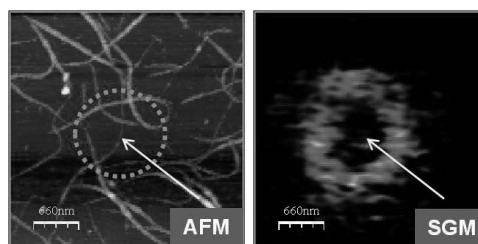


Fig.1 AFM image (left) and the corresponding SGM image (right) within the channel corresponding DGU process.

[1] M. Bockrath *et al*, Science **291**, 283 (2001).

[2] M. Freitag *et al*, Appl. Phys. Lett. **79**, 3326 (2001).

[3] M. T. Woodside and P. L. McEuen, Science. **296**, 1098 (2002).

[4] X. Wei *et al*, Jpn. J. Appl. Phys.**51**, 04DN05 (2012).

Corresponding Author: X. Wei

Tel: +81-43-290-3430, Fax: +81-43-290-3427, E-mail: weixiaojun@graduate.chiba-u.jp

Polymer Solar Cells with PEDOT:PSS / SWCNTs and MWCNTs Composite as Hole Transport Layer

○Naoki Kishi¹, Junki Hayashi¹, Takeshi Saito², Tetsuo Soga¹, Takashi Jimbo³

¹*Department of Frontier Materials, Nagoya Institute of Technology,
Nagoya 466-8555, Japan*

²*Nanotube Research Center, National Institute of Advanced Industrial Science and
Technology (AIST), Tsukuba 305-8565, Japan*

³*Research Center for Nano-Device and System, Nagoya Institute of Technology,
Nagoya 466-8555, Japan*

Polymer solar cells have attracted much attention in recent years for their potential application as a low cost approach to solar energy conversion. Hole transport layer, which is formed between a hole correcting anode and a photovoltaic layer in the solar cell structure, plays an important roll on the controlling the hole injection to the anode electrode. Several kinds of polymer materials such as poly(3,4-ethylenedioxythiophene) : poly(styrenesulfonate) (PEDOT:PSS) have been investigated as hole transport materials for organic solar cells. Recently, we reported that the device performance of polymer solar cells can be improved by introducing SWCNTs into the hole transport layer [1]. However, further studies on PEDOT:PSS/CNT composite hole transport layer are required to develop photovoltaic devices with high photo conversion efficiency.

In this study, we reported the effects of incorporating different types of CNTs (SWCNTs and MWCNTs) into PEDOT:PSS hole transport layer on the solar cell performance. The optimum solar cell structure with SWCNTs incorporation shows improved short circuit current density and fill factor. On the other hand, the addition of MWCNTs decreased photo conversion efficiency due to increment of the leakage current of the devices. The performance of the solar cells will be discussed in detail.

[1] N. Kishi *et al.*, Nano, 6 (2011) 583.

Corresponding Author : Naoki Kishi

E-mail : kishi.naoki@nitech.ac.jp

Tel&Fax : 052-735-5147

High efficiency carbon nanotube/silicon heterojunction solar cells fabricated using high quality carbon nanotube network film

Feijiu Wang¹, Daichi Kozawa¹, Yuhei Miyauchi^{1,2},
Shinichiro Mouri¹, Yutaka Ohno³, and Kazunari Matsuda¹

¹*Institute of Advanced Energy, Kyoto University, Uji, Kyoto 611-0011, Japan*

²*Japan Science and Technology Agency, PRESTO, 4-1-8 Honcho Kawaguchi, Saitama 332-0012, Japan*

³*Department of Quantum Engineering, Nagoya University, Furocho, Chikusa-ku, Nagoya 464-8603, Japan*

Single-walled carbon nanotubes (SWNT) have attracted a great deal of attention for photovoltaic applications due to their excellent properties such as high carrier mobility, high-efficiency carrier multiplication effects, and tunable band gap by controlling their diameters. Recently, the heterostructures of SWNTs and Si have been extensively studied for highly efficient photovoltaic cells [1, 2]. It was found that the key to realize the highly efficient solar cell is the use of high quality SWNTs network film with both low resistivity and high transparency from the analysis of photovoltaic properties of SWNTs/Si solar cells [3]. We have fabricated the SWNTs/Si solar cells using the high quality SWNTs network film and evaluated the photovoltaic properties of the cells.

The high quality SWNTs network films fabricated by the floating catalytic CVD method [4] was used for the cells. Figure 1 shows the current density voltage (J - V) characteristics of SWNT/Si heterojunction solar cell with high photovoltaic conversion efficiency. From this J - V curve, the conversion efficiency (η), current density (J_{sc}), fill factor (FF) and open circuit voltage (V_{oc}) are 10.6 %, 29 mA/cm², 67 % and 0.549 V, respectively. This photovoltaic conversion efficiency is greater than previously reported highest value of SWNT/Si solar cells without doping treatment [2]. This high conversion efficiency is attributed to the greatly decrease of power loss due to lower inter-nanotube series resistance of the high quality network film with very longer nanotube [4]. We also evaluated the photovoltaic conversion efficiency during 10 days for the check of stability of the devices, and only the small decrease of efficiency (~ 1.5 %) was observed, which is much smaller than the previously reported value (~ 6 %) during 6 days [1].

[1] E. Shi *et al.*, *Sci. Rep.* **2**, 884 (2012).

[2] P. Wadhwa *et al.*, *Nano Lett.* **10**, 5001 (2010).

[3] D. Kozawa *et al.*, *Appl. Phys. Exp.* **5**, 042304 (2012).

[4] A. Kaskela *et al.*, *Nano Lett.* **10**, 4349 (2010).

Corresponding Author: Kazunari Matsuda

Tel: +81-774-38-3460, Fax: +81-774-38-3460

E-mail: matsuda@iae.kyoto-u.ac.jp

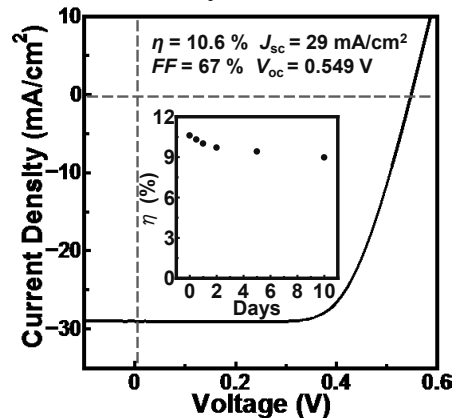


Fig. 1: J - V curve of SWNTs/Si solar cell. Inset shows the stability of this solar cell.

P-N junction in Carbon Nanotube Electric Double Layer Transistor

○Ryo Shimizu¹, Yijin Zhang², Kazuhiro Yanagi³, Yoshihiro Iwasa², Taishi Takenobu¹

¹ Department of Applied Physics, Waseda University, Shinjuku 169-8555, Japan

² Quantum-Phase Electronics Centre and Department of Applied Physics,
The University of Tokyo, Tokyo 113-8656, Japan

³ Department of Physics, Tokyo Metropolitan University, Hachioji 192-0397, Japan

Single-walled carbon nanotubes (SWCNTs) are next-generation semiconducting materials due to their extraordinary properties such as high mobility, flexibility, and ambipolar transistor operation. Moreover SWCNTs are prospective materials for optoelectronics in infrared region owing to their narrow energy bandgap. The fundamental optoelectronic elements such as LED and solar cell require p-n junction and it is already realized by chemical doping [1] and ambipolar transistor operation. However, it is very difficult to obtain stable p-n junction by chemical method. Moreover, p-n junction based on ambipolar characteristics always needs gate voltage application and it is not realistic method for future applications. To solve these problems, we realized pseudo stable p-n junction on the channel of SWCNT ambipolar electric double layer transistor (EDLT) by fixing ions in liquid-gate insulator with low temperature.

Ionic gel was adopted as gate insulator which consists of 1-Ethyl-3-methylimidazolium bis(trifluoromethylsulfonyl)imide and polystyrene-poly(methyl methacrylate)-polystyrene. Figure 1 describes an ambipolar carrier accumulation using EDLT. Both holes and electrons can be accumulated at the same time by controlling electric voltage between electrodes. A p-n junction is formed in between hole-accumulated region and electron-accumulated region. To fix this p-n junction, we froze the ionic gel by low temperature with applying $V_{GS} = -1.0$ V and $V_{DS} = -2.0$ V. Figure 2 shows current-voltage characteristics of the device after fixing p-n junction. Inset represents I-V curve before freezing ionic gel. As shown by these plots, rectification behavior has appeared by fixing ions in gel. Furthermore, photocurrent was observed by irradiating white light to the device. These results indicate that p-n junction has formed successfully.

In summary, we have demonstrated pseudo stable p-n junction on the channel of SWCNT ambipolar EDLT by coinstantaneous accumulation of holes and electrons. This result can be building block of next-generation optoelectronic devices.

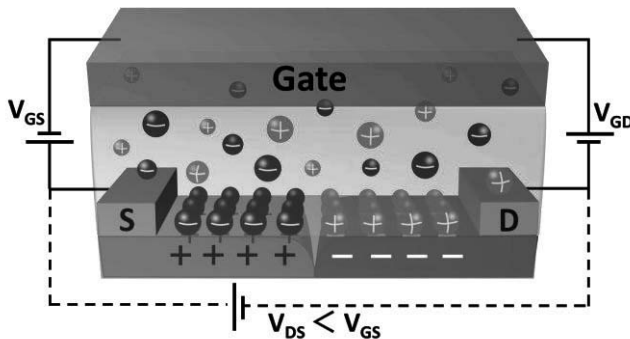


Fig.1 Ambipolar carrier accumulation and formation of p-n junction

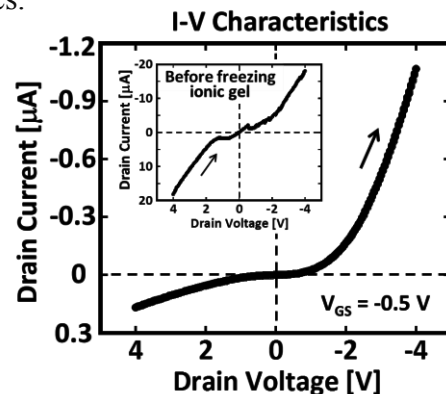


Fig.2 I-V characteristics after freezing ionic gel

[1] C. Biswas, S. Y. Lee, T. H. Ly, A. Ghosh, Q. N. Dang, and Y. H. Lee, ACS Nano **5**, 9817 (2011).

Corresponding Author: Taishi Takenobu, Tel&Fax: +81-3-5286-2981, E-mail: takenobu@waseda.jp

High-mobility, flexible, n-type carbon nanotube thin-film transistors

○Tomohiro Yasunishi, Yutaka Ohno, Shigeru Kishimoto, and Takashi Mizutani

Department of Quantum Engineering, Nagoya University, Nagoya 464-8603, Japan

The control of the conduction type (p/n control) of carbon nanotube thin-film transistors (CNT TFTs) is an issue that must be addressed for the various circuit applications. Techniques for p/n control have been proposed by utilizing chemical doping [1,2]; however, the mobility of the n-type devices are still poor. Here, we realized high-mobility n-type carbon nanotube TFTs on a plastic film, on the basis of the transfer process and chemical doping technique.

Bottom-gate TFTs were fabricated on a PEN substrate. After forming of gate electrodes (Ti/Au: 10/100 nm) with conventional photolithography, electron-beam evaporation, and lift-off process, a 50-nm Al₂O₃ insulator layer was deposited on the substrate by an atomic layer deposition technique. Contact windows for the gate electrodes were then opened by photolithography and reactive-ion etching. Then, the CNT film was transferred from the membrane filter to the substrate having patterned electrodes as previous work [3]. Subsequently, source and drain electrodes were formed by the lift-off process. CNTs outside the channel area were removed by oxygen plasma. The channel length and width are both 100 μm. We used polyethylenimine (PEI, MW 800) for electron donor as reported previously [1]. PEI was dissolved in methanol (0.8 vol%) and dropped on the substrate. Before the solvent evaporated, the solution was removed by nitrogen blow.

Figure 1 shows the I_D - V_{GS} characteristics of a fabricated device. Device measurement was performed in ambient air. Before chemical doping with PEI, the device showed *p*-type characteristics with an on/off ratio of $\sim 10^6$ and a mobility of 85 cm²/Vs for the rigorous model.

After chemical doping with PEI, the device polarity changes to *n*-type, whose mobility is 57 cm²/Vs with a high on/off ratio of $\sim 10^6$. The obtained mobility is the highest value compared to previous *n*-type CNT TFTs to our knowledge.

Acknowledgments: This work was partially supported by '08 NEDO Grant, R&D promotion scheme funding international joint research promoted by NICT, ALCA-JST, and Grant-in-Aid of JSPS.

[1] Y. X. Zhou *et al.*, Nano Lett., 4, 2031 (2004).

[2] Y. H. Lee *et al.*, Acs Nano, 5, 2369 (2011).

[3] D.-M. Sun, *et al.*, Nature Nanotech. 6, 156 (2011).

Corresponding Author: Y. Ohno

Tel: +81-52-789-5387, Fax: +81-52-789-5387,

E-mail: yohnno@nuee.nagoya-u.ac.jp

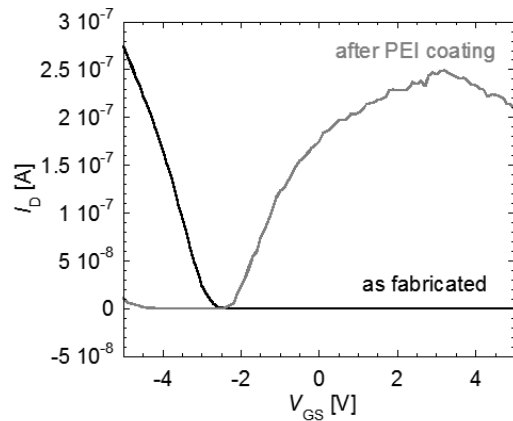


Fig. 1 I_D - V_{GS} characteristics of a CNT TFT measured at $|V_{DS}| = 0.5$ V before and after chemical doping with PEI.

Functionalization of Carbon Nanotubes with Antibody for Immunoassay

Yoko Iizumi¹, Toshiya Okazaki¹, Yuzuru Ikehara², Mutsuo Ogura³, Masako Yudasaka¹

¹ Nanotube Research Center, ² Research Center for Medical Glycoscience

³ Nanosystem Research Institute, National Institute of Advanced Industrial Science and Technology, Tsukuba, Ibaraki, Japan

Optical absorption, fluorescence, and Raman scattering of single-walled carbon nanotubes (CNT) in near infrared (NIR) range are potentially useful for imaging diseased sites in the body because the NIR lights have high transparency for the biological materials. Recently, the mouse blood vessels are visualized by the CNT NIR fluorescence [1]. The advantages of CNTs optical properties are potentially useful in biosensors to increase the detection limit of the objective materials. In our proof of principle study, the CNTs were used as a fluorescent label for immunoassay: IgG antibody was labeled with CNT and the usefulness of CNT label was demonstrated via specific coupling of IgG with protein G.

The CNTs (CoMoCAT) were dispersed in phosphate buffer by coating the CNT surface with phospholipid PEG (PLPEG). Rabbit IgG was attached to PLPEG by the reaction of IgG with NHS, an end group of PLPEG. The obtained complex was designated as CNT-IgG. The CNT-IgG dispersed in phosphate buffer homogenously and stably. It showed the fluorescence spectrum and Raman scattering spectrum characteristic of CNTs. Following a typical immunoassay process, the CNT-IgG was mixed with protein G magnetic beads (Pr.G-beads), and the CNT-IgG/Pr.G-beads were taken out and washed. The CNT-IgG/Pr.G-beads showed fluorescence spectra and Raman spectra of CNTs, indicating IgG, Pr.G, and magnetic beads did not alter the optical properties of CNTs. At the last stage, CNT-PEG was eluted from Pr.G-beads. The eluted solution showed the CNT fluorescence spectra. These results suggest that the CNTs will become useful as the NIR fluorescent label for immunoassay.

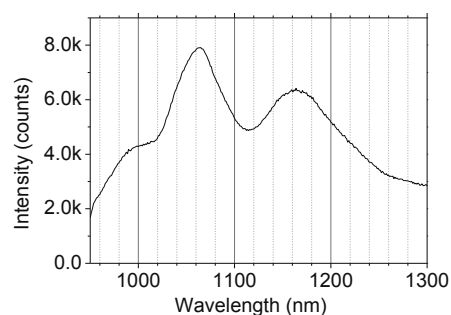


Figure 1. Fluorescence spectrum of CNT-IgG/Pr.G-beads. (Ex.660 nm)

[1] G. Hong et al. Nature Medicine 18, 1841(2012).

Corresponding Authors:

T. Okazaki, E-mail: toshi.okazaki@aist.go.jp,

M. Yudasaka, E-mail: m-yudasaka@aist.go.jp

Arc Production of SWNTs under Controlled He Gas Temperature

○Tetsu Mieno, Takashi Suzuki

Dept. Physics, Shizuoka University, 836 Ooya, Suruga-ku, Shizuoka 422-8529, Japan

By means of the arc discharge method, single-walled carbon nanotubes (SWNTs) and other carbon nano-materials can be produced. However, as the control of production condition is difficult, it is hard to produce high-quality and long SWNTs. In order to develop applications of SWNTs and other carbon nano-material, study of the arc production process is important.

When SWNTs are arc-produced in He gas, strong thermal convection flows up the He gas and sublimated gaseous carbons, and the carbon reaction-time under hot He gas is limited. When this thermal convection is suppressed under the gravity-free condition, carbons thermally diffuse and long reaction-time can be realized, where the hot gas region becomes much larger and spherical. The cooling rate of carbons is also much smaller. [1] In order to realize this convection-free reaction, the parabolic flight experiments were carried out using a jet plane. During 20 sec of the gravity-free times, SWNTs were produced, by which production of SWNTs was considerably improved. [2-4]

Here, we have developed an arc reactor as a ground experiment, in which gas temperature can be controlled by an electric furnace, and the gradient of gas temperature can be decreased. In a vertical and cylindrical metal chamber (50 mm in diameter), two arc electrodes are set, and the arc discharge can be generated (Fig. 1). By using a carbon/Ni/Y composite rod, SWNTs are arc-produced, where $p(\text{He})= 50$ kPa, $I_a= 50$ A. Figure 2 shows a typical TEM image of produced SWNTs under furnace temperature of 700 C. It can be observed that content of SWNTs increases by increasing the gas temperature.

- 1) T. Mieno, Plasma Phys. Controlled Fusion, **46** (2004) 211.
 - 2) T. Mieno, M. Takeguchi, J. Appl. Phys. **99** (2006) 104301.
 - 3) T. Mieno, New Diamond and Frontier Carbon Technol., **16** (2006) 139.
 - 4) T. Mieno, G-D Tan, "Carbon Nanotubes", ed. S. Yellampalli, INTECH, 2011, pp. 61-76.
- TEL & FAX: +81-54-238-4750, E-mail: sptmien@ipc.shizuoka.ac.jp

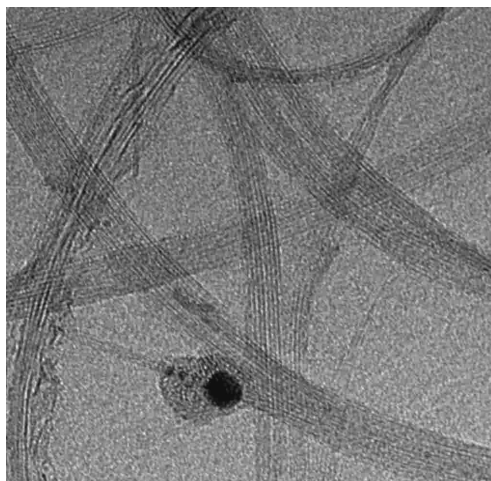
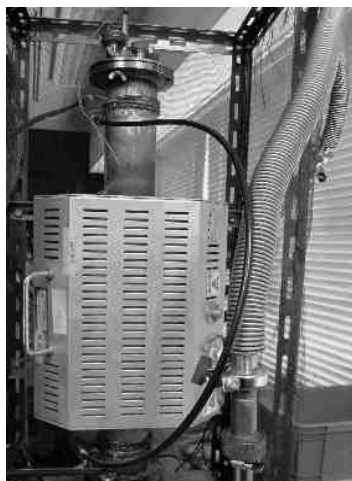


Fig. 1 (left):
Photo of the reactor.
Fig. 2 (right):
A TEM image of SWNTs.
 $T_{gas}= 700$ C.

Electric-field-induced layer formation of metallic and semiconducting single-wall carbon nanotubes in D₂O – H₂O mixtures

°Fusako Sasaki¹, Hideaki Numata^{1,2}, Takeshi Saito^{1,3}, Fumiyuki Nihey^{1,2}

¹Technology Research Association for Single Wall Carbon Nanotubes (TASC), Tsukuba 305-8565, Japan

²Smart Energy Research Laboratories, NEC Corporation, Tsukuba 305-8501, Japan

³National Institute of Advanced Industrial Science and Technology (AIST), Tsukuba 305-8565, Japan

Separation of metallic and semiconducting single-wall carbon nanotubes (SWCNTs) has been intensively studied both for fundamental interests and for electronic applications such as thin-film transistors. We have proposed a method to separate metallic and semiconducting SWCNT solution by electric-field-induced layer formation (ELF) method [1, 2]. Previously, deuterium oxide (D₂O) has been used as solvent to disperse SWCNTs. Ihara *et al.* pointed out that the density gradient established in the solvent plays an important role for ELF [1]. In this presentation, ELF of SWCNTs in D₂O – H₂O mixtures was studied to elucidate the role of the solvent density. From a technological point of view, the reduction of D₂O consumption would make the ELF method cost-effective.

Several sets of polyoxyethylene (100) stearyl ether (Brij 700) solution (1 wt %) were prepared by using the mixtures of D₂O and H₂O with different ratios to obtain solutions with different densities (1.0 – 1.1 g/cm³). SWCNTs (eDIPS, 1.0 nm in diameter) were dispersed in each of the solutions by sonication and ultracentrifugation. Each solution was introduced into a modified separation cell [2] and applied by the voltage of 90 V for 190 hours. Figure 1 shows the initial (a) and final (b) images of the separation cell with SWCNTs in H₂O solution. Semiconductor-rich (lower) and metal-rich (upper) layers were successfully formed as shown in Fig. 1 (b) and (c). Similar results were obtained for SWCNTs in the D₂O:H₂O mixtures with different ratios. We also found that the purity of separated SWCNTs depends on the difference between the densities at the top and bottom of the cell, regardless of the density of solution itself (Fig. 2). We expect our present study paves the way for low-cost separation of metallic and semiconducting SWCNTs by ELF method.

This work was supported by New Energy and Industrial Technology Development Organization (NEDO).

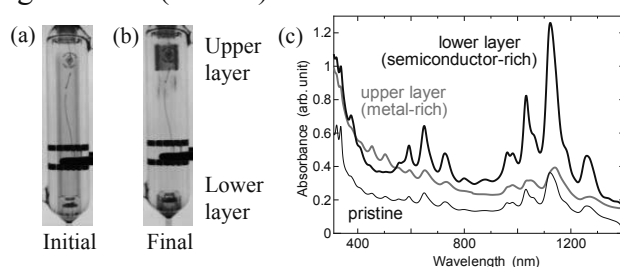


Fig. 1 (a) Initial and (b) final images of a separation cell with SWCNTs in H₂O solution. (c) Absorption spectra of the separated SWCNTs.

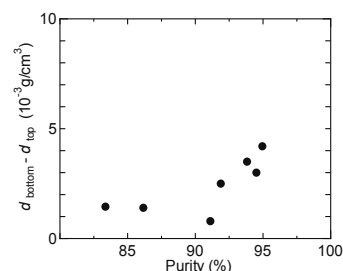


Fig. 2 Relationship between the density differences in the cell and semiconducting SWCNT purities.

References:

- [1] K. Ihara, H. Endoh, T. Saito, and F. Nihey, *J. Phys. Chem. C* **115**, 22827 (2011).
 [2] F. Sasaki, T. Saito, and F. Nihey, The 43th Symposium Abstract, p.85 (2012).

Corresponding Author: Fumiyuki Nihey

E-mail: nihey@tasc-nt.or.jp, **Tel:** +81-29-861-3772, **Fax:** +81-29-858-6330

Development of Substrate Heater System of Cold-Wall Chemical Vapor Deposition Equipment for Improvement of Single-Walled Carbon Nanotubes Quality

○Yusaku Tsuda¹, Satoshi Doi¹, Koji Ishii², Nobuyuki Iwata¹, Hirofumi Yajima², and Hiroshi Yamamoto¹

¹ Department of Electronics & Computer Science, College of Science & Technology, Nihon University, 7-24-1 Narashinodai, Funabashi, Chiba 274-8501 Japan

² Department of Applied Chemistry, Faculty of Science, Tokyo University of Science, 1-3 Kagurazaka, Shinjyuku-ku, Tokyo 162-0826, Japan

In our previous report, position selective growth of single-walled carbon nanotubes (SWNTs) is carried out on a surface treated SiO₂ (300nm)/Si substrate between electrodes by cold-wall chemical vapor deposition (CC-CVD) method in μm-scale^[1]. The SWNTs grow at the intermediate area between electrodes. In addition, chirality controlled growth of the SWNTs is also done by irradiating free electron laser (FEL) during CC-CVD growth. The grown SWNTs are all semiconducting investigated by a multi excited laser Raman analysis. However, the grown SWNTs length is limited to approximately 500 nm, and the value of the G/D ratio is still low around 30 using 532 nm excitation laser, probably due to the degradation of growth front by too much feeding carbon source. In this study we develop the new heater system and change a CC-CVD growth process, resulting in over 400 in the value of G/D ratio.

The new heater used in the CC-CVD process was SiC (EIG, NIKKATO Co.). The reaching temperature at the heater surface is approximately 1300°C. The heater was surrounded by a thermal insulating material, and the substrate holder was set above the heater with the distance of about 51.5mm. The heater system, including heater substrate, thermal insulating material, and thermal reflecting metals, was annealed in air to get rid of deposited carbon in advance. Surface treated substrate SiO₂(300nm)/Si in O₃ atmosphere was dipped in Mo dissolved solution followed by Co dissolved solution. The dipped substrate was annealed at 400°C after each dipping. The CC-CVD process was carried out at 700 °C, measured at the substrate surface by a thermocouple.

Figures 1 and 2 show surface images of the grown SWNTs using a ceramic heater and the new SiC heater, respectively. The length was more than about 1μm as shown in Fig.2. The value of G/D ratio was over 400 with 532 nm excitation laser. RBM peaks indicated the presence of SWNTs with 1.0 ~ 1.7 nm in diameter. Particles, probably catalysts covered by amorphous carbon, was also observed. The details will be discussed.

[1] K.Sakai, *et al.*, IEICE TRANS. Electron, E94-C (2011) 1861.

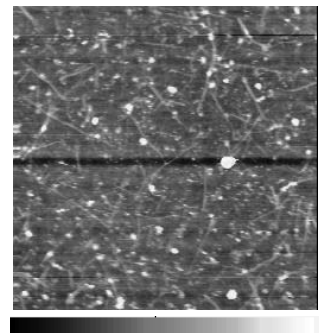


Fig.1 The previous surface image after CC-CVD process with the size of 2μm×2μm

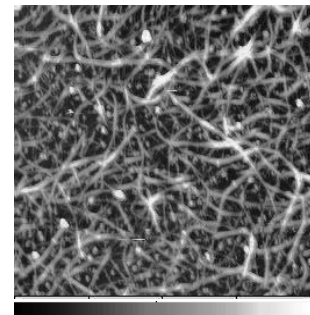


Fig.2 The surface image after CC-CVD process with the size of 2μm×2μm using new SiC heater.

Nitrogen-doped single-walled carbon nanotubes and their growth mechanism

○Theerapol Thurakitseree¹, Christian Kramberger¹, Akihito Kumamoto², Shohei Chiashi¹, Erik Einarsson¹, Shigeo Maruyama¹

¹ *Department of Mechanical Engineering, The University of Tokyo, Tokyo 113-8656, Japan*

² *Institute of Engineering Innovation School of Engineering, The University of Tokyo, Tokyo 113-8656, Japan*

An ongoing challenge in the field of nanotechnology is the controlled synthesis of single-walled carbon nanotubes (SWNTs). In particular, synthesis of SWNTs with uniform diameters or chiralities is critical for applications that rely on the SWNT optical properties. The presence of nitrogen during nanotube synthesis has been shown to strongly influence the nanotube diameter [1], making it a promising approach to controlling nanotube properties at the synthesis stage. We have recently demonstrated this effect is very strong when acetonitrile (CH_3CN) is introduced into ethanol feedstock, but the mechanism is not yet clear [2].

In the present study, we address the role of nitrogen on influencing the SWNT diameter. The mean diameter of vertically aligned SWNTs can be modulated along the nanotube array by simply switching between pure ethanol feedstock and a 5% acetonitrile mixture in ethanol [3]. The mean diameter changes from 2.1 nm for ethanol-grown SWNTs to approximately 1 nm when acetonitrile is added. This diameter change is reversible (Fig. 1), suggesting that nitrogen affects only the surface of the catalyst particle. We hypothesize that the presence of nitrogen reduces the effective flux of carbon into the catalyst nanoparticle, resulting in a change from a tangential to perpendicular growth mode [4], which results in a smaller diameter.

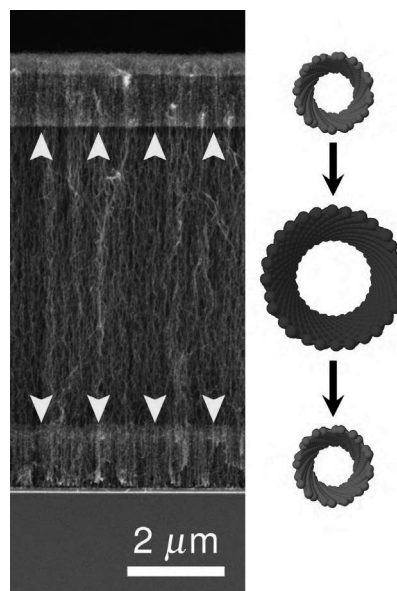


Fig.1 Scanning electron microscope images of triple-layered VA-SWNT array with different diameters along nanotubes synthesized from ethanol (blue) and 5% acetonitrile mixture in ethanol (red). Yellow arrows point at interface between layers.

[1] P. Ayala *et al.*, *Carbon*. **48**, 575 (2010).

[2] T. Thurakitseree *et al.*, *Carbon*. **50**, 2635 (2012).

[3] T. Thurakitseree *et al.*, under review.

[4] M.-F. C. Fiawoo *et al.*, *Phys. Rev. Lett.* **108**, 195503 (2012).

Corresponding Author: Prof. Shigeo Maruyama

Tel: +81-3-5841-6408, Fax: +81-3-5800-6983,

E-mail: maruyama@photon.t.u-tokyo.ac.jp

Selective synthesis of large amount of (6, 5) single-walled carbon nanotubes using pulse plasma CVD

○Koshi Murakoshi, Toshiaki Kato, Rikizo Hatakeyama, Toshiro Kaneko

Department of Electronic Engineering, Tohoku University, Sendai, 980-8579 Japan

One dimensional single-walled carbon nanotubes (SWNTs) are potential materials for future nanoelectronics. Since the electronic and optical properties of SWNTs strongly depend on their diameter and chirality, the selective synthesis of SWNTs with desired chiralities is one of the major challenges in nanotube science and applications. Recently, we have demonstrated a narrow-chirality distributed growth of SWNTs by time-programmed plasma CVD [1]. In this method, we used very short time growth of SWNTs. Based on the systematic investigations, it has been revealed that there is a close correlation between incubation time (t_i) and SWNT structures. Since t_i of the small diameter (or specific chirality) SWNTs is shorter than that of the larger (or other chiralities) one, selective growth of narrow-chirality distributed SWNTs has been realized by adjusting the growth time during plasma CVD. Due to the short growth time, however, only small amount of narrow-chirality distributed SWNTs can be grown with this method.

In this study, we have improved previous time-programmed plasma CVD and established a new strategy to realize the mass production of narrow-chirality distributed SWNTs using pulse plasma CVD. In the pulse plasma CVD, multiple short time growth of SWNTs is possible by repeating the plasma generation. In order to compare before and after pulse plasma irradiation at the same region, we carry out the mapping analysis. The amount of SWNTs is also estimated by the intensity of G-band, which is normalized by the intensity of Si. Chirality distribution of SWNTs is analyzed by optical measurements such as photoluminescence excitation-emission (PLE) spectroscopy and UV-vis-NIR absorption spectroscopy.

When we carry out the pulse plasma CVD for SWNTs growth, it is found that the amount of SWNTs increases with an increase in the total growth time. Interestingly, it is also revealed that the initial narrow-diameter distribution of SWNTs can be maintained even after the long time pulse plasma CVD. We think this is because that only specific diameter or chirality SWNTs can be grown during each pulse of plasma CVD due to their very short t_i . The results of optical measurements indicate the (6, 5) SWNTs are selectively synthesized by pulse plasma CVD. When we adjust the growth conditions, we can improve the purity of (6, 5) SWNTs up to 36%. These results indicate that it should be possible to realize the mass production of narrow-chirality distributed SWNTs with our established novel approach.

[1] T. Kato and R. Hatakeyama, ACS Nano **4**, 7395 (2010).

Corresponding Author: K. Murakoshi

Tel: +81-22-795-7046, Fax: +81-22-263-9225,

E-mail: murakoshi10@ecei.tohoku.ac.jp

Alcohol Catalytic CVD Synthesis of Single-Walled Carbon Nanotubes Using C₆₀ as the Catalysts

○Kenta Nakamura, Takanori Umino, Shohei Chiashi and Shigeo Maruyama

Department of Mechanical Engineering, The University of Tokyo, Tokyo 113-8656, Japan

Structure-controlled synthesis of single-walled carbon nanotubes (SWNTs) can make a breakthrough in applications of SWNTs. Carbon materials in nano-size such as diamond nano-particles and fullerenes are good candidates for the catalyst of the structure-controlled synthesis, because they can be controlled in size and hardly aggregate even at high temperatures. C₆₀ is one of those carbon materials, and was reported to act as catalysts for SWNT synthesis by CVD [1].

We performed CVD synthesis using C₆₀ as the catalyst. C₆₀ crystals were made on Si/SiO₂ substrate by dropping C₆₀-toluene solution on the substrate. Ethanol gas was used as a carbon source. The CVD temperature was 650~950 °C and the pressure of ethanol gas was 1.3 kPa. The samples were inserted into an electric furnace after the temperature reached 800 °C. Our CVD process does not include any oxidation or water-treatment which were used for SWNT growth from C₆₀ in previous reports [1, 2].

An SEM image of grown SWNTs is shown in Fig. 1. The SEM image indicates that SWNTs are grown from an agglomeration with size of approximately 5 μm. Although the agglomerations come from C₆₀, typical Raman signal of C₆₀ could not be observed from them. It suggested that C₆₀ clusters were thermally polymerized or deform. Raman spectrum of grown SWNTs is shown in Fig. 2. The split peak of G-band around 1590 cm⁻¹ proves the existence of SWNTs. Moreover, if the samples were located in the furnace during temperature elevation, no SWNTs were synthesized probably because of sublimation of C₆₀. These results indicate that the SWNTs grow from C₆₀ or carbon material generated from C₆₀ during CVD.

In addition, we examined the effect of temperatures and ethanol gas pressures of CVD on the production yield and structures of SWNTs grown from C₆₀. The tendency was compared with that of SWNTs synthesized from Co/Mo catalysts.

[1] X. Yu *et al.* Nano Lett. **10**, 3343 (2010).

[2] I. Ibrahim *et al.* ACS Nano **6**, 10825 (2012).

Corresponding Author: Shigeo Maruyama

Tel: +81-3-5841-6421, Fax: +81-3-5800-6983,

E-mail: maruyama@photon.t.u-tokyo.ac.jp

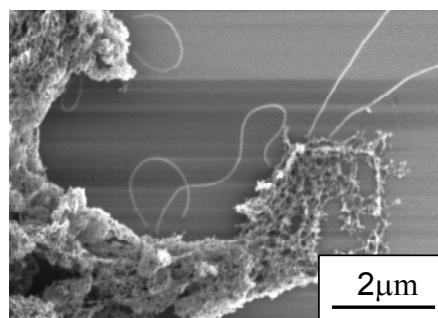


Fig.1 SEM image of SWNTs synthesized from C₆₀.

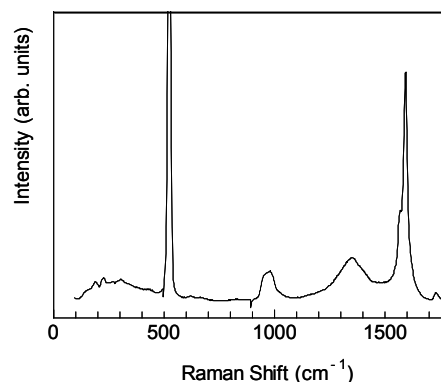


Fig.2 Raman scattering spectrum of SWNTs synthesized from C₆₀.

Characterization of Horizontally Aligned Single-Walled Carbon Nanotubes Grown on Crystal Quartz by Using Scanning Microscopy

○Daisuke Hasegawa, Taiki Inoue, Keigo Otsuka, Saifullah Badar,
Shohei Chiashi and Shigeo Maruyama

Department of Mechanical Engineering, The University of Tokyo, Tokyo, 113-8656, Japan

Characterization of single-walled carbon nanotubes (SWNTs) is of great importance especially for understanding of growth mechanism toward electronic applications such as field effect transistors. Scanning electron microscopy (SEM) has the advantage of facile observation in a wide range of magnifications, and atomic force microscopy (AFM) can measure surface nanostructure. Specific peaks, such as G-band or radial breathing mode (RBM), in a Raman spectrum of SWNTs provide information of quality, diameter and chirality. Horizontally aligned SWNTs (HASWNTs) have been reported to grow along a particular orientation on the single crystal quartz substrates with several cutting angles [1, 2]. Low density, little entanglement and high straightness of HASWNTs compared to other morphologies have the advantage of easier characterization of individual SWNTs in the axial direction.

In this study, we used scanning Raman spectroscopy, AFM and SEM to investigate as-grown HASWNTs synthesized by alcohol catalytic chemical vapor deposition on crystal quartz in the exact same measurement area. Raman scattering, AFM and SEM images are shown in (a-c), (d) and (e) of Fig. 1, respectively. Through comparison of these measurements, G-band, RBM, height profiles and length of each SWNT can be assigned each other. Approximately 40% and 10% of HASWNTs seen in SEM images can be observed in Raman images of G-band and RBM signals using a 532 nm excitation laser, respectively.

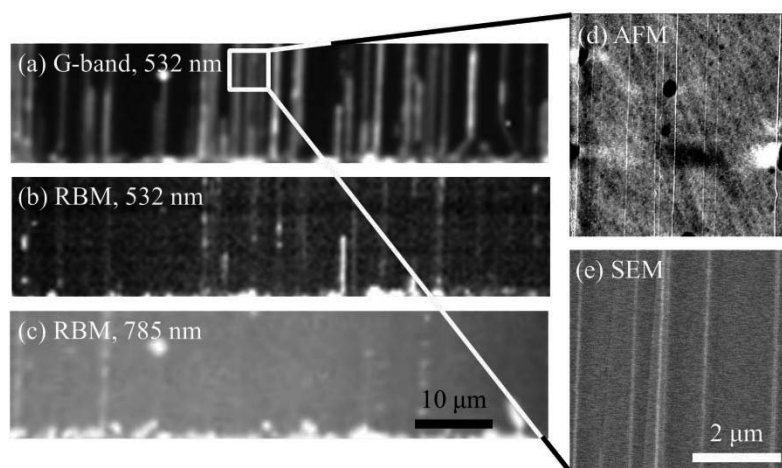


Fig. 1 Images of HASWNTs observed by using (a-c) Raman spectroscopy, (d) AFM and (e) SEM. Intensity mapping of (a) G-band and (b) RBM using a 532 nm excitation laser and (c) RBM using a 785 nm excitation laser are shown. Note that holes and scratch lines clearly seen in (d) come from the fabrication process of quartz substrates.

[1] C. Kocabas *et al.* *Small* **1**, 1110 (2005).

[2] S. Chiashi *et al.* *J. Phys. Chem. C* **116**, 6805 (2012).

Corresponding Author: S. Maruyama

TEL: +81-3-5841-6421, FAX: +81-3-5800-6983

Email: maruyama@photon.t.u-tokyo.ac.jp

String-like Aggregates of Aligned (6,5) Single Wall Carbon Nanotubes

○H. Kawai¹, K. Hasegawa¹, T. Nakatsu², Y. Naitou³, Y. Takagi⁴, T. Takenobu⁴, K. Yanagi¹

¹ Tokyo Metropolitan Univ., ² Kyoto Univ., ³ AIST, ⁴ Waseda Univ.

Single wall carbon nanotubes (SWCNTs) show various properties depending on their chiralities. Recently, it becomes possible to obtain high-purity SWCNTs with a single chirality by density gradient ultracentrifugation and gel chromatography and so on. Those techniques enable us to investigate the physical properties of SWCNTs with uniform electronic structure, however, typical properties of such high-purity SWCNTs have been often investigated in randomly distributed networks. How to obtain aligned purified SWCNTs systems is an important subject to improve device performances.

In our study, we investigated to control aggregation processes of SWCNTs, which are enriched (6, 5) chirality, dispersed in solutions with surfactants. We found that temperature of the solutions and reaction time significantly influenced their aggregation processes and morphologies of the aggregates. Fig. 1 shows pictures of solutions when the vial was heated at several different temperatures and reaction times. If the temperature was below 70 degrees, no aggregation was observed. When the temperatures were set at 80~100 degrees for over 3 hours, disordered aggregations (alga-like aggregations) were dominantly generated. However when the temperature and the reaction time were adjusted to a proper condition, string-like aggregates were formed. Micro-Raman measurement clearly shows that the (6, 5) SWCNTs were aligned to string axis in the aggregates. In addition, clear alignments of SWCNT bundles were observed in SEM images. Moreover, we succeeded to control conductance of the string-aggregates by electric double layers techniques. This result will be a first step toward crystallization of SWCNTs.

Corresponding Author: K. Yanagi

Tel: +81-42-677-2494, Fax: +81-42-677-2483,

E-mail: yanagi-kazuhiro@tmu.ac.jp

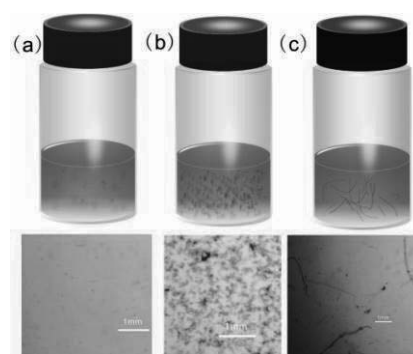


Fig1. (a) Temperatures at 10°C ~70°C, reaction time more than 1 day. (b) at 80°C~100°C for more than 3 hours. (c) at 80°C~100°C for 1 hour.

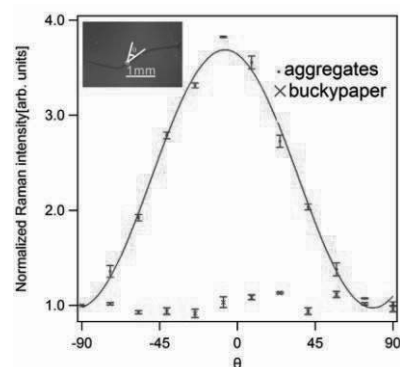


Fig2. G-band intensities of aggregates and buckypaper as a function of polarization angles of excitation light.

Super Growth: Unexpectedly High Yield Carbon Nanotube Synthesis from Low Activity Carbon Feedstocks at High Concentrations

○Hiroe Kimura^{1,3}, Jundai Goto¹, Satoshi Yasuda¹, Shunsuke Sakurai¹, Motoo Yumura¹,
Don N. Futaba*¹ and Kenji Hata*^{1,2,3}

¹*Nanotube Research Center, National Institute of Advanced Industrial Science and Technology (AIST), Tsukuba, 305-8565, Japan.*

²*Japan Science and Technology Agency (JST), Kawaguchi, 332-0012, Japan.*

³*Tsukuba University, Department of Pure and Applied Sciences, Tsukuba University, Tsukuba, 305-8573, Japan*

When a carbon feedstock is delivered into the reaction chamber of a CVD system, the concentration is a critical parameter because for a given growth process (*i.e.* flow rate, temperature, catalyst composition, catalyst amount, *etc.*) an optimum carbon feedstock concentration exists for the yield. In general, it is well-known that as the carbon feedstock concentration increases, the yield increases, peaks, and then drops. This is because at low feedstock concentrations, the rate-limiting factor is the supply of carbon, while at high feedstock concentrations, the rate limiting factor is the short catalyst lifetime. Therefore, the current trend for CNT synthesis is the use of highly active carbon feedstocks, such as acetylene, ethylene at low concentrations. However, when a growth enhancer is added at even ~100 ppm levels, this optimum carbon concentration can be greatly increased which leads to a dramatic increase in growth yield as exemplified by water-assisted CVD (Super-growth method ^[1]).

Here, we report an entirely different approach using the Super Growth CVD method, where, in contrast to using highly active carbon feedstocks at low concentrations, low activity carbon feedstocks are used in high concentrations, exceeding the saturation concentrations for active sources, to achieve unprecedented and superior CNT growth yields. We found that when an unsaturated, chain feedstock, such as butane, was used as the carbon feedstock, the yield linearly increased with carbon concentration, and did not show saturation or a peak as observed with the other groups of hydrocarbons. As a result, we could achieve 2.5-fold optimum growth yield higher than using ethylene. We propose that the mechanisms for the growth kinetics for high and low reactivity carbon feedstocks are fundamentally different where the latter benefits from a longer catalyst lifetime because of a relatively low production rate of carbon impurities.

References:

[1] K. Hata *et al*, *Science*, **306**, 1241 (2004)

*Corresponding Author: Kenji Hata, Don N. Futaba

TEL: (029) 861-4654, FAX: (029) 861-4851, E-mail: kenji-hata@aist.go.jp, d-futaba@aist.go.jp

Pressure dependence of High-temperature Pulsed-arc Discharge

○Hayato Kikuchi¹, Katsuhide Terada², Toshiki Sugai¹

¹ *Department of Chemistry, Toho University, Chiba 274-8510, Japan*

² *Faculty of Pharmaceutical Sciences, Toho University, Chiba 274-8510, Japan*

A high-temperature pulsed-arc discharge (HTPAD) has been developed to produce nanocarbon materials. The system utilizes width controlled pulsed arc discharge for the vaporization of electrode in temperature controlled ambient rare gas. With this width and temperature control, novel materials have been produced by the system such as high-quality double wall carbon nanotubes[1]. Furthermore by utilizing the low energy consumption of pulse mode operation we can shrink the system size and increase the working pressure compared to the standard steady arc discharge around 2 atm[2]. Here, we present the pressure dependence of production of carbon nanotubes by the pulsed arc discharge up to 4 atm.

The system consists of a furnace with a ceramic tube inside, an Ar gas flow and pressure control system, an HV pulse voltage controller, and a water cooling trap. Electrodes made of graphite containing catalytic metals (Ni/Y 4.2/0.5 at. %:Toyo Tanso Co. Ltd.) were located in the ceramic tube. The pulsed arc discharges (0.6 ms, 50 Hz, and 100 A) vaporized the electrodes and produced nanotubes in the high-temperature (1250 °C) and high-pressure (up to 4 atm) Ar gas in the ceramic tube. The products were collected on the trap and were characterized by Raman spectroscopy with excitation laser of 633 nm together with weight analyses.

Figure 1 shows the pressure dependence of G/D ratio of the Raman spectra. The ratio increases as the pressure increases showing the graphitization of the produced nanotubes is enhanced by the pressure. Figure 2 shows the ratio between the mass of trapped product and that of the vaporized electrodes. Since the produced nanotubes are selectively collected on the trap, the result shows that concentration of nanotubes in the vaporized materials is also increased by the pressure. These results clarified that the production processes are controlled by the pressure and that there exists some frontier to improve the productivity through the high pressure of 4 atm which have been not utilized by the steady arc discharge[2].

[1] T. Sugai *et al.*, *Nano Lett.* **3**, 769 (2003).

[2] Y. Saito, Y. Tani, and A. Kasuya, *J. Phys. Chem. B.* **104**, 2495 (2000).

Corresponding Author: T. Sugai Tel: 047-472-4406 E-mail: sugai@chem.sci.toho-u.ac.jp

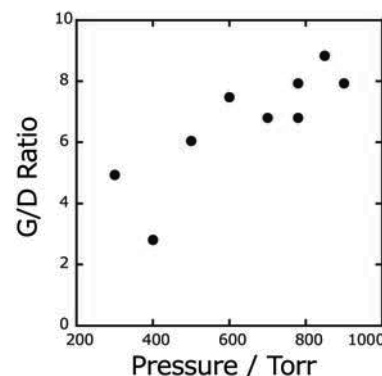


Fig. 1 Pressure Dependence of G/D ratio

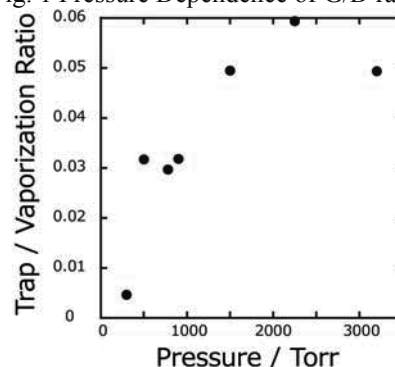


Fig. 2 Pressure Dependence of Trap vs. Vaporization Ratio

ESR Measurements of N@C₆₀ with [10]Cycloparaphenylene in Solution

○Mitsuhiro Okamoto¹, Takahiro Iwamoto², Shigeru Yamago², and Tatsuhisa Kato^{1,3}

¹ *Department of Interdisciplinary Environment, Graduate School of Human and Environmental Studies, Kyoto University, Kyoto 606-8501, Japan*

² *Institute for Chemical Research, Kyoto University, Uji 611-0011, Japan*

³ *Institute for the Promotion of Excellence in Higher Education, Kyoto University, Kyoto 606-8501, Japan*

Cycloparaphenylenes (CPPs) are molecules with the simplest structure unit of armchair carbon nanotubes in which paraphenylene structures are linked in a cyclic manner. The concave cavity of the CPPs should act as a host for π -conjugated molecules with a convex surface, such as fullerenes. Yamago group of author succeeded in syntheses of [n]CPPs (n=8-13)^[1] and reported the size selective encapsulation of C₆₀ by [10]CPP^[2]. We report here ESR studies of N@C₆₀ encapsulated complex by [10]Cycloparaphenylene in solution by using a X band-ESR spectrometer

The ESR spectra of N@C₆₀-[10]CPP complex in toluene-d₈ solution are shown in Fig.1. Spectra were recorded at temperatures above and below the freezing point of solvent, T_{freezing} =178K. Comparing with spectra of intact N@C₆₀ in toluene-d₈ solution, it is noticeable that the sharp triplet peaks are still observed even below the freezing temperature of solvent. The rotation of N@C₆₀ within the encapsulated complex should reflect on the prominent feature of the sharp line width of ESR spectra below the freezing point of solvent.

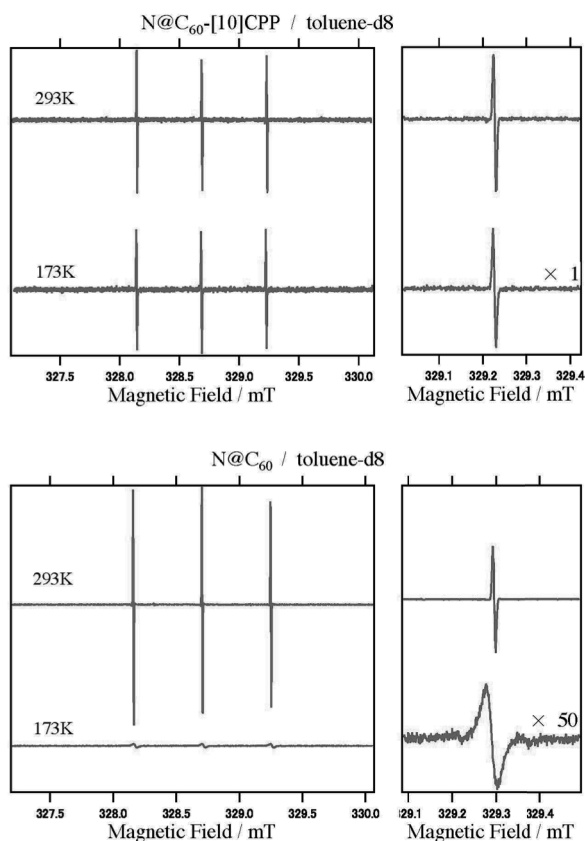


Fig.1 ESR spectra of N@C₆₀-[10]CPP complex and intact N@C₆₀ in toluene-d₈ solution at the temperatures above and below the freezing point of 178K.

[1] T. Iwamoto *et al.* J. Am. Chem. Soc. **133**, 8354 (2011).

[2] T. Iwamoto *et al.* Angew. Chem. Int. Ed. **50**, 8342 (2011).

Corresponding Author: T. Kato

Tel: +81-75-753-6695, Fax: +81-75-753-6695,

E-mail: kato.tatsuhisa.6e@kyoto-u.a.cjp

Polythiophene encapsulated in carbon nanotubes as a high-throughput Raman imaging marker

○Kenshi Miyaura, Yasumitsu Miyata, Ikuya Wakamori, Boanerges Thendie,
Ryo Kitaura, Hisanori Shinohara

*Department of Chemistry & Institute for Advanced Research, Nagoya University,
Nagoya 464-8602, Japan*

Raman imaging of carbon nanotubes is one of the most powerful tools for the high-throughput measurement of nanotube location, density, and orientation on arbitrary substrates and even in living cells [1,2]. However, complete Raman imaging of nanotubes requires multiple-wavelength laser excitations because the resonance energies of CNTs vary sensitively depending on the chirality. To solve this problem, we have focused our attention to the use of encapsulated molecules inside nanotubes as an imaging marker. In our previous study [2], we reported the encapsulation of polythiophene (PT, Fig.1a), a representative pi-conjugated polymer, and its high filling yield, a single resonance band, and strong Raman signals. These findings have tempted us to further investigate the optical properties of individual nanotubes encapsulating PT.

Here, we demonstrate that the encapsulated PT can be used as an efficient marker of individual CNTs for Raman imaging with a single-wavelength laser excitation. PT/CNT complexes were obtained by a vapor-phase doping of oligothiophenes and were purified with density gradient ultracentrifugation. The individual nanotubes were then deposited on a SiO₂/Si substrate and measured on confocal Raman imaging with a 488 nm excitation laser. As shown in Figs.1b-c, as compared with the G-band intensity image of nanotubes (Fig.1b), the Raman image of PT shows more points in the same area (Fig.1c). In some locations, only the PT-derived peaks can be observed because of off-resonance of outer nanotubes at the present excitation wavelength (Fig.1d). These results indicate that the present nanotube system possesses a high potential of PT markers for versatile imaging of CNTs in electronics and biological applications.

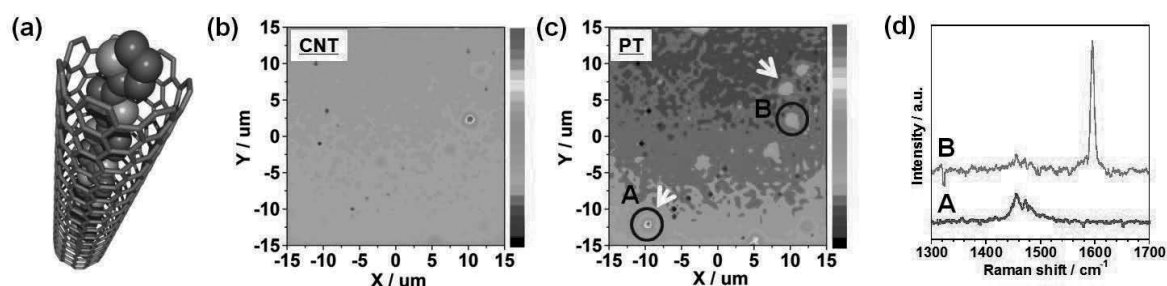


Figure 1. (a) Schematic illustration of the PT/CNT complex. Raman images of (b) G-band intensity of CNTs and (c) PT-derived peak intensity. (d) Raman spectra at different points marked by circles of A and B in Fig. 1c.

[1] R. Haverner *et al.*, *ACS Nano* **6**, 373 (2011), [2] J. W. Kang *et al.*, *Nano Lett.* **12**, 6170 (2012),

[3] K. Miyaura *et al.*, The 43th FNTG General Symposium.

Corresponding Author: Hisanori Shinohara

Tel: 052-789-2482, **Fax:** 052-747-6442, **E-mail:** noris@nagoya-u.jp.

Biodegradation of Single-Wall Carbon Nanohorns

○Minfang Zhang¹, Mei Yang¹, Cyrill Bussy², Hanene Ali-Boucetta², Sumio Iijima^{1,3},
Kostas Kostarelos², Masako Yudasaka¹

¹ *Nanotube Research Center, National Institute of Advanced Industrial Science and Technology,
1-1-1 Higashi, Tsukuba 305-8565, Japan*

² *Nanomedicine Lab, University College London (UCL) School of Pharmacy,
London WC1N 1AX, United Kingdom*

³ *Department of Materials Science and Engineering, Meijo University, 1-501 Shiogamaguchi,
Tenpaku, Nagoya 468-8502, Japan*

With the rapid development in the applications of nanocarbons, such as carbon nanohorn (CNH), carbon nanotube and nanographene in biomedicine, the concerns of long-term fate, excretion, and degradation of these materials are very important. Recently, some reports have shown that carbon nanotubes and graphene can be biodegraded under certain conditions [1], but the biodegradation of CNH has still remained unclear. In this study, we have investigated the biodegradation of CNHs in *ex vitro* and *in vitro* experiments.

CNHs treated with light assisted oxidation (LAOx-CNHs) [2] were incubated with a low concentration of hydrogen peroxide (40 μ M) supplemented with two simulated biological solutions. One was enzyme of human myeloperoxidase (*h*MPO) solution and another was phagolysosomal stimulant fluid (PSF). PSF is a medium that mimics the acidic oxidizing environment typically presented in endosomes and phagolysosomes. Our results showed that CNHs degraded slowly in PSF solution and about 50% CNHs were removed after 2 months. On the other hand, about 40% CNHs were removed in 5 days when *h*MPO was used.

In order to investigate the cellular degradation of CNHs, we incubated human leukemia macrophage cells (THP-1) with LAOx-CNHs (10 μ g/ml). Quantities of CNHs in the cells were estimated from optical absorption intensities (700 nm) of CNHs in the cell-lysis. The amounts of CNHs in the cells decreased with longer incubation periods and about 30 % CNHs were degraded after 9 days.

The small-sized (20-50 nm) CNHs [3] having more carboxylic groups than LAOx-CNHs (sizes ca. 100 nm) were prepared and their biodegradation was similarly studied. The degree of degradation for small-sized CNHs was about 12% in *ex vivo* studies and 20% in cell cultures using the THP-1 cell line. The reason why the kinetics of degradation for the small-sized CNHs seemed to be slower than the large-sized CNHs has been revealed and will be further investigated as will be discussed in the presentation.

[1] B. L. Allen et al. *Nano let.* **8**, 3899 (2008); *J. Am. Chem. Soc.* **131**, 17194 (2009); V. E. Kagan, et al. *Nat. Nanotechnol.* **5**, 354 (2010). X. Liu, et al. *Carbon* **48**, 1961 (2010).

[2] M. Zhang, et al. *ACS Nano* **1**, 265 (2007). [3] M. Zhang, et al. *Small* (2012).

Corresponding Author: M. Zhang, K. Kostarelos, M. Yudasaka

E-mail: m-zhang@aist.go.jp; k.kostarelos@ucl.ac.uk, m-yudasaka@aist.go.jp

Carbon nanohorns induced RAW264.7 apoptosis: Lysosomal membrane destabilization caused reactive oxygen species generation, leading cell apoptosis

○Mei Yang¹, Minfang Zhang¹, Yoshio Tahara¹, Sumio Iijima^{1,2}, Masako Yudasaka¹

¹ *Nanotube Research Center, AIST 5-2, Tsukuba, Japan*

² *Department of Material Science and Engineering, Meijo University, Nagoya, Japan*

In recent years, nanocarbons have gained enormous popularity and offered a wide range of potential applications. With increasing industrial productions of nanocarbons, public concern on their environmental and health effects is growing rapidly. Animal studies show that intravenously injected nanocarbons are easily captured by tissue macrophages and retained in the tissues for long periods. This accumulation in macrophages could potentially lead to long-term toxicity, which may limit the bio-application of nanocarbons. In this context, negative effects, such as inflammatory response, oxidative stress and thrombus induction have been found both *in vitro* and *in vivo* studies [1-3]. Recently, *in vitro* experiments show that nanocarbons causes apoptosis at high uptake conditions [4-5], but its mechanism of how the nanocarbons induce apoptosis has not been clarified. Therefore, we have studied the mechanism of apoptosis induced by single-walled carbon nanohorns (SWNHs), a type of nanocarbons, in macrophages.

We used SWNHs treated by light-assisted oxidation with hydrogen peroxide. They were dispersed in cell culture medium without using any dispersants, and used for the cell experiments of RAW264.7 macrophage. It was found that SWNH caused cell proliferation inhibition, reactive oxygen species (ROS) generation and caspase activation in a SWNH concentration and incubation time dependent manner. Lysosomal membrane destabilization was determined by acridine orange staining method. Lysosomal membrane destabilization occurred just 1 hour after SWNHs treatment and enhanced gradually for 6 hours, while ROS generation started 1 h after SWNHs treatment and kept low level, but suddenly increased after 24 hours. Cathepsins (lysosomal enzymes) inhibitors suppressed ROS generation. The results suggest that the high accumulation of SWNHs in lysosomes caused the lysosomal membrane destabilization, which induced the ROS generation, leading to the cell apoptosis.

[1] AA Shvedova, *et al.* Am. J. Physiol. Lung Cell. Mol. Physiol., **289**, L698, (2005).

[2] G Jia, *et al.* Environ. Sci. Technol, **39**, 1378(2005).

[3] S K Singh, *et al.* ACS nano, **5**, 4987(2011).

[4] Y Tahara, *et al.* Biomaterials, **33**, 2762(2012)

[5] WW Cheng, *et al.* Int. J. Biochem. Cell Biol., **43**, 564(2011).

Corresponding Author: M. Yang and M. Yudasaka.

Tel:029-861-4818, TEL/Fax: +81-29-861- 6290

E-mail: m-yan@aist.go.jp (M. Yang), m-yudasaka@aist.go.jp (M. Yudasaka).

Nitrogen-doped carbon nanohorn aggregates with electrocatalytic activity for oxygen reduction

○Ryota Yuge¹, Takashi Manako¹, Shunji Bandow⁴, Masako Yudasaka², Kiyohiko Toyama¹,
Takashi Yamaguchi³, Sumio Iijima⁴, and Kaichiro Nakano¹

¹ *Smart Energy Research Laboratories, NEC Corporation, Tsukuba 305-8501, Japan*

² *Nanotube Research Center, National Institute of Advanced Science and Technology (AIST),
Tsukuba, 305-8565, Japan*

³ *Institute for Advanced Research, Nagoya University, Nagoya, 464-8602, Japan*

⁴ *Department of Materials Science and Engineering, Meijo University, Nagoya 468-8502,
Japan*

Single-wall carbon nanohorns (SWNHs) [1] are a kind of nano-carbon materials such as carbon nanotubes, and graphenes, which are attractive due to their excellent properties as support for metal particles [2]. Recently, it has been reported that non-metallic nitrogen-doped carbon nanotubes have the intrinsic catalytic properties for oxygen reduction reaction (ORR) [3]. This achieves not only the potentially low cost for noble metal free but also their better stability against CO poisoning compared to traditional platinum catalysts [3]. In this study, we tried to incorporate the nitrogen atom in graphene sheets of SWNHs and control the quantity of the nitrogen atoms. We also investigated the ORR electrocatalytic activity of them.

SWNHs were prepared by the CO₂ laser ablation, which was operated at 3.5 kW at room temperature. During 30 seconds laser ablation, the target was rotated at 2 rpm. The buffer gases were N₂, Ar, and N₂/Ar mixture. The gas flow rate and pressure were 10 L/min and 760 Torr, respectively. The obtained samples are denoted as N₂-SWNHs, Ar-SWNHs, and N₂/Ar-SWNHs.

Shapes of N₂-SWNHs, Ar-SWNHs, and N₂/Ar-SWNHs observed by a scanning electron microscopy and scanning transmission electron microscopy were quite similar. However, from XPS, and ESR results, we found that the nitrogen atoms are incorporated in the carbon network of N₂-SWNHs and behave as acceptors. In oxygen-saturated 0.1 molar potassium hydroxide, electrocatalytic activity of N₂-SWNHs was superior to that of Ar-SWNHs, indicating that nitrogen atoms incorporated in graphene network acted as active sites of ORR. The details are shown in the presentation.

[1] S. Iijima *et al.* Chem. Phys. Lett. **309**, 165 (1999).

[2] T. Yoshitake *et al.* Physica B **323**, 124 (2002).

[3] K. Gong *et al.* Science **323**, 760 (2009).

Corresponding Author: R. Yuge

Tel: +81-29-850-1566, Fax: +81-29-856-6137

E-mail: r-yuge@bk.jp.nec.com

CVD Growth of Bernal Stacked Bilayer Graphene on Heteroepitaxial Cu(111) Film

○Shota Tanoue,¹ Kenji Kawahara,² Masaharu Tsuji,^{1,2} and Hiroki Ago^{*,1,2}

¹Graduate School of Engineering Sciences, Kyushu University, Fukuoka 816-8580

²Institute for Materials Chemistry and Engineering, Kyushu University, Fukuoka 816-8580

To overcome the problem of no bandgap in graphene, several methods have been proposed including the applying a vertical electric field to bilayer graphene (BLG). By using exfoliated BLG it was demonstrated that band gap is tunable up to 250 meV [1]. The non-zero bandgap is induced by breaking the inversion symmetry of the two layers. Thus, for application of graphene to semiconductor devices, the growth of uniform BLG with Bernal stacking (AB stacking) is demanded. Recently, several groups reported the CVD growth of large BLG sheets on Cu foil [2,3], but their Raman 2D band was broad and featureless without clear shoulder peak. Apparently, the observed 2D band of the CVD grown BLG [2,3] is different from that of exfoliated graphene [4], signifying the stacking is not highly ordered in the CVD grown BLG.

In this work, we report our attempt to grow Bernal stacked BLG by CVD. As illustrated in Fig. 1, we used heteroepitaxial Cu(111) film deposited on sapphire c-plane that was used to grow single-layer graphene whose lattice orientation is consistent with the underlying metal lattice [5]. We systematically studied the CVD growth and found that the simple increase of CH₄ concentration gives only monolayer graphene, but the appropriate amount of H₂ accelerates the CH₄ decomposition, stimulating the BLG growth (Fig. 2a,b). Under the optimized condition, the BLG coverage can be increased to 65% of the total graphene area (Fig. 2b). However, too high H₂ concentration resulted in etching of the graphene sheets (Fig. 2c). Furthermore we observed an anisotropic 2D peak with a clear shoulder peak, indicating the growth of Bernal stacked BLG on our heteroepitaxial Cu(111) film.

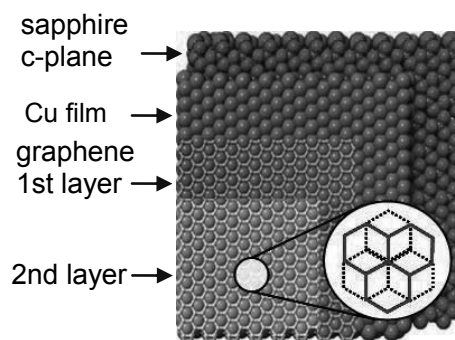


Fig.1 Schematic of Bernal stacked BLG on heteroepitaxial Cu(111) film.

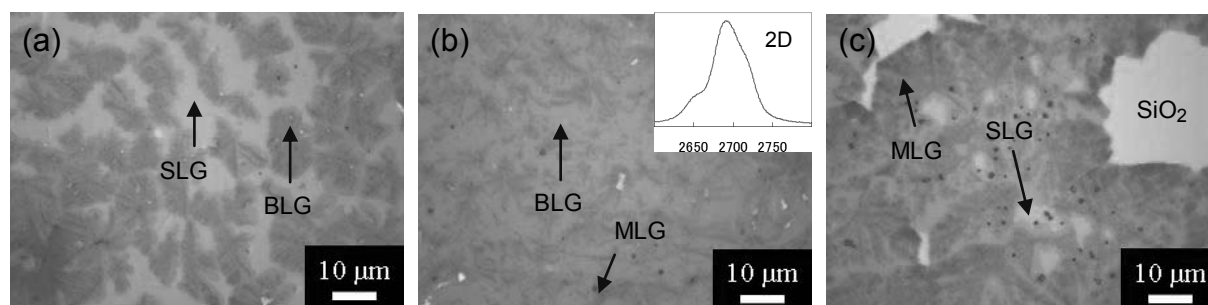


Fig. 2 Optical microscope images of graphene with the different hydrogen concentrations, (a) 7.0%, (b) 7.5%, and (c) 8.0%. Inset of (b) shows the Raman 2D band of the BLG area. SLG: single-layer graphene, MLG: multi-layer graphene.

References: [1] Y. Zhang *et al.*, *Nature*, **459**, 820 (2009). [2] L. Liu *et al.*, *ACS Nano*, **6**, 8241 (2012). [3] Z. Sun *et al.*, *ACS Nano*, **6**, 9790 (2012). [4] A. C. Ferrari *et al.*, *Phys. Rev. Lett.*, **97**, 187401 (2006). [5] C. M. Orofeo *et al.*, *Carbon*, **50**, 2189 (2012).

Corresponding Author: Hiroki Ago (Tel&Fax: +81-92-583-7817, E-mail: ago@cm.kyushu-u.ac.jp)

Scalable processing of crystallographic etching for graphite powder using supercritical fluid

○Takaaki Tomai, Naoki Tamura, Itaru Honma

*Institute of Multidisciplinary Research for Advanced Materials, Tohoku University, Sendai
980-8577, Japan*

The characteristics of finite-sized graphene, which is strongly affected by the edge type, such as armchair and zigzag, have attracted much attention. Crystallographic etching of graphene/graphite is one of the most promising methods for selective introduction of zigzag edge to the graphene/graphite surface [1]. Crystallographic etching of graphite surface is conducted by Ni, Co nanoparticle under reductive environment and by Ag nanoparticle under oxidative environment.

Recently, we succeeded in the crystallographic etching of graphite surface in supercritical water (SCW, critical point of water: 374 °C, 22 MPa) environment. The Ag-supported graphite was treated in SCW with oxygen. The treated temperature and time was 500 °C and 10 min, respectively. In the case of usage of graphite substrate, we confirmed many straight trenches formed on the surface by etching due to catalytic oxidation by SEM observation. We also observed an apparent increase in the etching rate with increasing water density when we varied the water density from 0 to 0.2 g/ml. This result indicates that the water contributes to the enhancement of the etching reaction. Although the mechanism is still not fully understood, efficient removal of adsorbed gaseous products (CO, CO₂) from the catalyst surface by the SCW might promote the catalytic carbon gasification. Moreover, after supercritical treatment, suspended materials in the water are observed. It is highly supposed that the anisotropically-etched graphene layer was isolated from the surface of graphite due to the exfoliation effect of supercritical fluid [2]. By using transmission electron microscopy (TEM), it is revealed that the graphene with zigzag edges which is introduced.

To check the scalability, we applied this method to dispersed graphite powder. To verify that the treatment progressed efficiently for the bulk, we conducted a Raman spectroscopic analysis. It has been reported that the D band at around 1350 cm⁻¹ and the D' band at around 1620 cm⁻¹ can be attributed to the defects and the graphite edges. Moreover, the D band intensity from a zigzag edge is weaker than that from an armchair edge, while the D' band intensity doesn't show the dependence on the edge type [3]. In the case of the graphite powder with Ag nanoparticles after SCW treatment, the average intensity ratio between the D band and the D' band ($I_D/I_{D'}$) value was smaller than that in the case of SCW-treated graphite powder without Ag nanoparticles. This result indicates that zigzag edges are effectively introduced by crystallographic etching in SCW even to the dispersed graphite powder.

Further details of process and the characteristics of zigzag-edge-introduced graphite powder will be presented in FNTG44.

[1] L. Ci *et al.* Nano Res. **1**, 116 (2008).

[2] T. Tomai, Y. Kawaguchi and I. Honma, Appl. Phys. Lett. **100**, 233110 (2012).

[3] L. G. Cancado *et al.* Phys. Rev. Lett. **93**, 247401 (2004).

Corresponding Author: T. Tomai

Tel: +81-22-217-5816, Fax: +81-22-217-5828,

E-mail: tomai@tagen.tohoku.ac.jp

***In situ* RHEED Study on Growth Process of Graphene by Chemical Vapor Deposition**

○Takuro Minato, Hitoshi Nakahara, Koji Asaka, and Yahachi Saito

Department of Quantum Engineering, Nagoya University, Furo-cho, Nagoya 464-8603

In situ observations of graphene growth have been carried out by SEM and LEEM. In these previously reports, the segregation of graphene on metal substrates with high solubility of carbon was observed during cooling process after chemical vapor deposition (CVD). In this study, graphene growth process during CVD was studied by *in situ* reflection high energy electron diffraction (RHEED).

Graphene was synthesized by CVD using ethanol gas. In order to investigate the effect of carbon solubility, vacuum deposited films of copper (Cu), which has low carbon solubility of 0.04 at.% at 1000 °C, and cobalt (Co), which has high carbon solubility of 3.41 at.% at 1000 °C, were used as catalyst metal. These films were prepared using electron beam deposition on silica-coated silicon substrates. The base pressure of CVD chamber was at 5×10^{-6} Pa to minimize the effect of the residual gas on the graphene growth. The substrate was heated at 900 °C, and the ethanol pressure was kept at 0.1 Pa for 5 minutes during CVD. After CVD, the substrates were taken out from the CVD chamber followed by Raman spectroscopy and atomic force microscopy (AFM) characterization.

Figures 1(a),(b) show electron diffraction patterns of the Cu and Co films during CVD, respectively. Streaks due to graphene reflections 10 were observed in both Cu (Fig. 1(a)) and Co films (Fig. 1(b)), suggesting that graphene has already grown on the substrates before cooling the substrates. It took 60 and 10 seconds until these streaks appeared in CVD process on Cu and Co films, respectively. It is considered that this difference was due to the higher catalytic activity of Co than Cu films. After cooling the substrates, electron diffraction patterns of Cu and Co films changed (Figs. 1(c),(d)); For Cu, Debye rings due to graphene appeared, and for Co, streaks due to graphene became clearer.

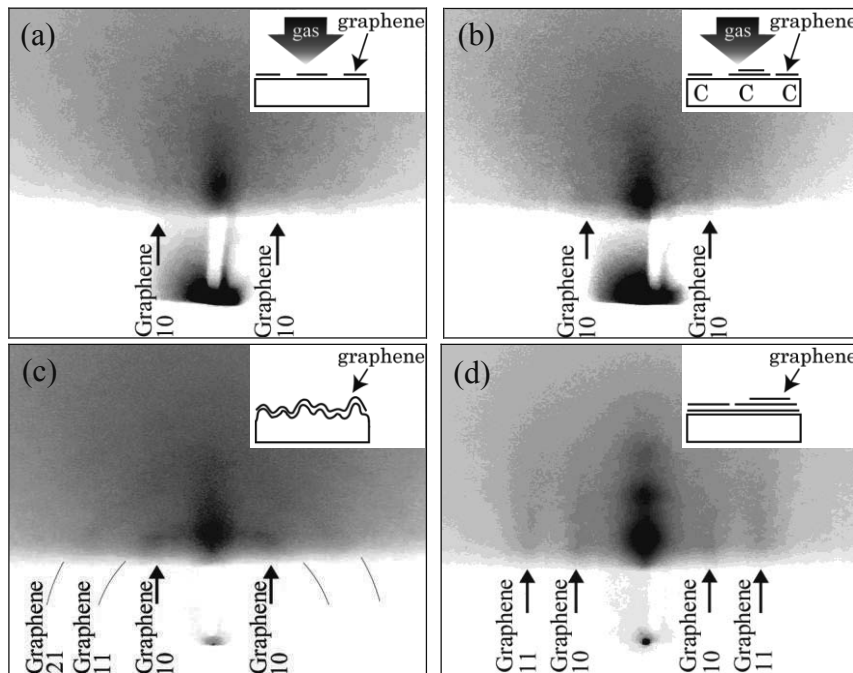


Fig. 1. RHEED patterns from (a) Cu film during CVD. (b) Co film during CVD. (c) Cu film after CVD. (d) Co film after CVD. Insets in each figure illustrated graphene growth process.

Corresponding Author: T. Minato

Tel&Fax&E-mail: +81-52-789-3714, +81-52-789-3703, minato@surf.nuqe.nagoya-u.ac.jp

Influence of applied potentials for electrochemical exfoliation of graphite

○Haruya Okimoto, Syun Takabayashi, Yuhei Sobe, Masahito Sano

¹ *Department of Polymer Science and Engineering, Yamagata University, Yonezawa, 992-8510, Japan*

Chemical exfoliation of graphite, such as Hummers method, is an attractive technique for the synthesis of graphene at room temperature. However, it needs several strong oxidants (KMnO_4 , NaNO_2) and a reductant (N_2H_2). Recently, we have reported a new method of electrochemical exfoliation of graphite without strong oxidants. It is known that electrochemical reactions on graphite involve many processes such as intercalation, anodic oxidation, and electrolysis, depending on the applied potential. It is important to elucidate a reaction at a given potential to control chemical characteristics of the resulting graphene. In this study, we report a systematic study of exfoliation of graphite over several applied potentials.

All electrochemical measurements were recorded in a conventional three-electrode potentiostat (working electrode: Grafoil as a raw material for graphene, counter electrode: Pt plate, and reference electrode: Ag/AgCl). Sulfuric acid system (H_2SO_4 or NaSO_4) and nitric acid system (HNO_3 and NaNO_3) were used as an electrolyte for exfoliation of graphite. Chronoamperometry were used for constant-voltage electrochemical exfoliation. After electrochemical exfoliation for 20 min, the exfoliated graphene was dispersed in DMF. The solution was cast on silicon and dried to measure the thickness, size, and functional moiety by AFM, SEM, XPS.

Figure 1 shows a cyclic voltammogram in Na_2SO_4 solution. A small peak at +1.8 V is known as an intercalation reaction in the case of H_2SO_4 . This result suggested that the Na_2SO_4 is also intercalated to graphite at the same potential as H_2SO_4 . Exfoliation of graphite is estimated to occur at the potentials +1.7, +1.8, and +2.1 V in Na_2SO_4 solution. The graphite electrode does not react below +1.7 V, which is just beneath the intercalation potential. On the other hands, the graphite is expanded and exfoliated over +1.8 V. Figure 2 shows the histograms of graphene thickness measured by AFM. The thickness of exfoliated graphene is not affected by the applied voltage. This result means that +1.8 V is a threshold value for the electrochemical exfoliation of graphene.

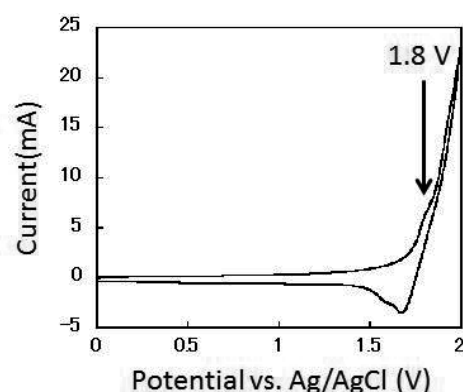


Fig 1 Cyclic voltammogram recorded at Grafoil in 1 M Na_2SO_4 .

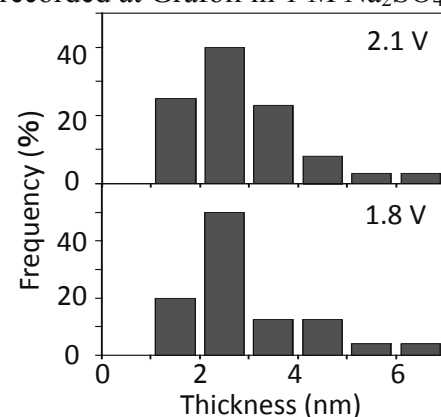


Fig 2 Histograms of graphene thickness made at different potentials.

Corresponding Author: H. Okimoto
Tel/Fax: +81-238-26-3074
E-mail: haruya@yz.yamagata-u.ac.jp

CVD synthesis of shape-controlled graphene and boron nitride heterostructures

○Eriko Maeda, Yasumitsu Miyata, Ryo Kitaura, and Hisanori Shinohara*

Department of Chemistry & Institute for Advanced Research, Nagoya University, Nagoya

Atomic-layer lateral heterostructures of graphene and hexagonal boron nitride (hBN) have attracted much attention because of their unique interface-originated properties as well as applications in electronics. Recently, the synthesis of such heterostructures has been reported by three different groups including the present group [1-3]. These works demonstrate that firstly-grown graphene can be used as a patterning mask and its edges behave as nucleation site of secondary-grown hBN in chemical vapor deposition (CVD).

Here, we show a shape-controlled growth of graphene/hBN heterostructures using hydrogen etching process of graphene. Individual grains of single-layer graphene are first grown from methane on a copper foil, and then the graphene is etched under hydrogen atmosphere. This etching process can produce hexagonal-shape hole and ribbon-shape gap in graphene grains depending on etching conditions. Shape-controlled hBN is then synthesized in the patterned graphene grains using ammonia borane CVD. The samples obtained are characterized by using optical spectroscopy and imaging, scanning and transmission electron microscope observations. As shown in Fig.1, the present process results in the growth of hexagonal and ribbon-shape hBN in each graphene grains. In the presentation, the detail of growth process and structure of the products will be discussed.

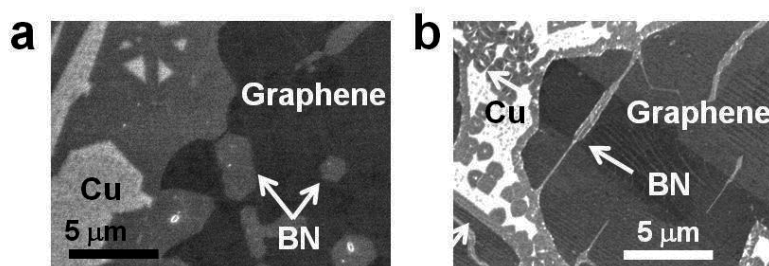


Fig.1 (a,b) Scanning electron microscope images of CVD-grown hBN/graphene heterostructures.

[1] Y. Miyata et al. Appl. Phys. Express 5 (2012) 085102.,

[2] M. Levendorf et al. Nature, 488 (2012) 627., [3] P. Sutter et al. Nano Lett., 12 (2012) 4869.

Corresponding Author: Hisanori Shinohara

Tel: 052-789-2482, Fax: 052-747-6442, E-mail: noris@nagoya-u.jp

Orientation Controlled Growth of NbS₂ Nanosheets on CVD Graphene

Wanyin Ge, Kenji Kawahara, Masaharu Tsuji, and Hiroki Ago*

Institute for Materials Chemistry and Engineering, Kyushu University, Fukuoka 816-8580

Recent development of graphene triggered the extensive interest in a new class of two-dimensional materials. In particular, quasi-two-dimensional transition metal chalcogenides show unique physical properties, and many chemical or physical approaches have been proposed to prepare the chalcogenide nanosheets. The primary emphasis so far has been put on semiconductor chalcogenides, such as MoS₂ and WS₂. On the contrary, very few works have been reported for metallic chalcogenide nanosheets. Niobium disulfide (NbS₂) is a metallic chalcogenide having a layered structure and shows superconductivity at transition temperatures of 1.7-6.3 K as well as unique anisotropic optical and magnetic properties [1]. Layered NbS₂ has been applied to a cathode material in secondary batteries, catalyst for the purification of petroleum, and humidity sensors. The preparation of nanosheets of NbS₂ is particularly important not only in these applications, but also in the fundamental research for the quasi-two-dimensional chalcogenide materials.

Here, we report ambient pressure chemical vapor deposition (CVD) growth of single-crystalline NbS₂ nanosheets with a controllable orientation. On SiO₂ substrates, NbS₂ nanosheets grow almost perpendicular to the substrate surface. However, when we use the transferred CVD graphene on SiO₂ substrate, NbS₂ nanosheets grow laterally lying on the graphene, as shown in Fig. 1. The as-grown NbS₂ sheets show mainly triangular shapes with the thickness of about 20-200 nm and several hundreds to micrometres in the lateral dimension. Analyses based on X-ray diffraction and Raman spectroscopy indicate that the NbS₂ nanosheets are single crystalline with a rhombohedra structure (3R-type) [2]. Our finding on the formation of highly aligned NbS₂ nanosheets on graphene gives new insight on the formation mechanism of NbS₂ and would contribute to the templated growth of various layered materials.

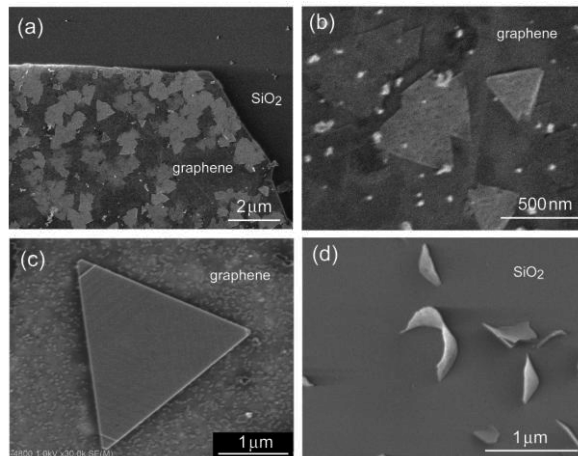


Figure 1 (a) SEM images of NbS₂ nanosheets grown on transferred graphene. The density of NbS₂ nanosheets is much lower than that on graphene. (b,c) NbS₂ nanosheets on graphene. (d) NbS₂ nanosheets grown on plain SiO₂ surface.

References:

- [1] W. G. Fisher, M. J. Sienko, *Inorg. Chem.*, **19**, 39 (1980).
 [2] W. Ge, K. Kawahara, M. Tsuji, H. Ago, submitted.

Corresponding Author: Hiroki Ago (Tel&Fax: +81-92-583-7817, E-mail: ago@cm.kyushu-u.ac.jp)

Nanocolumnar Crystal Growth of Organic Semiconductor Molecules on a Graphene-Modified Surface

○Satoshi Okada, Shunsuke Furukawa, Hideyuki Tanaka, Koji Harano, Eiichi Nakamura

Department of Chemistry, The University of Tokyo, Tokyo 113-0033, Japan

Morphological control of organic semiconductor molecules are important in organic solar cells to increase current density and enhance performance. Here, we solution-processed nanocolumnar structure of donor material tetrabenzoporphyrin (BP)^[1] onto graphitic sheets (reduced graphene oxide: rGO)-coated poly(3,4-ethylenedioxythiophene): poly(styrenesulfonate) (PEDOT:PSS). The nanocolumns are formed by sparsely rGO-covered PEDOT:PSS surface, which initiated nucleation of BP via acid-base interaction (Fig. 1). Graphitic sheets were synthesized by Hummers' method followed by reaction with isocyanate, and was spin coated on PEDOT:PSS and thermally reduced (Fig. 2)^[2] to obtain ca. 30%-covered surface.

On rGO-coated PEDOT:PSS, BP was solution processed from its soluble precursor CP followed by thermal treatment to obtain BP film. Flat domain structure was obtained on PEDOT:PSS (Fig. 3 left), while nanocolumnar structure with the height of 50-150 nm was formed on rGO-coated PEDOT:PSS (Fig. 3 right). The obtained nanocolumnar BP was applied for BP/C₆₀ p-n devices by thermally evaporating C₆₀ to obtain devices with 1.08-fold enhanced performance. The increase in performance was attributed to 1.16-fold increase in current density and 1.2-fold enlargement in surface area of BP.

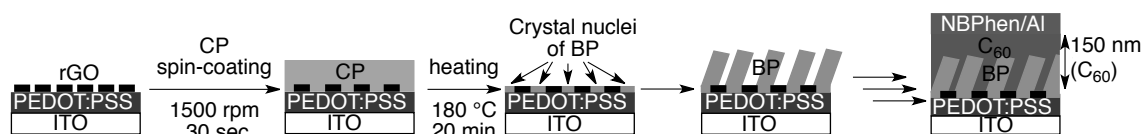


Fig. 1. Formation of nanocolumnar donor BP on rGO-masked PEDOT:PSS and solar cell fabrication

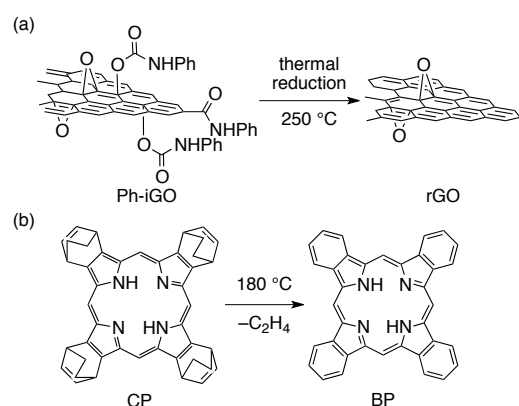


Fig. 2. Materials used in this study. (a) Preparation of graphitic sheets. (b) Preparation of BP from soluble precursor CP.

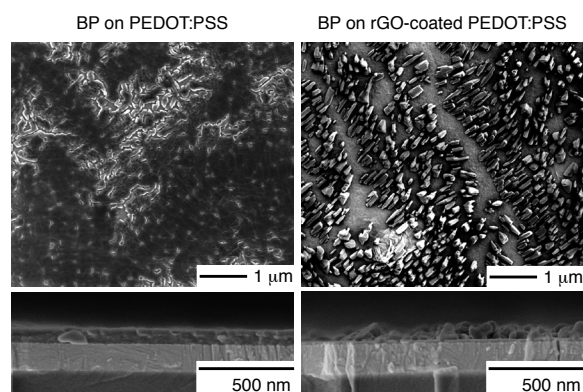


Fig. 3. SEM images of BP film. (left) BP on PEDOT:PSS. (right) BP on rGO-coated PEDOT:PSS. (top) Top view. (bottom) Cross-section image.

[1] Aramaki, S. *et al.* Appl. Phys. Lett. **84**, 2085 (2004).

[2] Stankovich, S. *et al.* Carbon **44**, 3342 (2006).

Corresponding Author: Eiichi Nakamura

Tel: +81-3-5841-1475, Fax: +81-3-5841-1475,

E-mail: nakamura@chem.s.u-tokyo.ac.jp

Imaging graphene lattice by the helium ion microscope: A prediction by *ab initio* simulations

○Yoshiyuki Miyamoto

Nanosystem Research Institute, National Institute of Advanced Industrial Science and Technology (AIST), Central 2, 1-1-1 Umezono, Tsukuba 305-8568, Japan

In the last general meeting, I introduced the feasibility of Helium ion microscope (HIM) as a new tool for getting image of suspended graphene. HIM can take images by secondary emitted electron induced by collision of high-speed helium ion to the samples. The amount of the emitted electrons depends on the position of the collision, thus ion-beam scanning can induce contrast of the intensity of the secondary emitted electron that makes the HIM image. The mechanism of the secondary electron emission was found to be impact ionization upon the collision by performing *ab initio* simulations based on the time-dependent density functional theory [1]. Further analysis considering finite beam-size of helium has been made to examine accessible experimental conditions to challenge for lattice image of graphene.

First, the similarity between the profile of secondary electron intensity as a function of He-ion-beam impact point and the profile of the valence charge density is demonstrated, see Fig. 1. Second, the guess of HIM image of graphene ribbon from the charge distribution is demonstrated considering possible focusing size of the He ion beam. The charge density profile has been modified by the Gaussian broadening technique mimicking the finite beam-size and necessary conditions for taking lattice image will be discussed [1].

This work was performed by using the Earth Simulator. The author is indebted to collaboration with Prof. H. Zhang and Prof. A. Rubio and to support by the Research organization for Information Science and Technology (RIST), Tokyo office.

[1] H. Zhang, Y. Miyamoto, and A. Rubio, *Phys. Rev. Lett.* **109**, 265505 (2012).

Corresponding Author: Yoshiyuki Miyamoto

Tel: +81-29-849-1498, Fax: +81-29-861-3171,

E-mail: yoshi-miyamoto@aist.go.jp

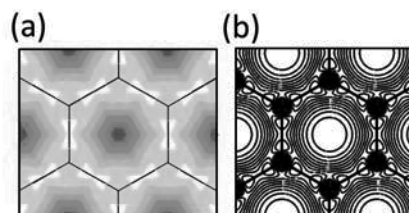


Fig.1 (a) Simulated HIM image and (b) charge density of graphene.

Anderson Localization of Edge-Disordered Graphene Nanoribbons

○Kengo Takashima¹, Yukihiro Takada², Takahiro Yamamoto^{1,2}

¹*Dept. of Electrical Engineering, Tokyo Univ. of Science, Chiyoda-ku, Tokyo 102-0073, Japan*

²*Dept. of Liberal Arts, Tokyo Univ. of Science, Chiyoda-ku, Tokyo 102-0073, Japan*

Graphene is a potential candidate for channel materials of field effect transistors (FETs) because of their high carrier mobility [1]. However, metallic behavior of graphene is a major hurdle to utilize it to the channel of FETs, because high on-off ratios are not achievable without an energy-band gap. One possible way to overcome the gap-opening problem is to process the graphene in the form of nanoribbon with nanometer width. Graphene nanoribbons has an energy gap and they have been successfully applied to FETs with high on-off ratio [2].

The channel length of cutting-edge GNR-FETs is less than 100nm (the minimum length is ~1nm). Because such channel lengths are shorter than the typical coherent length of GNRs, the GNRs is expected to exhibit remarkable electronic transport properties originating from the wave nature of electrons. A recent experiment reported that the resistance of GNRs increases exponentially with their length even at the room temperature [3]. This non-Ohmic behavior is believed to be due to Anderson's localization caused by the interference between coherent electrons scattered by the disordered edges of GNRs. However, the detail relation between the edge roughness and the coherent length L_ϕ of GNRs has not been clarified yet.

In this study, we have computationally investigated the coherent electronic transport in edge-disordered armchair GNRs (AGNRs). The edge disorder has been treated as randomly distributed carbon-pair vacancies on the edges of AGNR (Fig.1). We clarified (i) a relation between L_ϕ and the amount of edge carbon-pair vacancies, (ii) the chemical-potential dependence of L_ϕ , and (iii) the ribbon-width dependence of L_ϕ .

[1] Novoselov, *et al.*, *Science* **306**, 666 (2004).

[2] Schwierz, *Nature Nanotech.* **5**, 487 (2010).

[3] Xu *et al.*, *Nano Lett.* **11**, 1082 (2011).

[4] Roche, *Phys. Rev. B* **59**, 2284 (1999).

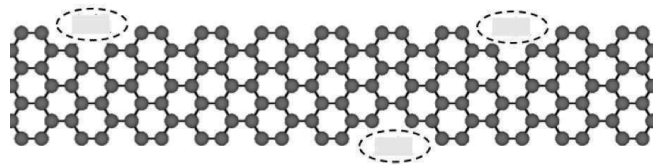


Fig.1: A schematic view of a edge-disordered GNR

Corresponding Authors: Takahiro Yamamoto

TEL&FAX: +81-3-5213-0990

E-mail: takahiro@rs.tus.ac.jp

Gapped and gapless graphene and graphene-nanoribbon/nanotube complex

Shota Kizukuri, Takashi Koretsune and Susumu Saito

*Department of Physics, Tokyo Institute of Technology,
2-12-1 Oh-okayama, Meguro-ku, Tokyo 152-8551, Japan*

Nanostructured carbon materials are of high importance as future device materials because of their variety of electronic properties. Here, we focus on graphene and armchair-edge graphene nanoribbon (AGNR)/carbon nanotube (CNT) complex. It is expected that the interlayer interaction between graphene and the periodically placed AGNRs/CNTs may modify the linear dispersion around the K point and open up the band gap. So, we study the band structure of graphene and AGNR complex by first-principles calculation. It is found that a gap actually appears in some cases depending on the stacking way of AGNR on graphene as well as the width of AGNRs and the stacking distance. Although, the graphene part in this complex system deforms from a flat-geometry sheet, its band structure is still gapless. However the whole complex system shows semiconducting property (Fig. 1), indicating the importance of interlayer interaction. Furthermore, by changing interlayer distance, the size of the band gap can be controlled. By calculating the total energy as a function of interlayer distance, we estimate the pressure value to be necessary for the band gap modulation.

We also study the band structure of graphene complex with thick CNTs. In the optimized system, the graphene deforms to fit the shape of collapsed CNTs. In addition, to consider more realistic systems, we also discuss the wiggle-like shaped AGNRs complex and AB-AC stacking AGNR complex.

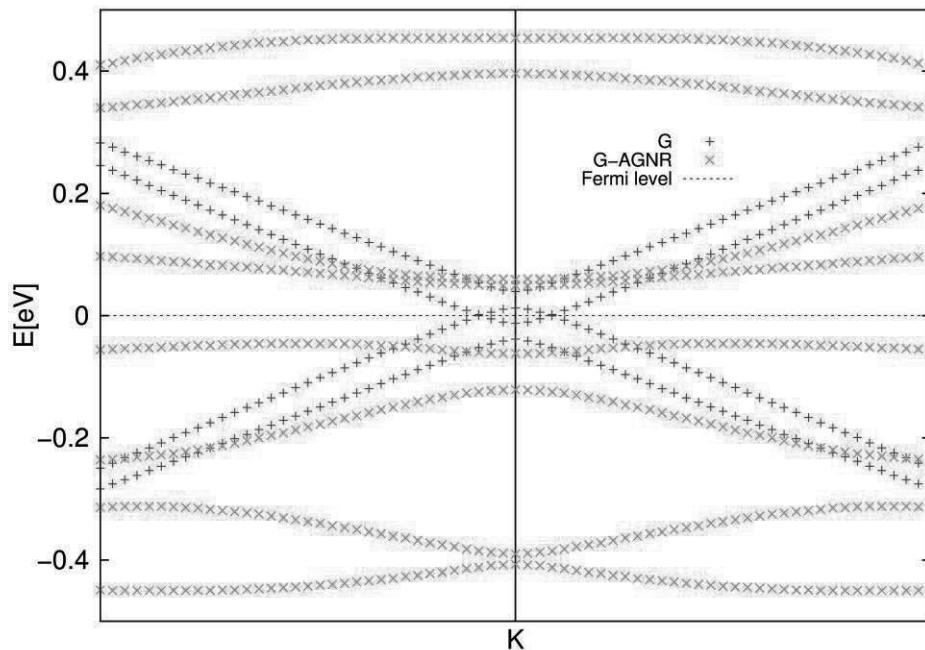


Fig. 1: Band structure of deformed graphene (G) and the GNRs-on-graphene complex (G-AGNR) around the K point.

SGM investigation of graphene nano structure

○Souhei Furuya, Kazuyuki Takai, Yoshiaki Sato, and Toshiaki Enoki

Department of Chemistry, Tokyo Institute of Technology, Ookayama, Meguro-ku, Tokyo 152-8551, Japan

Nano-structured graphene such as the graphene point contact is one of the most interesting systems in view of a study on the effect of potential barrier of the edge region of the sample and the carrier puddling at Dirac point on the transport properties of graphene. Scanning Gate Microscopy (SGM) is a powerful tool to investigate the effect of the local electronic structure on the transport properties [1]. In SGM, the effect of the local electrostatic modulation on the transport is obtained as the 2D conductance mapping as a function of the position of the scanning gate. In this study, the SGM instrument able to operate under UHV, at low temperature down to 2 K, in the magnetic field up to 8 T, is developed based on existing LT-STM system as schematically shown in Fig.1. Graphene point contact structure is characterized toward SGM investigation on graphene.

The point contact structure of few layer graphene was fabricated by annealing of SiC at 1750 °C and following photolithography and oxygen plasma etching processes, where the influence of the local potential by the scanning gate significantly affects on the electron scattering at a narrow bridging region between two electrodes. To compare the behavior of carriers in graphene with those in ordinary metals, we employed the Au point contact device on SiC as reference. SGM measurement was performed in lift-up manner, where tip went over 10 nm above the height mode scanned trajectory.

The point contact structure of graphene and Au having 700 nm channel width and 40 nm height was successfully fabricated as shown Fig. 2 a). SGM image of Au point contact showed no variation in the conductance, being consistent with the short mean free path and the higher Fermi energy of Au electron system.

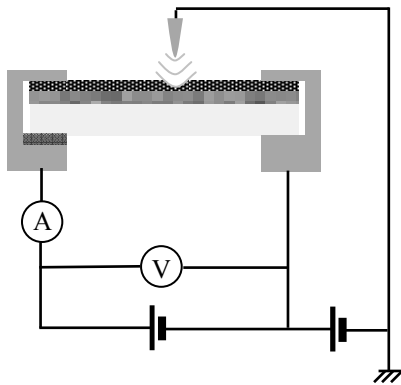


Fig. 1 Schematic diagram for SGM measurement

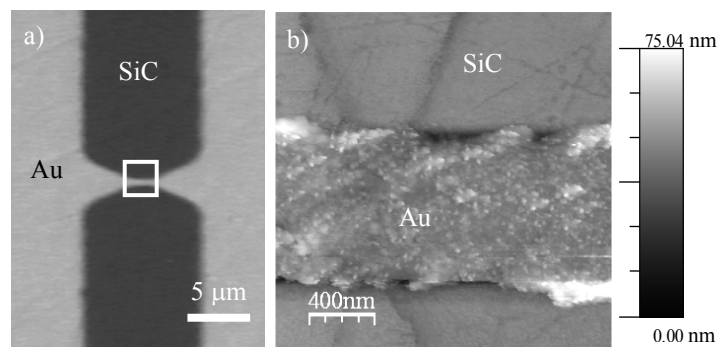


Fig. 2 a) Optical microscope image of Au point contact

b) STM height image of square region of a)

[1] M. A. Topinka, *et al.* SCIENCE **289**, 2323 (2000)

Corresponding Author: Souhei Furuya

Tel: +81-3-5734-2610, Fax: +81-3-5734-2242, E-mail: furuya.s.ab@m.titech.ac.jp

Raman spectroscopy of mechanically strained chemically functionalized graphene

○Mark A. Bissett, Masaharu Tsuji, and Hiroki Ago*

Institute of Materials Chemistry and Engineering, Kyushu University, Fukuoka, 816-8580

The unique properties of graphene make it an ideal candidate for applications in flexible electronics such as touch screens and displays. These properties include high conductivity, as well as transparency and mechanical flexibility. However, pristine graphene exists as a zero-band gap material and this must be overcome before being applicable to many functional devices. Previously, it has been shown that mechanical strain as well as chemical functionalization can alter the electronic structure of graphene and possibly introduce a band gap [1]. Thus, for optimizing the performance of graphene devices it is important to gain a thorough fundamental understanding of the effects of both strain and chemical functionalization on the electronic structure of graphene. In this work we utilize Raman spectroscopy to investigate the effect of mechanical strain on both pristine single-layer polycrystalline graphene on a flexible polydimethylsiloxane (PDMS) substrate and also graphene that has been chemically functionalized by an aryl diazonium molecule (4-NBD), as seen in Fig. 1a.

Our previous work has investigated the effect of strain on polycrystalline graphene and found that the presence of domain boundaries can affect the Raman spectra which indicate a change in electronic structure [2]. The reactivity of polycrystalline graphene was found to be greatly increased due to these domain boundaries compared to exfoliated single crystalline graphene. This high reactivity can be seen in Fig. 1b where we see an increase in the D/G ratio as well as a shift in the Raman peak positions. This shift in peak position is indicative of a doping effect taking place. Figure 1c shows the plots of the 2D peak width with increasing values of strain. The pristine graphene exhibits the expected linear trend; however, the functionalized graphene exhibits an unusual v-shaped trend. This unusual behavior is attributed to a combination of phonon splitting caused by the chemical functionalization and also morphological changes to the graphene lattice caused by the covalent bond formation [3].

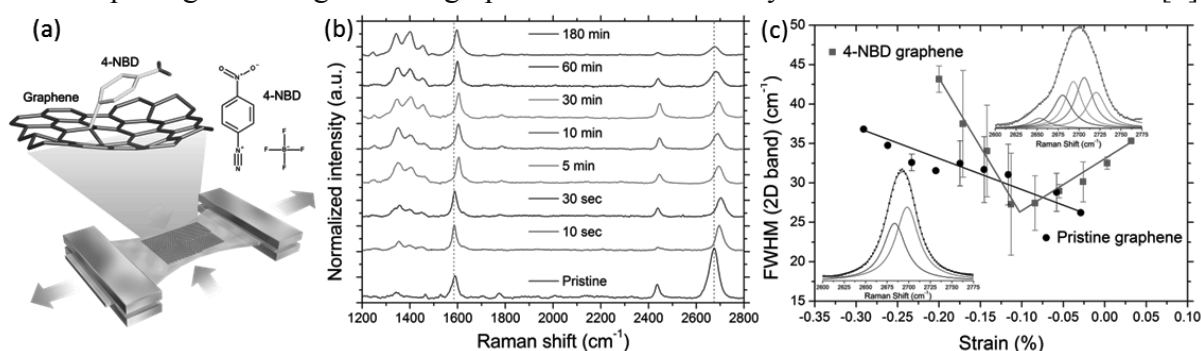


Figure 1: (a) Schematic of functionalized polycrystalline graphene on flexible PDMS. (b) Raman spectra with increasing 4-NBD functionalization times. (c) Plot of 2D bandwidth with increasing strain for both pristine and functionalized graphene. Inset shows peak fitting for each sample.

- [1] Zhan, D. *et al.*, *Adv. Mater.*, **24**, 4055 (2012).
 [2] Bissett, M. A. *et al.*, *ACS Nano*, **6**, 10229 (2012).
 [3] Bissett, M. A. *et al.*, *J. Phys. Chem. C*, submitted.

Corresponding Author: H. Ago, Tel: +81-92-583-7817, Fax: +81-92-583-7817, E-mail: ago@cm.kyushu-u.ac.jp

Magnetic Interactions between Nanographite and Oxygen Molecule

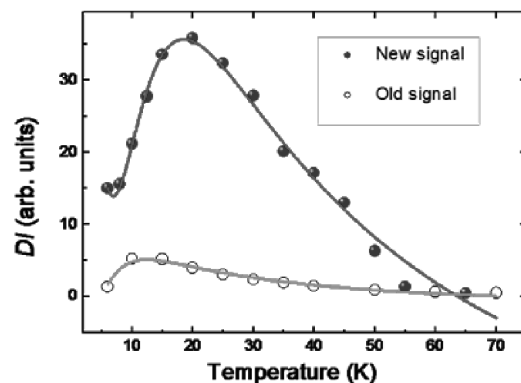
○Kazuyuki Takai¹, Alexander. I. Shames², Vladimir Yu. Osipov³, Alexander Ya. Vul³, Yutaka Kaburagi⁴, Takuya Hayashi⁵, Toshiaki Enoki¹

¹ Department of Chemistry, Tokyo Institute of Technology, 2-12-1 Oh-okayama, Meguro-ku, Tokyo 152-8551, Japan, ² Department of Physics, Ben-Gurion University of the Negev, 84105, Be'er-Sheva, Israel, ³ Ioffe Physical-Technical Institute, Polytechnicheskaya 26, 194021, St. Petersburg, Russia, ⁴ Faculty of Engineering, Tokyo City University, 1-28-2, Tamazutsumi, Setagaya-ku, 158-8557 Tokyo, Japan, ⁵ Faculty of Engineering, Shinshu University, 4-17-1 Wakasato, Nagano 380-8553, Japan

In nanographene, the edge state spins given by the presence of edges with π -electron nature form ferrimagnetic spin structure, where the exchange interactions among spins are mediated by conduction carriers [1]. In this view point, carbon onions (CO) derived from detonation nanodiamonds by prolonged heat treatment was interesting material, which is composed of well separated nanographene sheets and featured by its defective and hollow nature, giving magnetic interactions between edge-state spin and guest adsorbed molecules[2] [3]. In this study, π -electronic edge-localized spin magnetism in CO was investigated in terms of the molecular oxygen adsorption and microwave (MW) irradiation effect.

The linewidth of ESR spectra of CO under air atmosphere (oxygen pressure ~ 200 mbar) at low incident MW power ($P_{MW} \leq 200 \mu\text{W}$) shows progressive broadening of the edge-spin signal ($g = 2.0014(2)$) as the temperature decreases. At $T < 140$ K, the edge-spin EPR signal becomes unobservable, revealing weak narrow ESR signal with $g = 2.0022(1)$ ascribed to spins of localized defects (“Old”). Within the low temperature region ($T < 60$ K), the latter signal demonstrates unusual enhancement in the intensities and line width upon the irradiation of the larger MW power ($P_{MW} > 20$ mW) accompanied with a drastic upward deviations from the conventional saturation behavior. On abrupt reduction of P_{MW} back to low power ($P_{MW} < 1$ mW), the new intensive narrow EPR signal with the same $g = 2.0022(1)$ is observed with a non-Curie-Weiss behavior in the temperature range less than 60 K (“New”), where it turns back to the weak narrow signal (Old) (Fig. 1). The observed new magnetic entities in the oxygen adsorbed CO is explained by the antiferromagnetic coupling between the edge spins and negatively charged O_2^- oxygen molecules, which is generated through the charge transfer between nanographite and oxygen molecules in the process of desorption / adsorption of oxygen molecules caused by high power MW-irradiation and subsequent abrupt reduction of P_{MW} . The antiferromagnetic dimer model well explains the observed temperature-dependence of the ESR intensities.

Fig.1 The temperature dependence of ESR intensities for new and old signal in CO. Solid lines indicates the fitting results with the model of antiferromagnetic dimers.



[1] T Enoki and K Takai, *Solid State Communications* **149** 1144 (2009)

[2] V. Yu. Osipov, T. Enoki, K. Takai, et al, *Carbon* **44** 1225 (2006)

[3] A. Shames, A. M. Panich, V. Yu. Osipov, et al, *J. Appl. Phys.* 107 014318 (2010)

A new stage in the detonation nanodiamond research

Shuichi Sasaki, Ryoko Yamanoi, Eiji Ōsawa

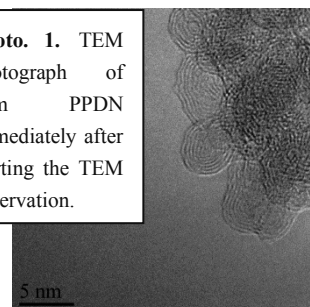
*NanoCarbon Research Institute, AREC, Faculty of Textile Science and Technology, Tokida 3-15-1,
Ueda, Nagano, 〒386-8567, Japan*

Optimization of operation conditions in the disintegration of crude detonation nanodiamond agglomerates by means of attrition milling with 30 μm zirconia beads according to Taguchi's method of the quality engineering, led to significant decrease in the average diameter of particle-size distribution from 4.8 to 3.7 nm in the primary particles of detonation nanodiamond (PPDN).¹⁾ We report here subsequent developments in our endeavor to develop a standard method to obtain ensemble of polydisperse PPDNs of potentially the most useful and interesting among the known nanocarbons from 4.8 to 3.7 nm carbons. A decisive improvement occurred when old beads were replaced with a new batch and a few runs have been completed to reach new low diameters of 3.0 to 3.3 nm. In view of the large difference in diameters between beads and PPDN ($10^4:1$), we interpret this high performance of new beads as the effect of being well-covered and adhered with the primary diamond particles, which are actually responsible for disintegration of nanodiamond agglomerates. This new mechanism of disintegration will be discussed in the presentation in more detail. The final diameter corresponds to an ensemble consisting of only the primary particles, while the larger diameters mean persistence of small agglomerates like dimers and trimmers.

In such a small size-range, the colloidal solution of PPDN looks clearer and acquires consistencies in the values of *pH* (5.8, 5 %), viscosity (2 cps, 5%) and ζ -potential (+53 mV). In addition to these expected behaviors of well-distributed ensemble, one remarkable size-effect was observed. Diamond-graphite transition in the 4.8 nm PPDN is known to occur at 800-900°C, considerably lower than that of bulk diamond (3000-4000°C). However, the 3.0 nm PPDN transformed quickly under irradiation of electron beam in a conventional TEM operating at 200KeV, to give well-dispersed 5-6 layered nano-onions. The transformation seems very fast as we could not recognize original nanodiamond particles at all in the TEM examination but completely transformed masses of nano-onion particles (**Photo 1**). Quantum confinement limit of the size of smaller nanoparticles has long been considered to be around 1nm, but this behavior of PPDM indicates the limiting size could be larger, around 2 nm.

- (1) "Optimized de-agglomeration of detonation nanodiamond," Sasaki, S.; Yamanoi, R.; Ōsawa, E. Presented before the 42nd Fullerenes-Nanotubes-Graphenes General Symposium, University of Tokyo, March 6-8, 2012, Abstract Book, p. 40.

Photo. 1. TEM photograph of 3nm PPDN immediately after starting the TEM observation.



Biomimetic approach toward tough nanodiamond materials

○Keita Fujiwara, Toshiki Ikami, Tadamasa Ito, Masaki Ozawa

Department of Materials Science and Engineering, Meijo University, Aichi 468-8502, Japan

Nacre is composed of alternating calcium carbonate layers and protein layers well known as “brick-and-mortar” structures. The former occupies about 93 %, while the latter about 5 %. Despite the brittleness of the main constituent, nacre shows outstanding toughness partly because of the characteristic structures. In addition, another mechanism was found working at a nanoscale. Each bricks are made of nanoparticles of calcium carbonate bound by proteins, and they rotate to dissipate stresses applied. These mechanisms working at different length scales make nacre 1000 times tougher than calcium carbonate alone [1]. In this study, fabrication of tough materials inspired by nacre were investigated by substituting nanodiamonds for calcium carbonate as well as polymer networks for proteins.

As we have an unique technique to facilitate surface functionalization of nanodiamond primary particles by using a powerful microtip-type sonicator in the presence of hard ceramic beads [2], detonation nanodiamond derivatives thus functionalized were at first examined to be incorporated in a polymer hydrogel, and then dried up to give nacreous bricks having nanostructures. Carboxylated or sulfonated nanodiamonds [3] were successfully integrated in a gel of polyacrylamide or gelatin, while they showed phase separation with, for example, a poly(2-acrylamido-2-methyl-1-propanesulfonic acid)] gel. As even sulfonated nanodiamonds are excluded from a polymer network having sulfo groups, integration is likely driven not by similarity of functional groups between diamonds and polymers, but by electrostatic attraction between them. Fig. 1 displays a composite gel with polyacrylamide. The product obtained after drying the gel was reasonably, but not outstandingly, tough, presumably due to the size of the particles being off the optimal values or to pores developed during the drying process.

On the other hand, the directional freezing technique [4] was employed to organize microscale nacreous structures. Ice grains are known to be utilized as templates upon freezing of colloids. A nanodiamond colloid mixed with monomers were directionally frozen prior to polymerization, and then a resultant composite gel was dried up to give a material consisting of nanodiamonds and polymer networks arranged like brick-and-mortars. Despite low nanodiamond concentration examined so far and considerable amount of pores developed in the product, a lamellar structure was successfully obtained as in Fig. 1(b).

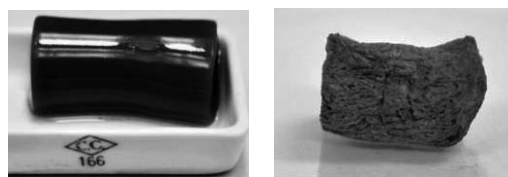


Fig.1 Composites of nanodiamonds with polymer networks. A puddingy hydrogel of polyacrylamide with nanodiamonds (a), and a dried nanodiamond-gelatin composite prepared using directional freezing (b).

- [1] X. Li *et al.* Nano Lett. **6**, 2301 (2006)
 [2] Y. Liang *et al.* ACS Nano **3**, 2288 (2009).
 [3] Y. Liang *et al.* J. Colloid Interface Sci. **354**, 23 (2011).
 [4] W. Mahler, M. F. Bechtold Nature **285**, 27 (1980).

Corresponding Author: T. Ito

Tel: +81-52-838-2410, Fax: +81-52-831-1170,

E-mail: 123434005@ccalumni.meijo-u.ac.jp

Kinetic consideration on the formation of polyyne-iodine complex by photoinduced reaction

○Yoriko Wada and Tomonari Wakabayashi

Department of Chemistry, Interdisciplinary Graduate School of Science and Engineering,
Kinki University, Higashi-Osaka 577-8502, Japan

Polyynes are linear hydrocarbon molecules which have sp-hybridized carbon chains. Hydrogen-end-capped polyynes, $H(C\equiv C)_nH$, are the simplest model compounds for linear carbon chain molecules. These molecules exhibit absorption bands for the allowed transition in the UV region and those for the forbidden transition in the near UV region [1,2]. We have reported that the absorption bands for the allowed transition disappeared and those for the forbidden transition are intensified by addition of iodine molecules into the polyyne solution under illumination with visible light. These spectral changes indicate that the formation of the molecular complex with polyyne and iodine molecules is proceeding [3]. The composition of the polyyne-iodine complex was determined to be 1:3 for polyyne:iodine molecules from iodine concentration dependence experiments.

In this work, we investigated the formation mechanism of the polyyne-iodine molecular complex by a reaction kinetic analysis. Mixed solutions of polyyne and iodine which have different concentrations of iodine were prepared. The 532 nm cw-laser light irradiates the mixed solution. Then, absorption spectra of the mixed solution were recorded. Figure 1 shows temporal changes in the UV/Vis absorption spectra of mixed solution of polyyne and iodine molecules (2.3 molar equivalent of $I_2/C_{10}H_2$ in hexane) upon irradiation for 0-136 s. Fig 1 a) shows UV absorption spectra for $C_{10}H_2$ and b) visible ones for I_2 . The insert shows the spectral component of $C_{10}H_2$ in a). The absorption band of I_2 at 520 nm decreased by 17% at 136 s. If the corresponding amount of I_2 was converted to $C_{10}H_2I_6$, the depletion in the $C_{10}H_2$ absorption should be 18%. However, the observed decrease in the $C_{10}H_2$ absorption was 54%. In order to understand this photoinduced decay process, we model chemical reactions, 1) $I_2 + h\nu \rightarrow I_2^*$, 2) $I_2^* \rightarrow I_2$, 3) $C_{10}H_2 + I_2^* \rightarrow D + I_2^*$. Reaction 1 represents photoexcitation of an iodine molecule, reaction 2 represents relaxation of the active molecular iodine I_2^* , and reaction 3 represents degradation of $C_{10}H_2$. Based on this model, reaction kinetics was considered for the observed temporal changes in the UV/Vis absorption spectra. As a result, it was clarified that the active molecular iodine I_2^* degrades $C_{10}H_2$ in the case of low concentrations of I_2 for the initial concentration.

[1] E. Kloster-Jensen et al., *Helv. Chem. Acta.* **57** (1974) 1731.

[2] T. Wakabayashi et al., *Chem. Phys. Lett.* **446** (2007) 65.

[3] Y. Wada et al., *J Phys. Chem. B* **115** (2011) 54.

Corresponding Author: T. Wakabayashi

Tel: +81-6-6730-5880 (ex. 4101), Fax: +81-6-6723-2721,

E-mail: wakaba@chem.kindai.ac.jp

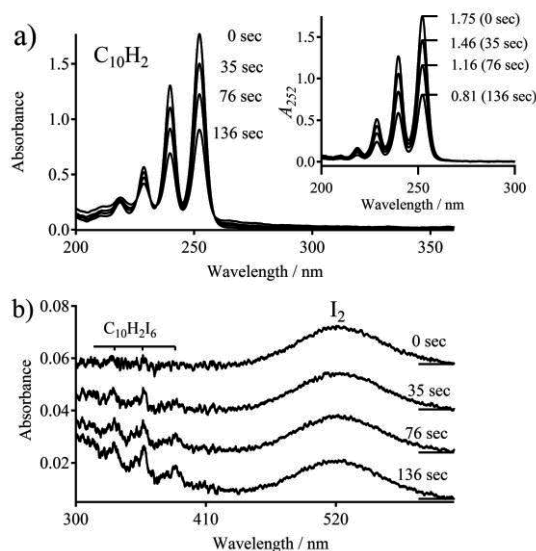


Figure 1. Temporal changes in UV/Vis absorption spectra of the mixture solution of polyyne and iodine (2.3 molar equivalent of $I_2/C_{10}H_2$ in hexane) upon irradiation for 0-136 s.

Improved Mechanical Property of Bucky Paper by Adding Carbon Nanocoil

○Koji Maruyama¹, Yoshiyuki Suda¹, Hideto Tanoue¹, Hirofumi Takikawa¹,
Hitoshi Ue², Kazuki Shimizu³, Yoshito Umeda⁴

¹ *Department of Electrical and Electronic Information Engineering,
Toyohashi University of Technology, Toyohashi, 441-8580 Japan*

² *Fuji Research Laboratory, Tokai Carbon Co., Ltd.*

³ *Shonan Plastic Mfg. Co., Ltd.*

⁴ *Toho Gas Co., Ltd., Tokai, Aichi 476-8501 Japan.*

Bucky paper which is made of carbon nanotube (CNT) is expected for application of electric double layer capacitor (EDLC) electrode, because of high electrical conductivity and large specific surface area of CNT. Although EDLC using bucky paper electrode has high specific capacitance, the mechanical property of the electrode is weak. The approach in this work is to improve the mechanical property of bucky paper by combining CNT with carbon nanocoil (CNC).

To prepare the electrode, different amounts of multi-walled CNT (MWCNT) (10–15 nm diameter, 3 μm length) and CNC (500–800 nm coil diameter, 20–30 μm length) were ultrasonicated separately in the aqueous (SDC 1 wt% solution) and mixed. The solution was filtered through a 0.22 μm cellulose membrane and rinsed with deionized water to obtain the electrodes. Fig. 1 shows the fracture surface of the CNT/CNC electrode. To measure the mechanical property, we conducted testing of the electrode in tension (Fig. 2). Young's modulus was calculated from slopes of the lines in Fig. 2. The results show that Young's modulus was improved from 1.4 GPa to 1.81 GPa by adding CNC.

This work has been partly supported by the Research Project of the Venture Business Laboratory from Toyohashi University of Technology (TUT); the Core University Programs (JSPS-CAS program in the field of "Plasma and Nuclear Fusion") from the Japan Society for the Promotion of Science (JSPS); and a Grand-in-Aid for Scientific Research from JSPS.

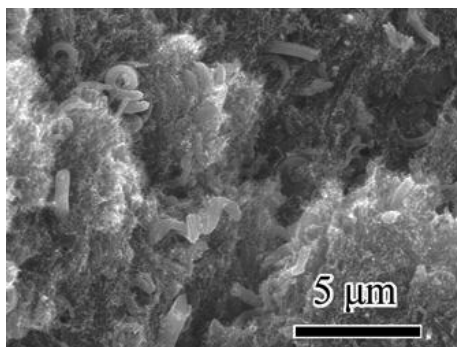


Fig. 1 SEM image of fracture surface of CNT/CNC electrode.

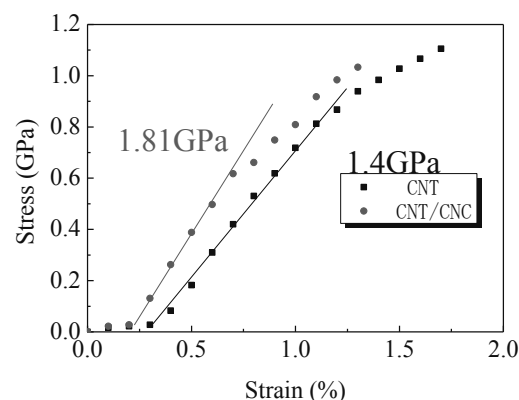


Fig. 2 Tensile stress curve of CNT and CNT/CNC electrodes.

Corresponding Author: Yoshiyuki Suda

Tel: +81-532-44-6726, Fax: +81-532-44-6757, E-mail: suda@ee.tut.ac.jp

Measurement of electric resistance of a single carbon nanocoil

○Ryuji Kunimoto¹, Taiichiro Yonemura¹, Yoshiyuki Suda¹, Hideto Tanoue¹, Hirofumi Takikawa¹, Hitoshi Ue², Kazuki Shimizu³, Yoshito Umeda⁴

¹ Department of Electrical and Electronic Information Engineering, Toyohashi University of Technology, Toyohashi 441-8580, Japan

² Fuji Research Laboratory, Tokai Carbon, Co., Ltd., Oyama 410-1431, Japan

³ Development Department, Shonan Plastic Mfg. Co., Ltd., Hiratsuka 254-0807, Japan

⁴ Toho Gas Co., Ltd., Tokai, Aichi 476-8501, Japan

Carbon nanocoil (CNC) is predicted to have a high mechanical strength^[1], and we focus on the elongation behavior of CNC. The purpose of this study is to measure the electrical resistance of CNC when it is elongated under the tensile load. CNC was synthesized in our laboratory by chemical vapor deposition^[2]. Fig. 1 shows that the SEM image of a prepared sample. We have prepared a CNC sample using focused ion beam (FIB), and fixed the end of CNC to Au film on SiO₂/Si substrate. Silver paste was used to bond Au film with a stage of SEM. The stage of SEM was connected to the manipulator tip through a source meter. We approached the manipulator tip to the CNC and measured the electrical resistance of CNC.

Table 1 shows the measurement results of the electrical resistances of CNC. Electrical resistance measurements were carried out by making the tip contact point A and point B in Fig. 1. Measured value of the former is a resistance of the whole measurement system without CNC. Therefore, the resistance of CNC was obtained by subtracting the value of the former from that of the latter. It was measured that the electrical resistance of CNC is in the order of several hundred kΩ.

This work has been partly supported by the Research Project of the Venture Business Laboratory from Toyohashi University of Technology (TUT); the Core University Programs (JSPS-CAS program in the field of "Plasma and Nuclear Fusion") from the Japan Society for the Promotion of Science (JSPS); JSPS KAKENHI Grant Number 24360108; and MEXT KAKENHI Grant Number 24110708.

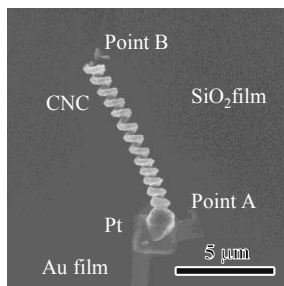


Fig. 1 Preparation of measurement sample of CNC

Table 1 Measurement of electrical resistance of three CNC samples.

	Sample 1	Sample 2	Sample 3
Coil length [μm]	11.7	5.5	12.5
Coil diameter [nm]	730	1400	1240
Wire diameter [nm]	600	500	677
Resistance [kΩ]	290	80	621

[1] S. Motojima, et al: Diamond & Related Materials, 13, 1989 (2004)

[2] K. Takimoto, et al., The 37th Fullerene-Nanotubes General Symposium (2009) 3P-30

Corresponding Author: Yoshiyuki Suda

Tel: +81-532-44-6726, Fax: +81-532-44-6757, E-mail: suda@ee.tut.ac.jp

ESR Measurements of Series of [n]Cycloparaphenylene Cation Radicals in Solution

○Takahiko Kouyama¹, Eiichi Kayahara², Shigeru Yamago², and Tatsuhisa Kato^{1,3}

¹ Department of Interdisciplinary Environment, Graduate School of Human and Environmental Studies, Kyoto University, Kyoto 606-8501, Japan

² Institute for Chemical Research, Kyoto University, Uji 611-0011, Japan

³ Institute for the Promotion of Excellence in Higher Education, Kyoto University, Kyoto 606-8501, Japan

Cycloparaphenylenes (CPPs) are molecules with the simplest structure unit of armchair carbon nanotubes. Yamago group of author succeeded in selective syntheses of [n]CPPs.^[1] The systematic study of the electric structure of the series of CPPs would attract the theoretical attention. We report here ESR studies of radical cations prepared by the oxidation of [n]CPPs (n=6,8,10,12) with SbCl₅ in CH₂Cl₂ solvent by using a X band- ESR spectrometer.

The ESR spectra of [n]CPPs (n=6,8,10,12) radical cations in CH₂Cl₂ solution were obtained at 293K. All observed spectra were well reproduced by the computer simulation, as shown in Fig 1. The ESR parameters of g factors, ¹H hyperfine coupling (hfc) constants, and line widths ΔH_{pp} determined by the simulation are tabulated in Table 1. It is noticeable that the g factors are greater than the value of free electron, g_e = 2.0023, and that the smaller ¹H hfc constants are obtained for the bigger size of paraphenylene ring.

Table 1. g factors and hfc constants obtained by simulation

	g factor	hfc constant	ΔH _{pp}
[6]CPP	2.0028	0.0429 / mT	0.0128 / mT
[8]CPP	2.0023	0.0343	0.0194
[10]CPP	2.0031	0.0293	0.0180
[12]CPP	2.0030	0.0249	0.0156

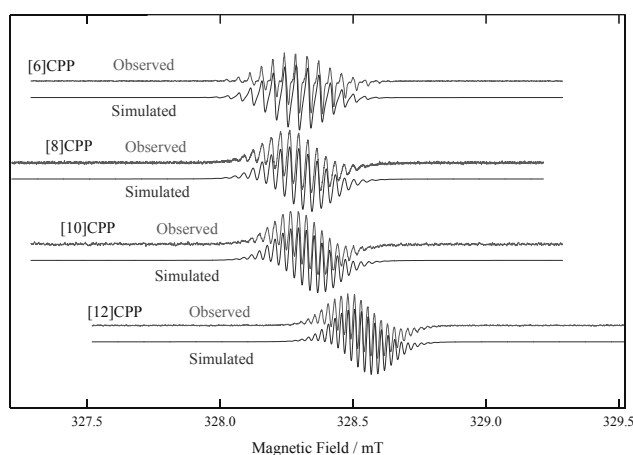


Fig.1 ESR spectra of [n]CPPs (n=6 - 12) radical cations in CH₂Cl₂ solution recorded at 293K.

[1] T. Iwamoto *et al.* J. Am. Chem. Soc., **133**, 8354 (2011).

Corresponding Author: T. Kato

Tel: +81-75-753-6695, Fax: +81-75-753-6695,

E-mail: kato.tatsuhisa.6e@kyoto-u.ac.jp

Isolation and Properties of a Cyclopentadiene Adduct of Lithium-ion Encapsulated [60]Fullerene

○Hiroki Kawakami, Hiroshi Okada, Yutaka Matsuo

Department of Chemistry, School of Science, The University of Tokyo, 7-3-1 Hongo, Bunkyo-ku, Tokyo 113-0033, Japan

There have so far been many reports on functionalization of fullerene by the Diels-Alder reaction [1]. Cyclopentadiene (CpH), which is a conjugated diene used in the Diels-Alder reaction, reacts with [60]fullerene smoothly to give an adduct C₆₀-CpH [2]. Its thermal stability and kinetic parameter have been reported [3]. In the endohedral metallofullerene research field, the reversible and regioselective addition of CpH to La@C₈₂ has been reported in 2005 [4].

We investigated reactivity between lithium-ion-encapsulated fullerene (Li⁺@C₆₀) and CpH. The reaction of [Li⁺@C₆₀]PF₆⁻ with CpH immediately proceeded and produced a mono-adduct ([Li⁺@C₆₀(CpH)]PF₆⁻) and bis-adducts ([Li⁺@C₆₀(CpH)₂]PF₆⁻). [Li⁺@C₆₀(CpH)]PF₆⁻ was isolated with electrolyte-associated HPLC technique. The HPLC charts before and after isolation are shown in figure 1. Then, the behavior of desorption and addition of CpH was compared with that of empty C₆₀ adduct (C₆₀(CpH)). Light absorption and electrochemical properties of [Li⁺@C₆₀(CpH)]PF₆⁻ will be also presented.

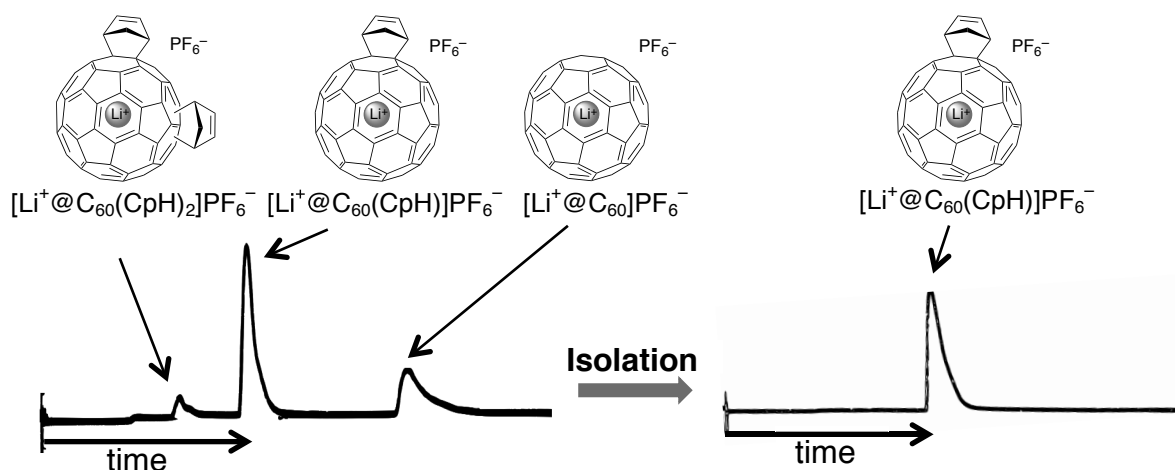


Figure 1. Analytical HPLC charts of [Li⁺@C₆₀]-CpH adducts before and after isolation. Buckyprep column with an eluent system of *o*-dichlorobenzene and acetonitrile (95:5 v/v) containing 30 mM tetrabutylammonium hexafluorophosphate (Bu₄NPF₆)

[1] Śliwa, W. *Full. Sci. Techn.* **1997**, 5, 1133–1175.

[2] Rotello, V. M. *et al. Tetrahedron Lett.* **1993**, 1561-1562.

[3] a) Pang, L. S. I.; Wilson, M. A. *J. Phys. Chem.* **1993**, 97, 6761–6763. b) Howard, B. J.; Rotello, M. V. *et al. J. Phys. Chem.* **1993**, 97, 8560–8561.

[4] Hasegawa, T.; Akasaka, T.; Nagase, S. *et al. J. Am. Chem. Soc.* **2005**, 127, 12190–12191.

Corresponding Author: Y. Matsuo

Tel: 03-5841-1476, Fax: 03-5841-1476, E-mail: matsuo@chem.s.u-tokyo.ac.jp

Solution-phase Synthesis of Dumbbell-Shaped Dimer C₁₂₀ by the Use of FeCl₃

Masahiko Hashiguchi¹, Hiroshi Inada² and Yutaka Matsuo²

¹ Fullerene Development Group, Performance Products Division, Mitsubishi Chemical Corporation, 1-1 Kurosakishiroishi, Yahatanishi-ku, Kitakyushu 806-0004, Japan

² Department of Chemistry, School of Science, The University of Tokyo, 7-3-1 Hongo, Bunkyo-ku, Tokyo 113-0033, Japan

Fullerene chemists and carbon cluster scientists have devoted much attention to fullerene dimers, because of their unique structures that are thought to be intermediates in fullerene polymerization. Among them, special attention has been paid to buckminsterfullerene dimer, C₁₂₀, which is composed of only carbon atoms [1]. The first reported C₁₂₀ synthesis used high-speed vibration milling [2-4]. On the other hand, a solution-phase synthesis of the dimer C₁₂₀ has yet to be reported. Solution-phase synthesis offers certain advantages: the synthesis can be conducted by using common laboratory glassware and etc.

C₆₀ was converted into C₁₂₀ in the presence of FeCl₃ in 1,1,2,2-tetrachloroethane at 150 °C under nitrogen atmosphere. Aromatic organic solvents such as toluene and xylene are often used in synthesis of fullerene derivatives. However they are not suitable for this reaction because they cause a side reaction [5-9].

C₁₂₀ was characterized with electrospray ionization mass spectrometry, attenuated total reflection fourier transform infrared spectrometry, and X-ray crystal structure analysis. We will discuss the proposed reaction mechanism in this presentation. These findings will provide opportunities for further investigation to obtain polymeric structures of fullerenes in the solution phase as well as to expand applied research on C₁₂₀.

[1] J. L. Segura *et al.* Chem. Soc. Rev. **29** 13 (2000).

[2] G-W. Wang *et al.* Nature. **387** 583 (1997).

[3] K. Komatsu *et al.* J. Org. Chem. **63** 9358 (1998).

[4] K. Komatsu *et al.* Carbon **38** 1529 (2000).

[5] G. A. Olah *et al.* J. Am. Chem. Soc. **113** 9387 (1991).

[6] A. Iwashita *et al.* Angew. Chem. Int. Ed. **46** 3513 (2007).

[7] S. H. Hoke II *et al.* Rapid Commun. Mass Spectrometry **5** 472 (1991).

[8] M. Hashiguchi *et al.* Org. Biomol. Chem. **9** 6417 (2011).

[9] M. Hashiguchi *et al.* Org. Lett. **14** 3276 (2012).

Corresponding Author: Y. Matsuo

Tel: +81-3-5841-1476, Fax: +81-3-5841-1476

E-mail: matsuo@chem.s.u-tokyo.ac.jp

Growth and Electric Properties of C₆₀ Whiskers Directly Grown between Electrodes by Surface Treatment

○Katsuya Uruchida Nobuyuki Iwata and Hiroshi Yamamoto

*Department of Electronics & Computer Science, College of Science & Technology,
NihonUniversity, 7-24-1 Narashinodai, Funabashi-shi, Chiba, 274-8501 Japan*

C₆₀-whisker has been paid attention from its shape, scale and electric properties depending on the degree of polymerization for nano-scale application[1,2]. The C₆₀-whiskers are synthesized from evaporating C₆₀ dissolved solution and/or liquid-liquid interfacial precipitation method[3]. Those processes are rather easier than a traditional evaporation method considering an organic FET application[4]. In this study, we aim at bridge of the C₆₀-whisker between electrodes directly on the surface treated substrate with electrodes. Indeed the crystal structure, crystallinity, shape, growth direction, and polymerization are expected to depend on solvent, dipping speed, and solution temperature, electrode's shape, difference in surface tension between solvent and the substrate surface, and so forth. The degree of the polymerization and electric properties of the bridged C₆₀-whiskers were investigated. The triangular electrodes Au/Cr were deposited by an evaporation method on SiO₂/Si substrates. Then the area of electrodes and between electrodes was exposed in the ozone atmosphere to be hydrophilic for 30 minutes. The C₆₀-whisker was self-assembly grown between electrodes from solution by dipping method with the speed of 1 μm/s. The used solvent was *m*-xylene.

The C₆₀ crystal shape, grown on untreated substrate, was examined by an optical microscope (OM) as shown in Fig.1. The C₆₀-whisker randomly grew on overall substrates, and whiskers did not bridge the electrodes. Figure 2 shows the OM image of the C₆₀-whisker grown on the substrate with hydrophilic treatment. We can see the bridged C₆₀-whisker between electrodes. The surface of SiO₂ and Au is normally hydrophilic and hydrophobic, respectively. By the ozone treatment, the intermediate area between electrodes was more hydrophilic than the other SiO₂ surface. Considering the hydrophobic property of *m*-xylene solvent and treated hydrophilic Au surface, it is speculated that a spherical drop on the Au electrode was getting bigger as pulling up the substrate during dipping process, then reached the edge of the Au. The drop was wet and the surface of the drop was expanded on the hydrophilic SiO₂ surface, simultaneously the solvent evaporated, resulting in the crystallization of C₆₀-whisker and bridge the electrodes.

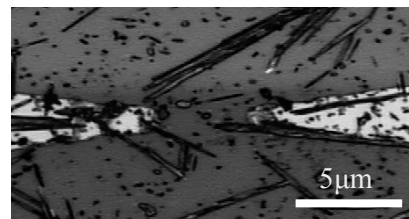


Fig.1 The result of the C₆₀-whisker grown on untreated substrate with Au electrodes.

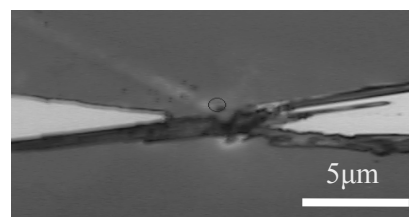


Fig.2 The result of the C₆₀-whisker growth on the substrate surface with hydrophilic treatment.

- [1] M. N.-Regueiro, et al., PRL 74 (1995) 278.
- [2] M. P. Larsson, et al., ECS Trans. 2 (2007) 27.
- [3] K. Miyazawa, et al., J. Mater. Res. 17 (2002) 83.
- [4] M. Kitamura and Y. Arakawa, Jpn. J. Appl. Phys. 50 (2011) 01BC01.

Cycloadditions to $\text{La}_2@C_{80}$ and vibronic coupling density analysis

◦ Naoki Haruta¹, Tohru Sato^{1,2}, Kazuyoshi Tanaka¹

¹*Department of Molecular Engineering, Graduate School of Engineering,
Kyoto University, Kyoto, 615-8510, Japan*

²*Unit of Elements Strategy Initiative for Catalysts & Batteries, Kyoto University,
Nishikyo-ku, Kyoto 615-8510, Japan*

The frontier orbitals of large molecules such as fullerenes are sometimes delocalized throughout the molecules. In such a case, the frontier orbital theory has difficulty in predicting their reactivity. To overcome this difficulty, we have clarified that it is effective to consider an electronic state as well as molecular vibrations [1, 2]. In this study, we discuss the reactivity of an endohedral metallofullerene $\text{La}_2@C_{80}$ from the view of vibronic (electron-vibration) couplings.

Vibronic coupling density and its integration, a vibronic coupling constant are discussed as reactivity indices. Vibronic coupling means the interaction between electrons and molecular vibrations. The vibronic coupling constant V_s and the vibronic coupling density $\eta_s(\mathbf{r})$ are expressed by

$$V_s = \int \eta_s(\mathbf{r}) d^3\mathbf{r}, \quad \text{where} \quad \eta_s(\mathbf{r}) = \Delta\rho(\mathbf{r}) \times v_s(\mathbf{r}).$$

$\Delta\rho(\mathbf{r})$ is the change of electron density in a reaction process. For example, for nucleophilic attacks, it is the electron density difference between neutral and anionic states. $v_s(\mathbf{r})$ is the potential derivative with respect to vibrational mode s . According to the Hellman–Feynman theorem, V_s is exactly equal to the gradient of the potential surface with an electronic state changed in a reaction process. V_s has therefore the physical meaning of the driving force to deform the molecule along the vibrational mode s in the early stage of a chemical reaction. $\eta_s(\mathbf{r})$ can be regarded as the local picture of a chemical reaction, which is illustrated on the basis of an electronic structure $\Delta\rho(\mathbf{r})$ and a vibrational structure $v_s(\mathbf{r})$.

In this study, we performed the DFT calculations (BP86 functional; all electron basis sets C: TZ2P, La: TZP) for the neutral and charge-transfer (ionic) states of $\text{La}_2@C_{80}$ including relativistic effects as ZORA with the ADF 2012.01 package. $\text{La}_2@C_{80}$ has a much unstable D_{5d} isomer, and D_{2h} , D_{3d} , C_{2h} and C_i isomers whose energy differences are less than 50 meV. At the room temperature, all the D_{2h} , D_{3d} , C_{2h} and C_i isomers are possible and averaged to be observed. Therefore, we here analyzed the reactivity of a D_{3d} isomer which has the highest symmetry of them. Fig. 1 shows the potential derivative $v_s(\mathbf{r})$ caused by an effective vibration for nucleophilic attacks. The double bonds indicated by arrows are more reactive than others, that is consistent with experimental facts [3]. In the present work, we will discuss the vibronic couplings on the basis of the electronic and vibrational structures in more detail.

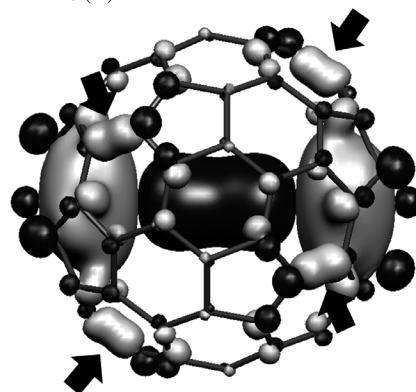


Fig. 1: The potential derivative $v_s(\mathbf{r})$ caused by an effective vibration for nucleophilic attacks.

[1] T. Sato *et al*, Chem. Phys. Lett. **531**, 257 (2012).

[2] N. Haruta *et al*, J. Org. Chem. **77**, 9702 (2012).

[3] M. Yamada *et al*, J. Am. Chem. Soc. **128**, 1402 (2006).

Corresponding Author: T. Sato

Tel: +81-75-383-2803, Fax: +81-75-383-2556,

E-mail: tsato@moleng.kyoto-u.ac.jp

A Novel Non-IPR Endohedral Metallofullerene: $\text{La}_2@C_s(17490)-C_{76}$

○Mitsuaki Suzuki,¹ Naomi Mizorogi,¹ Zdenek Slanina,¹ Xing Lu,^{1,2}
Shigeru Nagase,³ and Takeshi Akasaka¹

¹*Life Science Center of Tsukuba Advanced Research Alliance, University of Tsukuba,*

²*State Key Laboratory of Materials Processing and Die & Mould Technology, School of Materials Science and Engineering, Huazhong University of Science and Technology (HUST),*

³*Fukui Institute for Fundamental Chemistry, Kyoto University.*

Fullerenes are pure-carbon molecules consisting of exactly 12 pentagonal carbon rings and a varied number of hexagons, which depend on the cage size. Thus, fullerene chemistry has the very important experimental rule, that is, the isolated pentagon rule (IPR). The search for fullerene structures violating the IPR is of particular importance and of wide interest because non-IPR cages might exhibit different properties from those of IPR-compliant structures. Two strategies have shown practical effectiveness in generating non-IPR fullerene cages. One of them is the encapsulation of metallic species inside the fullerene cages, which generates hybrid molecules known as endohedral metallofullerenes (EMFs). Until now, a great number of endohedral metallofullerenes (EMFs) have been discovered. EMFs have very unique structures and properties because of the electron transfer from encapsulated species to fullerene cage. This also results in several prominent examples of EMFs that do not satisfy the IPR with cage sizes spreading from C_{72} to C_{84} . This serves as a solution for stabilizing non-IPR fullerene cages which seems more effective because many more examples of non-IPR EMFs have been obtained.¹

Herein, we report the isolation and systematic characterization of a new non-IPR EMF, *i.e.* $\text{La}_2@C_s(17490)-C_{76}$, including the first single-crystal X-ray diffraction crystallographic result of a non-IPR EMF possessing a C_{76} cage. Moreover, the motion of the two encapsulated La ions has been examined using variable-temperature ^{139}La NMR, providing new insights into the metal-cage interactions in these types of unconventional EMFs.

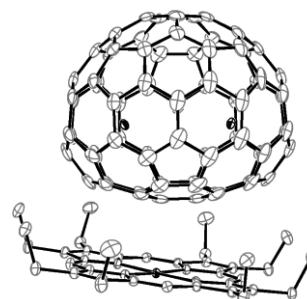


Fig. 1. X-ray structure of $\text{La}_2@C_{76}$. $\text{Ni}(\text{OEP})\cdot 2(\text{benzene})\cdot \text{CS}_2$. Solvent molecules and hydrogen atoms are omitted for clarity.

[1] (a) *Endofullerenes: A New Family of Carbon Clusters*, Akasaka, T.; Nagase, S. Eds.; Kluwer: Dordrecht, The Netherlands, **2002**. (b) Yang, S.; Dunsch, L. *Endohedral Fullerenes*, in *Nanomaterials: Inorganic and Bioinorganic Perspectives*, Lukehart, C. M. and Scott, R. A. Eds. John Wiley & Sons: Chichester, United Kingdom, **2008**, pp189-214. (c) *Chemistry of Nanocarbons*, Akasaka, T.; Wudl, F.; Nagase, S. Eds.; Wiley-Blackwell: London, **2010**. (d) Lu, X.; Akasaka, T.; Nagase, S. *Rare Earth Metals Trapped inside Fullerenes—Endohedral Metallofullerenes*, in *Rare Earth Coordination Chemistry: Fundamentals and Applications*, Huang, C. H. Ed. John Wiley & Sons: Singapore, **2010**, pp 273-308.

Corresponding Author: T. Akasaka

Tel: +81-29-853-6409, Fax: +81-29-853-6409,

E-mail: akasaka@tara.tsukuba.ac.jp

Magnetic Properties of Gd@C₈₂-PEG-b-PAMA-complexed Nanoparticle

○Toshihiro Aizawa¹, Yukichi Horiguchi², Yukio Nagasaki^{2,3,4}, Hisanori Shinohara⁵, and Tatsuhisa Kato^{1,6}

¹ Department of Interdisciplinary Environment, Graduate School of Human and Environmental Studies, Kyoto University, Kyoto 606-8501, Japan

² Graduate School of Pure and Applied Sciences, University of Tsukuba, Tsukuba 305-8573, Japan

³ Master's School of Medical Sciences, University of Tsukuba, Tsukuba 305-8573, Japan

⁴ Satellite Laboratory of International Center for Materials Nanoarchitectonics, National Institute of Materials Science, Tsukuba 305-8573, Japan

⁵ Department of Chemistry, Nagoya University, Nagoya 464-8602, Japan

⁶ Institute for the Promotion of Excellence in Higher Education, Kyoto University, Kyoto 606-8501, Japan

Gadolinium is a promising candidate for MRI contrast agent because of the significant variations in the water relaxation time. Nagoya group of author has reported that gadolinium fullerenol Gd@C₈₂(OH)_n exhibited the efficient reduction of relaxation time.^[1] Tsukuba group of author reported the solubilization of Gd@C₈₂ in water by synthetic block copolymers, poly(ethylene glycol)-b-poly [N,N-(dimethylamino) ethyl methacrylate] (PEG-b-PAMA).^[2] We report here the magnetic properties of Gd@C₈₂-PEG-b-PAMA by ESR spectroscopy.

The electron spin state of intact Gd@C₈₂ has been reported by Kyoto group.^[3] The charge transfer of three electrons of gadolinium outer electron shell gave the electronic state of Gd³⁺@C₈₂³⁻. And the spin (S = 1/2) on the π orbital of the fullerene cage was coupled with the octet spin (S = 7/2) of the encapsulated gadolinium in an antiferromagnetic manner, then the ground state of Gd@C₈₂ was characterized by an integer spin quantum number S = 3. In the solid powder form of Gd@C₈₂, the radical electrons canceled upon dimerization, and the resultant spin state of the dimer was described by two independent octet (S = 7/2) spins of the gadolinium. Thus the radical spin on the cage contributed to the peculiar spin state of Gd@C₈₂.

The ESR spectra of Gd@C₈₂-PEG-b-PAMA were obtained by X band ESR measurement in frozen solution of water with various pH at 5K, as shown in Fig.1. The sharp peak at the magnetic field of 3500 Gauss was prominent feature in the spectrum, whose line width varies with pH of solution.

[1] H. Kato *et al.* J. Am. Chem. Soc. **125**, 4391 (2003).

[2] Y. Horiguchi *et al.* Sci. Technol. Adv. Mater. **12**, 044607 (2011).

[3] K. Furukawa *et al.* J. Phys. Chem. A **107**, 10933 (2003).

Corresponding Author: T. Kato

Tel: +81-75-753-6695, Fax: +81-75-753-6695,

E-mail: kato.tatsuhisa.6e@kyoto-u.ac.jp

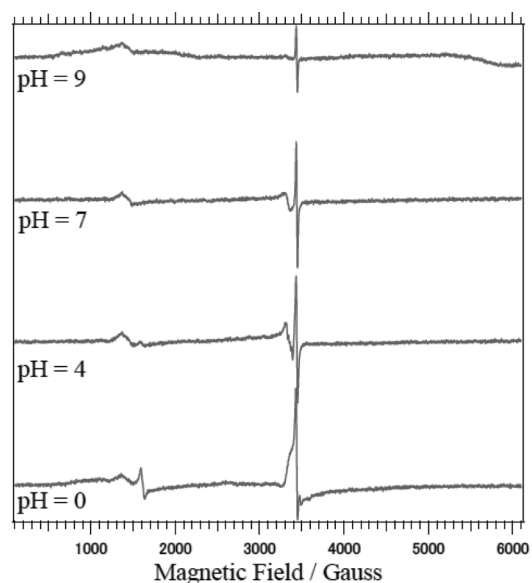


Fig.1 ESR spectra of Gd@C₈₂-PEG-b-PAMA in frozen solution of water with different pH at 5K.

Synthesis of C₇₀ Nanosheets by Liquid-Liquid Interfacial Precipitation Method

○Kana Osonoe, Ryosuke Kano and Masaru Tachibana

Department of Nanosystem Science, Yokohama City University, Yokohama 236-0027, Japan

C₇₀, one of the higher fullerenes, has narrow band gap than C₆₀. So C₇₀ is very interesting for the application to a nanoelectronic device. However, it is difficult to get a high quality C₇₀ crystal because C₇₀ has some phase transitions near room temperature and symmetry being lower than C₆₀. Therefore there are fewer studies on solid state properties of C₇₀ than C₆₀. Recently, for the control of the crystal shape, much attention has been paid for the solution growth. A liquid–liquid interfacial precipitation method (LLIP method) leads to not only the control of crystal shapes but also the short time growth for the crystals [1]. The LLIP method is expected as an effective method for practical use. In this paper, we report the synthesis of C₇₀ nanosheets by LLIP method.

C₇₀ nanosheets were prepared by LLIP method with an interface between C₇₀-saturated toluene with ferrocene and IPA. Fig. 1 shows optical microscopic image of the crystals grown for 24 hours by LLIP method. They exhibit hexagonal shapes with ~200 nm in thickness and 10 μm in diameter. Fig. 2 shows XRD pattern of C₇₀ nanosheets. From the XRD pattern, the structure of C₇₀ nanosheets exhibits a monoclinic structure including ferrocene ($a = 27.15\text{Å}$, $b = 10.21\text{Å}$, $c = 19.25\text{Å}$, $\beta = 121.73^\circ$). In addition, it should be noted that the monoclinic structure of C₇₀ nanosheets change to a face-centered cubic one with annealing. We present the growth method of C₇₀ nanosheets and the structural characteristic.

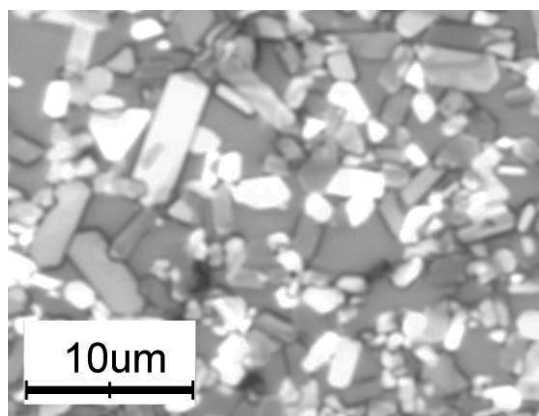


Fig. 1 The optical microspopepic image of C₇₀nanosheets.

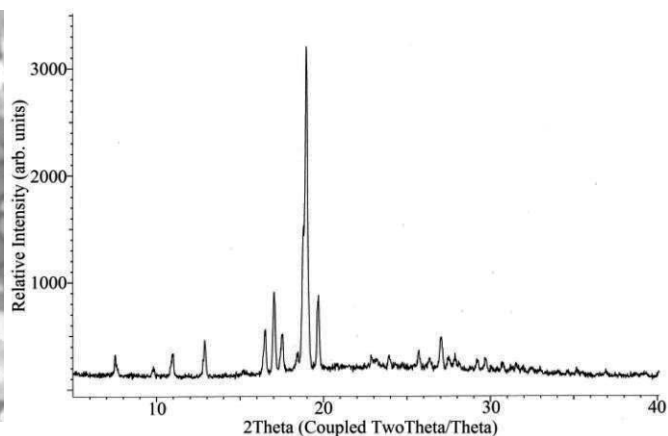


Fig.2 The XRD pattern of C₇₀ nanosheets

[1] T. Wakahara et al. J. Am. Chem. Soc 131 (2009) 6372

Corresponding author: Masaru Tachibana, YokohamaCity University, 22-2 Seto, Kanazawa-ku, Yokohama 2360027, Japan, Tel &Fax: +81-45-787-2360, E-mail: tachiban@yokohama-cu.ac.jp

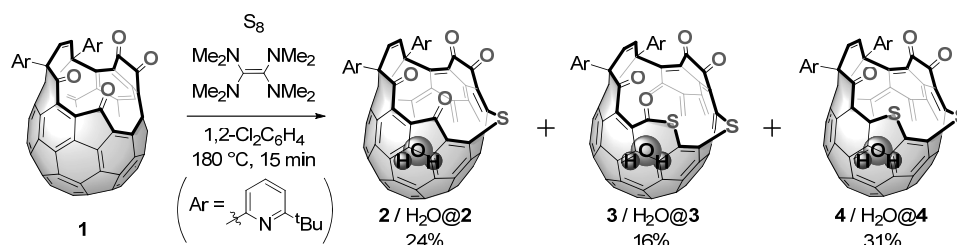
Synthesis of C₆₀ Derivatives Having a Sulfur-containing Opening and X-ray Structure of N₂ Encapsulated Molecule

○Tsukasa Futagoishi,¹ Michihisa Murata,¹ Yasujiro Murata^{1,2}

¹Institute for Chemical Research, Kyoto University, Uji, Kyoto 611-0011, Japan
²JST-PRESTO

We have already established methods to synthesize endohedral fullerenes encapsulating helium¹, dihydrogen², and water³, based on skeletal modifications of fullerenes by organic reactions.⁴ In order to further extend our research to the encapsulation of larger molecules, development of a method to enlarge the opening is required. In this work, we prepared C₆₀ derivatives with a large opening by using sulfur insertion as a key reaction.

Scheme 1



A sulfur insertion was carried out to tetraketo-C₆₀ derivative **1** with a 16-membered-ring opening under the presence of a reducing agent. This reaction afforded a novel open-cage C₆₀ derivative **2** having a 17-membered-ring opening by insertion of a sulfur atom to the rim of the opening. Furthermore, we unexpectedly found that new sulfur-containing compounds also formed in this reaction; an insertion of two sulfur atoms to the opening of **1** gave **3** and subsequent loss of one carbonyl group gave **4** (Scheme 1). ¹H NMR and X-ray structural analysis showed that a water molecule was encapsulated in **2-4**.

Then an insertion of dinitrogen to **2** was studied. After powder of **2**/H₂O@**2** was heated under vacuum, the powder was subjected to nitrogen gas (10 atm). In order to inhibit the release of dinitrogen, one of the carbonyl groups of **2** was immediately reduced (Scheme 2).⁵ Although the product was a mixture of **5** encapsulating dinitrogen or water, N₂@**5** was found to be separated from the mixture by HPLC (Buckyprep column). X-ray structural analysis of N₂@**5** clearly showed that dinitrogen was present at the center of the C₆₀ cage of **5** (Fig. 1).

Scheme 2

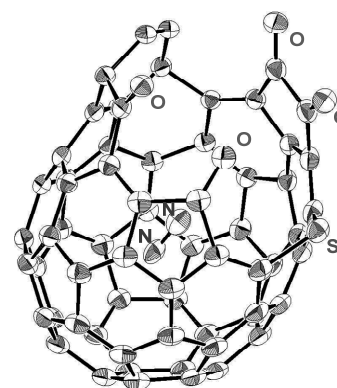
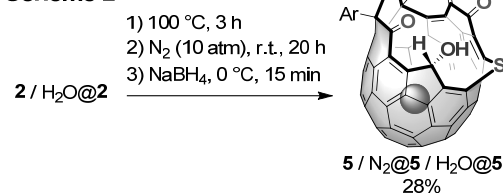


Fig. 1 X-ray structure of N₂@**5**. Aryl groups are omitted for clarity.

[1] Y. Morinaka, F. Tanabe, M. Murata, Y. Murata, K. Komatsu, *Chem. Commun.* **2010**, 4532. [2] K. Komatsu, M. Murata, Y. Murata, *Science* **2005**, *307*, 238. [3] K. Kurotobi, Y. Murata, *Science* **2011**, *333*, 613. [4] M. Murata, Y. Murata, K. Komatsu, *Chem. Commun.* **2008**, 6083. [5] S.-C. Chuang, Y. Murata, M. Murata, K. Komatsu, *Chem. Commun.* **2007**, 1751. Corresponding Author: Y. Murata Tel: +81 774-38-3172, Fax: +81 774-38-3178, E-mail: yasujiro@scl.kyoto-u.ac.jp

Polymerization in C₆₀ thin films deposited under *in situ* UV light irradiation

○Daijiro Arai^{1,2}, Hisanori Tanimoto¹, Manabu Ohtomo², Shiro Entani², Yoshihiro Matsumoto², Seiji Sakai²

¹ Institute of Materials Science, University of Tsukuba, Tennodai 1-1-1, Tsukuba, Ibaraki 305-8573, Japan

² Advanced Science Research Center, Japan Atomic Energy Agency, Shirakata-Shirane 2-4, Tokai, Ibaraki 319-1195, Japan

[Introduction] Polymerized C₆₀ film is of interest for some attractive property, such as high electrical conductivity due to the unique electronic structure[1]. While there have been several reports on the polymerization method of C₆₀, light irradiation has advantages of simplicity and controllability for nano-scale fabrication. However, since the light penetration depth into C₆₀ films is limited to ~100 nm, it is difficult to fabricate homogeneous C₆₀ films essential for electronic applications. In the present study, microstructures are investigated for the C₆₀ films deposited under *in situ* UV light irradiation by using X-ray diffraction (XRD), micro-Raman spectroscopy and X-ray photoelectron spectroscopy (XPS). It is demonstrated that the *in situ* UV light irradiation leads to a growth of FCC crystal with high polymerization degree of C₆₀ comparable to that in the high-pressure phase through the entire thickness.

[Experimental] C₆₀ films of 100's nm thickness were deposited on Si substrates at room temperature. To perform *in situ* UV light ($\lambda = 365$ nm) irradiation, the substrate was tilted with respect to the directions of a Knudsen-Cell and incident light source. After the deposition, the lattice parameter and degree of polymerization were estimated from the XRD data. The thermal stability of the C₆₀ photopolymer was investigated for the change of the Raman spectrum by thermal annealing. The electronic structures were also investigated by XPS.

[Result & Discussion] Figs. 1(a) and 1(b) show the XRD patterns obtained for the C₆₀ films deposited without and with UV light irradiation (pristine and *in situ* UV irradiated C₆₀ film), respectively. For the *in situ* UV irradiated films, the diffraction peaks due to the (111), (220), and (310) reflections of the FCC lattice are observed; however, the peak positions are shifted to higher angles compared with the pristine C₆₀ film. The estimated lattice constant is 1.355 nm, which is 4% smaller than that of pristine C₆₀. From the micro-Raman measurements, it is also confirmed that C₆₀ molecules in the *in situ* UV irradiated films are uniformly polymerized. The number of the covalently-bonded C₆₀ around a C₆₀ molecule was estimated to be about 6 from the lattice constant, which is larger than that reported for the C₆₀ photopolymer by post light irradiation[2] and comparable to that in the high-pressure phase[1]. More details including the XPS results will be reported on the presentation.

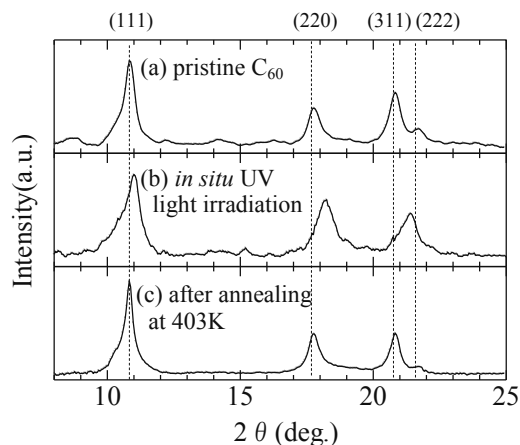


Fig. 1 XRD patterns of the C₆₀ films. (a) pristine C₆₀ film, (b) *in situ* UV light irradiated C₆₀ film (80 mW/cm², 300 nm thick), (c) and the same film after annealing at 403 K.

[1] T. L. Makarova, Semiconductors **35**, 243(2001)

[2] E. Kovats *et al.* J. Phys. Chem B **109**,11913(2005)

Chirality dependence of exciton diffusion in air-suspended single-walled carbon nanotubes

○A. Ishii, A. Yokoyama, M. Yoshida, T. Shimada, Y. K. Kato

Institute of Engineering Innovation, The University of Tokyo, Tokyo 113-8656, Japan

In single-walled carbon nanotubes, exciton diffusion affects the photoluminescence quantum efficiency through substrate- and defect-induced nonradiative decay of the excitons, and therefore quantitative characterization of exciton diffusion is important. In the case of air-suspended nanotubes, exciton diffusion lengths can be determined by analyzing the dependence of photoluminescence intensity on nanotube length [1]. As this method requires ~30 nanotubes for a particular chirality, we have constructed an automated micro-photoluminescence system which allows us to characterize over five hundred individual carbon nanotubes in a day. A three-dimensional programmable stage is used to automatically locate and list the positions of bright nanotubes. Excitation wavelength, intensity, and polarization angle are automatically controlled to fully characterize these nanotubes. Using this system, hundreds of as-grown air-suspended carbon nanotubes are characterized, and data from high quality individual tubes are selected to investigate the chirality dependence of exciton diffusion length.

This work is supported by SCOPE, KAKENHI, KDDI Foundation, The Sumitomo Foundation, and the Photon Frontier Network Program of MEXT, Japan. The samples are fabricated at the Center for Nano Lithography & Analysis at The University of Tokyo.

[1] S. Moritsubo *et al.*, Phys. Rev. Lett. **104**, 247402 (2010).

Corresponding Author: Y. K. Kato
Tel: +81-3-5841-7702, Fax: +81-3-5841-7772,
E-mail: ykato@sogo.t.u-tokyo.ac.jp

Electric Double Layer Transistors using Thick Films in Single Chiral States of (6,5) and (11,10) Single-Wall Carbon Nanotubes

○Kudo Hikaru¹, M. Kawai¹, H. Tomoyuki¹, Yuki Nobusa², Taishi Takenobu², Kazuhiro Yanagi¹

Tokyo Metropolitan Univ.¹, Waseda Univ.²

Recent progress of purification techniques enables us to obtain metallic, semiconducting and single chiral SWCNTs, and then purified semiconducting SWCNTs have been used as field effect transistor applications. In the case of typical SWCNT thin film transistors, device performances have been significantly influenced by the morphologies of the networks of the semiconducting SWCNTs. Thus, how the electronic structures of the semiconducting SWCNTs affect the performances has not been well revealed. In the case of electric double layer transistors (EDLT), transistor performances depend on the electronic structures of SWCNTs because quantum capacitance, which is related to the density of states of SWCNTs, influences the capacitance of the channel at low voltages. Thus we investigated device properties of EDLTs of (6,5) and (11,10) SWCNTs, which were obtained by gel and ultracentrifugation purifications [1], and clarified their differences.

Figure 1 shows transfer characteristics of (6,5) and (11,10) SWCNTs EDLT. The on/off ratios of both transistors were more than 10^4 , and mobilities were 50 to $80 \text{ cm}^2 \text{ V}^{-1} \text{ s}^{-1}$. As shown in Fig. 1, distinct differences were observed in the threshold voltages of EDLTs. Threshold voltages of (11, 10) was smaller than those of (6,5), reflecting the band-gap widths of the SWCNTs. The backgrounds of the distinct threshold voltages are differences in their capacitance characteristics (Fig. 2). Quantum capacitance due to the densities of states of (6,5) and (11,10) SWCNTs influenced the threshold voltages of the EDLTs of the SWCNTs.

[1] H. Liu et al., Phys. Stat. Solidi B 248, 2524 (2011), M. Kawai et al., J. Am. Chem. Soc. **134**, 9545 (2012).

Corresponding Author: K. Yanagi
Tel: +81-42-677-2494,
Fax: +81-42-677-2483,
E-mail: yanagi-kazuhiro@tmu.ac.jp

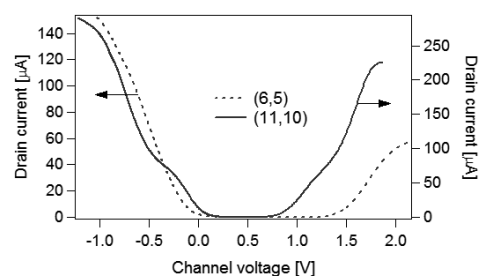


Fig. 1 Transfer characteristics of EDLTs of (6,5) and (11,10) SWCNTs

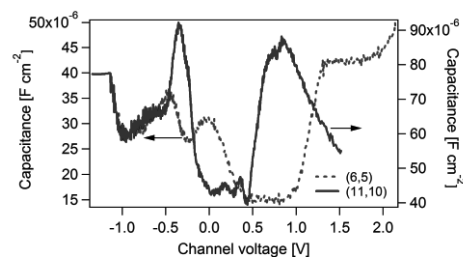


Fig. 2 Capacitances of EDLTs of (6,5) and (11,10) SWCNTs

Existence of two distinct equilibrium states in the exchange reaction of sodium cholate and oligo DNA on single-walled carbon nanotubes

○Yuichi Kato¹, Yasuro Niidome^{1,2}, Naotoshi Nakashima^{1,2,3}

¹*Department of Applied Chemistry, Kyushu University, Fukuoka 819-0395, Japan*

²*WPI-I2CNER, Kyushu University, Fukuoka 819-0395, Japan*

³*JST-CREST, Chiyoda-ku, Tokyo 102-0075, Japan*

A deep understanding of the solubilization of the single-walled carbon nanotubes (SWNTs) is essential from the viewpoints of fundamental science and applications. Although surfactant micelles are the most typical SWNT solubilizers, quantitative analysis on the concentration dependence of surfactant on the SWNTs has been very limited. In general, SWNT solubilization requires a certain concentration of surfactants. These concentrations do not coincide with the critical micelle concentration (CMC) in some cases.^[1]

Previously, based on thermodynamics, we provided the equilibrium constants ($K_{exchange}$) and thermodynamical parameters of the exchange reactions of DNAs and sodium cholate (SC) (concentration below the CMC) on the SWNTs.^[2,3] Here, we describe the finding that two distinct equilibrium states exist in the exchange reaction of sodium cholate and DNAs on the surfaces of the SWNTs.

We prepared SC dispersed SWNT solutions by sonication and centrifugation. The SC-SWNT solutions, DNA solutions and buffer solutions were mixed. The DNA concentration ($[DNA]$) was adjusted from 0 to 0.14 mM. The SC concentration ($[SC]$) was adjusted from 1.2 to 4.8 mM. The absorption spectra were measured. In order to compare the exchange reactions with different SC concentrations, we plotted the $[DNA]$ where the surface coverage of the SC (θ_{SC}) equals the surface coverage of the DNA (θ_{DNA}) as a function of $[SC]$ (Fig. 1). Note that the plots showed a linear relation; however, two slopes were observed in the different $[SC]$ range. Fig. 1 represents the existence of two states of the SC-SWNTs. The transition in the two states occurs in a very small $[SC]$ range.

The surface tensions of the SC solutions revealed that the CMC is approximately 14 mM, which is much higher than the observed break points in Fig. 1. Both absorption peak wavelengths and zeta potentials of the SC-SWNTs with different $[SC]$ values do not show any signs. These results suggest the transitions of the adsorption structure at certain SC concentrations with different chiral-types of SWNTs under the CMC of SC.

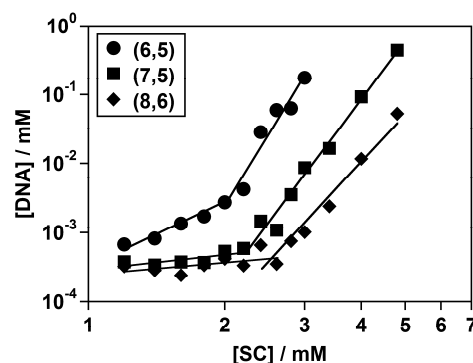


Fig. 1 Plots of DNA concentrations as a function of the SC concentrations in which the surface coverages (θ_{SC} and θ_{DNA}) were equivalent.

[1] A. Ishibashi, N. Nakashima, *Chem. Eur. J.* **12**, 7595–7602 (2006).

[2] Y. Kato, Y. Niidome, N. Nakashima, *Chem. Lett.* **40**, 730–732 (2011).

[3] Y. Kato, A. Inoue, Y. Niidome, N. Nakashima, *Sci. Rep.* **2**, art. no. 733 (2012).

Corresponding Author: N. Nakashima

Tel: +81-92-802-2840, Fax: +81-92-802-2840

E-mail: nakashima-tcm@mail.cstm.kyushu-u.ac.jp

Control of UV Optical Absorption of Single-Wall Carbon Nanotubes Using Electro-chemical Doping Techniques

○Toru Igarashi¹, Kai Hasegawa¹, Tomoyuki Funabasama¹, Shimpei Ono², Kazuhiro Yanagi¹

¹ Department of Physics, Tokyo Metropolitan University, 2. CRIEPI

Steep optical absorption line-shapes of single-wall carbon nanotubes (SWCNTs) are due to one-dimensional characteristics, quantized conditions along circumference direction, and excitonic effects in the SWCNTs. However, the physical backgrounds of a broad optical line-shape, which is sometimes observed in bundled SWCNTs and has absorption maximum at about 4.5 eV (here the band is termed as U-band), have still been under discussion. In previous studies, the detailed investigations of the U-band are sometimes prohibited by the presence of un-identified amorphous carbon species and different chiralities. However, high-purity SWCNTs in a single-chiral state have been obtained by recent purification techniques, and made it possible to discuss the details of the U-band. Figure 1 shows optical absorption spectra of (6,5) SWCNTs in a solution and their films. In the solution, although there were absorption bands in UV region, which will be due to the π - π^* transitions, U-band was not significant. However, in a film where the SWCNTs were bundled, the absorbance of U-band became dominant in the spectra. Therefore, it is clear that physical phenomena in the SWCNT-bundles play important roles for the U-band.

The presence of the U-band is a bottle-neck for electrochromic applications of SWCNTs,¹ and also understanding of the background of the U-band is of fundamental interest. Therefore, in this study, we investigated the physical backgrounds of the U-bands using electro-chemical doping techniques. To reduce chemical reactions during electro-chemical doping, we performed opto-electrochemical measurements at $-26\text{ }^{\circ}\text{C}$. Figure 2 shows the optical absorption spectra of (6,5) SWCNTs upon different potentials. Remarkably, the line-shape of U-band is changed when the potential is shifted, in addition to the disappearance of S_{11} and S_{22} , and the shift of S_{33} . Such changes were stable and reversible because the measurements were performed at a low temperature. The broadening of U-band by doping, which was expected from Fano-mechanisms, was not observed, thus contributions from free-carrier states will be small. The results suggest that optical absorption bands originated from π - π^* transitions can be controllable even if the bands are located at UV-region.

[1] Yanagi et al., Adv. Mater. 23, 2811 (2011)

Corresponding Author: K. Yanagi

Tel: +81-42-677-2494, Fax: +81-42-677-2483

E-mail: yanagi-kazuhiro@tmu.ac.jp

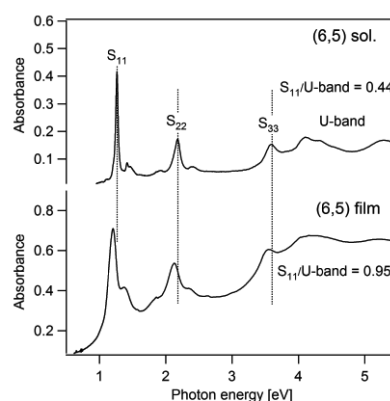


Fig. 1 Optical absorption spectra of (6,5) SWCNTs in a solution and in a film

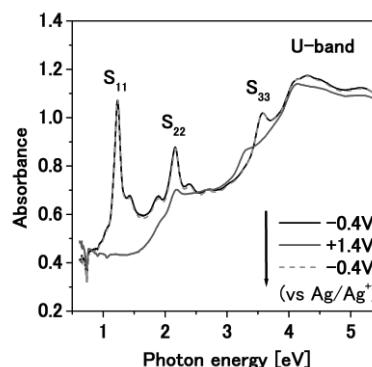


Fig. 2 Changes of optical absorption spectra of (6,5) SWCNTs by electrochemical doping at $-26\text{ }^{\circ}\text{C}$

Thermodynamics for the exchange reaction of sodium cholate and double-stranded DNA on single-walled carbon nanotubes

○Akiko Tsuzuki¹, Ayaka Inoue¹, Yuichi Kato¹, Yasuro Niidome^{1,2},
and Notoshi Nakashima^{1,2,3}

¹Department of Applied Chemistry, Graduate School of Engineering, Kyushu University,
²WPI I2CNER, ³JST-CREST

DNA is one of the well-known solubilizers for single-walled carbon nanotubes (SWNTs). DNA-SWNT hybrids are useful materials for studies on biosensors, electron transfer, length fractionation, and chirality separation of SWNTs. Previously, we have reported thermodynamics on soluble SWNTs, in which the exchange of sodium cholate (SC) and single stranded DNAs (ssDNA) was analyzed[1,2].

In this work, we focused on thermodynamics on the exchange reaction of double-stranded DNA (dsDNA) and SC on SWNTs.

CNTs that were individually solubilized in a SC solution (2 mM) were mixed with various concentrations of ssDNA ($d(G)_{20}$, 0–800 μM) and dsDNA ($d(G)_{20}$ - $d(C)_{20}$, 0–400 μM). After keeping the samples for three days at 14 °C, the near-IR absorption spectra were measured at 22 and 30 °C after 24 h-incubation.

Absorbance changes at 1190 nm that represent the fraction of the (8,6)SWNTs wrapped with ssDNA were plotted against the concentration of the ssDNA (Fig. 1).

From the analysis of the plots, we could calculate the equilibrium constants (K_a) of the exchanges of the solubilizers. Temperature dependences of $d(G)_{20}$ (dotted lines) indicated that the exchange of SC with $d(G)_{20}$ was endothermic. It was reported that $d(C)_{20}$ also showed endothermic reaction [1]. For the use of dsDNA, smaller K_a was found to obtain at the higher temperature (solid lines in Fig. 1), indicating that the exchange of SC with dsDNA was exothermic. Thus, the exchanges of SC with ssDNAs occur in a different manner from that using dsDNA. The thermodynamic parameters (ΔH , ΔS), which were obtained from the temperature dependence of K_a , suggested that the dsDNA-wrapped SWNTs remain the double stranded structure.

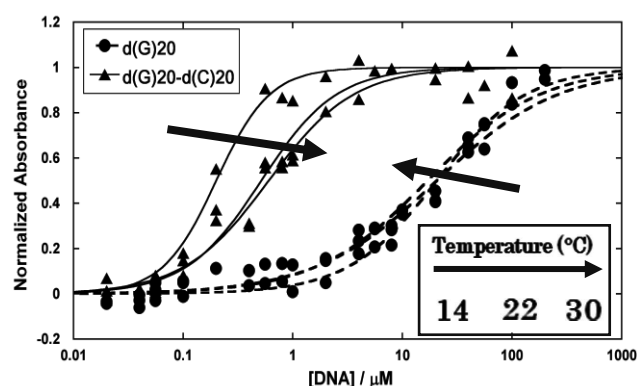


Figure 1 Semi-log plots of the normalized absorbance at 1190 nm. The absorbance changes indicated fractions of DNA-wrapped SWNTs in the presence of $d(G)_{20}$ and $d(G)_{20}$ - $d(C)_{20}$. Temperatures were 14, 22, and 30 °C.

[1] Y. Kato, Y. Niidome, N. Nakashima, *Chem. Lett.*, **40**, 730 (2011).

[2] Y. Kato, Ayaka Inoue, Y. Niidome, N. Nakashima, *Scientific Reports*, **2**, 733 (2012).

Corresponding Author: N. Nakashima

Tel: +81-92-802-2841, Fax: +81-92-802-2841

E-mail: nakashima-tcm@mail.cstm.kyushu-u.ac.jp

Improvement of CNT Properties through a Post Synthetic Treatment

○Naoyuki Matsumoto¹, Azusa Oshima¹, Motoo Yumura^{1,2}, Don N. Futaba^{1,2},
and Kenji Hata^{1,2}

¹ *Technology Research Association for Single Wall Carbon Nanotubes (TASC), Tsukuba
305-8565, Japan*

² *National Institute of Advanced Industrial Science and Technology (AIST), Tsukuba
305-8565, Japan*

Single-wall carbon nanotubes (SWCNTs) have attracted intense interest in numerous applications from MEMS devices, composites, sensors, filters to capacitor electrodes due to their unique inherent properties. However, despite great advances in synthesis, there remains a limitation with regards to the level of synthetic structural control and therefore the SWCNT properties. For example, floating catalyst CVD [1] can grow highly crystalline and small diameter SW- and DWCNTs, but cannot grow CNTs with great length, which is advantageous for long-range electrical, thermal, and strain transfer in macroscopic assemblies. In contrast, water-assisted CVD (Super-growth method [2]) has demonstrated the synthesis of high purity and millimeter-long SWCNTs in a forest but do not possess the high crystallinity of floating catalyst CVD. Therefore, effort has been placed on alternative approaches to overcome these synthetic limitations.

Here, we report the three-fold increase in electrical and thermal properties of Super-growth SWCNTs using a post-synthetic treatment to induce CNT structural change and improve crystallinity. This process consists of thermal annealing of the SWCNTs at high temperatures (1500-2000°C) in a neutral (argon) gas ambient based on the method reported by Yudasaka et al. [3],[4] to induce the improvement in crystallinity for improved thermal properties and/or the conversion of low purity SWCNTs into high purity MWCNTs for improved electrical conductivity. Detailed structural examination of the SWCNTs before and after treatment using Raman and TEM clarified the structural change to the individual nanotubes, which explains the improvement in the observed properties. Finally, this simple method affords several advantages: 1) high reproducibility, 2) the homogeneous treatment of gram-scale (or larger) SWCNT samples, and 3) no required vacuum, and therefore this method possesses the potential to integrate into a SWCNT mass production line.

[1] T. Saito *et al.* J. Nanosci. Nanotechnol., **8**, 6153 (2008).

[2] K. Hata *et al.* Nature, **306**, 1362 (2004).

[3] M. Yudasaka *et al.* Nano. Lett. **1**, 487 (2001).

[4] M. Yudasaka *et al.* Carbon **41**, 1273 (2003).

Corresponding Author: Don N. Futaba

Tel: +81-29-861-4656, Fax: +81-29-861-4851,

E-mail: d-futaba@aist.go.jp

Tensile strength of individual multi-walled carbon nanotube constituting MWCNT fiber

○Hideaki Suzuki¹, Yoshinori Sato¹, Go Yamamoto², Kenichi Motomiya¹, Toshiyuki Hashida², Kazuyuki Tohji¹

¹Graduate School of Environmental Studies, Tohoku University, Sendai 980-8579, Japan

²Graduate school of Engineering, Tohoku University, Sendai 980-8579, Japan

Carbon nanotube (CNT) is an attractive one-dimensional nanomaterial with extremely high tensile strength and Young's modulus [1, 2]. An issue remains concerning how to constitute macroscale CNT assemblies that can fully utilize the mechanical properties of individual CNT itself. As a means to solve this issue, binder-free multi-walled carbon nanotube (MWCNT) fibers have been produced twisting MWCNTs from vertically aligned MWCNT arrays (MWCNT forest) [3] in our laboratory. The tensile strength of MWCNT fibers is, however, not high enough because MWCNTs synthesized by chemical vapor deposition (CVD) are considered to have many defects. In this study, we measured the tensile strength of individual MWCNT constituting MWCNT fibers and evaluated the strength ratio of fiber to individual MWCNT.

Individual MWCNT was picked up from MWCNT forest which has the ability for fiber formation, and tensile tests of individual MWCNT were performed with a nanomanipulator inside a scanning electron microscope (SEM). Individual MWCNT was picked up by pushing up half of a copper transmission electron microscope (TEM) grid to the MWCNT forest (Fig. 1). The both side of the MWCNT was fixed to a cantilever and the TEM grid (Fig. 2), and then the cantilever was moved backward during tensile test. In the result, average tensile strength and specific tensile strength were 22.0 GPa and 10.1 GPa/g/cm³, respectively. The specific strength ratio of fiber to individual MWCNT was 7.3%. Hence, the reason for low strength of MWCNT fiber is due to not the low strength of individual MWCNT but the slippage between individual MWCNTs and/or the condition for spinning fiber.

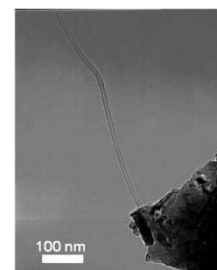


Fig.1 TEM image of individual MWCNT.

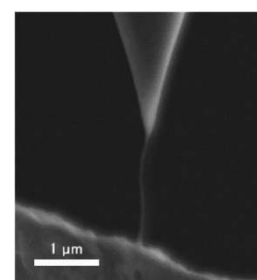


Fig.2 SEM photograph of individual MWCNT between cantilever and TEM grid.

[1] S. L. Mielke *et al.* Chem. Phys. Lett. **390**, 413-420 (2004).

[2] B. Peng *et al.* Nat. Nanotech. **3**, 626-631 (2008).

[3] M. Zhang *et al.* Science **306**, 1358-1361 (2004).

Corresponding Author: Y. Sato

Tel: +81-22-795-3215, Fax: +81-22-795-3215

E-mail: hige@ncsimd.kankyo.tohoku.ac.jp

Bending Properties of Single-Walled Carbon Nanotube Film Transistors

○Hiroki Hamahata¹, Yuki Nobusa¹, Yohei Yomogida¹, Kazuhiro Yanagi²,
Yoshihiro Iwasa³ and Taishi Takenobu¹

¹*Department of Applied Physics, Waseda University, Shinjuku 169-8555, Japan*

²*Department of Physics, Tokyo Metropolitan University, Hachioji 192-0397, Japan*

³*QPEC, School of Engineering, The University of Tokyo, Bunkyo 113-8656, Japan*

The recent technique for the separation of metallic and semiconducting SWCNTs opened a new route to high-performance SWCNT TFTs without the effect of metallic nanotubes [1,2]. However, the trade-off behavior between carrier mobility and on/off ratio was still a big open question. Very recently, we found clear answer for this longstanding issue, and realized very high-performance transistors with mobility of more than $100 \text{ cm}^2/\text{Vs}$ and on/off ratio of 10^4 - 10^5 using one of the solid electrolytes, ion gel [3]. For practical applications in flexible electronics, the co-existence of high performance and excellent flexibility is strongly required. Importantly, because both SWCNT high-density film and ion gel seem to be highly flexible materials, the obtained high-performance SWCNT transistors might have enough durability against extreme flexure strain. Therefore, in this study, we fabricated flexible SWCNT transistors using ion gel, and investigated the flexibility of these devices. Moreover, we also tested stretchability for same transistors on PDMS substrate.

We fabricated ion-gel gated SWCNT film transistors on flexible kapton film and realized high on/off ratio of 10^4 . We have tested bending durability of this device (composed of Au electrode, ion gel and semiconducting SWCNT film) up to bending angle of 180 degree (mountain and valley fold for tension and compression of SWCNT film, respectively, as shown in Fig.1) and any degradation was not observed. During the bending test, both on/off ratio and mobility of SWCNT ion-gel transistor were almost constant, and transistor kept on/off ratio of 10^4 and mobility of $100 \text{ cm}^2/\text{Vs}$ even at 180 degree. Under the angle of 180 degree, the directly measured curvature radius of SWCNT film was $270 \mu\text{m}$ for tension and $400 \mu\text{m}$ for compression. For the stretching test as shown in Fig.2, no degradation was observed by 14 % of strain. These results obviously show the ultra-high flexibility of ionic-gel gated SWCNT transistors and open the route to bendable and stretchable electronics based on SWCNT thick film and ion gel.

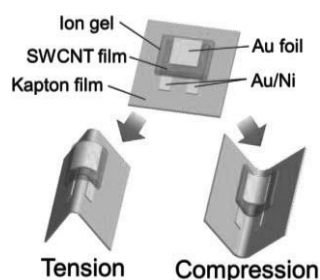


Fig.1 Schematic of bending device

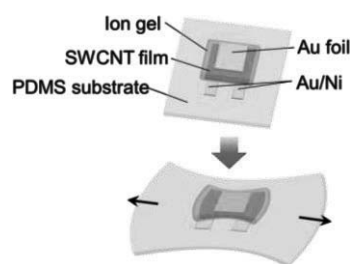


Fig.2 Schematic of stretching device

[1] M.S. Arnold *et al.* Nat. Nanotechnol. **1**, 60 (2006).

[2] K. Yanagi *et al.* Appl. Phys. Express. **1**, 034003 (2008).

[3] Y. Yomogida *et al.* The 42nd FNTGraphene General Symposium.

Corresponding Author: Taishi Takenobu

TEL/FAX: +03-5286-2981,

E-mail: takenobu@waseda.jp

High-performance, flexible carbon nanotube transparent conductive films of double layered structure

○Norihiro Fukaya¹, Yusuke Kataoka², Dong Young Kim^{2,3}, Shigeru Kishimoto¹,
Takashi Mizutani¹, Suguru Noda^{2,3}, and Yutaka Ohno¹

¹ Department of Quantum Engineering, Nagoya University, Nagoya 464-8603, Japan

² Department of Chemical System Engineering, The University of Tokyo, Tokyo 113-8656, Japan

³ Department Applied Chemistry, Waseda University, Tokyo 169-8555, Japan

Carbon nanotubes (CNTs) are quite promising material for transparent conductive films (TCFs) without resource problems because of various advantages such as good flexibility, and chemical stability, less haze, and so on. However, the resistance of CNT TCFs are still higher than other TCFs. In this study, we propose a novel CNT TCFs with double layered structure to reduce the sheet resistance. The double layered structure consists of a uniform layer and a grid layer of single-walled CNTs.

We fabricated the double layered CNT TCFs by utilizing the dry transfer technique based on floating-catalyst chemical vapor deposition technique (FC-CVD)¹. CNTs grown by FC-CVD were collect with a membrane filter and transferred on a polyethylenephthalate film with thickness of 100μm. For the grid formation, we used a membrane filter on which a photoresist layer was patterned as a grid. The patterned membrane filter was able to be used multiple times for the filtration and transfer process. After transferring both layers, the densification of CNTs with isopropanol and the chemical doping with nitric acid were carried out.

Figure 1 shows the transmittance at a wavelength of 550 nm versus sheet resistance. The closed and open circles represent CNT TCFs with and without the grid structured layer, respectively. The solid line is the fitted data using an equation², $T = \exp(-\alpha\rho/R)$, where α and ρ are an absorption coefficient and resistivity of CNT film, showing a tradeoff between the transmittance and sheet resistance determined by the material. By adding the grid structured layer, the performance of CNT TCFs were improved over the tradeoff curve. The sheet resistance at a transmittance of 80 % was reduced by 46 % from 95 Ω/sq. to 53 Ω/sq. This value is among the best data of CNT TCFs.

Acknowledgment: This work was supported by JST/ALCA.

[1] A. Moisala *et al.*, Chem. Eng. Science **61**, 4393 (2006).

[2] A. Kaskela *et al.*, Nano Lett. **10**, 4349 (2010).

Corresponding Author: Y. Ohno

Tel: +81-52-789-5387, Fax: +81-52-789-5387,

E-mail: yohno@nuee.nagoya-u.ac.jp

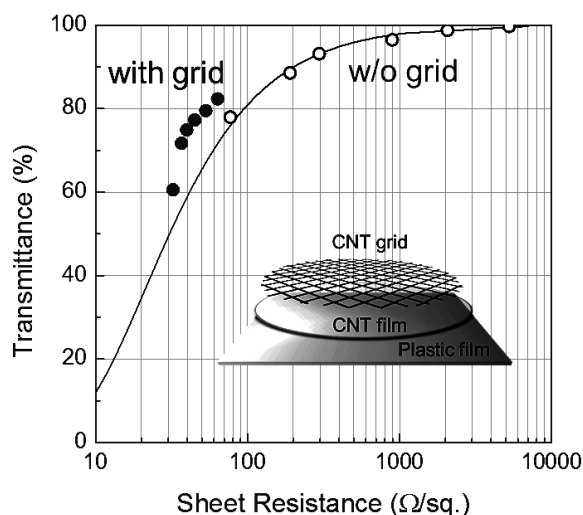


Fig.1 Transmittance versus sheet resistance for CNT TCF without (open circles) and with (closed circles) a grid structured layer.
Insert: Schematic of proposed double layered CNT TCF.

Evaluation of the contact resistivity at CNT/SiC interface using conductive AFM

○Megumi Shibuya¹, Masafumi Inaba¹, Kazuyoshi Oohara¹, Takumi Ochiai¹, Yoshiho Masuda², Atsushi Hiraiwa¹, Michiko Kusunoki², Hiroshi Kawarada¹

¹*School of Science and Engineering, Waseda University, Tokyo 169-8555, Japan*
²*Eco Topia Science Institute, Nagoya University, Aichi 464-8603, Japan*

1. Introduction

CNT synthesized with SiC surface decomposition method (CNT on SiC)^{[1][2]} exhibits the most densely packed CNT forest ($\sim 10^{13}$ cm⁻²) and is suitable for electrodes with high current density durability. CNTs can be important material for SiC, promising materials of power semiconductors, in cooperation with its high thermal conductivity and heat resistance. It is necessary for application as electrodes to evaluate the contact resistivity, we have revealed that CNT-metal contact resistivity is lower than $\sim 3 \times 10^{-9}$ Ωcm^2 ^[3]. In this study, we estimated the contact resistivity at CNT/SiC interface.

2. Lateral conduction blocking by focused ion beam (FIB)

CNT on SiC is synthesized on the C-face (000 $\bar{1}$) of on-axis n-type 4H- or 6H-SiC substrate (Nitrogen donor density: $\sim N_D \sim 10^{18}$ cm⁻³ and 10^{19} cm⁻³) with SiC surface decomposition method. In general, vertical conduction (parallel to CNT axis) is dominant comparing to lateral conduction. As shown in Fig.1 however, lateral conduction also coexists in the CNT on SiC because of its high tubedensity ($\sim 10^{13}$ cm⁻²). For confining lateral conduction to a certain area to estimate the contact resistivity at CNT/SiC interface, conducting islands were electrically isolated by FIB (Fig.2). Current-voltage property was measured by conductive AFM.

3. Estimation of the contact resistivity at CNT/SiC interface

CNT-AFM probe contact area is fixed, so CNT-AFM probe contact resistance is constant. Changing the island size to restrict conduction area makes it possible to estimate CNT/SiC interface contact resistance. Fig.3 shows the relationship between series resistance of CNT and area of islands within minimal isolated areas. Slope of approximate line at each CNT length represents the sum of the contact resistivity at CNT/SiC interface and the product of CNT length and resistivity component ($\rho_C^{CNT-SiC} + \rho_C^{CNT} \cdot l^{CNT}$). The intercept of that line corresponds to $\rho_C^{CNT-probe}$, the contact resistivity of probe-CNT, and it is the same order as our previous work^[3]. The contact resistivities at CNT/SiC interface are $\sim 10^{-2}$ Ωcm^2 and $\sim 10^{-3}$ Ωcm^2 at N_D of 10^{18} and 10^{19} cm⁻³, respectively. The corresponding Schottky barrier heights at CNT/SiC interface are ~ 0.5 eV and ~ 0.45 eV.

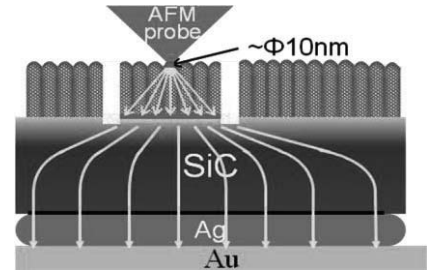


Fig.1 Schematic image of current paths at CNT/SiC system.

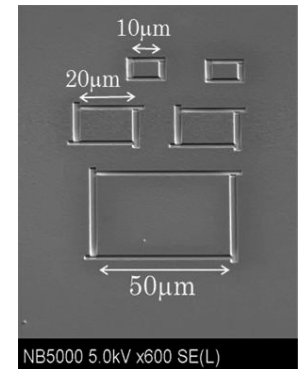


Fig.2 Islands formed by FIB to limit lateral conduction within them.

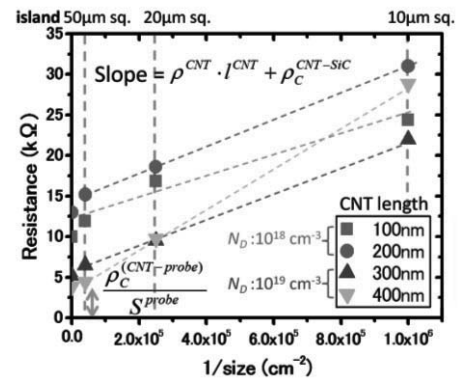


Fig.3 Resistance of CNT versus size of islands

[1] M. Kusunoki *et al.*, *Appl. Phys. Lett.* 77, 531 (2000)

[3] M. Inaba, H. Kawarada *et al.*, submitted

[2] M. Kusunoki *et al.*, *Appl. Phys. Lett.* 87, 103105 (2005)

Corresponding Author: M. Shibuya/Tel: 03-5286-3391, Fax: 03-5286-3391,

E-mail: seal_1030@fuji.waseda.jp

High-mobility carbon nanotube thin-film transistors fabricated on transparent plastic film by flexographic printing technique

○Kentarō Higuchi¹, Yuta Nakajima², Takuya Tomura², Masafumi Takesue², Shigeru Kishimoto¹, Takashi Mizutani¹, Katsuhiko Hata² and Yutaka Ohno¹

¹ Department of Quantum Engineering, Nagoya University, Nagoya 464-8603, Japan

² Research and Development Center, Bando Chemical Industries, LTD., Kobe 650-0047, Japan

Among many kinds of thin film transistors, carbon nanotube thin-film transistors (CNT-TFTs) have attractive features such as high mobility, flexibility, and transparency. In the previous work, we realized high performance CNT TFTs and functional integrated circuits (ICs) on a transparent plastic substrate by the simple gas-phase filtration and transfer process [1]. In this work, we introduce flexographic printing technique in the fabrication process of CNT TFTs. The devices are fabricated by fully lithography free and ambient pressure processes.

We fabricated bottom-gate-type CNT TFTs on a polyethylene naphthalate (PEN) film with the flexographic printing technique, which is a kind of high-speed typographic prints with a flexible relief plate made of photopolymer. The inks of silver nanoparticles and polyimide were respectively used for the electrodes and insulator. First, the gate electrode and insulator were printed by a flexographic printer. A carbon nanotube thin film grown by the floating-catalyst CVD was transferred as our previous work [1]. Then, the source and drain electrodes were printed. After printing the resist material, CNTs outside the channel region were etched by the ambient pressure plasma with O₂.

Figure 1 shows (a) an array of CNT TFTs fabricated on a 15-cm-square PEN film, (b) optical micrograph of a CNT TFT, and (c) I_D - V_{GS} characteristic of a device. The channel length and channel width were 115 μm and 130 μm , respectively. The device showed high mobility of 157 cm^2/Vs for the rigorous model (112 cm^2/Vs for parallel plate model) with on/off ratio of about 10^4 . The obtained mobility is the highest value for printed TFTs to our knowledge.

This work was partially supported by '08 NEDO Grant, R&D promotion scheme funding international joint research promoted by NICT, ALCA-JST, and Grant-in-Aid of MEXT.

[1] D.-M. Sun, *et al.* Nature Nanotech. **6**, 156 (2011).
Corresponding Author: Y. Ohno
Tel: +81-52-789-5387, Fax: +81-52-789-5387,
E-mail: yohno@nuee.nagoya-u.ac.jp

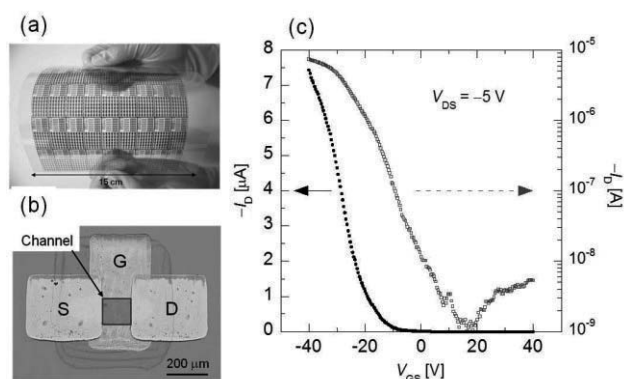


Fig. 1 (a) CNT TFT array printed on 15-cm-square PEN film. (b) optical micrograph and (c) I_D - V_{GS} characteristic of CNT TFT.

Effect of gas atmosphere on the photovoltaic characteristics of semiconducting single-walled carbon nanotubes/Si heterojunction photovoltaic cells

○Mao Shoji^{1,3}, Atsushi Nakano² and Hironori Ogata^{1,2,3}

¹Graduate School of Engineering, Hosei University, Koganei, 184-8584, Japan

²Department of Faculty of Bioscience and Applied Chemistry, Hosei University, Koganei, 184-8584, Japan

³Research Center for Micro-Nano Technology, Hosei University, Koganei, 184-0003, Japan

Single-walled carbon nanotubes (SWNTs) are expected to the application to various kinds of the electronic devices, because the high carrier mobility of the SWNTs. Especially, The use of semiconducting SWNTs (S-SWNTs) in photovoltaic applications is attractive because the optical bandgap of S-SWNTs can be varied by controlling the nanotube diameter.¹⁾ S-SWNTs are reported to show unipolar p-type behavior under ambient conditions. Various chemical doping have been reported to convert from p-type to n-type.²⁾ In this study, we report the effects of the electronic energy level evolution of S-SWNTs films by exposed to air or oxygen on the photovoltaic characteristics of both p-type SWNTs/n-Si and chemically doped (n-type) SWNTs/p-Si heterojunction photovoltaic cells.

The SWNTs (CoMoCAT method, 0.8 ± 0.1 nm in diameter) dispersed in 1,2-dichlorobenzene at 0.5 mg/mL by ultrasonication and SWNTs thin film was fabricated using airbrush on the Si substrate. N-type doping of the S-SWNTs was performed by dropped reduced benzyl viologen (BV) solution (5 mM) on the SWNTs thin films. The schematic of SWNTs/Si device is showed in Figure 1. The current density-voltage (J - V) characteristics were measured in the dark and under light (AM1.5G, 100 mW/cm^2) condition in the vacuum (44 Pa), oxygen (760 Torr) and air (ambient atmospheric pressure) conditions.

Figure 2 shows the time dependences of PCE for p-type (undoped) SWNTs/n-Si or viologen doped-SWNTs/p-Si devices under each gas atmosphere. The value of power conversion efficiency (PCE) increases gradually for the p-type SWNTs/n-Si device. However, that decreases for viologen doped-SWNTs/p-Si device by exposed to oxygen. The detailed results will be presented.

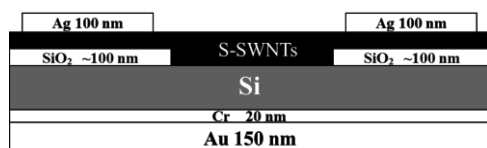


Figure 1 The structure of SWNTs/Si device.

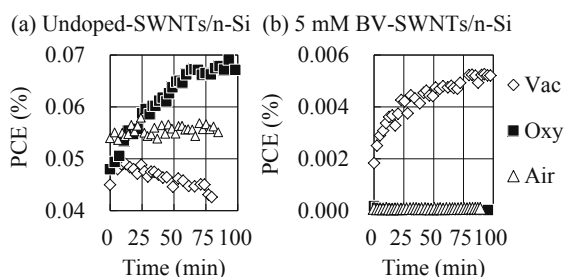


Figure 2 Time dependences of PCE of (a) p-type SWNTs/n-Si or (b) viologen doped SWNTs/p-Si devices in each gas atmosphere.

1) P.-L. Ong, *et al.*, *Nanotechnology* **21** (2010) 105203.

2) S. M. Kim *et al.*, *J. Am. Chem. Soc.* **131** (2009) 327.

Corresponding Author: Hironori Ogata,

Tel: +81-42-387-6229, Fax: +81-42-387-6229, E-mail: hogata@hosei.ac.jp

Effect of oxidized Al support property for millimeter-scale SWCNT growth

Kei Hasegawa and Suguru Noda

Department of Applied Chemistry, Waseda University, Tokyo 169-8555, Japan

After millimeter-scale growth of single-walled carbon nanotubes (SWCNTs) in 10 min was realized by adding small amount of water to $C_2H_4/H_2/He$ during chemical vapor deposition (CVD) [1], many groups have studied this growth method and realized that alumina support is one of the most important keys for the tall CNT forests. By using our combinatorial catalyst library, we found that Al-Si-O support prepared by annealing of aluminum on SiO_2 is effective for millimeter-scale growth of SWCNTs [2]. This time, we examined the effect of Al-Si-O support property for SWCNT growth.

Gradient thickness profiles of Al (50-2.0 nm) and Fe (10-0.30 nm) were orthogonally prepared on an SiO_2 substrate and CVD was carried out on it. The sample was set in a tubular CVD reactor, heated to and kept at 800 °C for 5 min in 5 vol% $H_2/50$ ppmv H_2O/Ar , and then CVD was carried out by switching the gas to 0.30 vol% $C_2H_2/50$ ppmv H_2O/Ar under ambient pressure. Samples were monitored in real-time by a digital camera [3] and CVD was continued until CNTs stopped growing.

Figure 1 shows photographs of CNTs grown on the binary combinatorial catalyst library. CNT height largely depended on both Al and Fe thicknesses. When Al thickness was between 7-12 nm, millimeter-tall SWCNTs were grown from thin Fe (below 1.0 nm). For both thinner and thicker Al layer than this window, CNTs got shorter and the threshold Fe thickness for tall CNTs got larger. Because CNTs get multi-wall for large Fe thickness, this result shows that millimeter-tall SWCNTs grew only in a limited window for the Al thickness. Some properties of Al-Si-O support, which depend on Al thickness, largely affect the CNT growth. During annealing process, redox reaction occurs between Al and SiO_2 , which results in the mixed oxide [4]. The formation process and property of oxide support depends on Al thickness and the surface composition and density of the oxide support will influence the Ostwald ripening and/or sub-surface diffusion of Fe particles and CNT growth. Effect of Al-Si-O surface structure for Fe catalyst and CNT growth will be discussed.

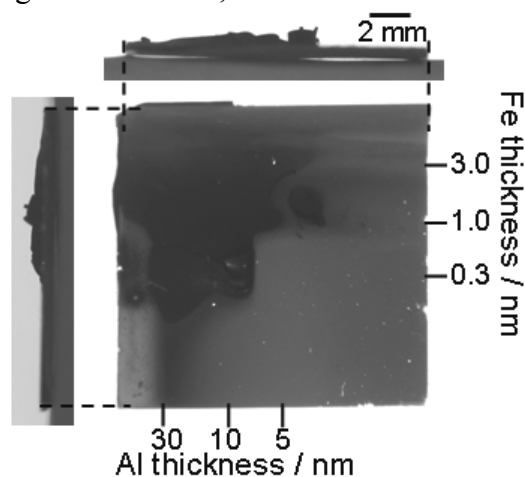


Fig. 1 Top- and side-view photos of CNTs grown on a combinatorial catalyst library.

[1] K. Hata, et al., *Science* **306**, 1362 (2004). [2] S. Noda, et al., *Jpn. J. Appl. Phys.* **46**, L399 (2007). [3] K. Hasegawa, et al., *Jpn. J. Appl. Phys.* **49**, 085104 (2010). [4] K. Hasegawa and S. Noda, *ACS Nano* **2011**, 5, 975–984 (2011).

Corresponding Author: Suguru Noda, TEL/FAX: +81-3-5286-2769, E-mail: noda@waseda.jp

CNT Synthesis by Laser Ablation Method Using Carbon and Nickel Double Target

○Koji Ishii¹, Nobuyuki Iwata², Hiroshi Yamamoto² and Hirofumi Yajima¹

¹ Department of Applied Chemistry, Faculty of Science, Tokyo University of Science, 1-3 Kagurazaka, Shinjyuku-ku, Tokyo 162-0826, Japan

² Department of Electronics & Computer Science, College of Science & Technology, Nihon University, 7-24-1 Narashinodai, Funabashi, Chiba 274-8501, Japan

Carbon nanotubes (CNTs) have potential for application to nano-scale devices because of the physical and chemical properties. Practically, a large amount of high quality CNTs are required for application. Conventional laser ablation method has a disadvantage of a low synthesis rate because of the molar ratio of carbon to catalyst at the target surface. The ratio gradually changes as proceeding the synthesis¹⁾. We propose the novel laser ablation method, called double laser ablation (DLA) method, as shown in Fig.1. In the DLA method, two ablated plasma plumes, including both of carbon and catalytic metal particles, are merged to be introduced into the furnace to synthesize CNTs. In this work, single walled carbon nanotubes (SWNTs) were synthesized by the DLA apparatus with two separated double target, graphite target and Ni catalyst target. The quartz tube was filled with 66.6kPa argon gas and the flow was 100ccm. The electric heater was controlled up to 1000°C at the rate of 10°C/min. The second harmonics of YAG laser pulse was focused on the targets and synthesized for 30 minutes.

Figure 2 shows the typical Raman spectrum of obtained deposits with 532nm excitation laser. The spectrum revealed G-band at 1582 cm⁻¹ and D-band at 1350cm⁻¹, respectively. However radial breathing mode (RBM) was not detected. Figure 3 shows the image of transmission electron microscopy (TEM). It was demonstrated that tubular materials was synthesized by the DLA apparatus.

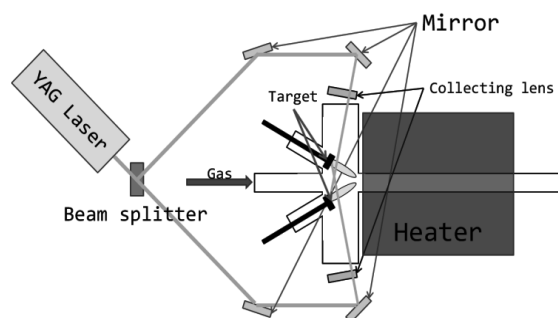


Fig.1. The schematic DLA apparatus

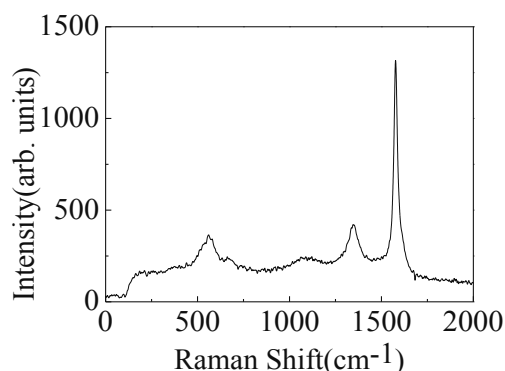


Fig.2. The typical Raman spectrum of deposits obtained by the DLA method with excitation wavelength of 532nm.

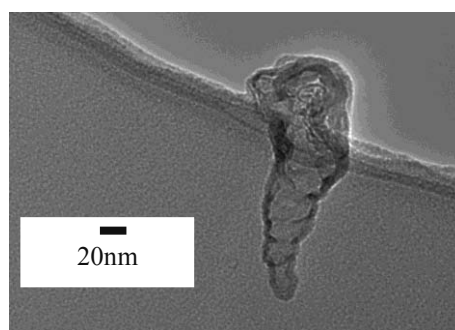


Fig.3. The TEM image of sample synthesized by the DLA method.

[1] M. Yudasaka, T. Komatsu, T. Ichihashi, and S. Iijima, *chem phys lett* **278**(1997)102-106.
Tel and Fax : +81-469-5457
E-mail : chem_spdf_orbital@yahoo.co.jp

Solubilization of single-walled carbon nanotubes using a flavin derivative in organic solvents

○Yuichi Kato¹, Yasuro Niidome^{1,2}, Naotoshi Nakashima^{1,2,3}

¹ Department of Applied Chemistry, Kyushu University, Fukuoka 819-0395, Japan

² WPI Research Center I2CNER, Kyushu University, Fukuoka 819-0395, Japan

³ JST-CREST, Chiyoda-ku, Tokyo 102-0075, Japan

We synthesized a flavin derivative as a solubilizer of single-walled carbon nanotubes (SWNT), and revealed that the compound showed a unique SWNT chiral selective dissolution behavior.

Due to the difficulty in the synthesis of single-walled carbon nanotubes (SWNTs) with a specific chiral indices (n,m), SWNT chirality sorting has been an anticipated technique for realizing practical applications of SWNTs, especially in the field of nano-electronic devices. Recently, several papers describing the separation of the chiral mixtures of semiconducting/metallic SWNTs.^[1] One of interesting chirality-sorting method is a selective extraction using polyfluorenes (PFOs) with long alkyl-chains and their derivatives which are known to dissolve only semiconducting SWNTs.^[2] This method is simple and powerful for the chirality-sorting; however, the removal of the PFO in the PFH/SWNT hybrids is difficult. The development of a method that allows easy removal of the solubilizers from the hybrids is thus required.

10-Dodecyl-7,8-dimethyl-10H-benzo[g]pteridine-2,4-dione (Fig. 1) is a small molecule that solubilizes SWNTs in organic solvents such as acetone or toluene.^[3] Here, we report that the compound shows a unique SWNT chiral selective dissolution behavior, which was revealed by vis-near IR absorption, photoluminescence, and Raman spectroscopies. Removal of the flavin from the nanotube hybrid will also be reported at the meeting.

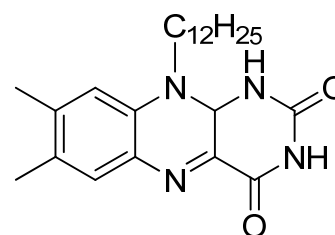


Fig. 1 Chemical structure of 10-Dodecyl-7,8-dimethyl-10H-benzo[g]pteridine-2,4-dione.

[1] M. C. Hersam, *Nature Nanotech.* **3**, 387–94 (2008).

[2] a) F. Chen, B. Wang, Y. Chen, L.-J. Li, *Nano Lett.* **7**, 3013-3017 (2007).

b) H. Ozawa, T. Fujigaya, Y. Niidome, N. Hotta, M. Fujiki, N. Nakashima, *J. Am. Chem. Soc.* **133**, 2651–2657 (2011).

[3] S. Ju, W. P. Kopcha, F. Papadimitrakopoulos, *Science* **323**, 1319–23 (2009).

Corresponding Author: N. Nakashima

Tel: +81-92-802-2840, Fax: +81-92-802-2840

E-mail: nakashima-tcm@mail.cstm.kyushu-u.ac.jp

SWNT growth from Pt catalysts on Al₂O_x buffer layer by Alcohol Gas Source Method in High Vacuum

○Naoya Fukuoka, Hiroki Kondo, Yuya Sawaki, Ranajit Ghosh, Shigeoya Naritsuka,
Takahiro Maruyama

Department of Materials Science and Engineering, Meijo University, Nagoya 468-8502, Japan

Single-walled carbon nanotubes (SWNTs) have been anticipated for applications in a lot of future nanodevices. To fabricate SWNT devices in a conventional LSI process, it is important to obtain SWNTs having homogeneous structures in high yield. To increase the SWNT yield, Al₂O_x have been widely used as buffer layers for transition metal catalysts in the CVD growth. Recently, we reported SWNTs having a narrow diameter distribution could be obtained from Pt catalysts on SiO₂/Si substrates. However, the Al₂O_x buffer layers have never been utilized for Pt. In this study, we carried out SWNT growth on Pt catalysts on Al₂O_x and investigated the effects of Al₂O_x on Pt catalysts.

Al₂O_x buffer layers were formed on SiO₂/Si substrates by oxidation of Al thin layers (3-30 nm). After deposition of Pt catalysts (0.2 nm) on the Al₂O_x using a pulsed arc plasma gun, the SWNT growth was carried out using alcohol gas source method in a high vacuum [1, 2]. The growth temperature was 700°C, and the ethanol pressure was 1×10⁻³ Pa. The grown SWNTs were characterized by SEM and Raman spectroscopy.

Figure 1 shows the Raman spectra of SWNTs grown from Pt catalysts on SiO₂/Si substrates and Al₂O_x buffer layers (Al thickness: 3nm). On the Al₂O_x buffer layer, the G band intensity was small, compared to that on the SiO₂/Si substrate, indicating that the SWNT yield was reduced on the Al₂O_x buffer layer. The Raman spectra in the RBM region shows that Raman shifts of SWNTs on the Al₂O_x were smaller than those on SiO₂/Si, suggesting that the diameters of SWNTs on the Al₂O_x were smaller than those on the SiO₂/Si. These results indicate that the effects of Al₂O_x buffer layers on Pt catalysts were fairly different from those on transition metal catalysts.

This work was partially supported by the Japan Society for the Promotion of Science (JSPS), Grant-in-aid for Scientific Research (c) 21510119 and the Instrument Center of the Institute for Molecular Science (IMS).

References

- [1] T. Maruyama et al., *J. Nanosci. Nanotechnol.* **10** (2010) 1.
[2] T. Maruyama et al. *Mater. Express* **1** (2011) 267.

Corresponding author: Takahiro Maruyama

Phone: +81-52-838-2386, Fax: +81-52-832-1172

E-mail: takamaru@meijo-u.ac.jp

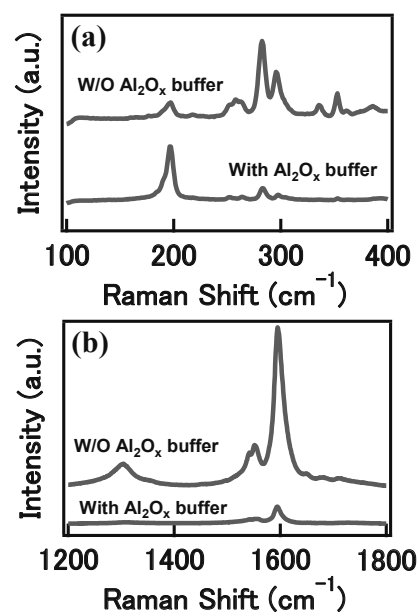


Fig. 1 Raman spectra of (a) RBM region and (b) high frequency region for SWNTs grown from Pt catalyst on Al₂O_x buffer layers and SiO₂/Si substrates.

Low temperature growth of dense carbon nanotube arrays on conductive underlayers

○Nuri Na^{1,2}, Yeong-Gi So³, Yuichi Ikuhara³ and Suguru Noda^{2,4,*}

¹ Department of Chemical System Engineering, The University of Tokyo, Japan

² Department of Applied Chemistry, Waseda University, Tokyo 169-8555, Japan

³ Institute of Engineering Innovation, The University of Tokyo, Japan

⁴ PRESTO, JST, Japan

Carbon nanotubes (CNTs) have been studied as a candidate for via interconnects in future large-scale integrated circuits (LSIs) because they have attractive electrical and thermal properties [1]. Rapid growth of millimeter-tall CNT arrays has been realized by chemical vapor deposition (CVD), however, such growth is achieved on insulating underlayer at high temperatures (~ 800 °C) with a porosity $> 90\%$ in CNT arrays. Dense CNT growth at 1×10^{12} cm⁻² on conductive underlayer at 450 °C [2] and at 15×10^{12} cm⁻² on insulating underlayer at 700 °C [3] are reported recently, which are not satisfactory for practical application yet.

In this work, we prepared Ni particles densely on conductive TiN layers on SiO₂/Si by sputter-deposition through their nucleation and growth and by stopping deposition prior to their percolation. We obtained a particulate structure as deposited by depositing nominally 0.6-nm-thick Ni at 400 °C slowly (8.1 pm/s) under a substrate bias of -20 V, which kept a particulate structure with a density as high as $\sim 2.8 \times 10^{12}$ cm⁻² after annealing in H₂/Ar at 400 °C (Fig. 1). We then performed CVD at 400 °C by feeding C₂H₂ at a pressure as low as 1-10 mTorr so as not to kill the catalyst and obtained CNT arrays, whose density proved as high as 1.1 g cm⁻³ by energy dispersive X-ray analysis by scanning electron microscopy (SEM). The CNT films were transferred to SiO₂/Si or transmission electron microscope (TEM) grids by etching SiO₂ layers and analyzed by atomic force microscopy (AFM) and high resolution transmission electron microscopy (HRTEM). The number density of CNTs and CNT walls were as high as 1.5×10^{12} cm⁻² and 12×10^{12} cm⁻², respectively (Fig. 2).

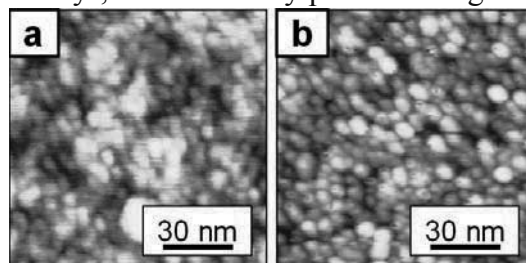


Fig. 1. AFM images of Ni particles. (a) As deposited and (b) after annealing.

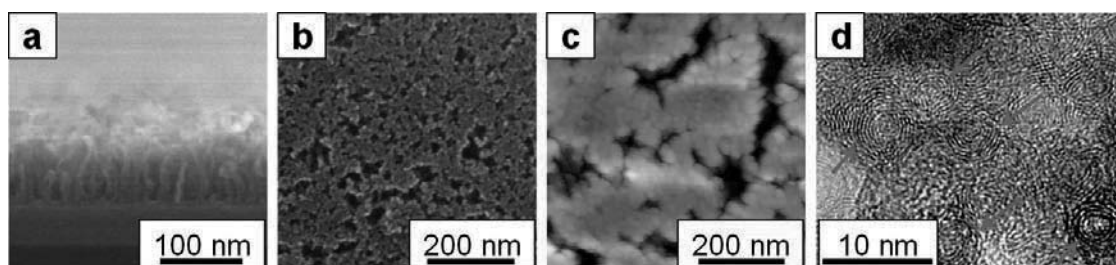


Fig. 2. (a) Cross-sectional SEM, bottom-view SEM (b) and AFM (c), and (d) plan-view TEM of CNT arrays.

[1] Y. Awano, et al., Phys. Stat. Sol. A 203, 3611 (2006).

[2] Y. Yamazaki, et al., Appl. Phys. Express 3, 055002 (2010).

[3] G. Zhong, et al., ACS Nano 4, 2893 (2012).

*Corresponding Author: Suguru Noda, Tel&Fax: +81-3-5286-2769, E-mail: noda@waseda.jp

Selective Removal of Metallic Single-Walled Carbon Nanotubes Utilizing Thermal Lithography of Molecular Glass Thin Films

○Keigo Otsuka, Taiki Inoue, Daisuke Hasegawa, Shohei Chiashi, Shigeo Maruyama

Department of Mechanical Engineering, The University of Tokyo, 7-3-1 Hongo, Bunkyo-ku, Tokyo, Japan

Single-walled carbon nanotubes (SWNTs) are a promising material for future electronics such as field effect transistors (FETs) due to their extraordinary electrical properties. For the realization of practical SWNT devices, it is one of the most important demands to obtain aligned arrays composed only of semiconducting SWNTs. Recently, selective etching of metallic SWNTs using a molecular glass film was reported [1]. The method could be applicable to the large-scale fabrication because it enables removal of whole length of metallic SWNTs in contrast to partial cutting of metallic SWNTs by electrical breakdown [2]. In this study, we attempted to remove metallic SWNTs using the method and considered its mechanism in order for improved processing.

Horizontally-aligned SWNTs grown on quartz substrates were transferred onto silicon substrates and used as channels of back-gated FETs. An SEM image of a fabricated FET device is shown in Fig. 1 (a). The current-voltage (I_D - V_{GS}) characteristic of the device (Fig. 2) shows that on/off ratio is 2.6, and this indicates the existence of metallic SWNTs along with semiconducting SWNTs. A thin film of molecular glass was fabricated on the FET by spin-coating, and a drain voltage of -4 V and a gate voltage of +10 V were applied to the FET for about 35 hours. After the application of the voltage, some trench structures along SWNTs were observed by AFM on the molecular glass film (Fig. 1(b)), which means that some of SWNTs originally embedded in the molecular glass were exposed. After oxygen plasma etching of the exposed SWNTs and dissolution of the molecular glass film (Fig. 1 (c)), the device shows on/off ratio of 34.5 (Fig. 2). The increase in on/off ratio indicates that metallic SWNTs were preferentially removed. The viscosity of the molecular glass around metallic SWNTs was considered to decrease with a temperature increase resulting from Joule heating of metallic SWNTs, and the trench structures were formed along metallic SWNTs.

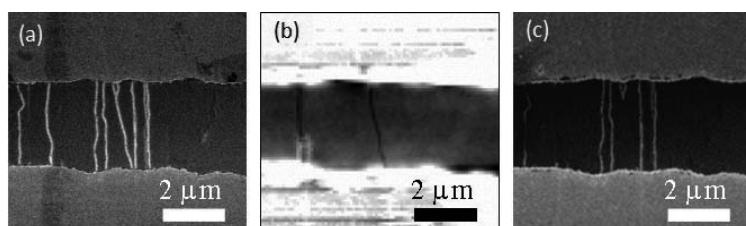


Fig. 1 (a) SEM image of an as-fabricated FET. (b) AFM image of the molecular glass film-coated FET after voltage application. (c) SEM image of the FET after oxygen plasma etching and dissolution of the molecular glass film.

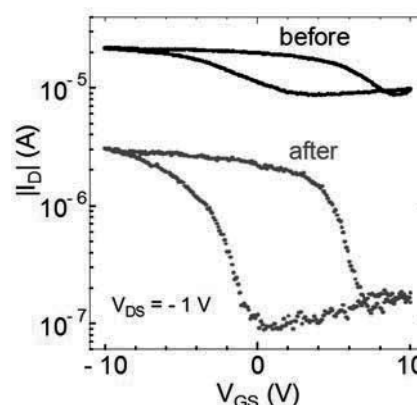


Fig. 2 Current-voltage characteristics of the FET before and after the treatment.

[1] J. Xiao *et al.* MRS Spring Meeting (2012).

[2] P. G. Collins *et al.* Science **292**, 706 (2001).

Corresponding Author: S. Maruyama

Tel: +81-3-5841-6421, Fax: +81-3-5800-6983

E-mail: maruyama@photon.t.u-tokyo.ac.jp

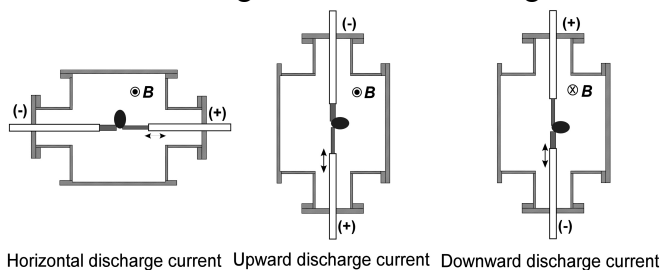
Effects of discharge current direction and magnetic field for the production of single-walled carbon nanotubes in the arc discharge method

○Mohammad Jellur Rahman¹, Tetsu Mieno²

¹ Graduate School of Science and Technology, Shizuoka University

² Department of Physics, Shizuoka University, Shizuoka 422-8529, Japan

Mass production of high-quality and diameter-controlled single-walled carbon nanotubes (SWNTs) are required to realize their various applications [1]. In the arc discharge method, SWNTs are produced in the hot He gas region near the arc plasma, where heat convection blows hot carbon species upward, and the reaction time is limited [2]. Therefore, if the discharge direction relative to gravity is changed, the production conditions of SWNTs in the hot gas region will be changed. When a magnetic field is applied perpendicular to the discharge current, the arc plasma jets out in the $\mathbf{J} \times \mathbf{B}$ direction and leads to the efficient production of SWNTs [2-4]. Therefore, SWNTs are synthesized by the arc discharge method in He gas where three directions of discharge current relative to gravity are selected. The soot production rate is larger for the upward discharge current. The qualities of the produced SWNTs for the three cases are almost the same. A steady magnetic field (3.0 mT), perpendicular to the discharge current direction ($\mathbf{J} \times \mathbf{B}$ arc discharge) increases the soot production rate for all the three discharge current directions. The estimated ratio of the number of SWNT bundles to the number of carbon particles is higher for the upward discharge current in the case of $B = 0$. This ratio increases significantly for the horizontal and downward discharge currents when a magnetic field is applied.



Horizontal discharge current Upward discharge current Downward discharge current
Fig. 1 Three discharge current directions and magnetic field.

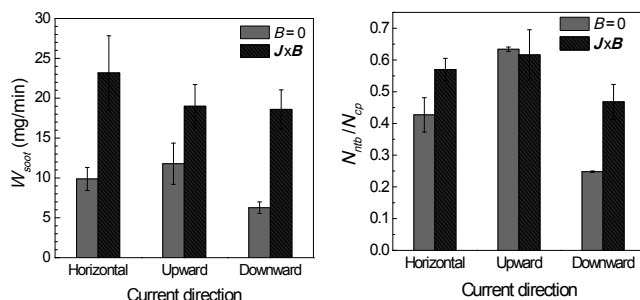


Fig. 2 Variation of the soot production rate, and nanotube bundles to carbon particles ratio in the three currents.

- [1] T. Yamamoto *et al.* in Carbon Nanotubes-Top. Appl. Phys., eds. A. Jorio, *et al.* (Springer, Berlin, 2008).
- [2] T. Mieno, *et al.* Jpn. J. Appl. Phys. **43**, L1527 (2004).
- [3] S. P. Doherty *et al.* Carbon **44**, 1511 (2006).
- [4] Y. Su *et al.* Carbon **50**, 2556 (2012).

Corresponding Author: T. Mieno, Tel. and Fax: + 81-54-238-4750, E-mail: sptmien@ipc.shizuoka.ac.jp

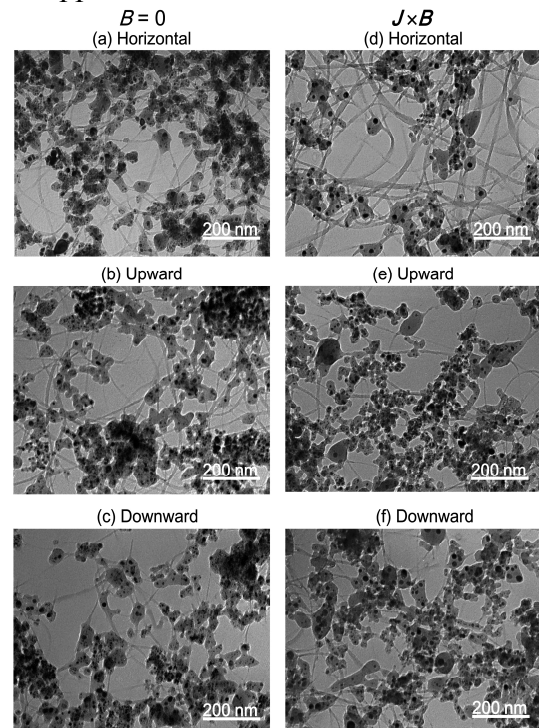


Fig. 3 TEM images of the soot for the $B = 0$ (a)-(c) and $\mathbf{J} \times \mathbf{B}$ (d)-(f) in the three discharge currents.

Chirality separation of metallic single-wall carbon nanotubes by gel column chromatography

○Takeshi Tanaka¹, Yasuko Urabe^{1,2} and Hiromichi Kataura^{1,2}

¹ *Nanosystem Research Institute, National Institute of Advanced Industrial Science and Technology (AIST), Tsukuba, Ibaraki 305-8562, Japan*

² *JST, CREST, Kawaguchi, Saitama, 332-0012, Japan*

As-produced single-wall carbon nanotubes (SWCNTs) contains various kind of structure (chirality). Recently we reported single chirality separation of semiconducting (S-) SWCNTs using dextran-based gel (Sephacryl S200) column chromatography [1]. In this separation, metallic (M-) SWCNTs were not adsorb to the gel and not separated each other. In this study we report chirality separation of metallic SWCNTs.

Proceeding chirality separation of M-SWCNTs, M/S separation of SWCNTs were conducted. HiPco-SWCNTs/0.5 % sodium dodecyl sulfate (SDS) aqueous solution were prepared by sonication and ultracentrifugation. The dispersion was applied to Sephacryl S200 column equilibrated with 0.5% SDS, and high-purity M-SWCNTs were obtained as unbound fraction (Fig. 1, bottom spectrum). The separated M-SWCNTs mixture were diluted twice with water and applied to long column (60 cm in length) packed with Sephacryl S200 equilibrated with 0.3% SDS. After flowing 0.3 % SDS, the concentration of elution solution changed to 0.4 and 0.5 SDS and 1% sodium cholate. From the optical adsorption spectra of eluted fractions (Fig. 1), clear difference of adsorption peaks were observed, indicating chirality separation of M-SWCNTs. The early and late eluted fractions tended to contain M-SWCNTs with optical absorption peaks of longer and shorter wavelengths, respectively. Detailed analyses containing the result of Raman spectroscopy will be presented.

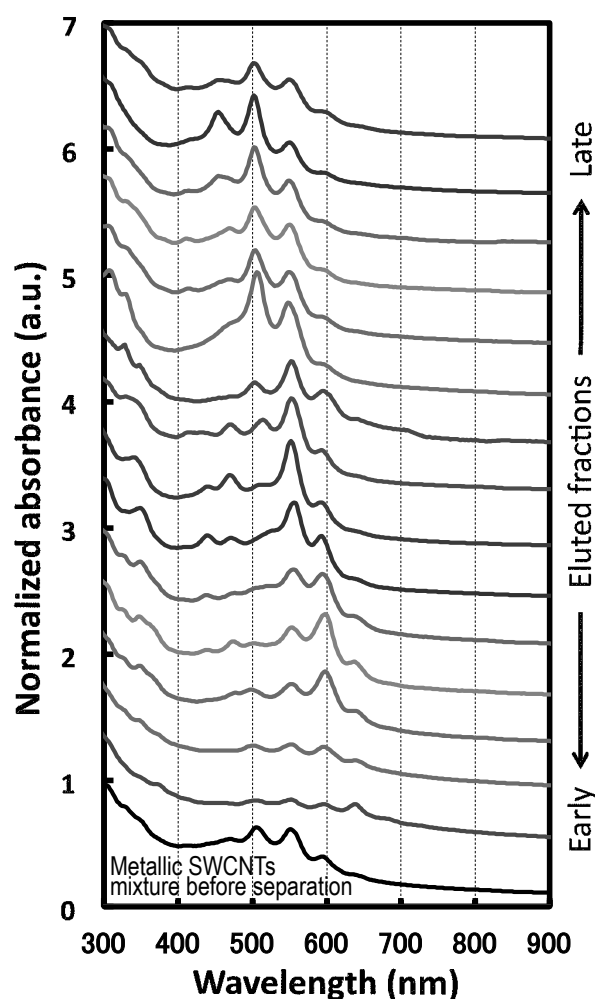


Fig. 1 Optical absorption spectra of chirality separated M-SWCNTs by Sephacryl S200 column (60 cm in length). The bottom spectrum is that of M-SWCNTs mixture before chirality separation.

References:

[1] H. Liu et al., *Nature commun.*, 2011, 2, 309

Corresponding Author: T. Tanaka

E-mail: tanaka-t@aist.go.jp

Encapsulation of superconductive metal carbide in the inner space of carbon nanotubes by template method

○Keita Kobayashi¹, Takeshi Saito^{2,3}, Masaharu Kiyomiya³, Hidehiro Yasuda¹

¹ *Research Center for Ultra-High Voltage Electron Microscopy, Osaka University, 7-1 Mihogaoka, Ibaraki, Osaka 567-0047, Japan*

² *Nanotube Research Center, National Institute of Advanced Industrial Science and Technology (AIST), Tsukuba 305-8565 Japan*

³ *Technology Research Association for Single Wall Carbon Nanotubes (TASC), Tsukuba305-8562, Japan*

The density of integrated circuits (ICs) should be increased for development of next-generation electric devices. However, the miniaturization of metal interconnections in ICs increases their risk of disconnection by electro migration [1]. Therefore, development of alternative materials to metal interconnections is crucial for producing ultra-fine wiring boards. Carbon nanotubes (CNTs) is expected as one of the candidates for the alternative materials due to their stability and structure [1]. Moreover, CNTs have been widely used as a template for producing one-dimensional nano-wires by encapsulating guest materials in their inner space [2]. Since wall of CNT prevents migration of the guest materials [3], it is expected to be applied to an useful ultra-fine conducting wire to develop further dense IC by encapsulation of good conductor in the inner space of CNT. Encapsulated superconductor materials in CNTs are particularly desirable, because they should produce high-efficiency ICs. However, fusion or vaporization of guest materials is necessary for encapsulation of the materials into inner space of CNT by the template method. Although the encapsulation of Pb (T_c : 7.2 K) and Sn (T_c : 3.7 K) in CNTs has been reported [4], any super conducting ceramics has not been encapsulated into CNTs by the method due to their higher melting point. The arc discharge method [5] and the laser vaporization method [6] have been used to synthesize multi-wall CNTs (MWCNTs) encapsulating refractory metals. However, these obtained products are not suitable for development of further dense IC because diameters of these MWCNT and guest materials are too large (>10 nm) for use as ultra-fine conducting wires. Therefore, development of novel method for encapsulating such refractory guest materials into CNTs is required.

Based on these backgrounds, we have tried to encapsulate superconductive guest materials with higher melting point to CNT having thinner diameter. Consequently, we developed a simple method for encapsulating niobium carbide (NbC; melting point: ~3000 K; T_c : 10.5 K) in the inner space of CNTs with diameter of 1-3 nm. In this presentation, we will report synthesis method of the NbC-encapsulated CNT and will outline their properties.

[1] in *Handbook of Carbon Nanotubes and Graphene*, The Fullerenes, Nanotubes and Graphene Research Society (Ed) (Corona Publishing, Tokyo, 2011).

[2] J. Sloan *et al.* *Inorg. Chim. Acta*, **330**, 1 (2002).

[3] K. Kobayashi *et al.* *Adv. Mater.* **22**, 3156 (2010).

[4] K. Kobayashi *et al.* *Small* **6**, 1279 (2010).

[5] A. Koshio, *J. Surf. Finish. Soc. Jpn.* **58**, 725 (2007).

[6] F. Kokai *et al.* *Appl. Phys. A* **97**, 55 (2009).

Corresponding Author: K. Kobayashi

Tel: +81-6-6879-7941, Fax: +81-6-6879-7942,

E-mail: kobayashi-z@uhvem.osaka-u.ac.jp

Energetics and Electronic Structures of C₆₀ Rolled in the Shortest Zigzag Carbon Nanotubes

○Shota Kigure and Susumu Okada

*Graduate School of Pure and Applied Sciences, University of Tsukuba,
1-1-1 Tennodai, Tsukuba, Ibaraki 305-8571, Japan*

Carbon nanotubes inherently possess nanometer scale space inside their one-dimensional covalent network. Such space can accommodate foreign atoms and molecules resulting in interesting hybrid structures with mixed dimensionality. Indeed, it has been demonstrated that fullerenes are encapsulated into inner space of carbon nanotubes exhibiting interesting electronic and structural properties. Recently, an experiment has reported that C₆₀ is rolled in cyclic-polyphenyl leading to interesting hybrid structures consisting of nano-scale materials with different topology. The hybrid structures can be regarded as sliced carbon peapods. In the present work, we aim to elucidate energetics and electronic structures of C₆₀ rolled in the shortest zigzag carbon nanotubes (cyclic polyacenes) whose diameters are 1.24 nm to 1.55 nm based on density functional theory with local density approximation.

Figure 1 show an energy gain upon the encapsulation of C₆₀ inside the cyclic polyacenes as a function of their diameter. For all polyacenes studied here, encapsulation reactions are exothermic indicating the fact that these short peapods are energetically stable. The calculated encapsulation energy strongly depends on the diameter of polyacenes. For the C₆₀, (17,0) nanotube (heptadecacene) give the largest encapsulation energy of about 1.3 eV which is the almost same as that for the peapods with infinite length. Encapsulation of C₆₀ leads to decrease the energy gap between the highest occupied and the lowest unoccupied states for the thick nanotubes.

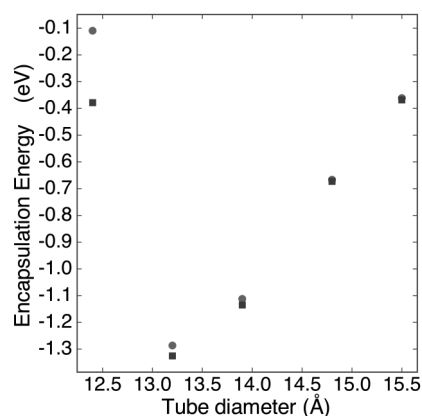


Fig. 1: Encapsulation energy of C₆₀ as a function of tube diameter.

Corresponding Author: S.Kigure
Tel: +81-29-853-5921, Fax: +81-29-853-5924,
E-mail: sokada@comas.frsc.tsukuba.ac.jp

Effect of inert gas on the growth of epitaxial graphene on Si-terminated SiC (0001)

○Akkawat Ruammaitree, Hitoshi Nakahara, Yahachi Saito

*Department of Quantum Engineering, Graduate School of Engineering,
Nagoya University, Nagoya 464-8601, Japan*

Graphene on SiC has a potential for technological application devices. In order to apply it to such devices, the uniform and ordered growth of graphene on SiC substrate is necessary. In this report, we have studied the growth of epitaxial graphene on Si-terminated SiC (0001) by annealing the SiC substrates in helium, neon and argon at pressure of 0.05 atm.

In the case of annealing the substrate in helium gas, AFM images (fig.1 (a) and (b)) show there are many pits at lower step edges and triangular graphene islands. For annealing the substrate in neon gas (fig.1 (c) and (d)), the pits at lower step edge still remain but the triangular graphene islands disappear from the terrace. In addition, the number of steps increases as compared with the sample annealed in helium gas. In the case of the substrate annealed in argon gas (fig.1 (e) and (f)), all of the pits at the lower step edge disappear. The triangular monolayer graphene islands are formed and enlarged until they merge with other graphene regions.

The SEM image (Fig.2 (a)) reveals that the triangular monolayer graphene islands will be formed on the wide terrace ($>1.5 \mu\text{m}$). The direction of triangular graphene which was formed on the same terrace pointed to the same direction. Fig. 2 (b) and (c) show moiré pattern at a triangular monolayer graphene island and the Fourier transform of Fig.2 (a), respectively.

Annealing in argon at 0.05 atm can be a candidate for creation of uniform and ordered monolayer graphene on SiC by merging graphene islands with graphene stripes at step edges before the formation of graphene bilayer.

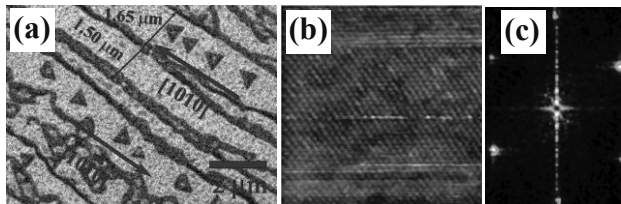


Fig.2 SEM (a), $50 \times 50 \text{ nm}^2$ STM (b) and Fourier transform (c) images of the sample which annealed in Ar gas

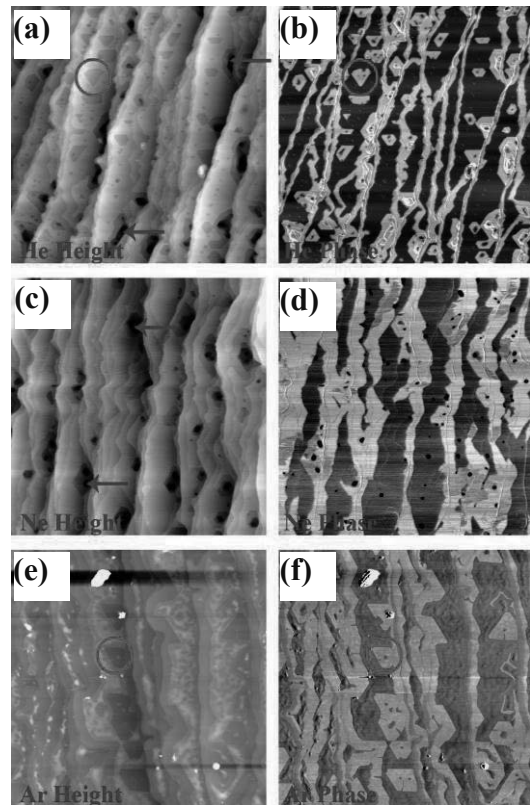


Fig.1 AFM $10 \times 10 \mu\text{m}^2$ topographic (a, c, e) and phase (b, d, f) images of the samples annealed in He (a and b), Ne (c and d) and Ar (e and f) gas. Bright regions in phase images represent graphene. Arrows indicate the pits at lower step edge. Circles indicate triangular graphene islands.

Corresponding Author: A. Ruammaitree

Tel: +8180-3823-3199

E-mail: akkawat@surf.nuqe.nagoya-u.ac.jp

Structural characterization of graphene edges using dark-field TEM

○Miho Fujihara, Yasumitsu Miyata, Ryo Kitaura, Eriko Maeda, Hisanori Shinohara*

Department of Chemistry, Nagoya University, Nagoya 464-8602, Japan

Graphene has attracted much attention for future electronics and spintronics applications due to their high carrier mobility and unique magnetism. Because the electrical and magnetic properties of graphene strongly depend on the edge structure [1], it is important to develop a preparation method of graphene with desired edge structure. Hydrogen etching is one of the most promising methods to produce clean edge with zigzag structure [2]. However, it is still unclear how grain boundary and morphology are affected by the etching process. In this work, we have investigated the edge structure of hydrogen-etched graphene by using dark field transmission electron microscopy (DF-TEM).

Graphene was grown on copper foil by chemical vapor deposition of methane. The hydrogen etching was then conducted by flowing Ar/H₂ at 1,050 °C. The etched graphene was transferred to a SiN grid for DF-TEM observation as reported previously [3]. DF-TEM observation was carried out a JEM-2100F operated at 80 kV.

As shown in Figs.1a-c, DF-TEM observations reveal that the hydrogen etching generates two different types of the etching pattern including polygonal and ribbon shape. In the former case, hexagonal and septagonal holes are located in single grain and at grain boundary, respectively (Figs.1a and b). Almost all edges observed correspond to zigzag type as confirmed by electron diffraction. In contrast, the latter can be found in single grains rather than at grain boundaries and has various types of edge structures including zigzag, armchair and chiral types. This suggests that the ribbon-shaped gaps are derived from the preferential etching of graphene wrinkle, which should have high reactivity due to its large C-C bond curvature. The present results provide a useful basis to prepare well-defined graphene edges with a desired structure.

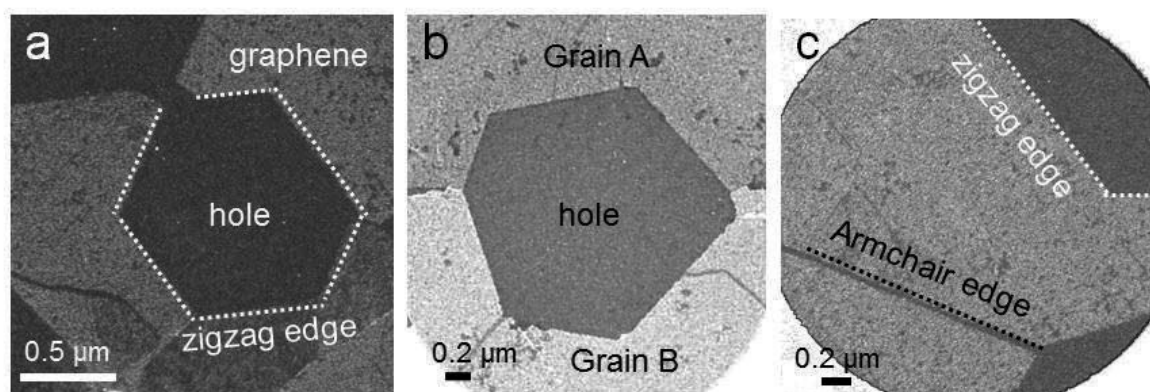


Fig.1 (a-c) DF-TEM images of graphene after hydrogen etching at different positions.

[1] M. Fujita *et al.* J. Phys. Soc. Jpn. **65**, 1920 (1996).

[2] R. Yang *et al.* Adv. Mater. **22**, 4014 (2010).

[3] P. Y. Huang *et al.* Nature **469**, 389 (2011).

Corresponding Author: H. Shinohara

Tel: +81-52-789-2482, Fax: +81-52-789-1169,

E-mail: noris@cc.nagoya-u.a.jp

Synthesis of Nitrogen-doped Carbon Materials Controlled Nitrogen Bonding Configuration

○Satoshi Yasuda^{1,2}, Li Yu¹, Kei Murakoshi¹

¹ Department of Chemistry, Hokkaido University, Sapporo, 060-0810, Japan

² JST-PRESTO, Kawaguchi, Saitama 332-0012, Japan

Nitrogen-doped carbon materials exhibit oxygen reduction reaction (ORR) catalytic activity, and paid attention to the metal free catalytic material for fuel cells [1]. There have mainly three common nitrogen bonding configurations within carbon, which are quaternary, pyridinic and pyrrolic nitrogen bonding configurations, and they are responsible for the ORR catalytic activities due to the reduced adsorption energy. However, in spite of numerous studies, it is still uncertain which configurations play important role in the actual activity for promoting ORR. To clarify the nitrogen configuration effect and realize high effective ORR catalytic material, development of selective synthesis technique of each nitrogen configuration in the carbon becomes a great challenge. Chemical vapor deposition (CVD) has been widely used as synthesis technique of conventional nitrogen-doped carbon materials. However, such high temperature process does not possess selective synthesis of the nitrogen configurations in carbon. In this study, we developed low temperature synthesis process based on surface polymerization of nitrogenous aromatic ring compounds as precursors, resulting in possibility of selective nitrogen configuration synthesis reflected on the molecular structure.

Low temperature CVD was employed below 500 °C to inhibit thermal decomposition of the feedstock molecule and polymerize them. As feedstock molecules, we used two kinds of nitrogenous aromatic ring compounds which are pyridine and julolidine molecules (Fig. (a)). The thermal polymerizations of each molecule are expected to allow selective synthesis of pyridinic and quaternary nitrogen configurations in carbon, respectively (Fig. (b)). Nitrogen-doped carbon sheets were synthesized on Cu foil below 500 °C for 30 ~ 120 min growth time at ambient pressure. Raman spectra for both samples made from pyridine and julolidine showed distinguishable D- and G-bands, indicating graphitic carbon formation. X-ray photoelectron spectra of both samples confirmed the existence of nitrogen in the carbon sheet with the N/C atomic ratio of 8 %. The binding energy of N1s peak of pyridine-made sheet was 398.2 eV, indicating a mainly pyridinic configuration, while julolidine-made sheet showed 401.4 eV of N1s peak, which is identical to quaternary one (Fig. (c)). These results indicate that the surface polymerization technique has potential to synthesize nitrogen-doped graphene contained desired nitrogen configuration in the graphitic carbon for ORR catalyst.

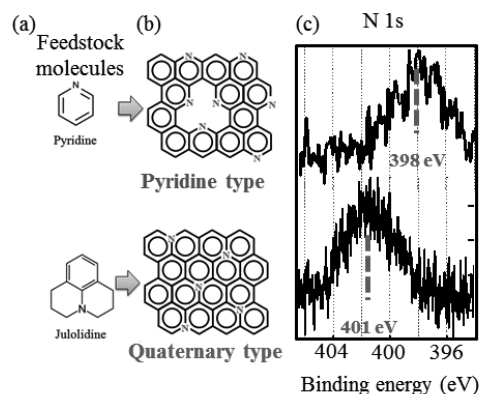


Fig. (a) Schematics of feedstock molecules and (b) synthesized structures. (c) XPS spectra of N1s.

[1] K. P. Gong *et al.* *Science* **324**, 760 (2009).

Corresponding Author: S. Yasuda

TEL & FAX: +81-(0)11-706-4811

E-mail: satoshi-yasuda@sci.hokudai.ac.jp

Preparation of High-Density Graphene Nanoribbons by Anisotropic Catalyst Cutting

○Yasumichi Kayo,¹ Pablo Solís-Fernández,² Kazuma Yoshida,¹
Masaharu Tsuji,^{1,2} and Hiroki Ago^{1,2,*}

¹Graduate School of Engineering Sciences, Kyushu University, Fukuoka 816-8580

²Institute for Materials Chemistry and Engineering, Kyushu University, Fukuoka 816-8580

Graphene, a two-dimensional sheet of carbon hexagons, is an attractive material for electronic applications, such as field-effect transistors, integrated circuits, and sensors, due to its unique structure and extraordinary high carrier mobility [1]. However, since graphene has no band gap, opening the band gap is a critical issue when one tries to apply graphene to semiconductor devices. Theoretical and experimental works have demonstrated that quantum confinement in one dimensional structure, so called graphene nanoribbons (GNRs), can potentially open the band gap [2,3]. Top-down lithography has been widely used to obtain GNRs, but the GNR edges are damaged by O₂ plasma treatment. The GNRs prepared by unzipping carbon nanotubes can be also damaged by gas phase or liquid phase oxidation processes [4,5]. Therefore, a new method based on bottom-up approach is expected.

Here, we developed a processing method to catalytically cut graphene along anisotropic crystalline orientation of underlying substrate, as illustrated in Fig. 1. This is similar to the CVD growth of horizontally-aligned single-walled carbon nanotubes (SWNTs) on crystalline sapphire and quartz [5], as Tsukamoto *et al.* showed recently [6]. We systematically investigated the anisotropic cuttings at different temperatures and different gas atmospheres for single-layer graphene grown by CVD. Various metal nanoparticles including Ni, Fe, and Cu gave anisotropic cutting lines, as seen in Fig. 2, and Ni nanoparticles were found to give the highest cutting density with more than 20 lines/μm. Moreover, we also observed that a cutting density is strongly dependent on the annealing temperature and H₂ concentration. Our results can be applied to large area fabrication of dense, highly aligned GNR arrays that can be developed to future carbon-based electronics.

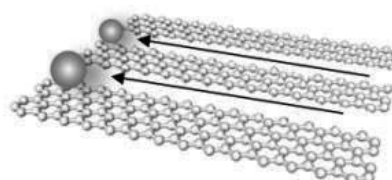


Fig. 1 Schematic of metal catalyzed anisotropic cutting of graphene to create GNR array.

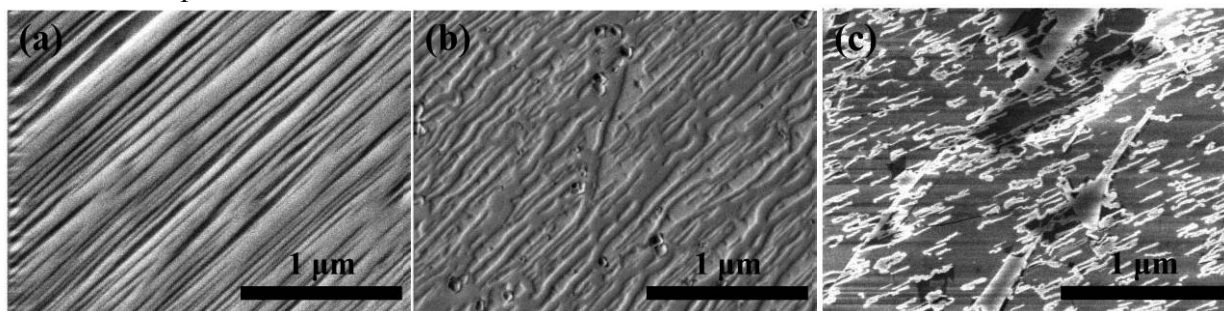


Fig. 2 SEM images of single-layer graphene measured after metal-catalyzed cutting using (a) Ni, (b) Fe, and (c) Cu. In (a), the cutting lines appear black and remaining graphene is gray. In (b) and (c), cutting lines appear as bright contrast.

References: [1] A. K. Geim, *Nat. Mater.*, **6**, 183 (2007). [2] K. Tanaka *et al.*, *Synth. Met.*, **17**, 143 (1987). [3] X. Li. *et al.*, *Science* **319**, 1229 (2008). [4] D. V. Kosynkin *et al.*, *Nature*, **458**, 872 (2009). [4] L. Jiao *et al.*, *Nat. Nanotechnol.* **5**, 321 (2010). [5] H. Ago *et al.*, *Chem. Phys. Lett.*, **408**, 433 (2005). [6] T. Tsukamoto *et al.*, *J. Phys. Chem. C*, **115**, 8580 (2011).

Corresponding Author: Hiroki Ago (Tel&Fax: +81-92-583-7817, E-mail: ago@cm.kyushu-u.ac.jp)

Transparent graphitic tiles synthesized from carbon nanowalls by shock compression

○Kazutaka Nakamura¹, Toshiyuki Atou², Keisuke Niwase³, Kazutaka G. Nakamura²
and Masaru Tachibana¹

¹ Department of Nanosystem Science, Yokohama City University, Yokohama 236-0027, Japan.

² Materials and Structures Laboratory, Tokyo Institute of Technology, Yokohama, 226-8503, Japan.

³ Hyogo University of Teacher Education, Hyogo 673-1494, Japan.

The transformation of graphite to diamond under high pressure is a long time issue. Shock compression and rapid quenching (SCARQ) technique is an effective method to obtain metastable carbon phase, transformed from the initial carbon phase in a short period of the shock compression [1]. The nature of transformed carbon phase, transition pressure and transition temperature should depend on the initial state of the starting material. For the understanding of the transformation mechanism, it is important to investigate the transformation of various kinds of carbon materials under high pressure.

Carbon nanowalls (CNWs) are two dimensional graphitic sheets vertically oriented to the substrate surface [2]. The nanostructure is composed of small and uniform graphite domains or crystallites with several tens of nanometers [3]. Such structural feature has been also demonstrated by transport properties such as Anderson weak localization [4] and novel electrochemical properties for fuel cells [5]. Thus, CNWs with such unique structure are also of great interest as a starting material for high-pressure transformation of graphite. Here we report the synthesis of transparent graphitic tiles from CNWs by the SCARQ method.

The transparent tiles (Fig. 1) are included in samples recovered from shock pressures more than 57 GPa [6]. They exhibit strong photoluminescence but no diamond Raman peak, similar to the case of amorphous diamond [7]. However, the electron energy-loss spectroscopy exhibits relatively intense π^* peak associated with graphite, that is inconsistent with the transparency. From these results, it is suggested that the transparent tile is a mixture of amorphous diamond and superhard graphitic material with the transparency [6]. Such carbon phase may come from the unique structural feature of CNWs as the starting material for the shock compression.

- [1] K. Kondo, *Diam. Relat. Mater.* **5**, 13 (1996).
- [2] S. Kurita *et al.*, *J. Appl. Phys.* **97**, 104320 (2005).
- [3] K. Kobayashi *et al.*, *J. Appl. Phys.* **101**, 094306 (2007).
- [4] S. Yamada *et al.*, *J. Phys. Soc. Jpn.* **79**, 054708 (2010).
- [5] S. C. Shin *et al.*, *J. Appl. Phys.* **110**, 104308 (2011).
- [6] K. Nakamura *et al.*, *J. Appl. Phys.* (in press)
- [7] K. Niwase *et al.*, *Phys. Rev. Lett.* **102**, 116803 (2009).

Corresponding Author: M. Tachibana
Tel & Fax: +81-45-787-2307
E-mail: tachiban@yokohama-cu.ac.jp

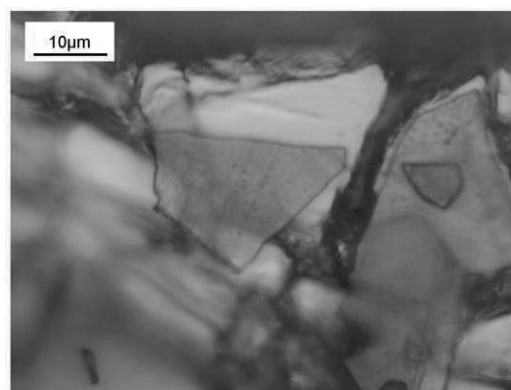


Fig. 1

Water-Soluble Graphene through Polyglycerol Grafting

○Toku Yasuda^{1,2}, Li Zhao¹, Gang Liu¹, Shuji Aonuma², Takahide Kimura¹, Naoki Komatsu¹

¹ Department of Chemistry, Shiga University of Medical Science, Otsu, 520-2192, Japan

² Department of Materials Chemistry, Osaka Electro-Communication University, Osaka, 572-8530, Japan

For applications of nanocarbons in biology and medicine, such as imaging probe and drug carrier, they have to be well solubilized in a physiological environment. In this context, surface chemical functionalization has been extensively investigated to impart strong hydrophilicity to nanocarbons. We found recently that polyglycerol-grafted nanodiamond (ND-PG) exhibited very high solubility in phosphate buffer (16 mg/mL) [1]. In this paper, we will present our recent result of PG grafting at the periphery of exfoliated graphene through ring-opening polymerization of glycidol to prepare PG-functionalized graphene (G-PG) soluble in PBS. We carried out the PG-functionalization of exfoliated graphene under similar reaction conditions to those of the ND-PG [1], but used graphene was prepared through wet-process of graphite exfoliation as a starting material. The strong Tyndall effects were observed in the aqueous solutions as shown in Fig. 1, suggesting that G-PG is solubilized both in the water and PBS. The existence of G-PG in these solutions was confirmed by UV and Raman spectroscopies. In the Raman spectra shown in Fig. 2, both G and G' bands are detected in the dried samples

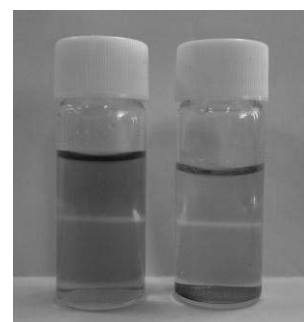


Fig. 1 Aqueous solutions of PG - functionalized graphene in water (left) and PBS (right).

from water and PBS solutions. From the ratio of G' / G and the symmetrical shape of G' band, a few-layer graphene is considered to be dominant in the G-PG. In addition, the intensity of the D band is very low, indicating that the G-PG does not have number of defects and that the process to prepare G-PG causes little damage to graphene.

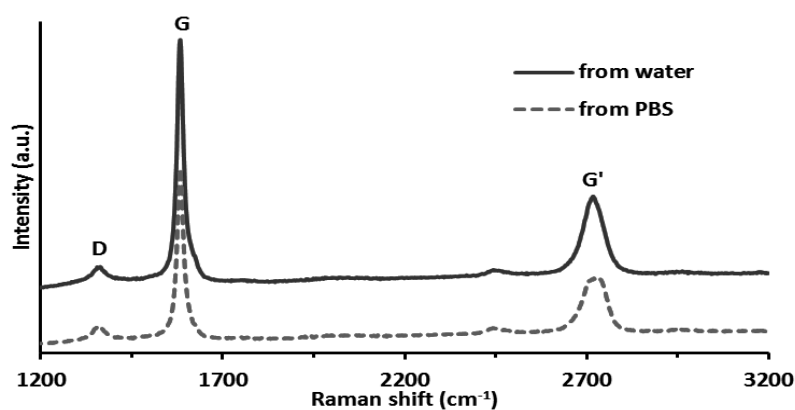


Fig. 2 Raman spectra of polyglycerol - functionalized graphene

[1] L. Zhao, T. Takimoto, M. Ito, N. Kitagawa, T. Kimura, N. Komatsu, *Angew. Chem. Int. Ed.*, 50, 1388 (2011).

Corresponding Author: Naoki Komatsu

Tel: +81-77-548-2102, Fax: +81-77-548-2405, E-mail: nkomatsu@shiga-med.ac.jp

Relationship between morphology, electric properties and field emission characteristics of carbon nanosheets films by microwave plasma-enhanced chemical vapor deposition

○¹Shohei Hayase, ²Zhipeng Wang and ^{1,3}Hironori Ogata

¹ Department of Chemical Science and Technology, Hosei University, Koganei 184-8584, Japan

² Institution for Sustainability Research and Education, Hosei University, 2-17-1, Fujimi, Chiyoda-ku, 102-8160 Tokyo, Japan

³ Research Center for Micro-Nano Technology, Hosei University, Koganei 184-0003, Japan

Carbon nanosheets (CNSs) consist of two-dimensional networks of almost vertically-aligned graphitic walls with sharp edges and a few to some tens of nanometers thick. Due to the high aspect ratio and the high in-plane continuity of the wall structures, CNSs are expected as the candidate for field emitters. As is well known, field emission (FE) properties strongly depend on the electric properties of the emitters and their morphological structures. Thus, the modification of the electronic structure or morphology of CNSs provides a possibility to enhance the FE performance of the CNSs. In this work, CNSs with various morphologies were fabricated by changing H₂ gas flow ratio and their FE properties were investigated. We also investigate the effect of nitrogen plasma treatments on the structure and FE properties of CNSs. The electron field emission properties of the films on NiFe substrate were measured in a parallel-plate configuration with ITO coated glass anode and a Teflon(100μm) interelectrode spacer at room temperature in high vacuum (below 10⁻³ Pa).

Figure 1 shows the FE-SEM image of the CNSs film before nitrogen plasma treatment. Figure 2 shows the *J-E* characteristic curve of FE from the CNSs. The turn-on electric field for the onset of emission at a $J=10^{-5}$ mA/cm² was found to be 5.2V/μm, the β value was fitted to be 2090. In this presentation, the detailed results will be presented.

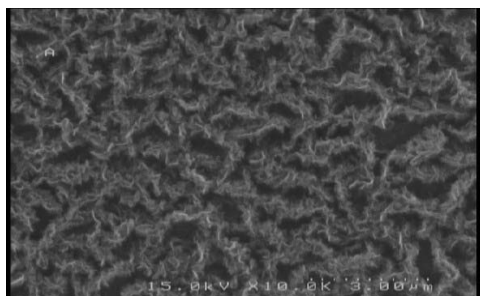


Figure 1. FE-SEM image of the CNSs.

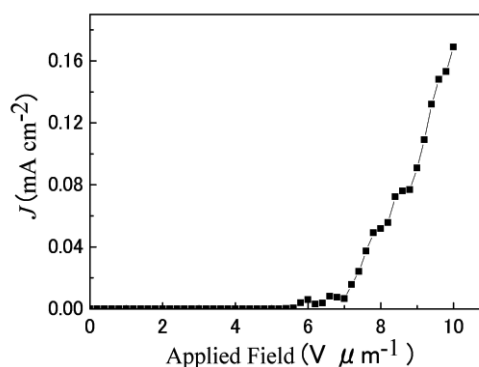


Figure 2. *J-E* characteristic curve of FE from the CNSs film.

Corresponding Author: Hironori Ogata,

Tel: +81-42-387-6229, Fax: +81-42-387-6229, E-mail: hogata@hosei.ac.jp

Characterization of Electrical Properties for Graphene Film Deposited by Microwave Plasma CVD

○Yuki Okigawa^{1,2}, Kazuo Tsugawa², Takatoshi Yamada^{1,2}
Masatou Ishihara^{1,2}, and Masataka Hasegawa^{1,2}

¹ *Nanotube Research Center, National Institute of Advanced Industrial Science and
Technology (AIST), Tsukuba 305-8565, Japan*

² *Technology Research Association for Single Wall Carbon Nanotubes (TASC), Tsukuba
305-8565, Japan*

We have developed the microwave plasma graphene CVD technique combined with the roll-to-roll process. In this method, a continuous deposition process of graphene film is expected at low temperature and few ten seconds [1]. Although higher quality of the graphene film is required, the electrical property of the graphene film deposited by plasma CVD technique is not fully understood. Hall effect measurement using van der Pauw devices is useful to measure the electrical property for graphene, which is expected to understand the mechanism of the electrical conductivity of graphene film. In addition, it is necessary to measure the electrical property for the different size of graphene, such as micrometer and centimeter size of graphene. In this study, we have measured the hall mobility by Hall effect measurement with van der Pauw devices.

The graphene film was deposited by microwave plasma CVD technique on Cu foil. Then, it was transferred to the quartz substrate. After that, the van der Pauw device was fabricated using conventional photolithography, metal deposition and lift-off processes. Figure 1(a) shows the optical microscopy image for a micrometer size of the device. For a centimeter size of device, the four electrodes were deposited using the silver paste, as shown in Fig. 1(b). These devices show that the mobility is estimated to be from 10 to 100 cm²/Vs. And these show the p-type conduction.

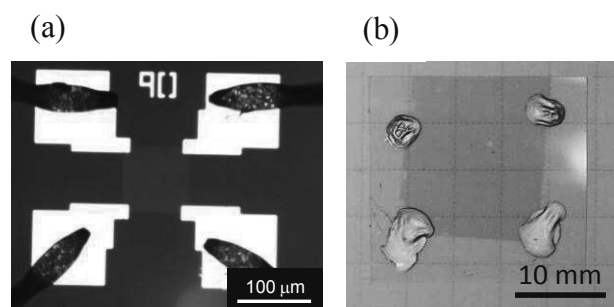


Figure 1 Optical microscopy images for van der Pauw devices.
(a) micrometer size (b) centimeter size.

[1] T. Yamada *et al.*, *Carbon*, **50**, 2615 (2012).

Corresponding Author: Yuki Okigawa

Tel: +81-29-861-2747, Fax: +81-29-861-4565,

E-mail: okigawa.yuki@aist.go.jp

Host-guest Interactions between Nanographene and Gas molecules

○Junichi Takashiro¹, Kazuyuki Takai¹, Manabu Kiguchi¹, Toshiaki Enoki¹
Takeo Yamada², Kenji Hata², Takafumi Ishii³, Takashi Kyotani³

¹Department of Chemistry, Tokyo Institute of Technology, Meguro, Tokyo, 152-8551, Japan

²Nanotube Research Center, National Institute of Advanced Industrial Science and Technology (AIST), Tsukuba, 305-8565, Japan

³Institute of Multidisciplinary Research for Advanced Materials, Tohoku University Sendai, 980-8577, Japan

The electronic properties of nano-sized graphene (nanographene) are influenced by the edges. Especially, in zigzag edges a non-bonding π state called “edge state” is created. Nanoporous activated carbon fibers (ACFs, Fig.1), which consist of 3D disordered network of nanographene sheets with their edges terminated by oxygen-containing functional groups, are good model system to investigate the effect of adsorbed guest chemical species on the electronic properties of nanographene [1]. In this work, we investigated the interaction between ACFs and gas species (O_2 , He, Ar and Xe) in terms of physisorption, charge-transfer, and chemical reaction.

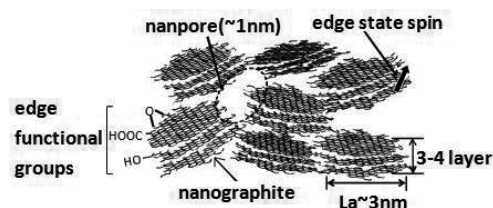


Fig.1 Activated Carbon Fibers (ACFs)

Pristine ACFs were pre-heat-treated at 1000°C to eliminate the foreign species terminating the nanographene edge. The time evolution of the resistivity was measured after 1atm of gas species was introduced to ACFs at room temperature. To investigate the details of interaction between nanographene and oxygen atoms, ACFs were exposed to O_2 atmosphere of 1-100Pa at T_{treat} ; 600-1300°C (oxidation). The oxidized samples were investigated by the resistivity, thermogravimetry, XPS, NEXAFS and thermal desorption measurements.

The resistivity increases upon gas adsorption, where the increment is in the order of $O_2 > Ar > He \cong Xe$. The large increase in the resistivity is caused by chemisorptions of O_2 to nanographene accompanied by charge transfer. For chemically inert noble gas species, the physisorption of larger diameter noble gas molecules except Xe works to expand the nanopore space to a larger extent, resulting in the resistivity increase owing to the elongation of inter-nanographene-sheet distance. Xe, whose diameter is larger than the nanopore size, shows only a small resistivity increase, as it cannot be accommodated into the nanopores.

Fig.2 shows (a) edge state intensities in C K-edge NEXAFS and (b) the atomic ratio of edge carbon atoms to total carbon atoms in nanographene (C_{edge}/C_{total}) obtained from TG for oxidized and non-oxidized ACFs. The NEXAFS intensity of the edge state originating from zigzag edges decreases with increasing in T_{treat} , irrespective of the increasing of C_{edge}/C_{total} . This is explained by the higher reactivity of zigzag edge than armchair edge due to its energetically unstable nature, suggesting that oxidation process in nanographene transforms zigzag edge into armchair edge.

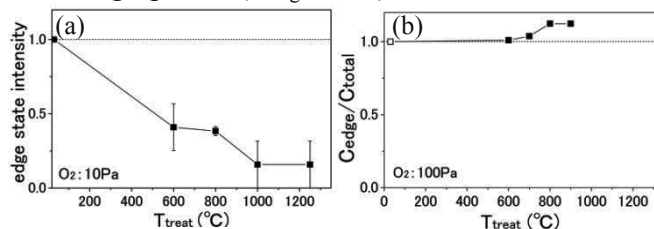


Fig.2 (a) Edge state intensity and (b) C_{edge}/C_{total} normalized with the value in the pristine state for ACFs at T_{treat} (■), and non-oxidized ACFs (□)

[1] T.Enoki and K.Takai *et al. Solid State Communications* **149** 1144 (2009)

Corresponding Author: T.Enoki

E-mail: enoki.t.aa@m.titech.ac.jp

Linear Dispersion Bands on Partially H-Terminated (111) Surfaces of Diamond Structure

○Junki Sone, Susumu Okada

*Graduate School of Pure and Applied Sciences, University of Tsukuba,
1-1-1 Tennoudai, Tsukuba, Ibaraki 305-8571, Japan*

Ever since exfoliation of graphene from bulk graphite, graphene has been attracting a lot of attentions due to their interesting electronic properties arising from their characteristic geometry. Graphene has a planer honeycomb structure due to sp^2 hybridization of carbon atoms. On this atomic sheet, π electrons are extended through out the network leading to the peculiar electronic structure at the Fermi level: A pair of linear dispersion bands emerges at the Fermi level. Such characteristic electronic structures result in a rich variety of physical properties and allow us to apply for electronic devices in the next generation. Besides the honeycomb sheet of C atoms, recently, a hexagonal atomic sheet consisting of Si has been synthesized. In the present work, we aim to explore the possibility of the emergence of liner dispersion bands on semiconductor surfaces. Here, we focus on the (111) surfaces of diamond structure of C and Si, whose topmost atoms are partially terminated by H atoms. In accord with the partial termination, unsaturated surface bonds form hexagonal network (Fig. 1). On these surfaces, we perform first-principles calculations based on density functional theory to elucidate their geometric and electronic structures.

Since a unit cell contains two dangling bonds, we find that two surface associated states emerge in the gap between valence and conduction bands. Due to the large spacing between the dangling bonds, these states have small dispersion of a few hundred meV. By focusing at K point, surprisingly, these states have linear dispersion as in the case of graphene (Fig. 2). In sharp contrast, calculated Fermi velocities of C and Si dangling bonds are 10 % of that of graphene. Thus, by controlling surface morphologies of semiconductors with appropriate adsorbates, we can easily obtained Dirac fermion systems on surface of matters and tune their electron correlation.

Corresponding Author: J.Sone
Tel: +81-29-853-5921, Fax: +81-29-853-5924,
E-mail: sokada@comas.frsc.tsukuba.ac.jp

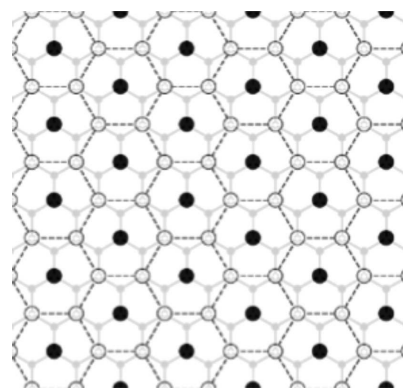


Fig.1 Geometric structure of partially H-terminated (111) surface of diamond. Circles denoted black and white are the atoms with hydrogenated and without hydrogenated.

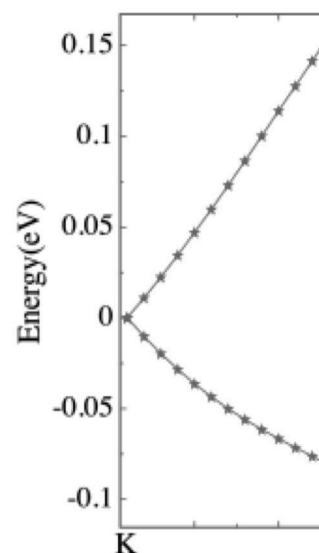


Fig.2 Electronic structure of dangling bond states of partially hydrogenated (111) surface of diamond near K point.

Influence of mechanical deformation on thermal properties of graphene

○Takashi Funatani¹, Takahiro Yamamoto², Matsuto Ogawa¹, Satofumi Souma¹

¹*Dept. of Electrical and Electronic Engineering, Kobe University, Kobe, 657-8501, Japan*

²*Dept. of Liberal Arts, Tokyo University of Science, Chiyoda, Tokyo 102-0073, Japan*

Recent rapid development of semiconductor technologies have been mainly achieved by the miniaturization of silicon MOSFET and their integration based on the Moore's law. However, as the device size is aggressively scaled down, the heat production in the device influences more seriously the device performance. As one of strategies to resolve such problem, graphene is attracting great attention since it has high thermal conductivity and thus useful for dissipating heat. On the other hand, from the view point of effective utilization of heat given off, thermoelectric devices are also drawing many attentions, where the material with low thermal conductivity is preferable. Therefore, it is interesting to explore the possibility to control the thermal conductivity of graphene.

With such motivation, in the present study we theoretically examine the effect of mechanical deformation on "phonon specific heat" in graphene, which is one of physical quantities that dominate its thermal conductivity. Our calculations have shown that the tensile strain applied along the zigzag direction (Fig. 1) modulates essentially the temperature dependence of the specific heat, where the specific heat is found to be increased by applying the strain when the temperature is higher than the threshold value (Fig. 2), meaning that the thermal conductivity of graphene is expected to be enhanced by the mechanical deformation. The detail of our analyses will be given in the presentation.

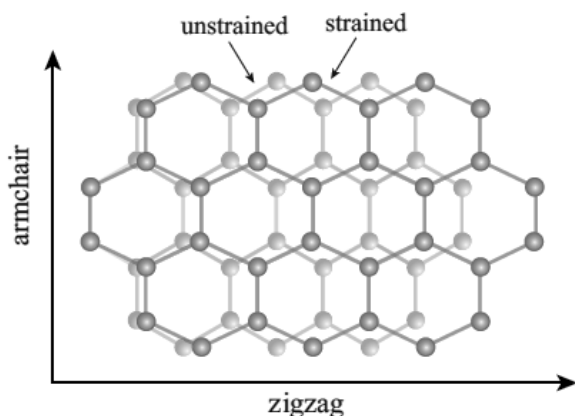


Fig. 1. Conceptual diagram of graphene strained along the zigzag direction

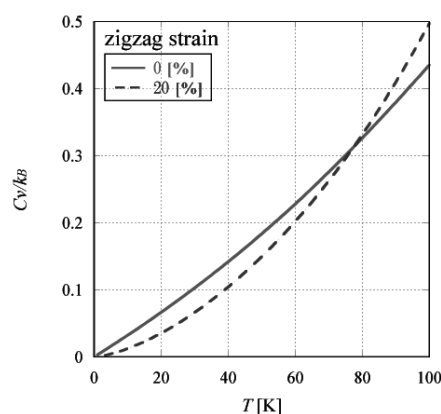


Fig. 2. Temperature dependence of phonon specific heat in graphene with 0 [%] and 20 [%] strain.

Corresponding Author: Satofumi Souma

Tel&FAX: +81-78-803-6087 E-mail: ssouma@harbor.kobe-u.ac.jp

First-principles study of edge-modified armchair graphene nanoribbons

○Hideyuki Jippo and Mari Ohfuchi

Fujitsu Laboratories Ltd., 10-1 Morinosato-wakamiya, Atsugi, Kanagawa 243-0197, Japan

Graphene nanoribbons (GNRs) have attracted attention as hopeful semiconducting nanostructures for electronic applications of graphene. Recently a bottom-up approach to atomically precise fabrication of armchair GNRs (AGNRs) has been reported [1]. This approach might also enable us to produce AGNRs with various edge terminations. OH-terminated AGNRs (OH-AGNRs) have been theoretically studied and shown to have rippled edges and different energy band gaps from H-terminated AGNRs (H-AGNRs) [2]. F- and Cl-terminated AGNRs (F- and Cl-AGNRs) have also shown rippled edges [2], but their electronic structures are still unclear. In this article, we investigate the electronic structures of the F- and Cl-AGNRs using first-principles methods.

We examine H-, F-, Cl- and OH-AGNRs with widths $N = 7$ and 19. They are most likely to be realized by the bottom-up approach. The most stable geometries of H-AGNRs have planar configurations, but those of F-, Cl- and OH-AGNRs have rippled edges as shown in Fig. 1. The ripples stem from steric hindrance between neighboring pairs of the termination atoms or groups and are strongly localized to the edges. We have found that F-AGNRs are the most stable owing to the strong C-F bonds despite their rippled edge structures. As shown in Fig. 2, the energy band gaps of F- and Cl-AGNRs are narrower than those of H-AGNRs. We have found that this is due to the structural deformations rather than the chemical effect. For OH-AGNRs, the chemical interactions between the adjacent OH groups further reduce the band gaps.

In summary, the energy band gaps of AGNRs have been shown to vary with the edge terminations. This seems to show the possibility of controlling their electronic properties by edge modifications.

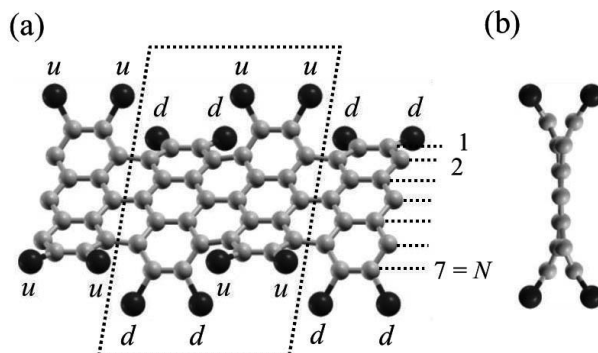


Fig.1. (a) Perspective and (b) side views of the most stable geometry for Cl-terminated armchair graphene nanoribbon with a width $N = 7$. The light and dark gray spheres represent C and Cl atoms, respectively. The symbols of u and d represent the edge moves “up” and “down” from the ribbon plane, respectively. The dotted lines indicate the unit cell.

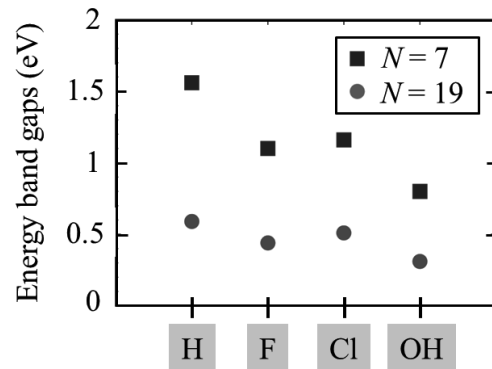


Fig.2. Energy band gaps of H-, F-, Cl and OH-terminated armchair graphene nanoribbons with widths $N = 7$ and 19.

[1] J. Cai *et al.*, Nature **466**, 470 (2010). [2] P. Wagner, *et al.*, Phys. Rev. B **84**, 134110 (2011).

Corresponding Author: H. Jippo

Tel: +81-46-250-8843, Fax: +81-46-250-8274, E-mail: jippo.hideyuki@jp.fujitsu.com

Enhancement of photo-induced current in the complex of iron oxide nanotubes and fullerenols

Yuki Shiraki, ○Yuki Mishina, Shunji Bandow

Department of Materials Science and Engineering, Meijo University,
1-501 Shiogamaguchi, Tenpaku, Nagoya 468-8502, Japan

Dye sensitized solar cell is most promising candidate for an effective absorber of the visible light. The principle of this composite is based on the charge transfer from the visible light excited electrons to the conduction band of the dye molecule to the conduction band of the host materials of metal oxides such as TiO_2 and WO_3 , etc. Since such charge transfer would take place at the interfacial region, it is effective to have a large surface area for the host material. A tube structure is a candidate for realizing such large surface area and we focus a material of iron-oxide or titanium oxide nanotube.

Since the metal oxides normally have hydrophilic nature, hydrophobic fullerene is not suitable for making the complex. In order to avoid this problem, we prepared fullerenols, $\text{C}_{60}(\text{OH})_n$, by the patent method [1]. Metal oxides nanotubes were prepared by the sol-gel (Fe-oxide NT) and strong alkaline reflux (Ti-oxide NT) methods reported [2,3].

The samples were made by mixing the colloidal solutions of metal-oxide NTs and fullerenols and kept for 1 day at RT. Responses of photo-induced current are in Figs. 1a (visible light) and 1b (UV) with the samples of 1) fullerenols only (C60-OH), 2) iron-oxide nanotube only (Fe-oxNT), 3) just after mixing Fe-oxNT and C60-OH (Fe-oxNT + C60-OH) and 4) after 1 day reaction (Fe-oxNT/C60-OH). As shown in the figure, an enhancement of the photo current and a remarkable visible light response can be identified only in the sample after 1 day reaction. Comparison of the light irradiation responses between the mixtures of Ti-oxNT/C60-OH and Fe-oxNT/C60-OH will be discussed.

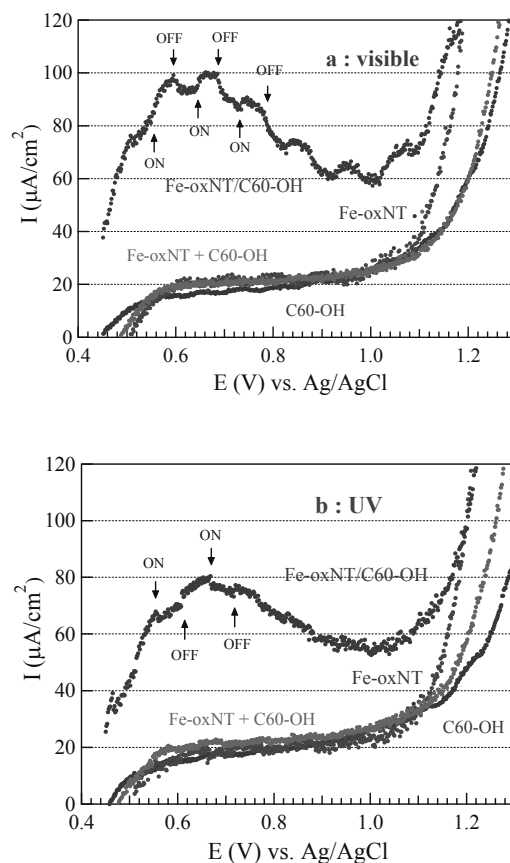


Fig. 1 Photo-induced current measured in an electrolyte of a 0.2 mol KHCO_3 aq. under irradiating a) visible light (halogen lamp) and b) UV (Hg lamp). Remarkable enhancement of the current and light irradiation effects can be seen in a Fe-oxNT/C60-OH complex under a visible light.

[1] P2007-031090 [2] Y. Mishina et al., The 41st FNTG (2011), **3P-10**.

[3] Y. Shiraki and S. Bandow, The 42nd FNTG (2012), **3P-49** and 43rd FNTG (2012), **3P-38**.

Corresponding Author: Shunji Bandow, **E-mail:** bandow@meijo-u.ac.jp, **Tel :** +81-52-838-2404

Development of Multi-stage Ion Trap Mobility System.

○Toshiki Sugai

Department of Chemistry, Toho University, Miyama 2-2-1 Funabashi, 274-8510, Japan

Ion mobility measurements have been utilized to analyze structures of nanocarbon materials[1]. Structures of Metal-fullerene show significant dependence on the number of metal atoms and the cage size. To study further, we have been developing an ion trap mobility system and structural changes of salt solution particles and solid polystyrene particles were monitored for more than 2 hours[2]. The measurements have revealed the stability and the sensitivity of the system. The salt water solution particles absorb water vapor in air and grow to larger particles whereas the rigid polystyrene particles keep their structures. Despite of these advantages, the trap system has low mobility resolution because of the small size of the trap. To improve the resolution, we have been developing the multi-stage ion trap mobility system. The details of the system will be presented.

[1] T. Sugai *et al.*, *J. Am. Chem. Soc.* **123**, 6427 (2001).

[2] T. Sugai *et al.*, The 38th symposium (2010) and The 44th symposium (2012).

TEL: +81-47-472-4406, FAX: +81-47-472-4406, E-mail: sugai@chem.sci.toho-u.ac.jp

Thermal Reactions of C₆₀ with Siliranes: Formation of Carbosilylated Fullerenes

○Ryosuke Iida¹, Kentaro Takagi¹, Masahiro Kako¹, Tadashi Hasegawa², Yutaka Maeda², Michio Yamada², Takeshi Akasaka³

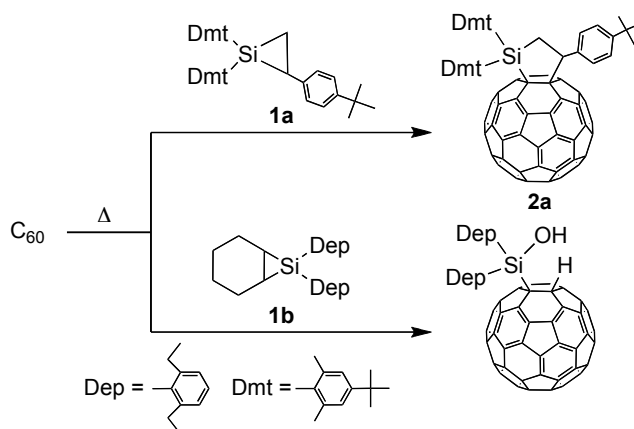
¹Department of Engineering Science, The University of Electro-Communications, Chofu, Tokyo 182-8585, Japan

²Department of Chemistry, Tokyo Gakugei University, Koganei, Tokyo 184-8501, Japan

³Life Science Center of Tsukuba Advanced Research Alliance, University of Tsukuba, Tsukuba, Ibaraki, 305-8577, Japan

Many research groups have investigated derivatization of fullerenes with various functional groups from both mechanistic and synthetic viewpoints. It has been demonstrated that introduction of heteroatoms such as electropositive silicon has induced remarkable changes in the electronic characteristics of fullerenes. In fact, the facile silylation reactions of fullerenes have been described using reactive silicon compounds such as disiliranes, silylenes, and silyl radicals [1]. These silylated derivatives have more negative charge on the cage than the parent fullerenes as revealed by electrochemical analyses and theoretical calculations. Nevertheless such silylation procedures are hitherto limited under photolytic conditions, and the decomposition of the silylated products were frequently observed under the photolytic conditions. Therefore, it is worthwhile to investigate alternative procedures for silylation of fullerenes without photoirradiation. Recently, we reported the photochemical carbosilylation of C₆₀ using siliranes indicating the production of the novel 1,2- and 1,4-adducts [1]. In our continuing research of silylation of fullerenes, we are investigating thermal reactivities of siliranes with C₆₀ for comparison with those of the photoreactions. Because siliranes are established as the precursors of silylenes, it is noteworthy that silylene addition and formal [2+3] cycloaddition are possible for siliranes. In addition, we also examined the thermal reactions of siliranes and fullerenes catalyzed by transition metal complexes as an alternative procedure for silylation.

When a toluene solution of C₆₀ and silirane **1a** was heated at 110°C for 24 h, a carbosilylated product compound **2a** was obtained in 68 % yield. Based on the spectroscopic analyses, **2a** was determined to be a 1,2-adduct on the [6,6] bond junction of C₆₀. On the other hands, the reaction of silirane **1b** and C₆₀ afforded the corresponding hydrolyzed silylene adduct. These results and related transition-metal catalyzed reactions will be discussed in detail.



Scheme 1.

[1] Nagatsuka, J.; Sugitani, S.; Kako, M.; Nakahodo, T.; Mizorogi, N.; Ishitsuka, M. O.; Maeda, Y.; Tsuchiya, T.; Akasaka, T.; Gao, X.; Nagase, S. *J. Am. Chem. Soc.* **2010**, *132*, 12106-12120, and references cited therein.

Corresponding Author: Masahiro Kako Tel: +81-42-442-5570 E-mail: kako@e-one.uec.ac.jp

Construction of an Opening on Fullerene C₇₀ and Encapsulation of a Water Molecule

○Rui Zhang,¹ Michihisa Murata,¹ Yasujiro Murata^{1,2}

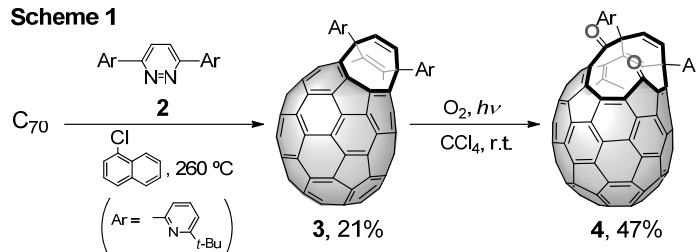
¹ Institute for Chemical Research, Kyoto University, Uji, Kyoto 611-0011, Japan

² JST-PRESTO

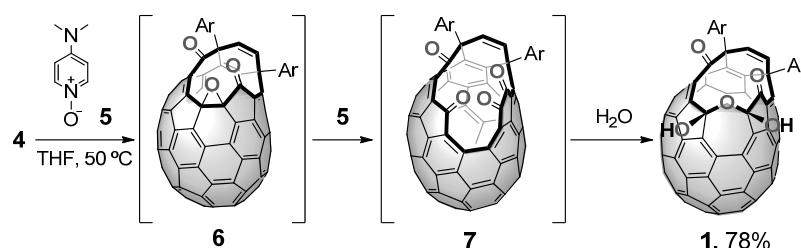
We have reported a synthetic method to produce endohedral fullerene C₆₀ encapsulating a water molecule.¹ In this work, by applying the similar procedure to C₇₀ with a larger inner space, open-cage C₇₀ derivative **1** with a 13-membered-ring opening was synthesized as a key compound for the insertion of a water molecule. We also studied the insertion of a water molecule by heating a solution of **1** under the presence of water.

We first prepared open-cage C₇₀ derivative **4** with a 12-membered-ring opening via thermal reaction of C₇₀ with pyridazine **2** and subsequent photo-oxidation of compound **3** (Scheme 1).² Then, by following the synthetic method for H₂O@C₆₀, we tried to enlarge the opening of **4** by using *N*-methylmorpholine *N*-oxide (NMO) as an oxidant.¹ This reaction resulted in a formation of

Scheme 1



Scheme 2



complex mixture and desired product **1** was not isolated. Thus, we used *N*-pyridine oxide **5** as a milder nucleophilic oxidant than NMO and succeeded in obtaining **1** in 78% yield. The plausible mechanism of this reaction is shown in Scheme 2. First a thermal reaction of **4** with **5** gives epoxide **6**, which again reacts with **5** to produce tetraketone **7**. Then a water molecule adds to one of the carbonyl groups of **7** to afford **1**.

Insertion of water molecule to **1** was achieved by heating a solution of **1** under the presence of water. ¹H NMR of the product showed a new singlet signal at $\delta = -18.16$ ppm in CDCl₃. Considering that the water molecule inside the corresponding open-cage C₆₀ derivative gave a singlet signal at $\delta = -9.87$ ppm in CDCl₃,¹ the water molecule encapsulated in **1** was subjected to the strong shielding effect from the C₇₀ cage. We will also present results of closing the opening toward the synthesis of endohedral fullerene H₂O@C₇₀.

[1] K. Kurotobi, Y. Murata, *Science* **333**, 613 (2011).

[2] Y. Murata, S. Maeda, M. Murata, K. Komatsu, *J. Am. Chem. Soc.* **130**, 6702 (2008).

Corresponding Author: Yasujiro Murata

Tel: +81-774-38-3172, Fax: +81-774-38-3178

E-mail: yasujiro@scl.kyoto-u.ac.jp

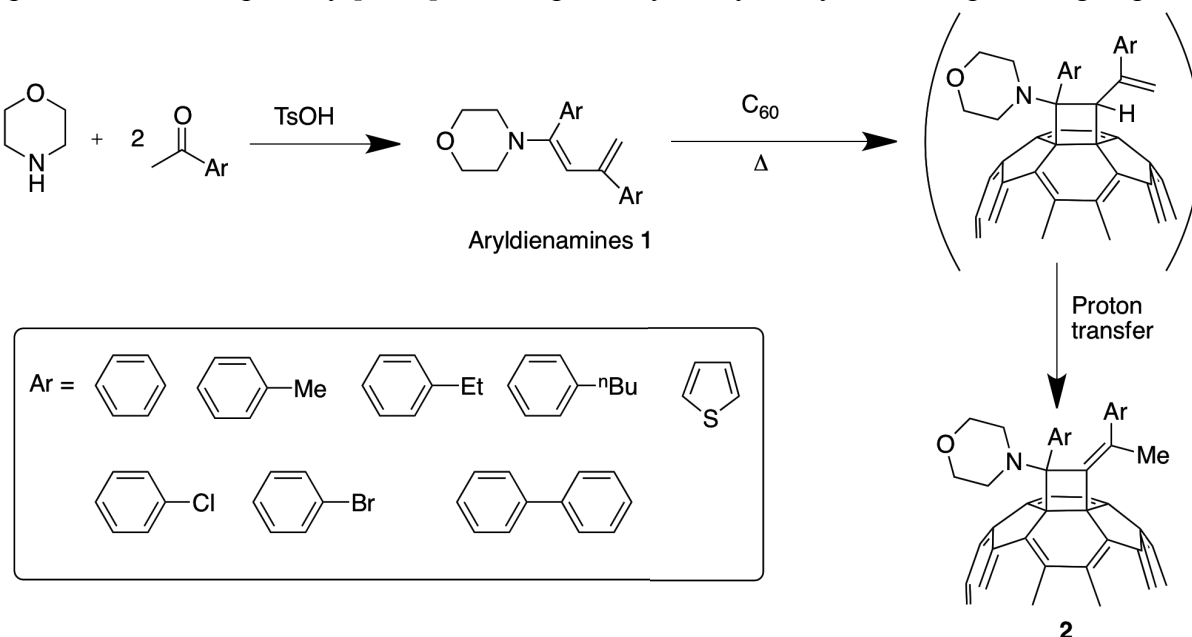
Thermal [2+2] cycloaddition of C₆₀ with aryl dienamines

○Naohiko Ikuma, Hiroyuki Yamamoto, Tsubasa Mikie, Ken Kokubo, Takumi Oshima

¹ *Division of Applied Chemistry, Graduate School of Engineering, Osaka University, Suita, Osaka, 565-0871, Japan*

Facile and highly selective functionalizations of C₆₀ without any undesirable by-products are required to obtain a variety of fullerene derivatives in reasonable costs. We are interested in the development of novel methodology in which the mono-addition of C₆₀ drastically reduces the further multi-additions due to the raise of its LUMO energy. In this context, we reported that reaction of C₆₀ with some morpholinoenamines proceeds via single electron transfer (SET) to give selectively monoadducts in very high yield[1].

Here, we extend this reaction to diaryl dienamines **1** derived from cycloamines and variously substituted acetophenones and report the successful formation of new [2 + 2] adduct **2** of C₆₀ with **1** in relatively high yields (up to 60%), depending on the aromatic substituents. On a radical trapping experiment with nitrosobenzene, this reaction seems to proceed via SET in a similar manner as morpholinoenamines. The NMR analysis of **2** indicated the occurrence of 1,3-proton transfer of primary [2 + 2] adducts probably catalyzed by basic morpholino group.



[1] T. Mikie, H. Asahara, K. Nagao, N. Ikuma, K. Kokubo, T. Oshima, *Org. Lett.* **13**, 4244 (2011).

Corresponding Author: N. Ikuma

Tel&Fax: +81-6-6879-4593,

E-mail: ikuma@chem.eng.osaka-u.ac.jp

Transport Characteristics of C₆₀ Photo-Polymers Fabricated by Focused Optical Vortex Irradiation

○Naoto Toriumi¹, Tatsuya Doi¹, Daiki Momiyama¹, Wataru Akiyama¹, Katsuhiko Miyamoto¹, Takashige Omatsu¹, Jonathan P. Bird², Yuichi Ochiai¹, and Nobuyuki Aoki¹

¹ Graduate School of Advanced Integration Science, Chiba University,
Chiba, 263-8522 Japan

² Department of Electrical Engineering, University at Buffalo, SUNY, Buffalo, NY
14260-1920, USA

Recently, a state of the art photo-polymerization of a C₆₀ thin film has been realized by irradiation of topological laser beam namely optical vortex (OV). Since the beam has a helical wavefront and a torque appears along the tangential direction, a confinement force can be expected along the peripheral direction of the beam and the polymerization takes a progress with a compressive photon-pressure under a high-beam-power density. Therefore, it can be expected to achieve a highly-packed and uniform photo-polymerization in a C₆₀ thin film. Moreover, combining with circular polarization, total angular momentum of light can be controlled [1].

In our study, thermally evaporated C₆₀ thin film was deposited 50 nm on a SiO₂ layer on top of a heavily doped Si substrate. A continuous-wave 532 nm laser beam was used for the optical source. The OV was produced by using a spiral phase plate and irradiated onto the sample through an objective lens.

We observed electric properties of C₆₀ thin film polymerized by OV irradiation and a peak shift of Raman spectrum corresponding to A_g(2) mode suggests a polymerization of the C₆₀ molecule [2]. Moreover, no significant cracks were confirmed in the polymerized region by OV. Therefore, non-conventional polymerization regime can be expected in the photo-polymer by OV irradiation. However, these characteristics have been confirmed in air after soaked in toluene for 3 minutes to remove non-polymerized C₆₀ films on the sample surface.

As the following step, we are trying to have in-site measurements of electric conduction properties just after the OV irradiation. Moreover, dose amount dependence of the transport properties and the thickness of the polymerized region will be discussed in the presentation.

[1] T. Omatsu *et al.*, Opt. Express **18** (2010) 17967.

[2] S. J. Duclos *et al.*, Solid State Commun. **80** (1991) 481.

Corresponding Author: N. Aoki
Tel: +81-43-290-3430, Fax: +81-43-290-3427,

E-mail: n-aoki@faculty.chiba-u.jp

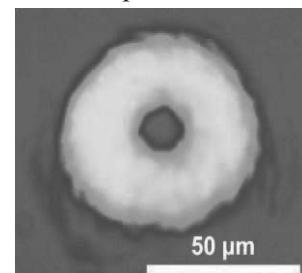


Fig1. Circular pattern on a C₆₀ thin film by OV irradiation.

Fabrication of bulk-heterojunction organic solar cells using PCBM and mixed donors of P3HT and phenylene–thiophene oligomer

○Shunjiro Fujii^{1,2}, Zongfan Duan³, Takanori Okukawa⁴, Yuichiro Yanagi⁴, Akira Yoshida⁴, Takeshi Tanaka¹, Yasuhiro Nishioka⁴, and Hiromichi Kataura^{1,2*}

¹Nanosystem Research Institute, National Institute of Advanced Industrial Science and Technology (AIST), Ibaraki 305-8562, Japan ²JST, CREST, Kawaguchi 330-0012, Japan ³School of Materials Science and Engineering, Xi'an University of Technology, Xi'an 710048, China ⁴Nihon University, Funabashi, Chiba 274-0851, Japan

Organic solar cells (OSCs) are of special interest owing to their advantages of low-cost and solution-processable fabrications. Each material for OSCs has different spectral sensitivity characteristics. Since the spectral distribution of sunlight has the maximum intensity around the wave length of 450 nm, OSCs are expected to have maximum incident photon-to-current conversion efficiency (IPCE) around 450 nm. Recently, we have reported the OSCs using a new phenylene-thiophene oligomer (PTO shown in Figure 1) as an electron donor [1]. The bulk-hetero junction (BHJ) OSCs fabricated from PTO and [6,6]-phenyl C61 butyric acid methyl ester (PCBM) showed a maximum IPCE around 400 nm. To improve the performance, the wavelength range of IPCE spectra is required to be widen and adjusted to the sunlight spectra. In this study, we fabricated BHJ-OSCs using two donors of PTO and poly(3-hexylthiophene) (P3HT), which have the maximum IPCE around 400 nm and 500 nm [2], respectively.

The active layers of BHJ-OSCs were fabricated by spincoating mixed solutions of chloroform solvent. The measured IPCE spectra of the OSCs using the two donors showed the maximum sensitivity around 450 nm, and had a wider sensitivity range (Figure 2). As a result, the OSC using the blend film of mixed donors and PCBM showed a power conversion efficiency of 0.90%, which was higher than that of PTO and PCBM (0.47%) or P3HT and PCBM (0.65%). In this presentation, detailed characteristics of the OSCs will be discussed.

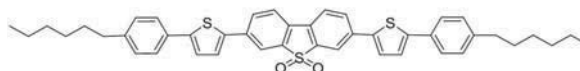


Figure 1 Molecular structure of oligomer

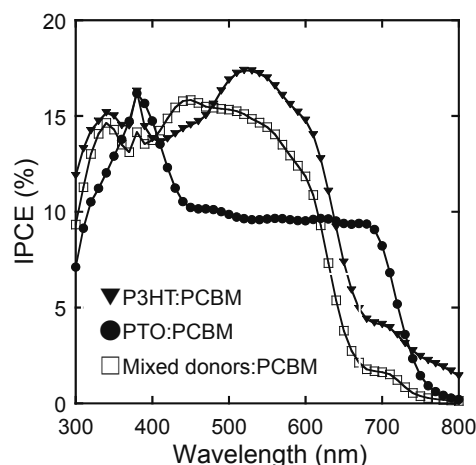


Figure 2 IPCE spectra of the OSCs with different active layers in the configuration of Glass/ITO/ PEDOT:PSS/active layer/Al.

[1] Z. Duan et al., Chem. Lett. 41, 363 (2012)

[2] F. Padinger et al., Adv. Funct. Mater., 13, 85 (2003)

Corresponding Author: Hiromichi Kataura
Tel: +81-29-861-2551, Fax: +81-29-861-2786,
E-mail: h-kataura@aist.go.jp

Reaction of Trimetallic Nitride Template-endohedral Metallofullerene (TNT-EMFs) with Aziridine

○Masato Kimura¹, Chihiro Ueda², Michio Yamada², Yutaka Maeda², Tadashi Hasegawa², Takeshi Akasaka¹

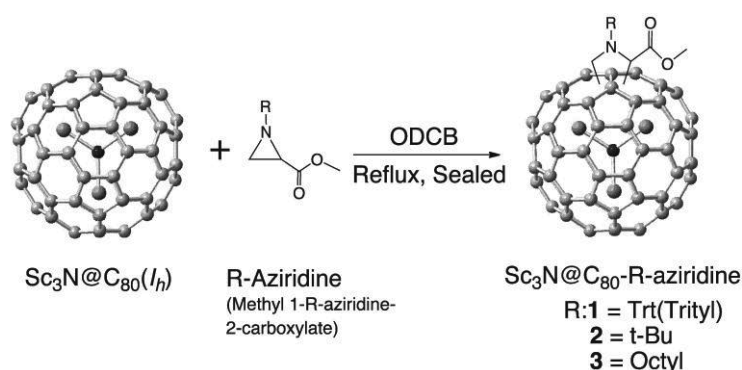
¹ Life Science center of Tsukuba Advanced Research Alliance, University of Tsukuba, Tsukuba, Ibaraki 305-8577, Japan

² Department of Chemistry, Tokyo Gakugei University, Koganei, Tokyo 184-8501, Japan

Endohedral Metallofullerenes (EMFs) have attracted interest for specific physical and chemical properties, as the result of electron transfer between the encapsulated metal species and the fullerene cage. Especially, TNT-EMFs, which encapsulated M₃N cluster, e.g. Sc₃N@C₈₀, are promising candidates for practical application in material science and biological science, because of its higher production yield than any other EMFs. For practical application, such as organic photovoltaic cells, it is essential to control its solubility or electronic properties by chemical modification. Prato et al. reported the reaction of C₆₀ or SWNTs with aziridine afford corresponding adducts.^[1] We focus on the aziridine, precursor of azomethyne ylide, for functionalization of metallofullerenes, because of the convenient synthesis of aziridine with various functional groups.

Herein, we report the reaction of TNT-EMFs, Sc₃N@C₈₀ with aziridine derivatives and characterization of **2**, **3** by HPLC, MALDI-TOF Mass, Vis-NIR, NMR, and electrochemical measurements.

Scheme 1



Reference

[1] Prato et al. *J. Am. Chem. Soc.* **2007**, *129*, 14580.

Corresponding Author: Takeshi Akasaka

Tel: +81-29-853-6409, **Fax:** +81-29-853-5881, **E-mail:** akasaka@tara.tsukuba.ac.jp

Extraction of unstable di-metallofullerenes using a mixed solvent of triethylamine and acetone

○Aimi Togashi, Takeshi Kodama, Wataru Fujita, Koichi Kikuchi, Yohji Achiba

Department of Chemistry, Tokyo Metropolitan University, Hachioji, 192-0397, Japan

$C_{80}(I_h)$ fullerene cage has been well known to be stabilized by transferring 6 electrons from the multiple metal atoms encapsulated inside the cage such as La_2 or Ce_2 . Actually, $La_2@C_{80}$ or $Ce_2@C_{80}$ species is easily extracted by conventional organic solvents such as CS_2 or 1,2,4-trichlorobenzene (TCB). However, until quite recently, the presence of $Y_2@C_{80}$ and $Sc_2@C_{80}$ has never been distinguished by the usual extraction method. In 2011, Kodama et al. have demonstrated for the first time that even $Y_2@C_{80}$ is able to be extracted by using a mixed solvent consisting of triethylamine (TEA) and acetone[1]. The differences in π electronic properties of the $C_{80}(I_h)$ common cage have strongly been suggested to give a significant influence on the extraction behaviors observed between La and Y systems. In this study, with use of a mixed solvent mentioned above, we have intended to extract $LaY@C_{80}$ as well as $Sc_2@C_{80}$ those have never been extracted so far by conventional organic solvents.

Soot containing metallofullerenes was produced by direct-current (60 A) arc discharge of La/Y/C composite rods (La:Y:C=1:1:98) or Sc/C composite rods (Sc:C=2:98) under a 500 torr He atmosphere. The raw soot was divided into two parts and each part was extracted for 8h with a mixed solvent of TEA and acetone or with TCB, respectively. Fig. 1 shows the typical LD-TOF-MS spectra of the mixed solvent extract and the TCB extract for LaY-metallofullerenes, and Fig. 2 shows the ones for Sc-metallofullerenes. The signals of $LaYC_{80}$ or Sc_2C_{80} are found in the mixed solvent extract, not in the TCB extract. Therefore, it is suggested that the two metal atoms are encapsulated in $C_{80}(I_h)$ for $LaYC_{80}$ and Sc_2C_{80} .

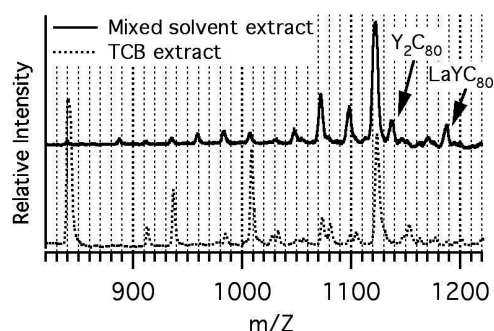


Fig. 1 LD-TOF-MS spectra of extracts for LaY-metallofullerenes.

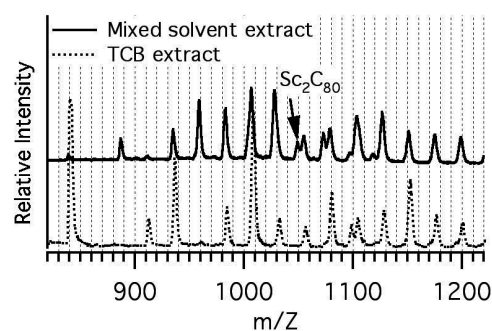


Fig. 2 LD-TOF-MS spectra of extracts for Sc-metallofullerenes.

[1] T. Kodama, et al. *The 41st Fullerenes-Nanotubes-Graphene General Symposium* 31 (2011).

Corresponding Author: Takeshi Kodama

E-mail: kodama-takeshi@tmu.ac.jp

Tel:+81-42-677-2530, Fax:+81-42-677-2525

Spin Configurations of Three Radicals on Fullerenes○Susumu Okada^(a) and Takahiro Yamamoto^(b)

(a) *Graduate School of Pure and Applied Sciences, University of Tsukuba, Tennodai, Tsukuba 305-8577, Japan*

(b) *Department of Liberal Arts (Physics), Faculty of Engineering, Tokyo University of Sciences, Kudanshita, Chiyoda Ku, Tokyo 102-0073, Japan*

Electronic structure of carbon allotropes with three-fold coordination is known to depend on their morphology, dimensionality, size, and boundary condition. Indeed, chemical modifications on fullerenes result in interesting π electron systems on the spherical networks. For instance, C_{60} derivatives with conical shape have been synthesized by attaching five aromatic molecules to C_{60} . Furthermore, deca-organo C_{60} have been also synthesized. In these materials, the aromatic molecules attached to C_{60} certainly modify the spherical π electron system of C_{60} . In the case of deca-organo C_{60} , attached aromatic molecules divide spherical π electron system into three parts: a short armchair nanotube and two pentagonal rings surrounded by molecules. According to these two pentagonal rings, this C_{60} derivative has two radical spins localized at these pentagonal, which are expected to possess interesting mutual arrangements. In this work, we aim to investigate the spin configuration of a radical spin trimer on fullerene surfaces by using both first-principles total-energy calculations and analytic calculations.

Our first-principles calculations show that the three radical spins exhibit peculiar spin-density distributions that are difficult to understand in terms of a classical spin picture. To reveal physical origin, we have analyzed the peculiar spin-density distributions based on a quantum spin model consisting of $S=1/2$ spins localized at the corners of a triangle. As a result, the spin-density distributions obtained by the first-principles calculations were well reproduced by the quantum spin model. In addition, we found from the model analysis that the modulation of exchange coupling between the spins induces a rich variety of spin configurations.

Corresponding Author: S. Okada

Tel: +81-29-853-5921, Fax: +81-29-853-5924,

E-mail: sokada@comas.frsc.tsukuba.ac.jp

Magnetic Properties of Deca-Methyl Fullerenes

○Haruna Nitta^a, Yutaka Matsuo^b, Eiichi Nakamura^b, Susumu Okada^a

^a *Graduate School of Pure and Applied Sciences, University of Tsukuba,
1-1-1 Tennoudai, Tsukuba, Ibaraki 305-8571, Japan*

^b *Department of Chemistry, The University of Tokyo, Hongo, Bunkyo-ku, Tokyo 113-0033, Japan*

It is known that electronic states of nanoscale materials consisting of sp^2 carbon atoms, such as grapheme nanoribbons, carbon nanotubes and fullerenes, strongly depend on their network topologies and dimensionalities. In addition to the intrinsic diversity of electronic structure of these carbon allotropes, both physical and chemical modifications also lead to unusual electronic properties on resultant systems. Indeed, C_{60} derivatives with conical shapes have been synthesized under controlled modifications of C_{60} by attaching five aromatic molecules [1] and have been reported to possess peculiar electronic structures. In addition to the penta-organo C_{60} , selective multiadditions of organic molecules to C_{60} and large fullerenes lead to many fullerene derivatives with interesting morphologies [2]. In this work, we study geometric and electronic structures of deca-methyl fullerenes, $(Me)_{10}C_{60}$, $(Me)_{10}C_{70}$, $(Me)_{10}C_{80}$, based on density functional theory. To investigate the interaction between radical spins on these deca-methyl fullerenes, we use local spin density approximation (LSDA) for the exchange correlation potential among the interacting electrons.

Our calculations clarified that the chemical adsorption of methyl groups results in segmentation of a spherical π electron system of fullerenes: Two pentagonal rings are isolated from the remaining sp^2 network leading to the spin polarization which are coupled in parallel and antiparallel arrangements. Further calculations unraveled that the antiparallel spin arrangement is the ground state for deca-methyl C_{60} s. With increase the size of fullerene, energy difference between the parallel and antiparallel arrangements decreases. In the case of the deca-methyl C_{70} , these two states almost degenerate each other indicating that the radical spins are freely arranged. Further increase the size, in the case of the deca-methyl C_{80} , the parallel arrangement is energetically favorable due to the substantial hybridization with the π states on a hexagonal network at the C_{80} equator. The facts indicate that the radical spin interaction on deca-methyl fullerenes is tunable by controlling the chemisorption site and the fullerene size.

References

[1] M. Sawamura, K. Kawai, Y. Matsuo, K. Kanie, T. Kato, and E. Nakamura: *Nature* **419**, (2003) 702.

[2] Y. Matsuo and E. Nakamura: *Chem. Rev.* **108** (2008) 3016.

Corresponding Author: H.Nitta

Tel: +81-29-853-5921, Fax: +81-29-853-5924,

E-mail: sokada@comas.frsc.tsukuba.ac.jp

Synthesis of non-IPR fullerenes from C₆₀ in liquid phase by irradiation of intense femtosecond laser pulses

○Takeshi Kodama, Tatsuya Fujino, Haruo Shiromaru, Yohji Achiba

Department of Chemistry, Tokyo Metropolitan University, Hachioji, 192-0397, Japan

Recently, the use of ultrashort pulsed lasers with extremely high intensity electric field have been started for the study of a new type of chemical reaction. In the field of carbon cluster science, polyynes were successfully synthesized by the femtosecond laser irradiation to organic solvents without any additional introduction of carbon sources[1,2]. Under such extreme laser condition, it has been believed that the atomization of solvent molecules and reconstruction of new C-C network formation take place very efficiently, resulting in the production of polyynes even in liquid phase. So the questions might arise what would happen when the ultrashort pulsed laser is irradiated to the fullerene cage in liquid phase.

According to our previous experiment[3], the irradiation of the femtosecond laser to the C₇₀ toluene solution, the black powder-like materials were generated and the mass spectroscopic analysis of these materials revealed that the C₆₈, C₆₆ and C₆₄ species were generated. Therefore, it was suggested that the successive C₂-loss process occurs and the resulting chemically unstable C₆₈, C₆₆ and C₆₄ would be easily changed into insoluble aggregates. In this study, we try to synthesize non-IPR fullerenes, C₅₈, from C₆₀ in liquid phase, because the isomer (#1205) with C_{3v} symmetry is expected as an energetically stable non-IPR fullerene via a C₂ ejection from C₆₀.

Fig. 1 shows the absorption spectra of C₆₀ before and after laser irradiation in toluene solution. After 10 min irradiation, characteristic peaks of C₆₀ almost disappear and the baseline becomes to be risen. Further 20 min irradiation gives rise of returning the baseline back to almost zero and black powder-like materials start to appear. The phenomenon of the rise of base line before 10 min irradiation suggests that some soluble non-IPR fullerenes are generated at the initial state.

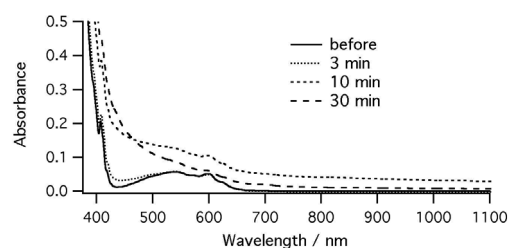


Fig. 1 Absorption spectral changes of C₆₀ before and after irradiation in toluene solution.

[1] A. Hu, et al. *Carbon* **46**, 1823 (2008).

[2] Y. Sato, et al. *Carbon* **48**, 1673 (2010).

[3] T. Kodama, et al. *The 40th Commemorative Fullerenes-Nanotubes General Symposium* 187 (2011).

Corresponding Author: Takeshi Kodama

E-mail: kodama-takeshi@tmu.ac.jp

Tel:+81-42-677-2530, Fax:+81-42-677-2525

Interaction of carbon nanotubes with homopolypeptides

○Atsushi Hirano ¹, Tomoshi Kameda ², Takeshi Tanaka ¹, Hiromichi Kataura ¹

¹ *Nanosystem Research Institute, National Institute of Advanced Industrial Science and Technology, Tsukuba, Ibaraki 305-8562, Japan*

² *Computational Biology Research Center, Advanced Industrial Science and Technology, Koto, Tokyo 135-0064, Japan*

With the progress of nanotechnology, nanoparticles including carbon nanotubes have raised concerns regarding the environmental and health issues. It is known that nanoparticles are associated with protein molecules in the biological systems once they are taken into the systems. The complexes of nanoparticles with proteins are termed “protein coronas” which are considered to be related with cytotoxicities [1]. Clarifying the mechanism of the formation of protein coronas is one of the important subjects in the development of the nanotechnology.

Several recent studies have showed that carbon nanotubes are associated with proteins and dispersed by them [2]. In particular, lysozyme, which is a protein from egg white, was found to interact with carbon nanotubes mainly through arginine residues by molecular dynamics (MD) simulation [3]. We also obtained a similar result about the interaction of the arginine residues with carbon nanotubes using MD simulation as a preliminary study (Figure 1). Thus, arginine is considered to play an important role in the interaction of protein with carbon nanotubes.

In this study, we compared the effect of poly-L-arginine (poly-R) on the dispersion of carbon nanotubes to that of poly-L-lysine (poly-K) for clarifying the side chain effect of arginine. Figure 2 shows spectra of carbon nanotubes dispersed by poly-R and poly-K. The amount of carbon nanotubes dispersed by poly-R was more than that by poly-K in the molecular weight range studied, indicating the affinity of arginine with carbon nanotubes. We will show the molecular mechanism of the interaction of arginine with carbon nanotubes obtained by experiments and MD simulations.

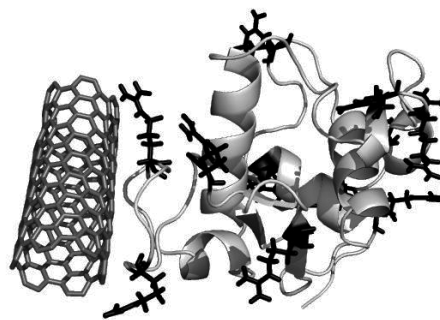


Fig. 1 Interaction of lysozyme with carbon nanotubes. Side chains of arginine are depicted by black sticks.

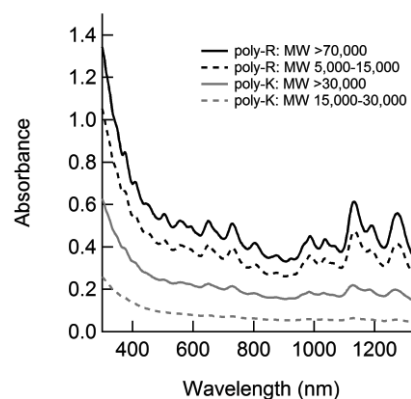


Fig. 2 Absorption spectra of carbon nanotubes dispersed by the homopolypeptides.

[1] T. Cedervall *et al.* Proc. Natl. Acad. Sci. USA **104**, 2050 (2007)

[2] A. Hirano *et al.* Langmuir **26**, 17256 (2010)

[3] M. Calvaresi *et al.* Chem. Eur. J. **18**, 4308 (2012)

Corresponding Author: T. Tanaka

Tel: +81-29-861-2903, Fax: +81-29-861-2786,

E-mail: tanaka-t@aist.go.jp

Molecular recognition of external grooves on bundled surfaces of single-walled carbon nanotubes

○JongTae Yoo¹, Tsuyohiko Fujigaya^{1,2}, and Naotoshi Nakashima^{1,2,3}

¹Department of Applied Chemistry, Graduate School of Engineering, Kyushu University, 744 Motoooka, Fukuoka 819-0395, Japan

²World Premier International (WPI), International Institute for Carbon-Neutral Energy Research, Kyushu University 744 Motoooka, Nishi-ku, Fukuoka 819-0395, Japan

³Japan Science and Technology Agency, CREST, 5 Sanbancho, Chiyoda-ku, Tokyo, 102-0075, Japan

Cylindrical and curvature structure of single-walled carbon nanotubes (SWNTs) often makes clear difference over planer analogues. Recently, one-dimensional nano-spaces in the bundle of SWNTs such as interstitial channel and external groove attract attentions in experimentally and theoretically due to their intense van der Waals interaction with molecules. Here, we investigated an effect of SWNT bundle for SWNT-molecular interaction using the affinity chromatography [1] incorporating SWNT bundles as a stationary phase.

In a preparation of the stationary phase, different concentrations of SWNT dispersions in 1-methyl-2-pyrrolidinone (NMP) were mixed with silica sphere and the precipitates were collected [2]. As shown in SEM images, bundled structures of SWNTs were observed on the silica surface prepared from higher concentration (**Fig. 1B**), while such a structure was hardly seen on that from lower one (**Fig. 1A**).

Quite interestingly, we noticed the changes of the order of retentions between isolated and bundled SWNTs caused by the unusual behavior of *p*-terphenyl in the chromatograms (**Fig. 2**) and the result suggests the specific recognition of bundled SWNTs for *p*-terphenyl. We consider that *p*-terphenyl strongly interacts with the one-dimensional external groove in the SWNT bundle due to its structure.

We believe that this unique aspect will provide a promising feature for new applications of SWNTs.

[1] J. Yoo et al., *Nanoscale* **2011**, 3, 2517.

[2] T. Fujigaya et al., *Carbon* **2011**, 49, 468.

Corresponding Author: Naotoshi Nakashima

E-mail: nakashima-tcm@mail.cstm.kyushu-u.ac.jp

Tel & Fax: +81-92-802-2842

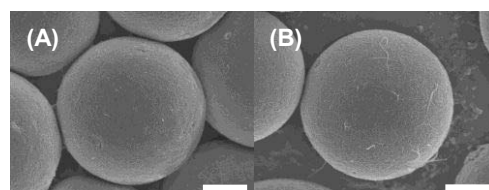


Fig. 1 SEM images of silica gel coated by (A) isolated and (B) bundled SWNTs. Scale bars: 1 μm .

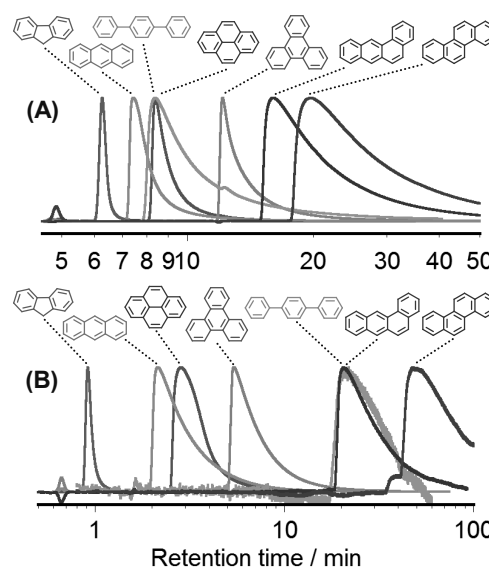


Fig. 2 Chromatograms of PAHs using (A) isolated and (B) bundled SWNTs as stationary phase at flow rates of (A) 0.1 and (B) 0.7 mL/min.

Enhancement of photoluminescence from single-walled carbon nanotubes by photonic crystal nanocavities

Ryosuke Watahiki¹, Takashi Shimada¹, Pei Zhao², Shohei Chiashi², Satoshi Iwamoto³, Yasuhiko Arakawa³, Shigeo Maruyama², and Yuichiro K. Kato¹

¹ *Institute for Engineering Innovation, The University of Tokyo, Tokyo 113-8656, Japan*

² *Department of Mechanical Engineering, The University of Tokyo, Tokyo 113-8656, Japan*

³ *Institute of Industrial Science, The University of Tokyo, Tokyo 153-8505, Japan*

Single-walled carbon nanotubes are bright nanoscale emitters, whereas photonic crystal nanocavities offer the possibility for efficient optical coupling at the nanoscale because of their small mode volumes and high quality factors. Here we report on the enhancement of photoluminescence from single-walled carbon nanotubes by L3 cavities in hexagonal lattice photonic crystals [1]. Free-standing photonic-crystal membranes are fabricated from silicon-on-insulator substrates, and micelle-encapsulated carbon nanotubes are dispersed on the devices. We observe sharp peaks with a typical spectral width of a 0.37 nm which corresponds to a quality factor of 3,800. As the peaks appear at wavelengths longer than those of Si photoluminescence, they are attributed to carbon nanotube emission coupled to the microcavity modes. We find that the photoluminescence intensity is enhanced by more than a factor of 50 compared to luminescence from a slab area.

This work is supported by SCOPE, Casio Science Promotion Foundation, Global COE and Photon Frontier Network Programs of MEXT, Japan.

[1] R. Watahiki *et al.*, *Appl. Phys. Lett.* **101**, 141124 (2012).

Corresponding Author: Yuichiro K. Kato
Tel: +81-3-5841-7702, Fax: +81-3-5841-7772,
E-mail: ykato@sogo.t.u-tokyo.ac.jp

Effect of Solvents on Electrochemical Band Gaps of Single-Walled Carbon Nanotubes

○Daigo Miyazaki¹, Yasuhiko Hirana¹, Yasuro Niidome^{1,2}, Naotoshi Nakashima^{1,2,3}

Department of applied Chemistry, Graduate School of Engineering, Kyushu University, 744 Motoooka, Fukuoka 819-0395, Japan

²WPI-I2CNER, Kyushu University, 744 Motoooka, Fukuoka 819-0395, Japan

³CREST, Japan Science and Technology Agency, 5 Sanbancho, Chiyoda-ku, Tokyo 102-0075, Japan

The electronic properties of single-walled carbon nanotubes (SWNTs) are one of the most fundamental properties. The redox properties (i.e. electronic densities, the Fermi levels, redox potentials) of SWNTs are related to the structures of SWNTs that have a specified diameter and chiral angle uniquely related to a pair of integers (n,m); the so-called chiral index. The redox properties of SWNTs are also strongly affected by the change of microenvironment conditions [1].

In this study, we have found that the electrochemical band gaps (ΔE_{electr}) of (n,m)SWNTs were strongly affected by the change of solvents. To determine the redox properties of SWNTs, in situ photoluminescence (PL) spectroelectrochemistry [2] of the films containing fifteen isolated (n,m)SWNTs cast on ITO electrodes was carried out in organic solvents to obtain ΔE_{electr} and Fermi levels of the (n,m)SWNTs (Fig.1). We have discovered that the ΔE_{electr} of the (n,m)SWNTs became greater as the solvent dipole moment of the SWNTs increased, which is in sharp contrast to the optical band gaps that show virtually no solvent dependence. Such a strong solvent dependence of ΔE_{electr} is due to the difference in the solvation energy of the charged SWNTs produced during the electrochemical oxidation or reduction of SWNTs. The present study provides useful information for a deep understanding of the fundamental electronic properties of isolated (n,m)SWNTs in solvents and is a key to the modulation of ΔE_{electr} of (n,m)SWNTs.

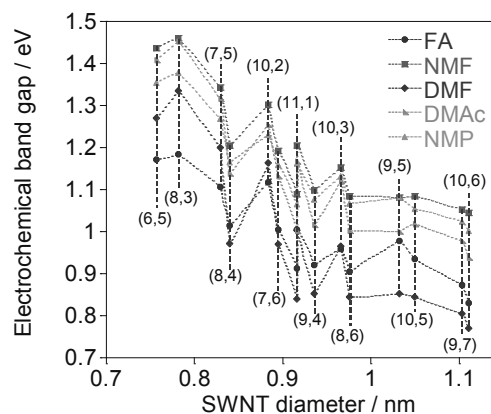


Fig. 1 Electrochemical band gaps of isolated (n,m)SWNTs in given solvents.

[1] Y. Hirana, Y. Tanaka, Y. Niidome, N. Nakashima et al. *J. Am. Chem. Soc.* **2010**, *132*, 13073-13077.

[2] Y. Tanaka, Y. Hirana, Y. Niidome, K. Kato, S. Saito, N. Nakashima, *Angew. Chem. Int. Ed.* **2009**, *48*, 7655-7659

Corresponding Author: Naotoshi Nakashima

E-mail: nakashima-tcm@mail.cstm.kyushu-u.ac.jp

Tel&Fax: +81-92-802-2840

Effects of OPO Laser Irradiation on the Structural Characteristics of Single- and Double-Walled Carbon Nanotubes

Tetsuya Oto, Akira Kumazawa, Yuka Nagaya, Koji Tsuchiya, Tadahiro Ishii, and Hirofumi Yajima

*Department of Applied Chemistry, Faculty of Science, Tokyo University of Science
1-3 Kagurazaka, Shinjuku-ku, Tokyo 162-8601, Japan*

As-synthesized single-walled carbon nanotubes (SWNTs) consist of various chiral structures responsible for metallic (m) and semiconducting (s) SWNTs. Selective separations of m- and s-SWNTs have been requested for practical and advanced applications. Thus, we have developed a new and promising selective separation technique for m-SWNTs with nanosecond pulsed optical parametric oscillator (OPO) laser operated with wavelength tunability.¹⁾ In the previous Conference, we have presented the effects of the laser wavelength and power on the selective separations of m-SWNTs from individually dispersed SWNTs with the dispersants such as carboxymethylcellulose (CMC) and sodium dodecylbenzenesulfonate (NaDDBS) in aqueous solutions.²⁾ Individually dispersed SWNTs exhibited the UV-vis-NIR absorption spectra with the characteristic peaks in three band regions (400-1600 nm) corresponding to m-SWNTs first transitions (M_{11}), and s-SWNTs first (S_{11}) and second (S_{22}) transition bands, respectively. The OPO laser with a peak wavelength in the S_{11} or S_{22} region brought merely about the destruction of the dispersed s-SWNTs through photo-thermal conversion process, while the m-SWNTs remained unchanged owing to their high thermal conductivity function. In the CMC dispersion system, the maximum collection efficiencies for m-SWNTs were achieved under the condition of a laser fluence of 6.4 MW/cm^2 at 778 nm (S_{22}) and 19.1 MW/cm^2 at 989 nm (S_{11}).²⁾ In the present study, in order to gain further insight into the effectivity of OPO laser irradiation for selective chirality separation of SWNTs and DWNTs, we focus on the resonance transition effect of the laser irradiation on SWNTs and DWNTs in their dispersion and solid states. Consequently, the 507 nm (M_{11})-laser irradiation to the solid state of as-synthesized SWNTs induced a decrease in the absorption peaks corresponding to m-SWNTs, while the peaks corresponding to s-SWNTs hardly changed. This result suggests that the separation of s-SWNTs from as-synthesized SWNTs can be achieved through the laser irradiation to the solid state of SWNTs.

1. I. Tajima et al. The 36th Fullerenes-Nanotubes General General Symposium (2009) 3P-5.
2. A. Kumazawa et al., The 40th Fullerenes-Nanotubes General General Symposium (2011) 2P-24.

*Corresponding Author: Hirofumi Yajima

TEL: +81-3-3260-4272(ext.5760), FAX: +81-3-5261-4631, E-mail: yajima@rs.kagu.tus.ac.jp

Vernier spectrum in finite-length armchair carbon nanotubes

○Yuki Tatsumi, Wataru Izumida, Riichiro Saito

Department of Physics, Tohoku University, Sendai, 980-8578, Japan

Many experiments of the transport through single-wall carbon nanotubes exhibit four-fold degeneracy reflecting the combination of the spin degeneracy and the valley degeneracy of the K and K' points in the Brillouin zone. However, some of the experiments show a gate voltage dependence of the degeneracy, for instance, two- and four-fold degeneracies alternately appear[1]. The recent theoretical study shows that the Fermi velocity of the right-going wave is different from that of left-going wave because of the curvature of the nanotube surface[2]. It has been argued that an effect of the velocity difference would appear as a vernier spectrum in a finite-length nanotube, in which the two- and four-fold degeneracies alternately appear as a function of the energy. The scenario of the vernier spectrum is as follows. A standing wave as a linear combination of a right- (left-) going wave in the K valley and a left- (right-) going wave in the K' valley would be an eigenfunction for the finite-length nanotube. The wave number is quantized because of the finite length and then the linear bands are quantized. There are two level separations reflecting the two different velocities. Therefore the system shows a vernier-like energy spectrum. However, it is not clear what conditions, for instance, which chirality and what type of the boundary conditions, are needed for the above scenario of the wavefunction. Here we perform a numerical calculation for finite-length armchair nanotubes, in which large difference of the velocities is expected, to study conditions of appearance of the vernier spectrum.

Energy spectrum, $\{\varepsilon_n\}$, for (5,5)-armchair nanotube near the half-filling is shown in Fig. 1 (a). The calculation is done for a tight-binding model with the nanotube length of 200nm. The ends of the nanotube are terminated by hydrogen atoms. The vernier-like spectrum is clearly seen: large and small peak separations appear alternately. Addition energy, $\mu_{n+1}=\varepsilon_{n+1}-\varepsilon_n$, shown in Fig. 1 (b) clearly exhibits the oscillatory behavior of the peak separation. It is confirmed that each wavefunction consists of a right- (left-) going wave in the K valley and a left- (right-) going wave in the K' valley. The vernier spectrum is also observed for a capped nanotube. An effective one-dimensional model explains the microscopic mechanism of the energy spectrum in finite-length armchair nanotubes.

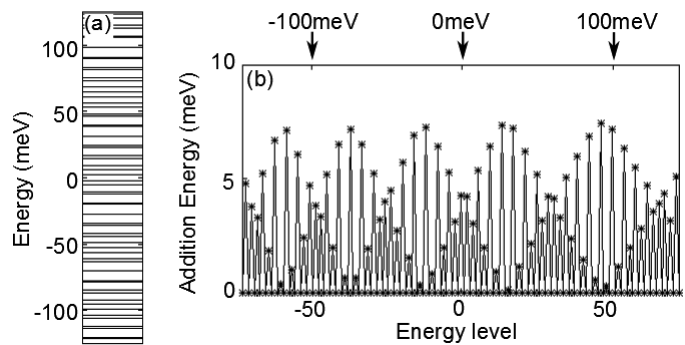


Fig. 1 (a) Energy spectrum for (5,5) armchair nanotube of length 200nm, near the half-filling, $\varepsilon=0$, and (b) addition energy. Each level is labeled by an integer number from HOMO of $n=0$ with ascending order of the energy. Note that $\mu_n=0$ for every two levels because of the two-fold degeneracy of the spin degree of freedom.

[1] A. Makarovski *et al.* Phys. Rev. B **74**, 155431 (2006), [2] W. Izumida *et al.* Phys. Rev. B **85**, 165430 (2012).

Corresponding Author: W. Izumida,

Tel: +81-22-795-6475, Fax: +81-22-795-6447, E-mail: izumida@cmpt.phys.tohoku.ac.jp

First-principles study of radial breathing modes in small-diameter carbon nanotubes

○Takashi Koretsune and Susumu Saito

Department of Physics, Tokyo Institute of Technology, Tokyo 152-8551, Japan

Radial breathing modes (RBMs) in carbon nanotubes (CNTs) play important roles for characterizing individual CNTs. There are several well-known empirical relations between frequencies of RBMs and diameters of CNTs. In small-diameter nanotubes, however, each RBM can deviate from the relations due to the curvature effect. Therefore, it is important to study this deviation from first principles. Furthermore, even in large-diameter nanotubes, it is not well understood to what extent the first-principles study can explain the empirical relations for all the nanotubes. To discuss RBMs in various situations such as carrier doping or encapsulation of molecules, it is of great importance to clarify the ability of predicting RBMs from first principles. Here, we demonstrate that the first-principles study based on the density-functional theory can actually predict RBMs in quite good accuracy by using two methods: the conventional plane-wave based method for small-diameter tubes and the method utilizing helical symmetry for large-diameter tubes.

Figure 1 shows the calculated RBMs for small-diameter nanotubes. It is found that the RBMs actually deviate from the empirical relations. In general, tubes with larger chiral angle have larger RBMs. We will discuss the reason of this chiral angle dependence.

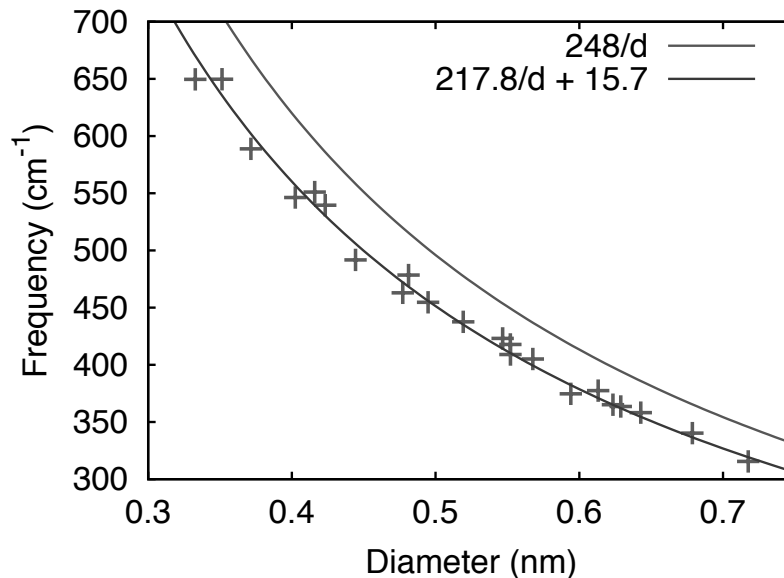


Fig. 1 Frequencies of RBMs for small-diameter nanotubes.

E-mail: koretune@stat.phys.titech.ac.jp

Electronic Properties of Capped Carbon Nanotubes with Accumulated Electrons by a Parallel Electric Field

○Ayaka Yamanaka, Susumu Okada

Graduate School of Pure and Applied Sciences, University of Tsukuba, Tennodai, Tsukuba 305-8577, Japan

In this decade, carbon nanotubes are attracting much attention due to its possible application for semiconductor electronic devices in the next generation. Therefore it is urging us to unravel fundamental properties of carbon nanotubes under an electric field for designing and fabricating nanotube-based electronic devices. In this work, we study the electronic properties of finite-length carbon nanotubes whose edges are capped by C_{60} hemispheres to unravel the effects of the external electric field on charge accumulation.

All calculations are performed by using the density functional theory. To express the exchange correlation potential among interacting electrons, we apply the local density approximation. We use an ultrasoft pseudopotential to describe the interaction between valence electrons and ions. The effective screening medium (ESM) method is applied to investigate behaviors of carbon nanotubes under the electric field in the framework of the first-principles calculations.

We study the electronic properties of capped finite-length armchair and zigzag nanotubes with 7-angstrom diameter under an electric field parallel to the nanotubes as shown in Fig. 1. We analyze the electrostatic potential and accumulated electrons to uncover how the nanotubes response to the electric field. By analyzing the calculated potential, we find that the potential modulation only occurs around the cap region (Fig. 2). We also find that injected electrons are accumulated around the cap region. The analyses unravel that there is a correlation between electrostatic potential and distribution of accumulated electrons.

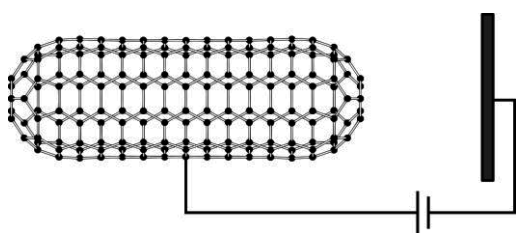


Fig.1 A structural model of nanotubes under the electric field.

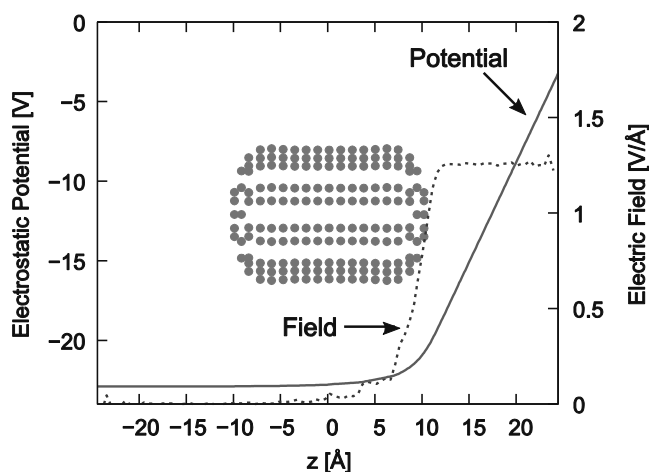


Fig.2 Plane-averaged electrostatic potential and electric field of capped carbon nanotube.

Corresponding Author: A. Yamanaka

Tel: +81-29-853-5600 (ext. 8233), Fax: +81-29-853-5924,

E-mail: ayamanaka@comas.frsc.tsukuba.ac.jp

Electronic Raman scattering and origin of the Fano resonance in metallic carbon nanotubes

○ Eddwi H. Hasdeo, Ahmad R.T. Nugraha, Kentaro Sato, and Riichiro Saito
Department of Physics, Tohoku University, Sendai 980-8578, Japan

Although most of excitonic physics in the Raman spectra of SWNTs has been investigated intensively, the origin of the asymmetric Breit-Wigner-Fano (BWF) lineshape of G-band in the metallic SWNTs (m-SWNTs) is still not well explained theoretically. Fano pointed out that the asymmetric feature of a broadened spectrum comes from interference between a discrete excitation spectrum with continuum spectra [1]. In m-SWNTs, electrons in the linear energy band plays an important role to give rise to the continuum spectra. However, the detailed mechanism remains a debatable topic [2-4]. Some reports suggest that the coupling of collective excitation (plasmon) with phonon could explain the origin of BWF asymmetry [2], and some others argue that the electron-hole pair and phonon coupling via Kohn anomaly is more dominant [3]. Farhat *et al.* have observed a new feature of the continuum spectra exclusively in m-SWNTs which is ascribed to the electronic Raman scattering (ERS) [4]. Compared to the G band, the ERS feature has broader spectral width ($\Gamma^{\text{ERS}} \sim 60 \text{ cm}^{-1}$, $\Gamma^{\text{G}} \sim 10 \text{ cm}^{-1}$) and smaller peak intensity ($I_{\text{ERS}} \sim 0.6 I_{\text{G}}$). The energy of inelastic scattered light in phonon Raman spectra changes as a function of excitation energy, while the ERS peak position does not; it keeps constant at M_{ii} (*i*-th van-Hove singularity transition energy). Therefore, instead of the phonon Raman contribution, the Coulomb interaction is relevant to the ERS. The calculated result shows that zero momentum transfer ($\mathbf{q} = 0$) vanishes in the direct Coulomb interaction because of the symmetry of the wave-function, thus a higher order Raman process is relevant to the ERS. By considering the second-order Raman process, we are able to reproduce experimental results for the ERS spectra consistently. Finally, the asymmetric BWF feature, i.e. an interference result between the G band and the ERS spectra is presented as a function of nanotube diameter and of laser excitation energy. We also theoretically predict a new feature that the RBM spectra of m-SWNTs give a similar asymmetric lineshape which requires an experimental confirmation.

[1] U. Fano, Phys. Rev. **124**, 1866–1878 (1961).

[2] S. D. M. Brown et al., Phys. Rev. B **63**, 155414 (2001), S. M. Bose et al. Phys. Rev. B **72**, 153402 (2005).

[3] M. Lazzeri et al., Phys. Rev. B **73**, 155426 (2006), Y. Wu et al. Phys. Rev. Lett. **99**, 027402 (2007).

[4] H. Farhat et al., Phys. Rev. Lett. **107**, 157401 (2011).

Corresponding Author: E. H. Hasdeo

TEL: +81-22-795-6442, FAX: +81-22-795-6447, E-mail: hasdeo@flex.phys.tohoku.ac.jp

Selective Dispersion of Single-Walled Carbon Nanotubes into Nano-Cage of Helical Conformation of Poly(*m*-phenylene-ethynylene) Derivatives

Fumito Kobayashi¹, Yuki Moriyama¹, ○Masahiro Takahashi¹,
Masayoshi Tange², Toshiya Okazaki², Keiki Kishikawa¹, Shigeo Kohmoto¹

¹ Faculty of Engineering, Chiba University, Chiba, 263-8522, Japan

² Nanotube Research Center, AIST, Tsukuba, 305-8565, Japan

As-synthesized single-walled carbon nanotubes (SWNTs) contain mixture of different diameters and chiralities. So separation of SWNTs is especially important for applications.

Diphenyl acetylene unit (*alias* Tolan) possesses small internal-rotational barrier. Corresponding Poly(phenylene-ethynylene) derivatives can be recognized as repetition of Tolan unit. Accordingly the polymers can transform into various high order structures, *i.e.* α -helix and zigzag, and random coil. Especially the α -helix structure of poly(phenylene-ethynylene) is attractive in recent years for supra molecular chemistry. The helical structure can construct at nano-cage at inner space of the helical structure. For example, polymer **1** can form nano-cage with *ca.* 0.9 nm in diameter at helical structure (Fig. 2). The nano-cage may include nano scale molecules, *i.e.* SWNTs. Further, an outside of the helical structure can be functionalized without degradation.

Poly(phenylene-ethynylene) **1** was obtained as orange solid by co-polymerization with dibromo and diethynyl compounds using of Sonogashira coupling reaction with Pd catalyst (Fig. 1, Table 1).

Table 1. Properties of polymer **1**.

$M_w^{a)}$	PDI ^{a)}	<i>n</i>
5.1×10^3	1.5 ₅	9.7

a) Measured by GPC with polystyrene standard.

Polymer **1** could stably disperse SWNTs (CoMoCAT) into THF solution. The dispersed solution show typical absorption spectra for high dispersed SWNTs. A TEM image of the cast film from the solution showed the SWNTs which was disaggregated and straightly extended for several micro meters (Fig. 3). We will report and discuss a selectivity of dispersed SWNTs with photoluminescence map.

Corresponding Author: M. Takahashi

Tel: +81-43-290-3397, Fax: +81-43-290-3401, E-mail: masahiro@faculty.chiba-u.jp

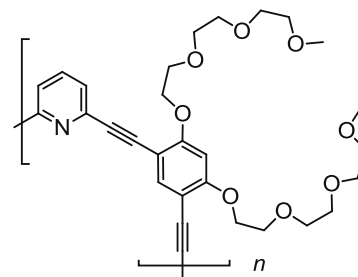


Fig.1 Poly(phenylene ethynylene) derivative **1**

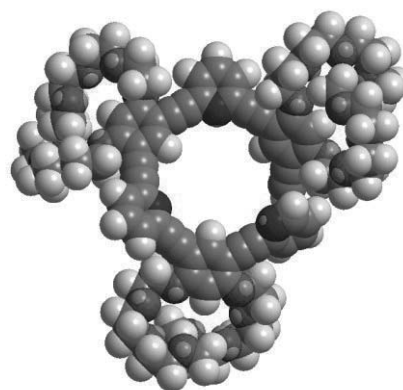


Fig. 2. Molecular modeling of oligomer of **1** (*n* = 3) optimized with MM2 calculation.

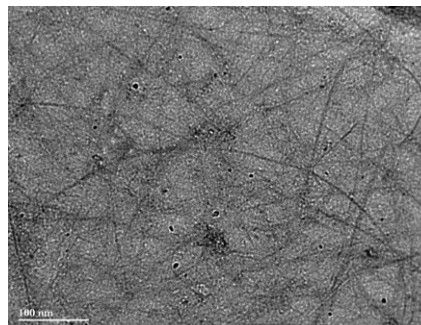


Fig. 3. TEM image of dispersed SWNTs (CoMoCAT) with **1**.

Chromatographic Separation of Highly Soluble SWNTs Prepared by Polyglycerol Grafting

○Keisuke Nakamura^{1,2}, Li Zhao¹, Shuji Aonuma², Takahide Kimura¹, Naoki Komatsu¹

¹ Department of Chemistry, Shiga University of Medical Science, Otsu, 520-2192, Japan

² Department of Materials Chemistry, Osaka Electro-Communication University, Osaka, 572-8530, Japan

For applications of nanocarbons in biology and medicine, such as imaging probe and drug carrier, they have to be solubilized in a physiological environment. Recently, we have found that surface functionalization with polyglycerol (PG) afford very good hydrophilicity to various nanocarbons (nanodiamond [1] and graphene [2]) as well as metal oxides (ZnO [3] or Fe₃O₄ [4]). In this paper, we will report PG functionalization, solubilization, and chromatographic separation of SWNTs. After cutting SWNTs through mixed acid treatment, they were functionalized with PG through ring opening polymerization of glycidol [1]. The SWNT-PG was solubilized in pure water (>8.5 mg/mL) and phosphate buffer (>8.5 mg/mL). Since these solutions were very stable without any precipitation for more than one month, they were subjected to size exclusion chromatography (SEC) to separate the SWNT-PG according to the size. Four fractions including SWNT-PG were collected and analyzed with STEM (Fig. 1) and DLS. Both the median size determined by DLS and the average length determined by STEM decreased from the fraction 1 to 4 in the SEC (Table 1).

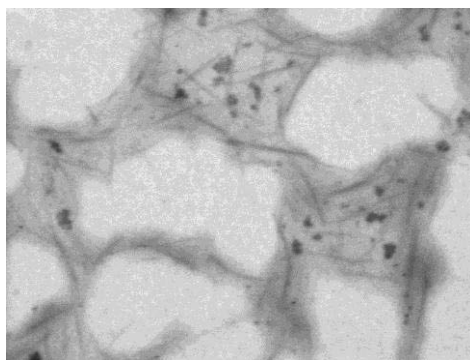


Fig. 1 STEM image of SWNT-PG after SEC separation (fraction 2).

Table. 1 Size and length of SEC-separated SWNT-PG determined by DLS and STEM, respectively.

Fraction (Retention time, min)	Median size (nm) in DLS	Average length (nm) in STEM
1 (19-20)	69	-
2 (20-21)	66	118
3 (21-22)	54	99
4 (22-23)	43	72

[1] L. Zhao, N. Komatsu, et al. *Angew. Chem. Int. Ed.*, **50**, 1388-1392 (2011)

[2] T. Yasuda, N. Komatsu, et al. The 43rd Fullerenes-Nanotubes-Graphene General Symposium, 1-14

[3] L. Zhao, N. Komatsu, et al. *J. Indian Chem. Soc.*, **88**, December, 1787-1790 (2011)

[4] L. Zhao, N. Komatsu, et al. *Adv. Funct. Mater.*, **22**, 5107-5117 (2012).

Corresponding Author: Naoki Komatsu

Tel: +81-77-548-2102, Fax: +81-77-548-2405, E-mail: nkomatsu@shiga-med.ac.jp

Electric double layer transistors of aligned carbon nanotube thin film

○Yoshifumi Wada¹, Jiang Pu², Yuki Takagi², Kazuhiro Yanagi³, and Taishi Takenobu^{1,2}

¹ *Department of Physics, Waseda University, Tokyo 169-8555, Japan*

² *Department of Applied Physics, Graduate School of Advanced Science and Engineering, Waseda University, Tokyo 169-8555, Japan*

³ *Department of Physics, Tokyo Metropolitan University, Hachioji 192-0397, Japan*

Electric double layer capacitors (EDLCs), which consist from two electrodes and electrolyte (fig.1), have huge capacitance [1]. This huge capacitance is due to very thin double charge layers formed with ions in electrolyte and carriers in electrode, which corresponds to capacitor with nano meter gap. We call this thin layer as electric double layer. Recently this EDLC is applied to MOS transistors as gate dielectric layer, which named as electric double layer transistors (EDLTs). It realized low voltage operation (< 3 V) of transistor and high carrier density at the semiconductor/electrolyte interface [2]. However, because ion movement in electrolyte is necessary to operate EDLTs, high speed operation is extremely difficult, which prevent them from actual use in electronic devices. Here we tried to investigate the ion motion in EDLC from electrochemical impedance spectroscopy (EIS) and realize 100 kHz response speed in EDLCs. Finally, we apply this structure to single-walled carbon nanotube (SWCNT) EDLTs, which is aligned by recent reported solution process [3].

We measured EIS of laminate structure EDLC using ionic liquid, 1-Ethyl-3-methylimidazolium bis(trifluoromethylsulfonyl)imide ([EMIM][TFSI]), and gold electrode. In particular, we could get high-speed response using asymmetric size electrode pair, which has different size of each electrode. With applying this structure, we realized response speed more than 100 kHz, which is very fast as EDLC.

Because we have succeeded in the fabrication of high speed EDLCs, we applied this technique into transistors. For this purpose, asymmetric structure is very important and, to fabricate asymmetric EDLTs, we used the aligned SWCNT film (fig. 2) as transistor channel because of its small channel area. Using the aligned SWCNT films and EDLT structure, we finally obtained high-response also in EDLTs, which might be 1st step for future high-speed electronics based on electrolyte.

[1] K. H. Lee *et al.*, *J. Phys. Chem. B.* **115**, 3315 (2011)

[2] S. H. Kim *et al.*, *Adv. Mater.* **17**, 1 (2012)

[3] H. Y. Li *et al.*, *J. Am. Chem. Soc.* **134**, 2760 (2012)

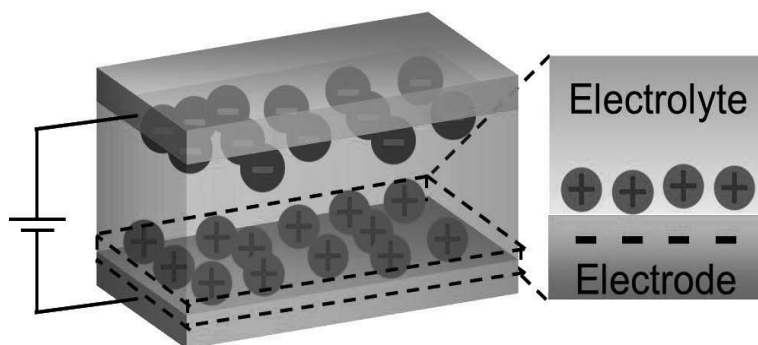


Fig.1 Electric double layer

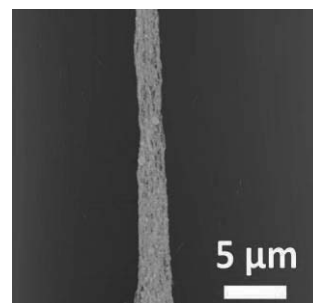


Fig.2 Aligned SWCNT film

Photo-thermoelectric power of single-walled carbon nanotube films

○Hajime Sakakibara¹, Yoshinori Sato¹, Kosuke Ino¹, Akihiko Ito²,
Tomokazu Matsue¹, Takashi Goto², Kenichi Motomiya¹, Kazuyuki Tohji¹

¹ Graduate school of Environmental studies, Tohoku University, Sendai 980-8579, Japan

² Institute for Materials Research, Tohoku University, Sendai 980-8577, Japan

Single-walled carbon nanotubes (SWCNTs) possess spike like density of states derived from one-dimensional van Hove singularity. The optical transitions occur between matching van Hove singularities in conduction and valence bands. In particular, semiconducting SWCNTs show several absorption peaks in the near-infrared light region, whereas metallic SWCNTs in the visible light region. Using their unique electric and optical characteristics, SWCNTs have been applied to photovoltaic devices as basic researches [1, 2].

Recently, it was reported that photovoltaic powers of thin SWCNT films arose when the films were asymmetrically illuminated by a near-infrared light. This photo-thermoelectric power was attributed to the temperature gradient of both ends of the film [3]. The thermal conductivity of an individual SWCNT is nearly $3500 \text{ Wm}^{-1}\text{K}^{-1}$ at room temperature [4]; on the other hand, the SWCNT mat is $35 \text{ Wm}^{-1}\text{K}^{-1}$ at room temperature [5]. Therefore, numerous tube-tube junctions are due to the dominant barriers to thermal transport in CNT mats. In this study, we investigated the influence of the different film thickness on photo-thermoelectric power of SWCNT films. In addition, we prepared thin/thick half SWCNT films with an interface of different film thickness in order to increase photo-thermoelectric power.

We prepared two type SWCNT films to measure the properties of photo-thermoelectric power of the films. One was uniform SWCNT films (Fig.1a) and the other was thin/thick half ones (Fig.1b). SWCNT films were prepared spraying SWCNTs/ethanol dispersion on a glass slide with Ag electrodes. We measured the photo-voltage and temperature difference of both ends of SWCNT films under asymmetrically solar light irradiation using an AM1.5 solar simulator with 100 mW/cm^2 . We will report the details of the results in this presentation.

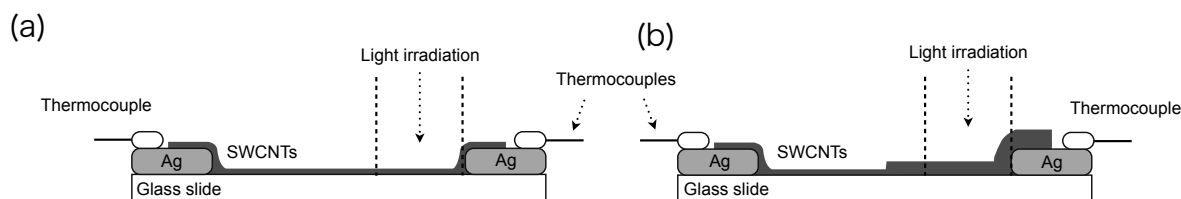


Fig.1 Schematic illustrations of (a) uniform SWCNT films cell and (b) thin/thick half ones.

- [1] K. Suzuki *et al.* Chem. Lett. **32**, 28 (2003).
- [2] Y. Jia *et al.* Adv. Mater. **20**, 4594 (2008).
- [3] M. Omari *et al.* Appl. Phys. Lett. **98**, 243113 (2011).
- [4] E. Pop *et al.* Nano Lett. **6**, 96 (2006).
- [5] J. Hone *et al.* Phys. Rev. B **59**, 2514 (1999).

Corresponding Author: Yoshinori Sato

Tel: +81-22-795-3215, Fax: +81-22-795-3215,

E-mail: hige@ncsimd.kankyo.tohoku.ac.jp

Specific biosensor based on biotin-labeled double-walled carbon nanotube FET

○Akihiro Kuno^{1,2}, Yuka Nagaya¹, Koji Tsuchiya¹, Akira Hida²
Koji Ishibashi², and Hirofumi Yajima¹

¹ *Department of Applied chemistry, Tokyo University of Science, Tokyo 162-8601, Japan*

² *Advanced Device Laboratory, RIKEN, Saitama 351-0198, Japan*

Biosensor devices based on carbon nanotube field effect transistors (CNT-FETs) are expected to be used as highly sensitive biosensing. Biosensing using CNTs has various advantages such as one-dimensional channel, high carrier mobility, and large surface area to volume ratio. Thus, highly sensitive and various types of single-walled CNT-FET biosensors have been reported [1]. Double-walled carbon nanotubes (DWCNTs) also have a potential for biosensors because of their unique inner-outer structure. Even if the outer layer is damaged due to surface modification, the electrical properties of the inner layer are protected by the outer layer.

In this study, we report the biosensing based on biotin-labeled DWCNT-FET. DWCNTs were oxidized by mixture of sulfuric acid and nitric acid (3:1) to create carboxyl groups on their surface. The oxidized DWCNTs were then allowed to react with 5-(biotinamido)pentylamine through amine coupling using 1-ethyl-3-(3-dimethylaminopropyl) carbodiimide hydrochloride (EDC) and sulfo-NHS.

Electrical property for the biotin-labeled DWCNT was largely changed when streptavidin solution was added (Fig.1), while nothing is detected with streptavidin by tiny changes of the electrical property for non-biotin-labeled DWCNT. This result revealed that the biotin-labeled DWCNT-FET device obtained in the present study had specific biosensing ability to streptavidin.

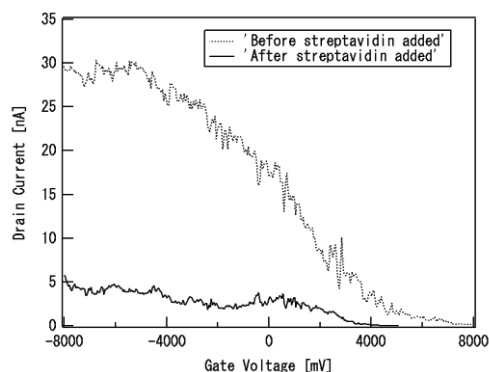


Fig.1 Gate characteristics of biotin-labeled DWCNT-FET biosensor.

[1] Brett Lee Allen, Padmakar D. Kichambare, and Alexander Star, *Adv. Mater.*, **19**, 1439, (2007)

*Corresponding Author: Hirofumi Yajima

Tel: +81-3-3260-4272(ext.5760), Fax: +81-3-5261-4631,

E-mail: yajima@rs.kagu.tus.ac.jp

Selective Solubilization of Semiconducting-Carbon Nanotubes by Using Weak-Bond Connecting Fluorene-Based Polymers

○Fumiyuki Toshimitsu¹, Fujigaya Tsuyohiko¹, Naotoshi Nakashima^{1,2}

¹ Department of Chemistry, Graduate School of Engineering, Kyusyu University, Fukuoka 819-0395, Japan

² JST-CREST, 5 Sanbancho, Chiyoda-ku, Tokyo 102-0075, Japan

Selective separation of single-walled carbon nanotubes (SWNTs) from various chirality is crucial issue for fundamental studies and applications toward next-generation nanotechnology. SWNTs' unique optical and electrical properties^[1,2] would be accomplished efficiently only when they are separated into certain chirality portions. It is desirable to develop strategic purification methods of separating SWNTs according to their chirality. We have previously reported polymer wrapping techniques which efficiently solubilize/extract semiconducting SWNTs with high chiral-selectivity by developing polyfluorene derivatives^[3, 4, 5, 6]. In order to expand this into more utilizable method, we introduced weak-bond connections, such as hydrogen-bond or metal-coordination-bond, which make polymers tunable for recognizing various chirality, and breakable so as to detachable from SWNTs.

In this study, a series of fluorene-based ligands were designed and synthesized to afford weak bond connected polymers. Ligand **1** and **2** recognized each other to form hydrogen-bond polymer in aprotic solvents. On the other hand, ligand **3** assembled into coordination polymers by treating with various metal ions. Each polymers solubilized/extracted SWNTs and exhibited different selectivity on SWNT chirality depending on the solvents, metal ions, and counter anions. The solubilized SWNT was confirmed by UV-Vis-NIR absorption and Raman spectroscopies. In order to ratiocinate these chiral specific recognition of the polymers on SWNT, conformation analysis of polymers on SWNTs by scanning tunneling microscopy (STM) direct observation and molecular mechanics simulation were performed upon the SWNTs wrapped with each polymers.

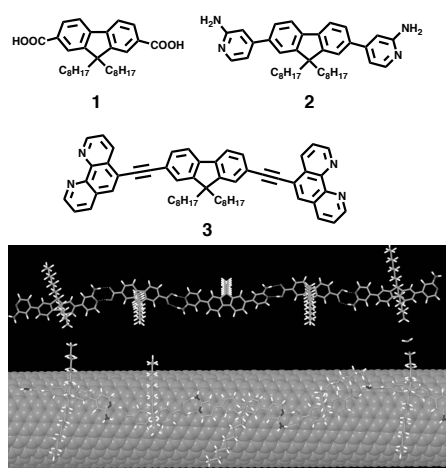


Figure 1. Chemical structures of ligands in this study (**1**, **2** and **3**), and simulated wrapping conformation on SWNT.

Referneces

- [1] J. Bernholc, D. Brenner, M. Buongiorno Nardelli, V. Meunier, and C. Roland, *Annu. Rev. Mater. Res.* **32**, 347 (2002).
 [2] H. J. Dai, *Acc. Chem. Res.* **35**, 1035 (2002).
 [3] H. Ozawa, N. Ide, T. Fujigaya, Y. Niidome, and N. Nakashima, *Chem. Lett.* **40**, 239 (2011).
 [4] H. Ozawa, T. Fujigaya, Y. Niidome, N. Hotta, M. Fujiki, and N. Nakashima, *J. Am. Chem. Soc.*, **133**, 2651 (2011).
 [5] K. Akazaki, F. Toshimitsu, H. Ozawa, T. Fujigaya, and N. Nakashima, *J. Am. Chem. Soc.*, **134**, 12700 (2012).

Corresponding Author: T. Tokyo

Tel: +81-42-677-1111, Fax: +81-42-677-2525,

E-mail: nakashima-tcm@mail.cstm.kyushu-u.ac.jp

Chirality Analysis of Single-walled Carbon Nanotubes Growth in Molecular Dynamics Simulation

○Tomoya Kawasuzuki, Kaoru Hisama, Yuki Takaki, Shohei Chiashi, and Shigeo Maruyama

Department of Mechanical Engineering, The University of Tokyo, Tokyo 113-8656, Japan

It is highly important to understand the growth mechanism of single-walled carbon nanotubes (SWNTs) in order to develop chirality-controlled growth techniques. For this purpose, we have performed classical molecular dynamics simulation (MD) of catalyst-nucleated SWNT growth process [1, 2]. However, the SWNTs obtained in MD simulation have defect structure so far and it is difficult to define their chirality (n,m). Therefore, we tried analyze the “local chirality” of SWNTs in MD simulation by calculating the distribution of angle between carbon-carbon bond and the “local axis”. As shown in Fig. 1, the tangential plane at a carbon atom has contact with SWNT on line. Here, the line is defined as the local axis of the carbon atom.

Figure 2 shows the probability density of the bonds against the angle between the C-C bond and the local axis of a grown SWNT in MD simulation (Co catalyst, 1600 K, after 220 ns). The structure and local axes are shown in the insert. This distribution has two peaks near 0° and 60° , which indicates that the part of this SWNT shows zigzag-like structure. Since this method can be applied widely to the SWNT structures of MD growth simulation, the relation between this local chirality and SWNT growth condition in MD simulation will be discussed.

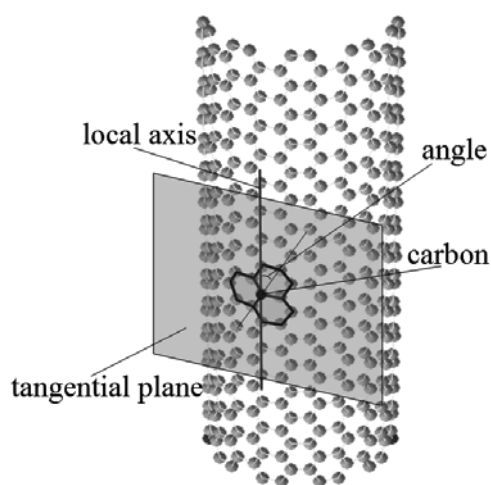


Fig. 1 Schematic diagram of the local axis and the tangential plane

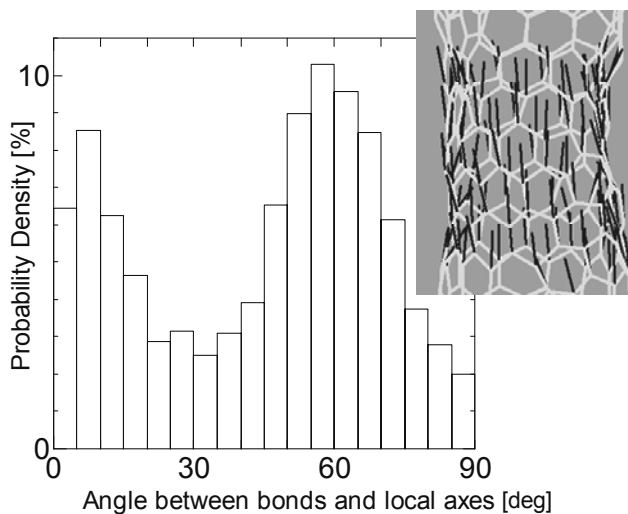


Fig. 2 Probability density of angle between C-C bond and the local axis.

[1] T. Matsuo *et al.*, to be submitted.

[2] Y. Shibuta and S. Maruyama, *Chem. Phys. Lett.*, **382** (2003) 381.

Corresponding Author: Shigeo Maruyama

Tel: +81-3-5841-6421, Fax: +81-3-5800-6983,

E-mail: maruyama@photon.t.u-tokyo.ac.jp

Methane-assisted CVD yielding millimeter-tall single-wall carbon nanotubes of smaller diameters

○Zhongming Chen^{1,2}, Dong Young Kim², Kei Hasegawa², Suguru Noda^{2,*}

¹ Department of Chemical System Engineering, The University of Tokyo, Japan

² Department of Applied Chemistry, Waseda University, Tokyo 169-8555, Japan

Growing taller carbon nanotubes (CNTs) with smaller diameters is an ever-lasting challenge. The rapid growth of millimeter-tall vertically aligned SWCNTs (VA-SWCNTs) by chemical vapor deposition (CVD) on substrates was realized in 2004, which attracted great attention [1], however the resulting SWCNTs proved to have rather large diameters of 3-4 nm [1,2]. Small catalyst particles are unstable and easily get coarsened during CVD, resulting in the gradual diameter increase in SWCNTs during their growth and abrupt growth termination [2,3]. In this work, we examined the use of low purity H₂ (96 vol% H₂ with 4 vol% CH₄ as a stimulant gas) for the low cost H₂ and unexpectedly found the dramatic effect of CH₄.

SWCNTs grew to millimeter-scale and formed vertically aligned arrays by CVD using C₂H₂/H₂/H₂O/Ar gas and Fe/Al-Si-O catalyst (Fig. 1). We found that the small CH₄ addition significantly improved their height (Figs. 1a,b). The sharp G-band peak (originating from graphitic structure) and radial breathing mode (RBM) peaks are characteristic for SWCNTs (Fig. 2). The small CH₄ addition significantly improved the quality of SWCNTs, as shown by the increased intensity ratio of G-band to D-band (originating from defects). Atomic force microscope analysis revealed that the smaller Fe particles formed at higher density when annealed under H₂ with CH₄. Real-time growth monitoring revealed that the growth lifetime was longer when CVD was carried out with CH₄. X-ray photoelectron spectroscopy revealed the annealing in CH₄/H₂ resulted in the carbon deposition at a small content on Fe particles without any CNT growth. The thin carbon layer formed on Fe particles possibly prevented the Fe particles from coarsening by reducing their surface energy while allowing them to grow SWCNTs from highly reactive C₂H₂. Further study is ongoing to clarify the underlying mechanism.

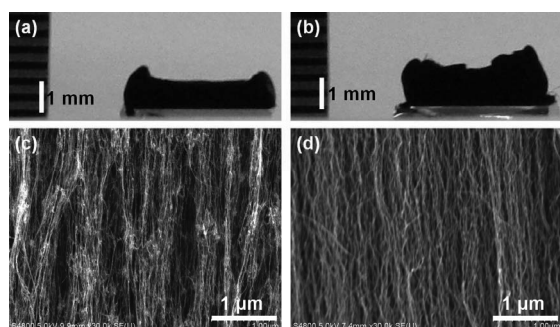


Fig. 1. Photographs (a, b) and SEM images (c, d) of the SWCNT arrays synthesized using (a, c) H₂ without CH₄ and (b, d) H₂ with CH₄. SEM images were taken at the middle of the arrays.

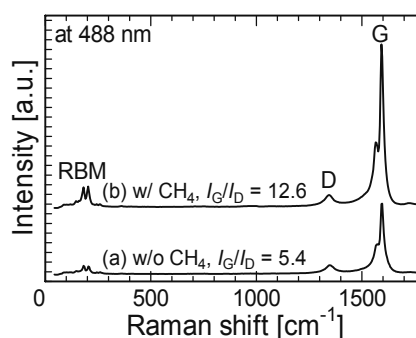


Fig. 2. Raman spectra of the SWCNT arrays taken at their top using an excitation wavelength of 488 nm

[1] K. Hata, et al., *Science* **306**, 1362 (2004).

[2] K. Hasegawa and S. Noda, *ACS Nano*, **5**, 975 (2011).

[3] K. Hasegawa and S. Noda, *Carbon*, **49**, 4497 (2011).

Corresponding Author: S. Noda

Tel: +81-3-5286-2769, Fax: +81-3-5286-2769, E-mail: noda@waseda.jp

Pyrene-based nanocalipers for selective extraction of metallic SWNTs

Gang Liu, Naoki Komatsu, Takahide Kimura

Department of Chemistry, Shiga University of Medical Science, Seta, Otsu 520-2192, Japan.

We have been working on separation of SWNTs with chiral nanotweezers through molecular recognition [1]. Quite recently, chiral porphyrin-based nanocalipers, a newly designed host molecule next to nanotweezers, have been found to discriminate not only diameter and handedness, but also metallicity [2]. In this paper, we modified the porphyrin-based nanocalipers to pyrene-based ones by replacing porphyrin moieties to 2-pyrenes (Fig. 1) and applied to the extraction of HiPco SWNTs.

After bath-sonication of the suspension of HiPco and the nanocalipers, the extract was concentrated, washed, and dispersed in D₂O/SDBS by use of a rosette cooling cell [3]. The Raman and absorption spectra of the washed solid and the D₂O dispersion, respectively, were measured as shown in Fig. 2. While semiconducting SWNTs were more abundant than metallic ones in the absorption spectrum of the HiPco, metallic SWNTs were significantly enriched after the extraction with nanocalipers (Fig. 2a). The metallic enrichment is supported by the Raman spectra (Fig. 2b, c); after the extraction, the peak in the metallic region in the RBM were almost dominant and BWF feature in the G band was more pronounced. The pyrene-based nanocalipers are found to exhibit preference for metallic SWNTs as the porphyrin-based ones.

[1] G. Liu, N. Komatsu, in *Handbook of carbon nano materials* (Eds.: F. D'Souza, K. M. Kadish), World Scientific, **2012**, vol. 3, pp. 203-232; X. Peng, F. Wang, A. F. M. M. Rahman, A. Bauri, N. Komatsu, *Chem. Lett.*, **2010**, 39, 1022.

[2] G. Liu, N. Komatsu, et. al., submitted.

[3] T. Yasumitsu, G. Liu, J.-M. Levêque, S. Aonuma, L. Duclaux, T. Kimura, N. Komatsu, *Ultrason. Sonochem.*, **2013**, 20, 37.

Corresponding Author: Naoki Komatsu

Tel: +81-77-548-2102, Fax: +81-77-548-2405. E-mail: nkomatsu@belle.shiga-med.ac.jp

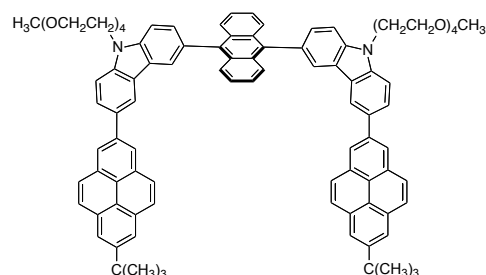


Fig 1. Structures of dipyrene nanocalipers

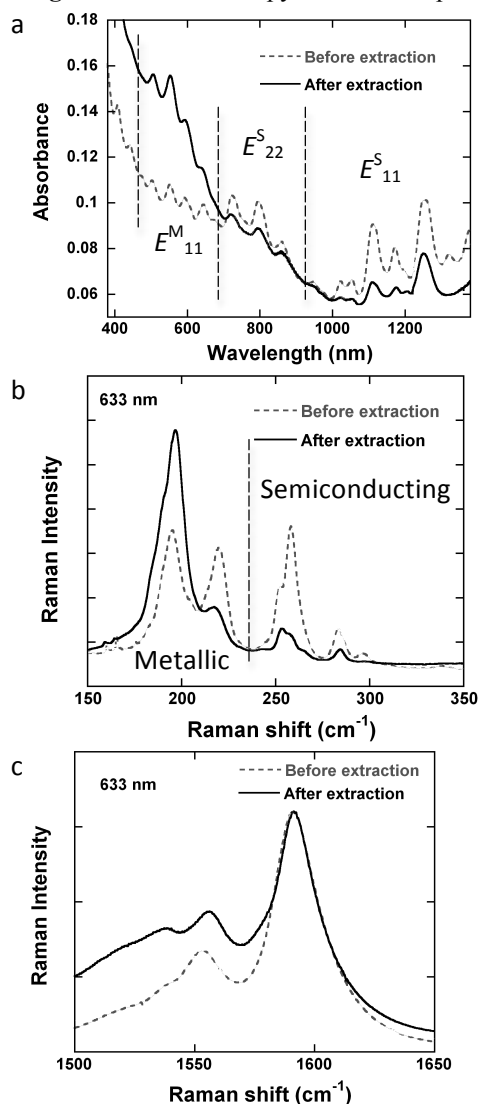


Fig. 2 Absorption (a) and Raman (b, c) spectra of SWNTs before and after the extraction

***In situ* Raman monitoring formation of SWNTs: process optimization and low temperature synthesis**○Ming Liu¹, Yuquan Su¹, Rong Xiang¹, Zikang Tang^{1,2}¹ *School of Physics and Engineering, Sun Yat-Sen University, Guangzhou 510275, China*² *Department of Physics, Hong Kong University of Science and Technology, Clear Water Bay, Hong Kong, China*

Raman scattering is a powerful approach to characterize single-walled carbon nanotubes (SWNTs). In principle, real time Raman monitoring the chemical vapor deposition (CVD) synthesis of SWNTs can give insights into both formation dynamics and structure evolution. However, since the very pioneer work,[1] there have been limited progress on *in situ* Raman measurement. One, if not the most, critical reason is that a Raman spectrum taken at a high temperature during the growth process usually has a low intensity, unable to provide enough signal-to-noise ratio to explicit the fingerprints of the obtained material (e.g. shape of G- peak or even radial breathing modes).

In this work, we are devoted to explore the possibility of increasing Raman signal using metal nano-particles mediated surface enhance Raman scattering (SERS). Unlike conventional SERS of SWNTs that has been extensively investigated, SERS during a CVD process involves high growth temperature, which brings more technical and scientific challenges. We perform a systematic study on the configuration, metal type, particle size. An enhancement up to ten is achieved at high temperature after this preliminary attempts.[2] After further optimization of the growth and measurement, RBM change during the CVD is obtained.[3] Also, we will report the formation of SWNTs at -196°C, the lowest temperature as far as we know. The formation process is clearly evidenced by *in situ* Raman, benefited from the clean background at this low temperature. [4]

[1] Chiashi S *et al.*, Chem. Phys. Lett., 386, 89 (2004).[2] Liu M *et al.*, submitted (2013)[3] Xiang R *et al.*, submitted (2013)[4] Su YQ *et al.*, submitted (2013)

Corresponding Author: Rong Xiang

E-mail: xiangr2@mail.sysu.edu.cn

One-Step Catalyst-Free Mist Flow CVD Growth of Single-Wall Carbon Nanotubes using C₆₀ Fullerenes

○Yun Sun, Ryo Kitaura, Jinying Zhang, Yasumitsu Miyata and Hisanori Shinohara

Department of Chemistry, Nagoya University, Nagoya 464 -8601, Japan

Due to their unique structural and electronic properties, single-walled carbon nanotubes (SWCNTs) have extensively studied during the past couple of decades. However, most of the techniques for the synthesis of SWCNTs are centered on metal catalysts supported CVD, which oftentimes leads to concomitant complicated purification processes. Contaminations can alter the quality and the intrinsic properties of as-grown SWCNTs. Because of this, catalyst-free growth of SWCNTs has been reported during the past decade. For example, various all-carbon routes have been developed, such as cloning SWCNTs from open-end SWCNT seeds [1]. The growth of SWCNTs via opened fullerenes as the nucleation is feasible in light of the previous study [2].

The so-called floating catalyst CVD, in contrast, is capable of continuously synthesizing SWCNTs from the gas phase onto a substrate by simultaneously supplying the catalyst precursor and carbon source.

Here a one-step catalyst-free CVD growth of SWCNTs has been investigated by using a colloidal aqueous C₆₀ solution [4] directly on the basis of the mist flow method [4]. It seems that C₆₀ fullerenes are considered as “the seed” during the formation of SWCNTs (Fig.1). Cap opening, nucleation and growing SWCNTs might be occurring successively during the growth. Consequently, under the optimum CVD reaction condition, the diameter distribution of as-grown SWCNTs becomes fairly narrow (from 1.0 to 1.5 nm) and a typical mean diameter is 1.28 nm, which is rather close to the diameter of individual C₆₀ molecules. Meanwhile, the uniform diameter of SWCNTs can be distinguished by the Raman spectra within RBM region measured at different positions of corresponding SEM image of as-grown products (Fig.2).

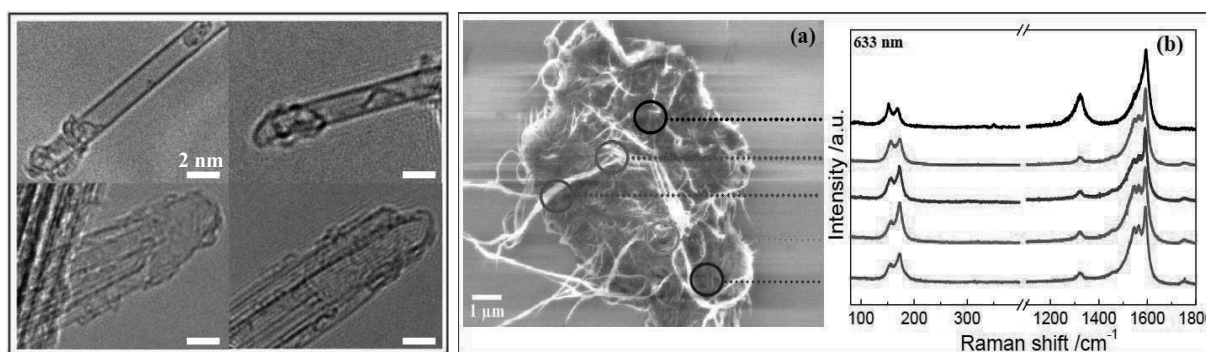


Fig.1 HRTEM images of cap structures. Fig.2 (a) SEM image and (b) corresponding Raman spectra, respectively.

References:

- [1] J. Liu *et al.* *Nat. Commun.* **3**, 1 (2012).
- [2] I. Ibahim *et al.* *ACS Nano* **6**, 10825 (2012).
- [3] Andrievsky *et al.* *Chem. Phys. Lett.* **300**, 392 (1999).
- [4] Y. Sun *et al.* *NANO* **7**, 1250045 (2012).

Corresponding Author: R. Kitaura and H. Shihohara

Tel: +81-52-789-2482, **Fax:** +81-52-747-6442,

E-mail: r.kitaura@nagoya-u.jp and noris@nagoya-u.ac.jp

Modeling the catalyst formation process to achieve diameter and density control of single-wall carbon nanotube forests

○Shunsuke Sakurai^{1,2}, Don N Futaba^{1,2}, Motoo Yumura^{1,2}, and Kenji Hata^{1,2}

¹*Nanotube Research Center, National Institute of Advanced Industrial Science and Technology (AIST), Tsukuba 305-8565, Japan*

²*Technology Research Association for Single Wall Carbon Nanotubes (TASC), Tsukuba 305-8565, Japan*

Catalyst particle array for single-walled nanotube (SWNT) forest requires small particle sizes (< 3 nm) and high particle density (below 20 nm spacing) at high temperature typically above 700 °C. The most widely used method to satisfy the above requirements is to use an AlO_x layer to support the Fe catalysts. In this method, H₂ annealing immediately prior to CNT growth (denoted as catalyst formation process), invoke the transformation of Fe thin film into a very high density array of small Fe catalysts array suited for SWNT forest growth.

Previously, we found essentially any Fe compounds spanning from Fe salts, nanoparticles and buckyferrocene could serve as catalysts for SWNT with nearly identical diameters (2.8-3.1 nm) [1]. Recently, we succeeded in continuously controlling the diameter of SWNT forest in the range of 1.9 nm to 3.2 nm, by changing temperature and gas flow rate during catalyst formation process [2].

These results indicate the understanding of the catalyst formation process is one of the key to control the SWNT forest growth. We found that subsurface diffusion of Fe atoms into the AlO_x support induced by hydrogen annealing induce the reconfiguration of remaining Fe atoms into small nanoparticles suitable for SWNT growth. In this paper, we present the model for the growth of catalyst particle during formation process, considering the offsetting effects of Ostwald ripening and subsurface diffusion. From this model, the growth of the particles stops at a specific size, where the effects of subsurface diffusion and Ostwald ripening are balanced (Figure 1). From analyses using this model, we conclude H₂ exposure increased catalyst surface energy and decreased diameter while increased temperature led to increased diffusion on the surface and to an increase in diameter.

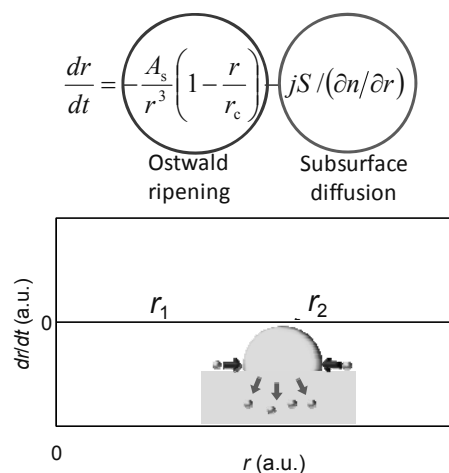


Figure 1: Calculation of the growth rate of catalyst particles.

[1] S. Sakurai, H. Nishino, D. N. Futaba, S. Yasuda, T. Yamada, A. Maigne, Y. Matsuo, E. Nakamura, M. Yumura, and K. Hata *J. Am. Chem. Soc.*, **134**, 2148 (2012). [2] S. Sakurai, M. Inaguma, D. N. Futaba, M. Yumura, K. Hata *submitted*

Corresponding Author: Don Futaba

TEL: +81-29-861-6205, FAX: +81-29-861-1169, E-mail: d-futaba@aist.go.jp

Simultaneous Growth Control of Position, Chirality, and in-plane Orientation of Single-Walled Carbon Nanotubes by Cold-Wall Chemical Vapor Deposition Method

○Takumi Sagara¹, Satoshi Doi¹, Nobuyuki Iwata¹, Hirofumi Yajima², and Hiroshi Yamamoto¹

¹ Department of Electronics & Computer Science, College of Science & Technology, Nihon University, 7-24-1 Narashinodai, Funabashi, Chiba 274-8501 Japan

² Department of Applied Chemistry, Faculty of Science, Tokyo University of Science, 1-3 Kagurazaka, Shinjyuku-ku, Tokyo 162-0826, Japan

In our previous report, position selective growth of single-walled carbon nanotubes (SWNTs) is carried out on a surface treated SiO₂ (300nm)/Si substrate between electrodes by cold-wall chemical vapor deposition (CC-CVD) method in μm -scale^[1]. The SWNTs grow at the intermediate area between electrodes. In addition, chirality controlled growth of the SWNTs is also done by irradiating free electron laser (FEL) during CVD growth. The grown SWNTs are all semiconducting investigated by a multi excited laser Raman analysis. The possible chirality is (14,0), (13,2), (10,6), (9,7), (13,0), (12,2), (10,5), and (8,7). The remained issue for applications of the field effect transistor (FET) using just one SWNTs is the in-plane alignment synthesis process. In this study, the CC-CVD growth was carried out on the *r*-cut sapphire substrate for the purpose of the in-plane alignment. The substrate was annealed in advance to obtain a step-terraces structure. The Co/Mo catalysts were adhered by dipping technique on the annealed substrate followed by firing.

Figure 1 shows the Raman spectrum of the SWNTs grown on sapphire substrates. The G and D peaks were observed around 1580 cm⁻¹ and 1350 cm⁻¹, respectively. The G/D ratio was 12. The observed radial breathing mode (RBM) around 160 cm⁻¹ mode indicated the growth of SWNTs with the diameter of 1.1 ~ 1.8 nm. Figure 2 shows the surface image of grown SWNTs. The observed needles are expected bundled-SWNTs bundles with a diameter of 3 ~ 5 nm. Position as well as chirality control growth of SWNTs on the *r*-cut sapphire substrate will be also discussed.

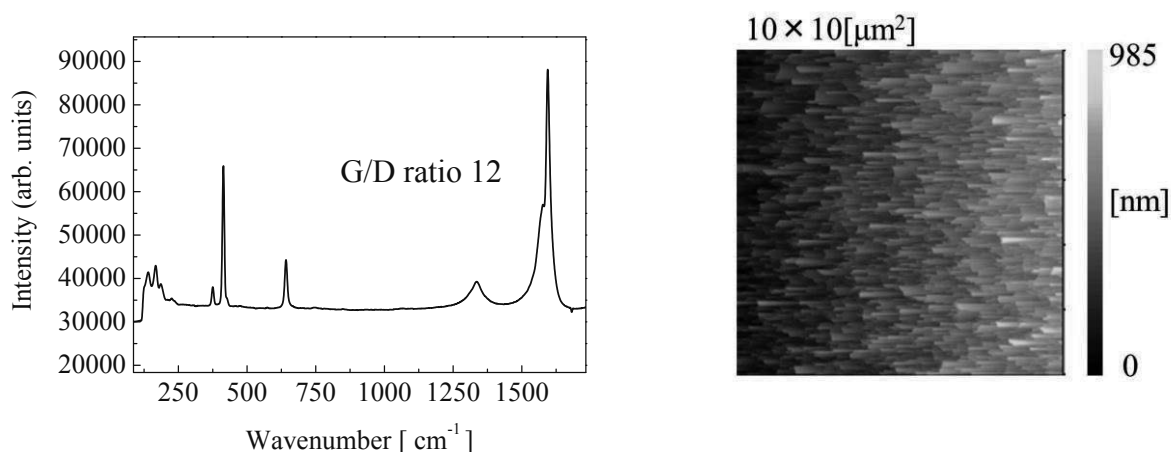


Fig1. The Raman spectrum of obtained SWNTs Fig2. The AFM image of the sample surface

[1] K. Sakai, S. Doi, N. Iwata, H. Yajima, and H. Yamamoto, *IEICE Trans. Electron.* **E94-C** (2011) 1861-1866.

Corresponding Author: T. Sagara

TEL/FAX: 047-469-5457, E-mail: cst12010@g.nihon-u.ac.jp

Diameter Dependent Interaction between Single-Walled Carbon Nanotubes and Encapsulated Ferrocenes

○Hironori Suzuki,^{1,2} Yoko Iizumi² and Toshiya Okazaki,^{2,1,*}

¹*Department of Chemistry, Tsukuba University, Tsukuba 305-8577, Japan*

²*Nanotube Research Center, AIST, Tsukuba 305-8565, Japan,*

Doping molecules to the inner spaces of single-walled carbon nanotubes (SWCNTs) is expected to be a useful technique for achieving realistic applications of SWCNTs. Organometallic compounds, ferrocenes, have been doped in SWCNTs by many researchers. However, the interaction between SWCNTs and the encapsulated ferrocenes, and their doping effects on the electronic and optical properties of SWCNTs are still controversial [1,2]. In this study, we characterize ferrocenes encapsulating SWCNTs (ferrocenes@SWCNTs) by photoluminescence (PL) spectroscopy over a wide range of tube diameters ($0.95 \text{ nm} < d < 1.5 \text{ nm}$). Figure 1 shows the two-dimensional PL maps of ferrocenes@SWCNTs and the empty SWCNTs (KH chemicals), respectively. Interestingly, the PL properties strongly depend on the tube diameter. In the smaller diameter region ($d < \sim 1.05 \text{ nm}$), the intensity of the PL signal is severely decreased. In the middle ($\sim 1.05 \text{ nm} < d < \sim 1.3 \text{ nm}$), the observed PL peak positions are shifted compared with those the original SWCNTs. For larger diameter tubes ($d > \sim 1.3 \text{ nm}$), their PL peak positions become similar to each other. The observed PL behaviors should reflect the difference in the interaction between SWCNTs and the encapsulated ferrocenes.

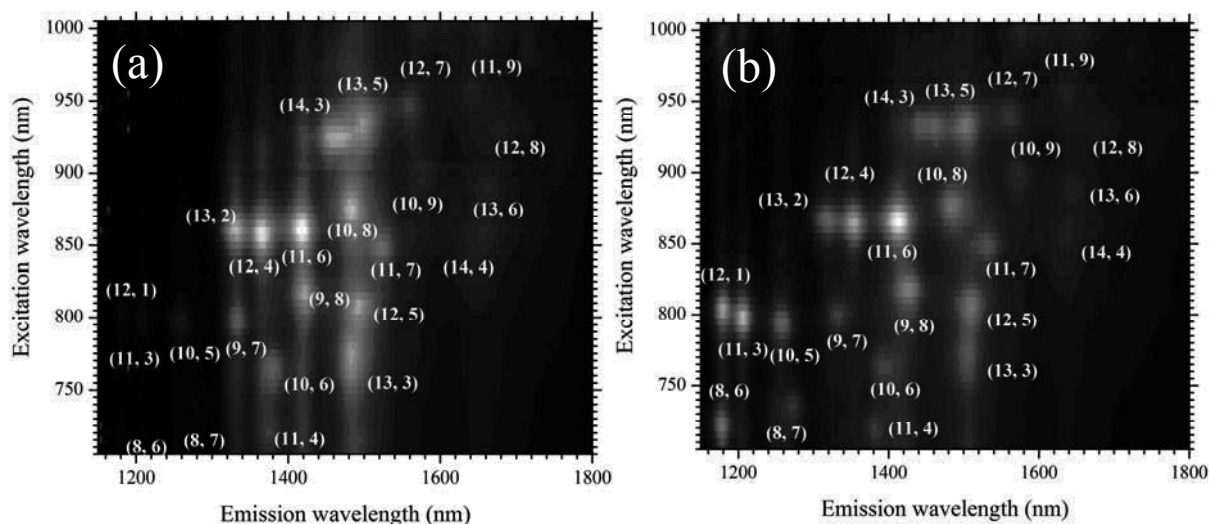


Fig. 1. Two dimensional PL maps of (a) ferrocenes@SWCNTs and (b) the original SWCNTs.

[1] H. Shiozawa *et al.*, *Phys. Rev. B*, **77**, 153402 (2008). [2] X. Liu *et al.*, *Adv. Funct. Mater.*, **22**, 3202 (2012).

Corresponding author: Toshiya Okazaki (toshi.okazaki@aist.go.jp)

Spectroscopic studies of single-wall boron nitride nanotubes synthesized in single-wall carbon nanotubes

○Ryo Nakanishi¹, Ryo Kitaura¹, Yuta Yamamoto², Shigeo Arai², Jamie H Warner³,
Yasumitsu Miyata¹ and Hisanori Shinohara¹

¹*Department of Chemistry & Institute for Advanced Research, Nagoya University, Nagoya,
464-8602, Japan*

²*Ecotopia Science Institute, Nagoya University, Nagoya, 464-8603, Japan*

³*Department of Materials, University of Oxford, Oxford, OX1 3PH, UK*

Boron nitride nanotubes (BNNTs) are nano-scale cylindrical tubes same as carbon nanotubes (CNTs), except that they are consisting of hexagonal boron nitride sheets. One of the most important features of BNNTs is that they possess a large band gap (~ 6.0 eV) irrespective of the chiralities [1]. Therefore, single-wall BNNTs (SWBNNTs) with narrow diameters can be considered as an ideal nano-scale vessel to explore physical properties of one-dimensional materials such as atomic wires. However, their selective and bulk synthesis is still in its infancy. Previously, we reported a novel synthesis method of SWBNNTs using single-wall CNTs (SWCNTs) with narrow diameter distribution (1.4 ± 0.1 nm) as a nano-template, from which SWBNNTs (0.7 ± 0.1 nm) with quite small and uniform diameter could be obtained selectively. Here, to explore the details of the reaction such as the efficiency, we have focused on spectroscopic studies of the SWBNNTs inside SWCNTs.

We have synthesized SWBNNTs inside SWCNTs according to the procedures previously reported: ammonia-borane complex (ABC) was used as a BN source, which was sealed into a glass tube with cap-opened SWCNTs under high vacuum (10^{-6} Torr) and encapsulated into them with heating at 823 K for 3 days. After capping those ends with C₆₀ and washing with deionized water, ABC encapsulated SWCNTs (ABC@SWCNTs) were annealed at 1,673 K for 3 days. From the analyses on electron energy-loss spectroscopy (EELS) inside transmission electron microscope (TEM), the B:C:N ratio of SWBNNT inside SWCNTs (SWBNNT@SWCNTs) is 14:71:15, whose B and N ratios are somewhat higher than that of ABC@SWCNTs (B:C:N = 10:81:9). Considering the yield of SWBNNTs (~ 50 %) obtained by TEM observation, this result suggests that the reaction efficiency from ABCs to SWBNNTs is extremely high (ca. 100 %). Further EELS analysis, Raman and absorption spectroscopy results will also be discussed in this presentation.

[1] N. G. Chopra *et al.*, *Science* 269, 966 (1995).

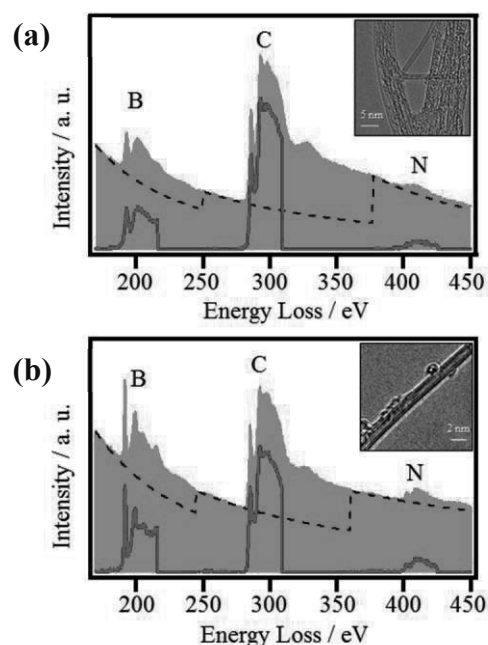


Figure 1. EELS spectra of (a) ABC@SWCNTs and (b) SWBNNT@SWCNTs taken at each inset region.

Corresponding Author: Ryo Kitaura and Hisanori Shinohara

Tel: +81-52-789-2483, Fax: +81-52-747-6442, E-mail: r.kitaura@nagoya-u.jp, noris@nagoya-u.jp

Molecular Dynamics Simulation of Multi-layer Graphene Growth by Catalytic CVD Method

○Yuki Takaki, Kaoru Hisama, Tomoya Kawasuzuki, Shohei Chiashi, Shigeo Maruyama

Department of Mechanical Engineering, The University of Tokyo, Tokyo 113-8656, Japan

Toward utilization of graphene in various applications, it is quite important to control the layer number of graphene in chemical vapor deposition (CVD) method. In order to understand the growth mechanism of graphene in atomic scale, we have performed molecular dynamics simulations. We adopted a newly developed Tersoff-type classical potential for carbon and several metal atoms, such as Co, Fe and Ni [1].

We annealed metal substrates ($17 \times 17 \times 15$ nm) for 100 ps, and supplied carbon atoms every 10 ps to keep constant pressure of carbon vapor at various temperatures; 1600, 1800 and 2000 K. We succeeded in the growth of single-layer graphene, as shown in Fig. 1. Figure 1 shows a snapshot of single-layer graphene grown on the iron substrate at 1800 K. The ratio of 6 membered rings indicates the quality of graphene. This ratio depends on growth temperature, and it shows the highest value at 1800 K in case of the iron substrate.

After the growth of the 1st graphene layer, we simulated the growth process of multi-layer graphene by directly supplying carbon atoms into metal substrates. This simulation reproduces the segregation of carbon atoms from metal substrates in cooling process in experimental graphene growth [2]. When the amount of carbon atoms in metal substrates excess the saturation point, carbon atoms appear in the interface between the 1st graphene layer and the metal surface, and form the 2nd graphene layer as shown in Fig. 2. Figure 2 show a snapshot of double-layer graphene grown on the iron substrate at 2000 K.

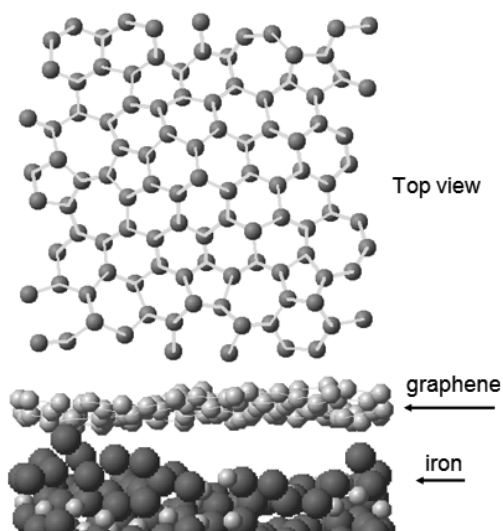


Fig. 1 Snapshot of single-layer graphene grown at 1800 K.

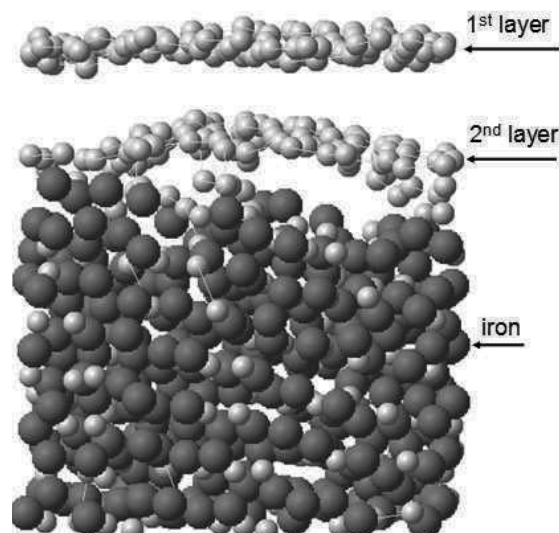


Fig. 2 Snapshot of double-layer graphene grown at 2000 K.

[1] T. Matsuo *et al.*, to be submitted.

[2] M. Liu *et al.* ACS Nano **6**, 10581 (2012).

Corresponding Author: Shigeo Maruyama

Tel: +81-3-5841-6421, Fax: +81-3-5800-6983,

E-mail: maruyama@photon.t.u-tokyo.ac.jp

Synthesis and characterization of large sized-grain, single-layer BN-doped graphene

○Yu Kobayashi, Yasumitsu Miyata, Eriko Maeda, Ryo Kitaura, and Hisanori Shinohara*

Department of Chemistry & Institute for Advanced Research, Nagoya University, Nagoya

Graphene has been considered as one of the promising candidates for various device applications in electronics and optics because of its excellent carrier mobility and optical transparency. However, due to the absence of a band gap in graphene, it is still highly required to develop cutting-edge methods to control its electronic structure. For this purpose, the substitutional doping of hetero atoms like boron and nitrogen provides a powerful way to modulate electronic properties of materials, which has been applied to the synthesis of boron and nitrogen-doped graphene (BN-doped graphene) [1,2].

Here, we report the synthesis and characterization of large sized-grain and single-layer BN-doped graphene produced by a thermal chemical vapor deposition (CVD). The doped graphene with large grain size was obtained through simultaneous supply of small amounts of methane and ammonia borane precursors. Interestingly, unlike the case of undoped graphene with hexagonal shape (Fig.1a), the BN-doped graphene is irregular in grain shape even though they have similar grain size of around 10 μm (Fig.1b). Raman spectra clearly present a significant increase of intensity ratio of D-mode to G-mode for the BN-doped graphene (Fig.1c). These results suggest that the atomic structural disorder leads to the change of microscopic grain shape, providing an important insight into the synthesis of high-quality BN-doped graphene.

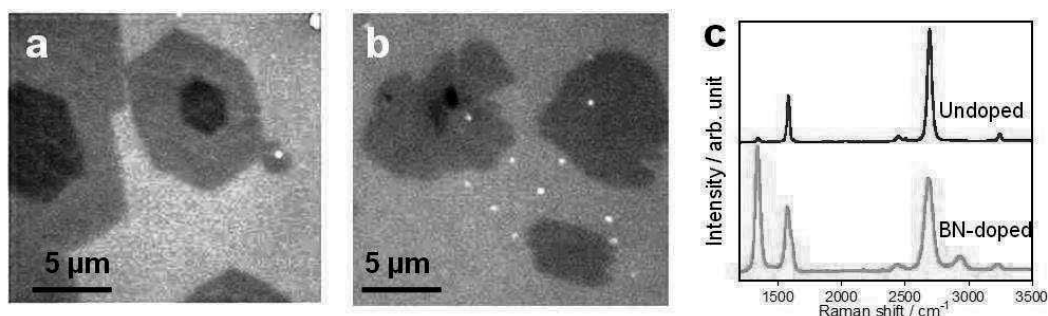


Fig.1 Optical microscope images of (a) undoped and (b) BN-doped graphenes. (c) Raman spectra of undoped and BN-doped graphenes.

[1] L Ci *et al.* Nat. Mater. 9 (2011) 430, [2] C. Chang *et al.* ACS Nano, in press.

Corresponding Author: Hisanori Shinohara,

E-mail: noris@nagoya-u.jp, Tel&Fax: 052-789-2482 & 052-747-6442

Synthesis and Characterization of Intercalated Graphite and Graphene for Room Temperature Superconductivity

○Shogo Sato, Hiroaki Ichikawa, Nobuyuki Iwata, Hiroshi Yamamoto

College of Science & Technology, Nihon University, 7-24-1 Narashinodai, Funabashi-shi, Chiba 2748501

Graphite intercalation compounds (GIC) is prepared on various substances. Superconducting transition temperature T_c of GIC with Ca are reported at 11.5K^[1]. Furthermore, recently, room temperature superconductivity (RTS) was demonstrated in the water-treated graphite powder, where clear typical superconducting diamagnetic hysteresis loop is observed^[2]. In this study we aim at realizing the RTS in a FeCl_3 or a metal intercalated graphite (FeCl_3 -GIC), double layers graphene, and/or a few layers graphene according to the BCS theory. The T_c is expected to be higher than room temperature as long as a disorder and a roughness of the graphite/graphene layers are much reduced.

Figure 1 shows the magnified Raman spectra between 1500 and 1700 cm^{-1} after the FeCl_3 was intercalated to a few layers graphene. The G peak was split to two peaks, indicating the presence of intercalated graphenes. The lower intensity peak at 1607 cm^{-1} than that of the bare G peak corresponds to the intercalation of one layer of FeCl_3 more or less every five layer graphene sheets, so-called stage 5^[3].

Figure 2 shows a resistivity of the stage 5 FeCl_3 intercalated graphene as a function of temperature. Resistivity lineally decreased as decreasing temperature with the remarkable change in resistivity behavior around 200K. The reason of the change is unclear at this moment, but it is speculated that the crystal structure transition is present. The intercalated double layers graphene, and/or a few layers graphene grown using Cu, Ni, Co and Fe foil by chemical vapor deposition will be discussed.

[1] N. Emery *et al.*, Phys. Rev. Lett. **95** (2005) 087003

[2] T. Scheike *et al.*, Adv. Mater, **24**(2012) 5826-5836

[3] F. Kang *et al.*, Carbon, **36**(1998) 383

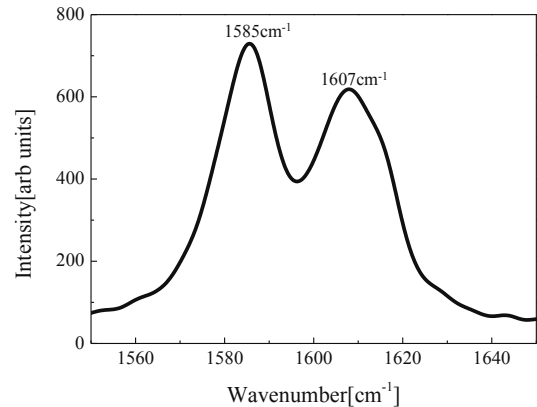


Fig.1. Magnified Raman spectra of the stage 5 FeCl_3 intercalated graphene.

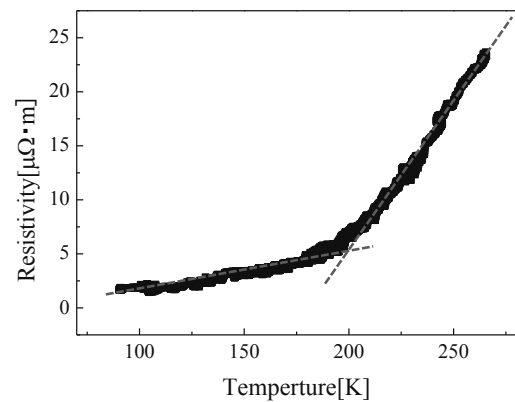


Fig.2. Temperature Resistivity characterization at 265 ~ 90 K.

Directional growth of graphene over Cu catalyst by face-to-face configuration CVD

○Tatsuya Masuda^{1,2}, Kenji Kawahara³, Hiroki Ago³, Suguru Noda^{2,4*}

¹ Department of Chemical System Engineering, The University of Tokyo, Japan

² Department of Applied Chemistry, Waseda University, Japan

³ Institute for Materials Chemistry and Engineering, Kyushu University, Japan

⁴ PRESTO, JST, Japan

Chemical vapor deposition (CVD) on Cu catalyst yields monolayer graphene owing to its self-terminating reaction [1]. Resulting graphene is, however, polycrystalline with grain boundaries at random positions. Epitaxial growth of graphene on epitaxial Cu or Co catalysts on single-crystalline sapphire or MgO substrates [2] is a promising approach, however it is still challenging to unify the grains without seams. Such problem arises from the nucleation at random positions and growth to random directions of graphene.

We have developed a face-to-face configuration (F2FC) preventing Cu sublimation during CVD by limiting the diffusion of Cu vapor to the bulk stream [3] (Fig. 1). When a less active reactant such as CH₄ is fed through a sub-millimeter gap (Fig. 1a), it is less consumed by the Cu catalyst and diffuses uniformly from the edge to the center of Cu [3]. If an active reactant such as C₂H₂ is fed through a sub-micrometer gap (Fig. 1b), it should be consumed by the Cu catalyst and graphene should selectively nucleate at the edge of Cu. When the graphene cover the edge of Cu, C₂H₂ should be fed and graphene should grow to inner region of Cu.

In this work, we used the epitaxial Cu catalyst on sapphire [2, 3] and prepared the counter substrate by partially etching the thermal oxide on Si substrates (Fig. 1b). The F2FC-substrates were set in the tubular CVD reactor, annealed under H₂/ Ar at 25 Torr and 1050 °C for 10 min, and CVD was carried out by flowing C₂H₂/ H₂/ Ar at 25 Torr and 1050 °C for 2 min. Typical results are shown in Fig. 2 with that with CH₄ as a reference. When CH₄ was used, graphene nucleate randomly, resulted in a number of grain boundaries in scanning electron microscopy (SEM) and a D-band in a Raman spectrum. Whereas when C₂H₂ was used, graphene selectively nucleated at the edge of Cu and grew inward and D-band was absent. We are now examining grain boundary distributions.

[1] X. Li, et al., *Science* 324, 1312 (2009).

[2] Y. Ogawa, et al., *J. Phys. Chem. Lett.* 3, 219 (2011)

[3] T. Masuda and S. Noda, The 43rd Fall Meeting of the Society of Chemical Engineers, Japan, U319 (2011).

*Tel&Fax:03-5286-2769, noda@waseda.jp

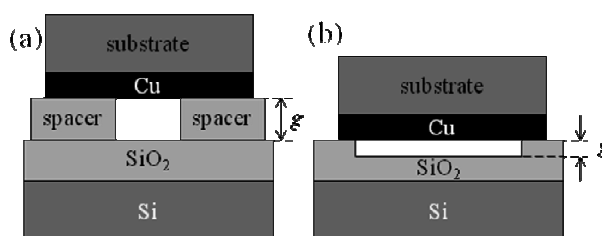


Fig.1 Schematics of F2FC-CVD.

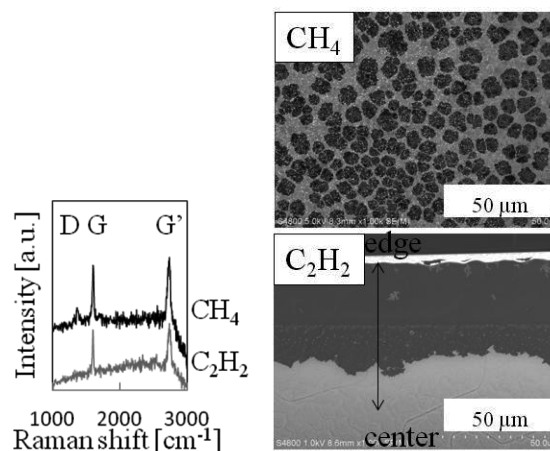


Fig.2 Raman spectra and SEM images of graphene on epitaxial Cu after F2FC-CVD.

Monte Carlo Particle Simulations of Local Heating Properties in Graphene-channel nano-FETs

○Shusuke Oki, Taichi Misawa and Yuji Awano

¹ *Department of Electronics and Electrical Engineering, Keio University, Yokohama 223-8522, Japan*

Due to high density integration of LSIs, thermal management becomes more and more important. Besides, Graphene has received much attention as an emerging research material for future nano-scale FETs and interconnects, because of its excellent electrical and thermal properties. In this paper, we report computer simulations on the electrical and thermal properties of Single layer Graphene (SLG) nano-FETs for the first time, using Monte Carlo particle model for both electron and phonon transport.

In devices scaled below or comparable to the size of electron mean-free path, Monte Carlo particle method would be the most reliable and accurate method of quantitative evaluation of electron transport [1]. Meanwhile, heat dissipation in the macro-scale devices has been analyzed as diffusion phenomena, while in nano-scale devices, cannot be treated the same way because the mean-free-path of the phonon becomes comparable to the size of device. Thus, we employed Monte Carlo particle method for not only electron but also phonon transport in Graphene-channel nano-scale FETs simulation. This simulation consists of two parts; the first part is electron transport simulation to obtain spatial distributions of phonons generated by electron-phonon interactions, the second part is phonon transport simulation in order to estimate local heating in the device (this phonon transport is then being feedback as a scattering rate to recalculate electron transport). We succeeded in calculating both electron and phonon transport phenomena self-consistently for a reasonable computing time by introducing two different time steps for electron and phonon transport simulations. The phonon velocity is derived from the phonon dispersion curve of SLG [2].

Using our new method, we succeeded in analyzing local heating phenomena in nano-scale SLG FETs quantitatively. Figure 2 shows the peak temperature of nano-scale SLG FET, comparing with that of GaAs. Although the heat generation rate of SLG is higher than that of GaAs because of higher optical phonon energy, the peak channel temperature in SLG is lower than that of GaAs, which is probably due to high speed optical and acoustic phonons in SLG. Our method can be applied for power devices in which local heating is more crucial in determining device performance.

[1] N. Harada, et al., APEX1 (2008) 024002.

[2] D. L. Mafra, et al., Phys. Rev. B 76 (2007), 233407.

Corresponding Author: Y. Awano Tel, Fax: +81-45-566-1506, E-mail: awano@elec.keio.ac.jp

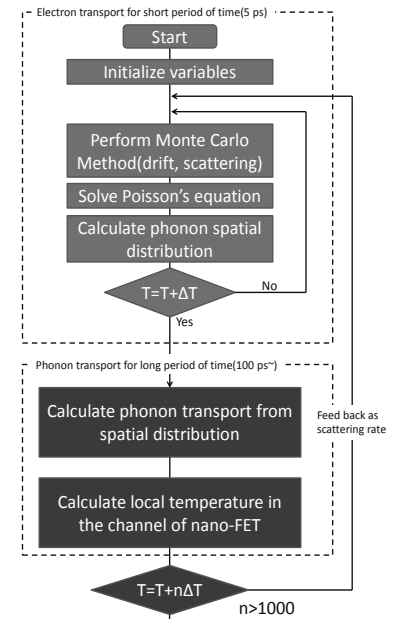


Fig. 1 Algorithm of a new model

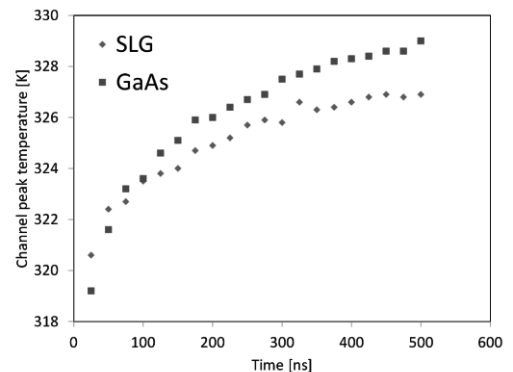


Fig. 2 Peak temperature in FET channel

Electrically driven ultra-high-speed black body emitters based on graphene

○Tomoya Yokoi¹, Yusuke Takayama¹, Tatsuya Mori¹, Daiju Tsuya², Hideyuki Maki¹

¹*Department of Applied Physics and Physico-Informatics, Faculty of Science and Technology, Keio University, Yokohama 223-8522, Japan*

²*NIMS Nanofabrication Platform, Tsukuba 305-0047, Japan*

Graphene is an ideal two-dimensional materials with interesting electrical, optical and thermal properties, and these unique properties have been utilized for the novel application in optoelectronics and photonics [1]. In this study, we fabricated a graphene-based emitter, and firstly observed high-speed blackbody emission with the response speed of > 1 GHz, which is $> 10^6$ times higher than that of a conventional incandescent emitter with a filament and is higher or comparable to a light-emitting diode (LED) and a laser diode (LD).

We used mechanical exfoliation technique (with a tape) to deposit graphene onto SiO₂ (90nm)/Si substrate, and the Ti/Pd(5/40nm) electrodes were deposited on it. Figure 1 shows the emission spectra under DC bias. Since these spectra can be fitted to Planck's law, these emissions can be explained by the blackbody radiation by Joule heating. The graphene temperature obtained from the fitting increased with increasing bias voltage.

The response speed of the emission from this device was evaluated by the time-resolved emission measurement under applying pulsed voltage. As shown in Fig. 2, the observed emission intensities quickly respond to the applied pulse voltage. In addition, we also experimentally demonstrated 1-ns-width pulsed light generation. We note that an emitter with a thick graphite (~ 3000 layers) has quite slow speed (~ 100 kHz). This high-speed response in graphene is explained by the extremely short temperature response time dominated by the high heat dissipation to the substrate owing to the direct heat dissipation to the substrate and the small heat capacity per unit area of graphene. This electrically driven, small footprint and ultra-high speed emitter may open novel applications of blackbody emission such as an integrated light source for integrated photonic or optoelectronic circuit, an ultrafast white light source (like a supercontinuum light) and so on.

This work was partially supported by Grants-in-Aid for the Encouragement of Young Scientists (no. 23686055) from the MEXT, Japan, by the A-STEP (no. AS242Z01485J) from JST, Japan and by NIMS Nanofabrication Platform in "Nanotechnology Platform Project" by MEXT, Japan.

[1] M. H. Bae, Z. Y. Ong, D. Estrada, and E. Pop, *Nano Lett.* **10**, 4787(2010).

Corresponding Author: H. Maki

Tel: +81-45-566-1643, Fax: +81-45-566-1587, E-mail: maki@appi.keio.ac.jp

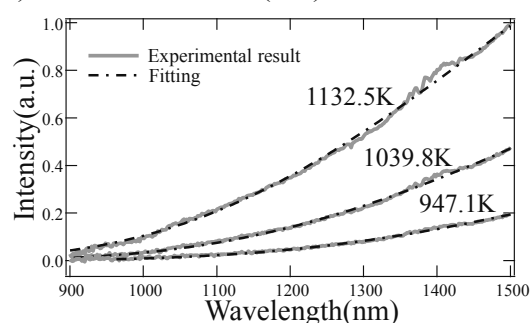


Fig. 1. Infrared spectrum of graphene black body radiation and temperature estimated from Planck's law fitting at $V_{ds} = 11, 13$ and 15 V.

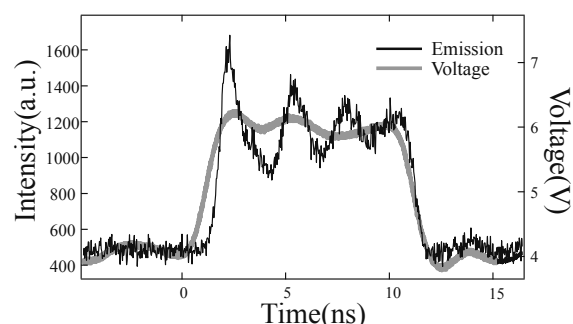


Fig. 2. Optical response of graphene black body radiation under applying pulse voltage (4 - 6 V).

Few-layer Graphene/silicon Heterojunction Photovoltaic Cells by Microwave Plasma-Enhanced Chemical Vapor Deposition

○Zhipeng Wang¹, Shohei Hayase², Mao Shoji², Hironori Ogata^{1,2,3}

¹*Institute for Sustainability Research and Education, Hosei University, fujimi, 102-8160, Japan*

²*Graduate School of Engineering, Hosei University, koganei, 184-8584, Japan*

³*Research Center for Micro-Nano Technology, Hosei University, koganei, 184-0003, Japan*

Graphene, a single layer of carbon atoms in a hexagonal lattice, has attracted great attention due to its outstanding and fascinating properties [1] and a wide range of interesting potential applications [2]. Recently, the graphene-based Schottky junction solar cells have been extensively investigated to optimize their power efficiencies [3, 4]. The graphene films used in their studies were usually grown on metal foils (eg. Cu, Ni) by chemical vapor deposition in Ar/H₂/CH₄ system at high temperatures (above 900 °C). Besides them, few-layer graphene (FLG) films which were fabricated by flame synthesis technique could be used to form a p-n junction solar cell with n-type silicon [5]. Recently, we have obtained the FLG films on the various metal substrates by microwave plasma enhanced chemical vapor deposition (MPECVD, 2.45GHz) with a solid carbon source. Fig. 1 shows the example of the FLG films consist of bi- or trilayer by MPECVD with a solid carbon source. In this presentation, we will present the fabrication and the optimized photovoltaic properties of FLG/n-type silicon heterojunction photovoltaic cells. The detailed results will be discussed in the presentation.

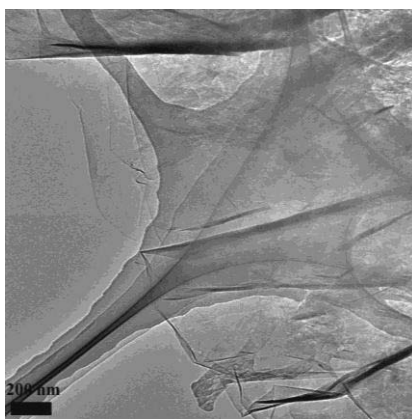


Fig. 1 Typical TEM image of few-layer graphene loading on the Cu mesh

[1] K. S. Novoselov *et al.*, *Science* **306**, 666 (2004).

[2] P. Avouris *et al.*, *MRS Bulletin*. **37**, 1225 (2012).

[3] X. Li *et al.*, *Adv. Mater.* **22**, 2743 (2010).

[4] X. Miao *et al.*, *Nano Lett.* **12**, 2745(2012).

[5] Z. Li *et al.*, *Chem. Commun.* **47**, 3520 (2011).

[6] Z. Wang *et al.* *preparing*

Corresponding Author: H. Ogata. Tel/fax: +81-42-387-6229. E-mail: hogata@hosei.ac.jp.

Degree of oxidation of centrifuged graphene oxide

○Hiroyuki Yokoi^{1,2}, Michio Koinuma^{1,2}, Kazuto Hatakeyama^{1,2}, Takaaki Taniguchi^{1,2},
Yasumichi Matsumoto^{1,2}

¹Graduate School of Science and Technology, Kumamoto University, Kumamoto, 860-8555,
Japan

²JST, CREST, K's Gobancho 6F,7 Gobancho, Chiyoda-ku, Tokyo, 102-0076, Japan

Graphene oxide (GO) is single-layered graphene modified with functional groups including oxygen. GO can be dispersed stably in water and become base material for many applications such as polymer composites, sensors, biomedical applications. As it is possible to synthesize GO in a large scale, this material has potential to utilize some of excellent features of graphene for industrial applications cost-effectively and massively. Though typical GO has low electrical conductivity, several approaches to reduce GO have been developed to improve the conductivity[1]. The reduced GO (rGO), however, loses dispersiveness instead, which spoils the handiness of GO. In this paper, we present a method to separate GO with the degree of oxidation comparable to rGO and the dispersiveness comparable to conventional GO.

In the experiments, GO was prepared following the Hummers' method from pure graphite powder (New Metals and Chemicals Ltd., 99.9999%) and washed several times with distilled water and then dried in an oven. The obtained GO was sonicated in distilled water with an ultrasonic bath for 2 h, and centrifuged at 15kG for 0.5 h to remove any aggregated GO. The supernatant liquid was centrifuged again at 11kG for 0.25 h. This two-stage centrifugation produced precipitation in spite that the centrifugal force and duration were smaller at the second stage than at the first stage. We mixed the precipitation with a small amount of the supernatant by shaking with a hand lightly and found that the precipitation dispersed very well in the liquid. We applied X-ray photoelectron spectroscopy (XPS) analysis to the precipitation and found that the precipitation was GO with the lower degree of oxidation than that of original GO as shown in Fig. 1. The XPS spectrum of precipitated GO (p-GO) was similar to that of rGO. Despite that the apparent degree of oxidation of p-GO is comparable to that of rGO, the dispersion has been stable for 5 months. Further studies on the Zeta potential and the electric properties of p-GO will be presented.

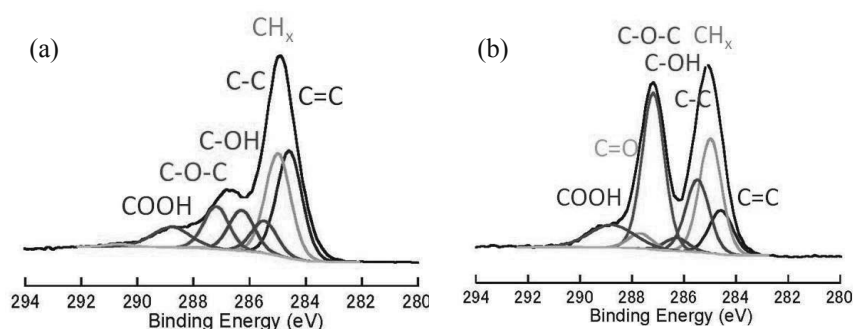


Fig. 1 XPS spectra of (a) precipitation of centrifuged GO suspension and (b) original GO

[1] Y. Matsumoto *et al.* ACS Appl. Mater. Interfaces, 2, 3461 (2010).

Corresponding Author: H. Yokoi

Tel: +81-96-342-3727, Fax: +81-96-342-3710,

E-mail: yokoihr@kumamoto-u.ac.jp

Spin polarization of hexagonal boron nitride/Ni(111) interface studied by spin-polarized metastable de-excitation spectroscopy.

○Manabu Ohtomo¹, Yasushi Yamauchi², Pavel V. Avramov¹, Shiro Entani¹,
Yoshihiro Matsumoto¹, Hiroshi Naramoto¹, and Seiji Sakai¹

¹ Advanced Science Research Center, Japan Atomic Energy Agency, Ibaraki 319-1195, Japan

² National Institute of Materials Science, Ibaraki 305-0047, Japan

1. Introduction

Hexagonal boron nitride (h-BN) has a large band gap (~5 eV) and a honeycomb lattice which makes it a promising insulating material for graphene spintronics. In this study, we present spin-polarized metastable de-excitation spectroscopy (SPMDS) of h-BN / Ni(111) “spinterface” in order to elucidate the spintronic structure and enhance the spin injection efficiency from Ni magnetic electrode into graphene overlayer through h-BN.

2. Experimental procedure

Substrate was a W(110) single crystal on which a Ni(111) film with thickness of 15 nm was epitaxially grown by molecular beam epitaxy (MBE) method. The h-BN was grown by ultra-high vacuum chemical vapor deposition technique (UHV-CVD) at the substrate temperature of 850°C. The precursor for UHV-CVD was borazine which has an analogous structure to benzene.

The SPMDS detect the de-excitation process of polarized metastable helium atoms (2^3S), which is governed by the Pauli principle and sensitive to surface spins. The spin polarized atom of the triplet states was produced by the optical pumping of metastable helium atom beam with circularly polarized light. All measurements and fabrication processes were performed in-situ conditions.

3. Results and discussion

As previously suggested by core-level excitation spectroscopy [1], it was confirmed that the $3d-\pi$ hybridization of Ni and N induces new electronic states in the band gap of h-BN. The SPMDS study revealed that the de-excitation process, which was mainly Auger neutralization (AN) in pristine Ni(111), changed into AN mixed with Auger de-excitation (AD) upon the formation of h-BN. This result indicates that the density of states around the Fermi level was significantly reduced. The spin asymmetry of SPMDS spectra showed that the induced gap states were spin-polarized along the Ni majority spins near the Fermi energy, which agrees well with the density functional theory (DFT) calculations of spin dependent band structure. According to the DFT calculations, the exchange splitting of the gap states were sufficiently large (0.6 eV). This result suggests that the splitting was mainly induced by coupling with Ni atoms.

[1] N. Mårtensson *et al.*, Phys. Rev. B **70**, 165404 (2004).

Corresponding Author: Dr. M. Ohtomo

Tel: +81-29-284-3802, Fax: +81-29-284-3802,

E-mail: ohtomo.manabu@jaea.go.jp

Tetragonal C₄ Polymer: A Two-dimensional Metallic sp² Carbon Allotrope

○Mina Maruyama and Susumu Okada

*Graduate School of Pure and Applied Sciences, University of Tsukuba, 1-1-1 Tennodai,
Tsukuba, Ibaraki 305-8571, Japan*

Carbon molecules are known to form various polygonal conformations due to flexibility of its bonding angle and length. These polygons can be a constituent unit for the various molecular patchworks with zero-, one-, two- and three-dimensions by sewing these polygons. In addition to graphene, it is interested in exploring the possibility of the other two dimensional carbon allotropes consisting of carbon polygons. Among the polygons, tetragons (cyclobutadiene: C₄) can completely cover up a two-dimensional plane. Although cyclobutadiene molecule is unstable under ambient condition, two-dimensional polymerized cyclobutadiene is expected to be stable due to the intermolecular covalent bonds. We study the geometric and electronic structures of a two-dimensionally polymerized C₄ based on the density functional theory with local density approximation.

We find that the polymerized C₄ is stable and keeps its tetragonal bonding network under the equilibrium lattice parameter of $a=0.34$ nm as shown in Fig. 1. Under the equilibrium lattice constant, the C₄ unit almost retains its tetragonal and planer structures: The optimized bond lengths for intra- and inter-unit are found to be 0.142 nm and 0.131 nm, respectively, and the bond angle in the unit is about 90 degree. Calculated total energy is higher than that of grapheme by 0.6 eV/atom. As shown Fig. 2, the polymerized C₄ is a metal with linear dispersion bands at the Fermi level.

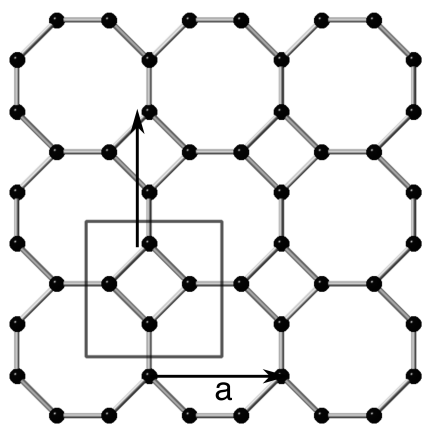


Fig. 1 The optimized structure of the polymerized C₄.

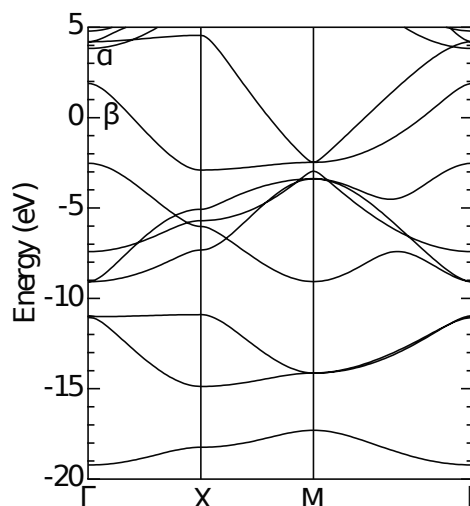


Fig. 2 Electronic structure of polymerized C₄. Energies are measured from that of the Fermi level.

Corresponding Author: Mina Maruyama

E-mail: mmaruyama@comas.frsc.tsukuba.ac.jp

Tel: +81-29-853-5600(ext: 8233)

Graphene-based nanomaterials prepared by laser ablation of graphite

○Maki Nakamura¹, Takazumi Kawai², Michiko Irie¹, Ryota Yuge², Sumio Iijima^{1,2,3},
Shunji Bandow³, Masako Yudasaka¹

¹ *Nanotube Research Center, AIST, 1-1-1 Higashi, Tsukuba 305-8565, Japan*

² *NEC Corporation, 34 Miyukigaoka, Tsukuba 305-8501, Japan*

³ *Meijo University, 1-501 Shiogamaguchi, Nagoya 468-8502, Japan*

Graphene-based nanomaterials are expected to have many applications in the fields of electrochemistry, biomedicine, and so on. We previously reported the oxidation of spherical graphene-based aggregates containing thin graphene sheets (TGSs) and single-walled carbon nanohorns (SWNHs) (Fig. 1) under mild condition, i.e., with hydrogen peroxide at room temperature for a certain period (from 1 hour to 56 days) [1]. By using high resolution thermogravimetric analysis (HR-TGA), we revealed the existence of two types of TGSs; one type (TGS1) was easily oxidized, while the other type was more resistant to oxidation (TGS2). The weight ratio of TGS1 and TGS2 was estimated to be 2:1, but their structures were not clear. In this report, we investigated the characteristics of TGSs, in terms of layer numbers, inter-layer distances, and structure of TGS1 and TGS2.

The spherical aggregates containing TGSs and SWNHs were prepared by CO₂ laser ablation of graphite in Ar (~760 Torr) without auxiliary heating. The weight ratio of TGSs and SWNHs determined by HR-TGA was 45:55. The layer numbers and inter-layer distances of TGSs were determined by using transmission electron microscopy (TEM) images.

The layer number histogram of TGSs showed a distinctive distribution: even-number layered graphenes (2-, 4-, 6- and 8-layers) were preferentially formed (~90%), and their population decreased as the layer number increased. Especially, bi-layers formed most abundantly (~60%). Assuming that TGS1 and TGS2 are attributed to surface layers and inner layers, respectively, the ratio of TGS1 and TGS2 (2:1) estimated in a previous study largely agreed with the layer number counting results. Therefore, it can be concluded that surface-selective oxidation on TGSs occurred by mild oxidation. The inter-layer distances estimated by TEM images were about 15% larger than that of bulk graphite (0.335 nm) in the bi-layer TGSs, and they approached the bulk value as the layer number increased. Supposed growth mechanism of even layer-number preferential growth is that single-layer graphenes are firstly formed, but they are unstable and bends to form bi-layers, and the bi-layers then go on to stack and form thicker TGSs (4-, 6- and 8-layers).

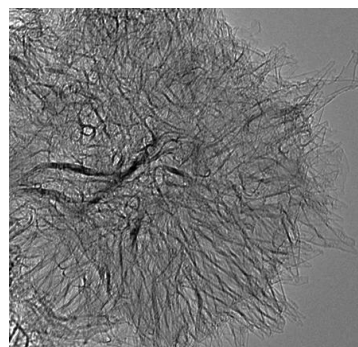


Fig.1 A TEM image of a spherical aggregate containing thin graphene sheets and carbon nanohorns.

[1] M. Nakamura *et al.* The 42th Fullerenes-Nanotubes-Graphene General Symposium, 2012.

Corresponding Author: M. Nakamura, M. Yudasaka

Tel: +81-29-861-6290, Fax: +81-29-861-6290,

E-mail: ma-ki-nakamura@aist.go.jp, m-yudasaka@aist.go.jp

Effects of etchant and synthesis temperature on the sheet-resistivity of nitrogen doped graphene film

Takahiro Mizuno, ○ Shunji Bandow

*Department of Materials Science and Engineering, Meijo University,
1-501 Shiogamaguchi, Tenpaku, Nagoya 468-8502, Japan*

A graphene film can be easily formed on the Cu substrate by the thermal chemical vapor deposition of methanol. In the previous study, we demonstrated that the nitrogen doping effectively lowered the magnitude of the sheet-resistivity by 1/4. However, actual value of the sheet-resistivity for a single sheet of N-doped graphene was still in the order $\sim 10\text{-}20\text{ k}\Omega/(\text{sq}\cdot\text{sheet})$, which is not low enough level. Hence, we study here that the effect of etching method on the sheet-resistivity and also the effects of methanol supplying rate and synthesis temperature on the sheet-resistivity.

First we checked the etchant effect on the sheet-resistivity for pristine un-doped graphene. Two kinds of etchants were used. One is ca. 6M-HCl/H₂SO₄ solution of CuSO₄ (CuSO₄ etchant) and the other is ca. 0.5M-HCl solution of FeCl₃ (FeCl₃ etchant). Same batch of a graphene formed on the Cu foil at 925 °C for 2 min was used, and various graphene samples were prepared by changing the liquid supplying rate between 0.1 and 0.8 cc/min. Figure 1 is a result of the number of graphene layers, which clearly indicates a decrease of the number of layers with decreasing the liquid supplying rate, and the number of layers does not depend on the etchants or acid concentrations. On the other hand, the magnitude of the sheet-resistivity per one graphene layer (normalized R_{sq}) was definitely different as indicated in Fig. 2. This suggests that the strong acid (CuSO₄ etchant) may destroy a one surface layer of stacked graphene and makes the defects, while FeCl₃ etchant does not give such significant effect to the graphene layer.

Next, we checked a synthesis temperature effect on the normalized R_{sq} between 900 and 1000 °C (T_{mp} of Cu is 1083 °C) with a liquid supplying rate 0.16 cc/min. In addition, we used a 0.03 % melamine containing MeOH for the N-doping. Results are in Fig. 3. Although the magnitude of the normalized R_{sq} does not indicate a distinct dependence, obvious drop of the normalized R_{sq} down to $\sim 5\text{ k}\Omega/(\text{sq}\cdot\text{sheet})$ can be seen when a small amount of melamine was added in the liquid source. Hence when we prepare a 5 layered N-doped graphene film, it can be realized the visible light transparency of $\sim 90\%$ and the sheet resistivity of $\sim 1\text{ k}\Omega/\text{sq}$.

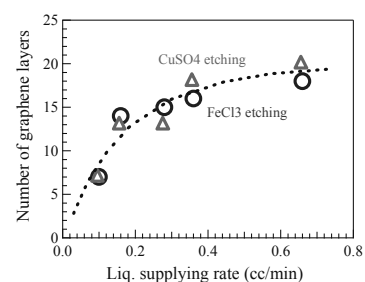


Fig. 1 Number of graphene layers after etching away the Cu. Neither etchant gives serious destruction to the graphene layer.

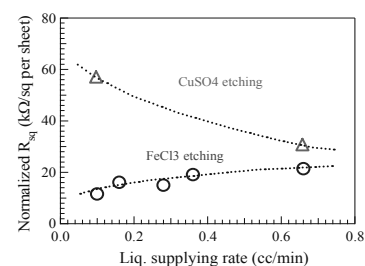


Fig. 2 Liq. supplying rate dependence on the normalized R_{sq} . A CuSO₄ etchant may give the atomic defects in the surface layer of graphene.

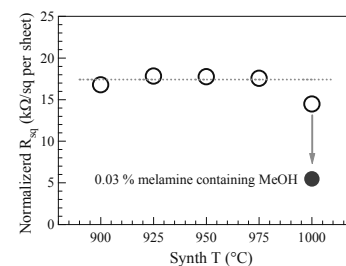


Fig. 3 Synthesis temperature dependence on the normalized R_{sq} .

Corresponding Author: Shunji Bandow, **E-mail:** bandow@meijo-u.ac.jp, **Tel :** +81-52-838-2404

発表索引
Author Index

Author Index

< A >

Achiba, Yohji 3-10, 3P-7, 3P-10
 Ago, Hiroki 1P-30, 1P-35, 1P-41,
 2-11, 2P-36, 3P-38
 Aizawa, Toshihiro 2P-7
 Akasaka, Takeshi 1S-1, 1-1, 2P-6,
 3P-1, 3P-6
 Akiyama, Wataru 3P-4
 Akizuki, Naoto 1P-8
 Ali-Boucetta, Hanene 1P-27
 Antipina, Liubov 2-9
 Aoki, Nobuyuki 1P-9, 3P-4
 Aonuma, Shuji 2P-38, 3P-21
 Aoyagi, Shinobu 3-11
 Arai, Daijiro 2P-10
 Arai, Miho 3S-8
 Arai, Shigeo 3P-34
 Arakawa, Yasuhiko 3P-13
 Aroua, Safwan 1-2
 Asaka, Koji 1P-32
 Atou, Toshiyuki 2P-37
 Avramov, Pavel 2-9, 3P-43
 Awano, Yuji 3P-39

< B >

Baba, Keisuke 1-5
 Baba, Yuji 2-9
 Badar, Saifullah 1P-21
 Bandow, Shunji 1P-29, 2P-45, 3P-45,
 3P-46
 Bird, Jonathan P. 1P-9, 3P-4
 Bissett, Mark 1P-41
 Bussy, Cyril 1P-27

< C >

Caiyu, Qiu 1-10
 Chan, M.Y. 2S-6
 Chaunchaiyakul, Songpol 2-4
 Chen, Zhongming 3P-27
 Chiashi, Shohei 1P-18, 1P-20, 1P-21,
 2-2, 2P-28, 3-2,
 3-6, 3P-13, 3P-26,
 3P-35
 Chiba, Takaaki 3-2
 Cui, Kehang 3-2

< D >

Doi, Satoshi 1P-17, 3P-32
 Doi, Tatsuya 3P-4
 Duan, Zongfan 3P-5

< E >

Eda, Goki 1S-3
 Einarsson, Erik 1P-18, 3-2, 3-6
 Enoki, Toshiaki 1P-40, 1P-42, 2-8,
 2P-41
 Entani, Shiro 2-9, 2P-10, 3P-43

< F >

Fedorov, Alexander 1-6
 Ferreira, A.A. 2S-6
 Fujigaya, Tsuyohiko 3P-12, 3P-25
 Fujihara, Miho 2P-34
 Fujii, Shunjiro 3-1, 3P-5
 Fujino, Tatsuya 3P-10
 Fujita, Wataru 3P-7
 Fujiwara, Keita 1P-44
 Fukaya, Norihiro 2P-19
 Fukuoka, Naoya 2P-26
 Fukuzumi, Shunichi 3-12
 Fumiyuki, Toshimitsu 3P-25
 Funabasama, Tomoyuki 2P-14
 Funatani, Takashi 2P-43
 Furukawa, Ko 1-1
 Furukawa, Shunsuke 1P-36
 Furuya, Souhei 1P-40
 Futaba, Don N. 1P-23, 2P-16, 3P-31,
 3-4
 Futagoishi, Tsukasa 2P-9
 Fuyuno, Naoto 1-7

< G >

Ge, Wanyin 1P-35
 Ghosh, Ranajit 2P-26
 Goto, Jundai 1P-23
 Goto, Takashi 3P-23

< H >

Hamahata, Hiroki 2P-18
 Harano, Koji 1P-36
 Harish, Sivasankaran 3-6
 Haruta, Naoki 2P-5
 Hasdeo, Eddwi 3-8, 3P-19

Hasegawa, Daisuke	1P-21, 2P-28	Imanishi, Masahiro	3-3
Hasegawa, Kai	1P-22, 2P-14	Inaba, Masafumi	2P-20
Hasegawa, Kei	2P-23, 3P-27	Inada, Hiroshi	2P-3
Hasegawa, Masataka	2P-40	Ino, Kosuke	3P-23
Hasegawa, Shigeki	3-3	Inoue, Ayaka	2-5, 2P-15
Hasegawa, Tadashi	3P-1, 3P-6	Inoue, Taiki	1P-21, 2P-28, 3-2
Hashida, Toshiyuki	2P-17	Irie, Michiko	3P-45
Hashiguchi, Masahiko	2P-3	Irle, Stephan	1-6, 3-7, 3-11
Hashimoto, Kenro	3-10	Ishibashi, Koji	1P-9, 3P-24
Hata, Katsuhiko	2P-21	Ishihara, Masatou	2P-40
Hata, Kenji	1P-23, 2P-16, 2P-41, 3-4, 3P-31	Ishii, A.	1P-3, 2P-11
Hatakeyama, Kazuto	3P-42	Ishii, Koji	1P-17, 2P-24, 3P-32
Hatakeyama, Rikizo	1P-19, 2-10	Ishii, Tadahiro	3P-15
Hayakawa, Yoshio	1P-4	Ishii, Takafumi	2P-41
Hayase, Shohei	2P-39, 3P-41	Ishikawa, Kei	3-6
Hayashi, Junki	1P-10	Isobe, Hiroyuki	1-3
Hayashi, Takuya	1P-42	Ito, Akihiko	3P-23
Hida, Akira	3P-24	Ito, Tadamasu	1P-44, 2-7
Higuchi, Kentaro	2P-21	Ito, Yasuhiro	3-1
Hino, Shojun	3-13	Iwamoto, Satoshi	3P-13
Hirai, Daisuke	1P-5	Iwamoto, Takahiro	1P-25
Hiraiwa, Atsushi	2P-20	Iwamura, Munechiyo	1P-8
Hirana, Yasuhiko	2-1, 3P-14	Iwasa, Yoshihiro	1P-12, 2P-18
Hirano, Atsushi	3P-11	Iwata, Nobuyuki	1P-17, 2P-4, 2P-24, 3P-32, 3P-37
Hirao, Norie	2-9	Izumi, Noriko	3-11
Hisama, Kaoru	3P-26, 3P-35	Izumida, Wataru	3P-16
Hitosugi, Shunpei	1-3		
Homma, Naoki	2-2	< J >	
Homma, Yoshikazu	2-2	Jimbo, Takashi	1P-10
Honda, Kazumasa	1P-4	Jippo, Hideyuki	2P-44
Honma, Itaru	1P-31		
Horiguchi, Yukichi	2P-7	< K >	
Hunabasama, Tomoyuki	2P-12	Kaburagi, Yutaka	1P-42
< I >		Kako, Masahiro	3P-1
Ichikawa, Hiroaki	3P-37	Kameda, Tomoshi	3P-11
Igarashi, Toru	2P-14	Kaneko, Toshiro	1P-19, 2-10
Iguchi, Kazuyuki	3S-8	Kano, Ryosuke	2P-8
Iida, Ryosuke	3P-1	Kataoka, Yusuke	2P-19
Iijima, Sumio	1P-27, 1P-28, 1P-29, 2-3, 3P-45	Kataura, Hiromichi	1P-2, 2P-30, 3-1, 3P-5, 3P-11
Iizuka, Ryosuke	1-3	Kato, Tatsuhisa	1-1, 1P-25, 2P-1, 2P-7
Izumi, Yoko	1P-14, 3P-33	Kato, Teppei	3-5
Ikami, Toshiki	1P-44	Kato, Toshiaki	1P-19, 2-10
Ikehara, Yuzuru	1P-14	Kato, Yuichi	2-5, 2P-13, 2P-15, 2P-25
Ikuhara, Yuichi	2P-27		
Ikuma, Naohiko	3P-3	Kato, Yuichiro K.	1P-1, 1P-3, 2P-11, 3P-13
Imamura, Saneyuki	1P-1		

Katsuno, Shunsaku	2-7	Kramberger, Christian	1P-18
Kawahara, Kenji	1P-30, 1P-35, 2-11, 3P-38	Kudo, Hikaru	2P-12
Kawai, Hideki	1P-22	Kumamoto, Akihito	1P-18
Kawai, Masatoshi	2P-12	Kumazawa, Akira	3P-15
Kawai, Takazumi	3P-45	Kunimoto, Ryuji	1P-47
Kawakami, Hiroki	2P-2	Kuno, Akihiro	3P-24
Kawarada, Hiroshi	2P-20	Kusunoki, Michiko	2P-20
Kawashima, Yuki	3-12	Kuwahara, Yuji	2-4
Kawasuzuki, Tomoya	3P-26, 3P-35	Kyakuno, Haruka	1P-2
Kayahara, Eiichi	2P-1	Kyotani, Takashi	2P-41
Kayo, Yasumichi	2P-36	< L >	
Kiguchi, Manabu	2P-41	Li, S.-L.	2S-6
Kigure, Shota	2P-32	Liu, Gang	2-4, 2P-38, 3P-28
Kikuchi, Hayato	1P-24	Liu, Ming	3P-29
Kikuchi, Koichi	3P-7	Lu, Xing	2P-6
Kim, Dong Young	2P-19, 3P-27	< M >	
Kimura, Hiroe	1P-23	Machida, Tomoki	3S-8
Kimura, Masato	3P-6	Maeda, Eriko	1P-34, 2P-34, 3P-36
Kimura, Takahide	2-4, 2P-38, 3P-21, 3P-28	Maeda, Kenji	1P-9
Kinoshita, Hidenori	3-2	Maeda, Yutaka	3P-1, 3P-6
Kishi, Naoki	1P-10	Maki, Hideyuki	3P-40
Kishikawa, Keiki	3P-20	Manako, Takashi	1P-29
Kishimoto, Shigeru	1P-13, 2P-19, 2P-21	Maniwa, Yutaka	1P-2
Kitaura, Ryo	1-7, 1P-26, 1P-34, 2P-34, 3-9, 3-11, 3P-30, 3P-34, 3P-36	Maruyama, Koji	1P-46
Kiyomiya, Masaharu	2P-31	Maruyama, Mina	3P-44
Kizukuri, Shota	1P-39	Maruyama, Shigeo	1P-18, 1P-20, 1P-21, 2P-28, 3-2, 3-6, 3P-13, 3P-26, 3P-35
Kobayashi, Fumito	3P-20	Maruyama, Takahiro	2P-26
Kobayashi, Keita	2P-31	Mase, Kentaro	3-12
Kobayashi, Yu	3P-36	Masubuchi, Satoru	3S-8
Kodama, Takeshi	3-10, 3P-7, 3P-10	Masuda, Tatsuya	3P-38
Kohmoto, Shigeo	3P-20	Masuda, Yoshiho	2P-20
Koinuma, Michio	3P-42	Matsuda, Kazunari	1-7, 1-8, 1P-8, 1P-11, 2-1
Kokubo, Ken	3P-3	Matsue, Tomokazu	3P-23
Koma, Kazunari	2-6	Matsumoto, Naoyuki	2P-16
Komatsu, Katsuyoshi	2-11	Matsumoto, Yasumichi	3P-42
Komatsu, Koichi	1S-2, 1-1, 2S-6	Matsumoto, Yoshihiro	2-9, 2P-10, 3P-43
Komatsu, Naoki	1-7, 2-4, 2P-38, 3P-21, 3P-28	Matsunaga, Masahiro	1P-9
Konabe, Satoru	1-9	Matsuo, Yutaka	2P-2, 2P-3, 3S-9
Kondo, Hiroki	2P-26	Mieno, Tetsu	1P-15, 2P-29
Koretsune, Takashi	1P-39, 3P-17	Mikie, Tsubasa	3P-3
Kostarelos, Kostas	1P-27	Minato, Takuro	1P-32
Kouyama, Takahiko	2P-1	Misawa, Taichi	3P-39
Kowalczyk, Tim	3-11	Mishina, Yuki	2P-45
Kozawa, Daichi	1-7, 1P-11	Miura, Ryohei	1P-1

Miyamoto, Katsuhiko	3P-4	Nakashima, Naotoshi	2S-5, 2-1, 2-5,
Miyamoto, Yoshiyuki	1P-37		2P-13, 2P-15, 2P-25,
Miyashita, Masahiro	2-11		3P-12, 3P-14, 3P-25
Miyata, Yasumitsu	1P-2, 1P-26, 1P-34,	Nakatsu, Touru	1P-22
	2P-34, 3-9, 3P-30,	Namba, Ryoichi	3-3
	3P-34, 3P-36	Naramoto, Hiroshi	2-9, 3P-43
Miyauchi, Yuhei	1-7, 1-8, 1P-8,	Narita, Ayumi	2-9
	1P-11, 2-1	Naritsuka, Shigeya	2P-26
Miyaura, Kenshi	1P-26	Nihey, Fumiyuki	1P-16
Miyazaki, Daigo	3P-14	Niidome, Yasuro	2-5, 2P-13, 2P-15,
Miyazaki, H.	2S-6		2P-25, 3P-14
Miyazaki, Takafumi	3-13	Nikawa, Hidefumi	1-1
Mizorogi, Naomi	1-1, 2P-6	Nishi, Tatsuhiko	3-13
Mizuno, Takahiro	3P-46	Nishibori, Eiji	3-11
Mizutani, Takashi	1P-13, 2P-19, 2P-21	Nishimura, Yoshifumi	1-6, 3-7
Momiyama, Daiki	3P-4	Nishioka, Yasushiro	3P-5
Mori, Tatsuya	3P-40	Nitta, Haruna	3P-9
Morikawa, Sei	3S-8	Niwa, Hiroyuki	3-13
Morinaka, Yuta	1-1	Niwase, Keisuke	2P-37
Moriyama, Hiroshi	1-4	Nobusa, Yuki	2P-12, 2P-18
Moriyama, Yuki	3P-20	Noda, Shoko	3-13
Motomiya, Kenichi	2P-17, 3P-23	Noda, Suguru	2P-19, 2P-23, 2P-27,
Mouri, Shinichiro	1-7, 1-8, 1P-8,		3P-27
	1P-11, 2-1	Nugraha, Ahmad	3-8, 3P-19
Murakoshi, Kei	2P-35	Numata, Hideaki	1P-16
Murakoshi, Koshi	1P-19		
Murata, Michihisa	1-1, 2P-9, 3P-2	< O >	
Murata, Shigeaki	3-3	Ochiai, Takumi	2P-20
Murata, Yasujiro	1-1, 2P-9, 3P-2	Ochiai, Yuichi	1P-9, 3P-4
< N >		Ogata, H.	3P-41
Na, Nuri	2P-27	Ogata, Hironori	1-5, 2P-22, 2P-39
Nagasaki, Yukio	2P-7	Ogawa, Matsuto	2P-43
Nagase, Shigeru	1-1, 2P-6	Ogawa, Yui	2-11
Nagaya, Yuka	3P-15, 3P-24	Ogura, Mutuo	1P-14
Naitou, Yasuhisa	1P-22	Ohfuchi, Mari	2P-44
Nakahara, Hitoshi	1P-32, 2P-33	Ohkubo, Kei	3-12
Nakaharai, S.	2S-6	Ohno, Yutaka	1P-11, 1P-13, 2P-19,
Nakai, Yusuke	1P-2		2P-21
Nakajima, Yuta	2P-21	Ohta, Kazutoku	1P-4
Nakamura, Eiichi	1P-36	Ohta, Tomona	3-13
Nakamura, Kazutaka	2P-37	Ohtomo, Manabu	2-9, 2P-10, 3P-43
Nakamura, Keisuke	3P-21	Okada, Hiroshi	2P-2
Nakamura, Kenta	1P-20	Okada, Satoshi	1P-36
Nakamura, Maki	3P-45	Okada, Susumu	1-9, 2P-32, 2P-42,
Nakanishi, Ryo	3P-34		3P-8, 3P-18, 3P-44
Nakanishi, Yusuke	3-13	Okamoto, Mitsuhiro	1P-25
Nakano, Atsushi	2P-22	Okazaki, Toshiya	1P-14, 2-3, 3P-20,
Nakano, Kaichiro	1P-29		3P-33
		Oki, Shusuke	3P-39

Okigawa, Yuki	2P-40	Sekiguchi, Tetsuhiro	2-9
Okimoto, Haruya	1P-33	Shames, Alexander. I.	1P-42
Okukawa, Takanori	3P-5	Shibata, Okinaga	2-6
Omatsu, Takashige	3P-4	Shibuya, Megumi	2P-20
Ono, Shimpei	2P-14	Shimada, Takashi	2P-11, 3P-13
Ono, Taizo	1P-4	Shimizu, Kazuki	1P-47
Onuki, Masahiro	3S-8	Shimizu, Maki	3-1
Oohara, Kazuyoshi	2P-20	Shimizu, Ryo	1P-12
Osawa, Eiji	1P-43	Shimoyama, Iwao	2-9
Oshima, Azusa	2P-16	Shinohara, Hisanori	1-7, 1P-26, 1P-34,
Oshima, Takumi	3P-3		2P-7, 2P-34, 3-9,
Oshima, Yugo	1P-6		3-11, 3-13, 3P-30,
Osipov, Vladimir Yu	1P-42		3P-34, 3P-36
Osonoe, Kana	2P-8	Shiomi, Junichiro	3-6
Oto, Tetsuya	3P-15	Shiraki, Yuki	2P-45
Otsuka, Keigo	1P-21, 2P-28	Shiromaru, Haruo	3-10, 3P-10
Ozawa, Masaki	1P-44, 2-7	Shoji, Mao	2P-22, 3P-41
		Simizu, Kazuki	1P-46
< P >		Slanina, Zdenek	2P-6
Pu, Jiang	3P-22	So, Yeong-Gi	2P-27
		Sobe, Yuhei	1P-33
< R >		Soga, Tetsuo	1P-10
Rahman, Mohammad Jellur	2P-29	Solis-Fernández, Pablo	2P-36
Ruammaitree, Akkawat	2P-33	Sone, Junki	2P-42
		Sorokin, Pavel	2-9
< S >		Souma, Satofumi	2P-43
Sado, Yuki	3-11	Su, Yuquan	3P-29
Sagara, Takumi	3P-32	Subramaniam, Chandramouli	3-4
Saito, Riichiro	1-10, 3-8, 3P-16,	Suda, Yoshiyuki	1P-46, 1P-47
	3P-19	Sugai, Toshiki	1P-24, 2P-46
Saito, Susumu	1P-39, 3P-17	Sugimoto, Kunihisa	3-11
Saito, Takeshi	1P-10, 1P-16, 2P-31	Suguru, Noda	3P-38
Saito, Yahachi	1P-32, 2P-33	Sun, Yun	3P-30
Sakai, Seiji	2-9, 2P-10, 3P-43	Susumu, Okada	3P-9
Sakakibara, Hajime	3P-23	Suzuki, Hideaki	2P-17
Sakamoto, Shingo	1P-7	Suzuki, Hironori	3P-33
Sakurai, Shunsuke	1P-23, 3P-31	Suzuki, Mitsuaki	2P-6
Sano, Masahito	1P-33	Suzuki, Takashi	1P-15
Sasaki, Fusako	1P-16		
Sasaki, Shuichi	1P-43	< T >	
Sasaki, Yuki	3-13	Tachibana, Masaru	2P-8, 2P-37
Sato, Kentaro	3P-19	Tadera, Shin	1P-2
Sato, Satoru	1-1	Tahara, Yoshio	1P-28
Sato, Shintaroh	2-2	Takabayashi, Syun	1P-33
Sato, Shogo	3P-37	Takada, Yukihiro	1P-38
Sato, Tohru	2P-5	Takagi, Kentaro	3P-1
Sato, Yoshiaki	1P-40, 2-8	Takagi, Yuki	1P-6, 1P-22, 3P-22
Sato, Yoshinori	2P-17, 3P-23	Takahashi, Masahiro	3P-20
Sawaki, Yuya	2P-26		

Takai, Kazuyuki	1P-40, 1P-42, 2-8, 2P-41	Umeda, Yoshito	1P-46, 1P-47
Takaki, Yuki	3P-26, 3P-35	Umino, Takanori	1P-20
Takashima, Kengo	1P-38	Urabe, Yasuko	2P-30
Takashiro, Junichi	2P-41	Uruchida, Katsuya	2P-4
Takayama, Yusuke	3P-40	Usui, Shinji	3-5
Takenobu, Taishi	1P-6, 1P-12, 1P-22, 2P-12, 2P-18, 3S-7, 3P-22	< V >	
Takesue, Masafumi	2P-21	Vul' Alexander, Ya	1P-42
Takikawa, Hirofumi	1P-46, 1P-47	< W >	
Tamura, Naoki	1P-31	Wada, Yoriko	1P-45, 2-6
Tanabe, Fumiyuki	1-1	Wada, Yoshifumi	3P-22
Tanaka, Hideyuki	1P-36	Wakabayashi, Tomonari	1P-45, 2-6
Tanaka, Kazuyoshi	2P-5	Wakamiya, Atsushi	1-1
Tanaka, Takeshi	2P-30, 3-1, 3P-5, 3P-11	Wakamori, Ikuya	1P-26
Tang, Zikang	3P-29	Wang, Feijiu	1P-11
Tange, Masayoshi	2-3, 3P-20	Wang, Feng	2-4
Taniguchi, Takaaki	3P-42	Wang, Jian	3-11
Taniguchi, Takashi	3S-8	Wang, Zhipeng	2P-39, 3P-41
Tanimoto, Hisanori	2P-10	Warner, Jamie	3P-34
Tanoue, Hideto	1P-46, 1P-47	Watahiki, Ryosuke	1P-1, 3P-13
Tanoue, Shota	1P-30	Watanabe, Kenji	3S-8
Tatsumi, Yuki	3P-16	Watanabe, Satoshi	1P-5
Terada, Katsuhide	1P-24	Wei, Xiaojun	1P-9
Thendie, Boanerges	1P-26	Witek, Henryk	1-6, 3-7
Thurakitseree, Theerapol	1P-18, 3-2	< X >	
Ting, Yu	1-10	Xiang, Rong	3P-29
Togashi, Aimi	3P-7	< Y >	
Tohji, Kazuyuki	2P-17, 3P-23	Yahagi, Taturou	1P-9
Tomai, Takaaki	1P-31	Yajima, Hirofumi	1P-17, 2P-24, 3P-15, 3P-24, 3P-32
Tominaga, Masato	1P-7	Yamada, Michio	3P-1, 3P-6
Tomura, Takuya	2P-21	Yamada, Takatoshi	2P-40
Toriumi, Naoto	3P-4	Yamada, Takeo	2P-41, 3-4
Toyama, Kiyohiko	1P-29	Yamago, Shigeru	1P-25, 2P-1
Tsuchiya, Koji	3P-15, 3P-24	Yamaguchi, Takashi	1P-29
Tsuda, Yusaku	1P-17	Yamaguchi, Takehiro	3S-8
Tsugawa, Kazuo	2P-40	Yamakoshi, Yoko	1-2
Tsuji, Masaharu	1P-30, 1P-35, 1P-41, 2-11, 2P-36	Yamamoto, Go	2P-17
Tsukagoshi, Kazahito	2S-6, 2-11	Yamamoto, Hiroshi	1P-17, 2P-4, 2P-24, 3P-32, 3P-37
Tsuya, Daiju	3P-40	Yamamoto, Hiroyuki	3P-3
Tsuzuki, Akiko	2P-15	Yamamoto, Kazuhiro	1P-4
< U >		Yamamoto, Takahiro	1P-5, 1P-38, 2-2, 2P-43, 3-5, 3P-8
Uchiyama, Kouya	1-4	Yamamoto, Yuta	3P-34
Ue, Hitoshi	1P-46, 1P-47	Yamanaka, Ayaka	3P-18
Ueda, Chihiro	3P-6		

Yamanoi, Ryoko	1P-43
Yamasaki, Takashi	1-3
Yamauchi, Yasushi	3P-43
Yamawaki, Hiroshi	1P-4
Yanagi, Kazuhiro	1P-2, 1P-6, 1P-12, 1P-22, 2P-12, 2P-14, 2P-18, 3P-22
Yanagi, Yuichiro	3P-5
Yang, Mei	1P-27, 1P-28
Yasuda, Hidehiro	2P-31
Yasuda, Satoshi	1P-23, 2P-35
Yasuda, Toku	1-7, 2P-38
Yasunishi, Tomohiro	1P-13
Yokoi, Hiroyuki	3P-42
Yokoi, Tomoya	3P-40
Yokoyama, A.	1P-3, 2P-11
Yomogida, Yohei	2P-18
Yonemura, Taiichiro	1P-47
Yoo, JongTae	3P-12
Yoshida, Akira	3P-5
Yoshida, Kazuma	2P-36
Yoshida, M.	1P-3, 2P-11
Yoza, Kenji	1-4
Yu, Li	2P-35
Yudasaka, Masako	1P-14, 1P-27, 1P-28, 1P-29, 3P-45
Yuge, Ryota	1P-29, 3P-45
Yumura, Motoo	1P-23, 2P-16, 3P-31, 3-4
 < Z >	
Zhang, Jinying	3P-30
Zhang, Minfang	1P-27, 1P-28
Zhang, Rui	3P-2
Zhang, Yijin	1P-12
Zhao, Li	2P-38, 3P-21
Zhao, Pei	3-2, 3P-13
Zhao, Sihan	3-9
Zheng, Ming	2S-4

複写をご希望の方へ

フラーレン・ナノチューブ・グラフェン学会は、本誌掲載著作物の複写に関する権利を一般社団法人学術著作権協会に委託しております。

本誌に掲載された著作物の複写をご希望の方は、(社)学術著作権協会より許諾を受けて下さい。但し、企業等法人による社内利用目的の複写については、当該企業等法人が社団法人日本複写権センター((社)学術著作権協会が社内利用目的複写に関する権利を再委託している団体)と包括複写許諾契約を締結している場合にあっては、その必要はございません(社外頒布目的の複写については、許諾が必要です)。

権利委託先：一般社団法人学術著作権協会

〒107-0052 東京都港区赤坂 9-6-41 乃木坂ビル 3階

TEL : 03-3475-5618 FAX : 03-3475-5619 E-mail : info@jaacc.jp

注意：複写以外の許諾(著作物の引用、転載・翻訳等)に関しては、(社)学術著作権協会に委託致していません。直接、フラーレン・ナノチューブ・グラフェン学会へお問い合わせください。

Reprographic Reproduction outside Japan

- Making a copy of this publication

Please obtain permission from the following Reproduction Rights Organizations (RROs) to which the copyright holder has consigned the management of the copyright regarding reprographic reproduction.

- Obtaining permission to quote, reproduce; translate, etc.

Please contact the copyright holder directly.

Users in countries and regions where there is a local RRO under bilateral contract with Japan Academic Association for Copyright Clearance(JAACC) are requested to contact the respective PROs directly to obtain permission.

Users in countries or regions in which JAACC has no bilateral agreement are requested to apply for the license to JAACC.

Japan Academic Association for Copyright Clearance (JAACC)

Address : 9-6-41 Akasaka, Minato-ku, Tokyo 107-0052 Japan

Website : <http://www.jaacc.jp/>

E-mail : info@jaacc.jp TEL : 81-3-3475-5618 FAX : 81-3-3475-5619

2013年3月11日 発行

第44回フラーレン・ナノチューブ・グラフェン総合シンポジウム 講演要旨集

<フラーレン・ナノチューブ・グラフェン学会>

〒113-8656 東京都文京区本郷 7-3-1

東京大学 大学院工学系研究科 機械工学専攻

丸山研究室内

TEL / FAX : 03-3830-4848

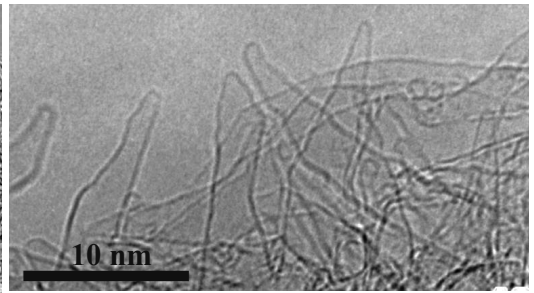
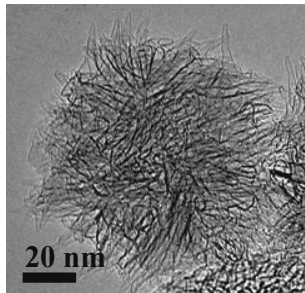
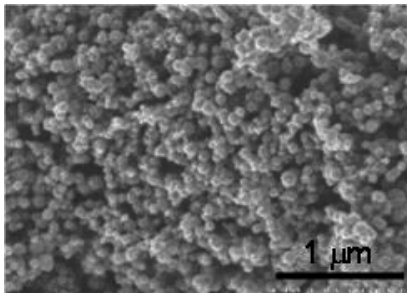
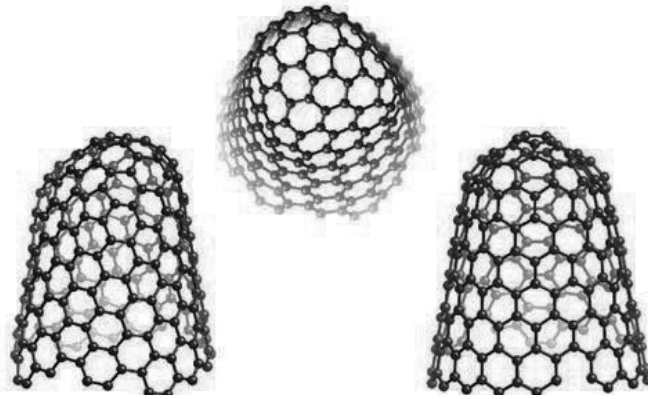
E-mail : fntg@photon.t.u-tokyo.ac.jp

URL : <http://fullerene-jp.org/>

印刷 / 製本 (株) 創志企画

グリーンイノベーションに貢献する革新的で実用向きの材料

カーボンナノホーン



日本電気株式会社
共通ソリューション開発本部

〒108-8423 東京都港区芝五丁目21-6(芝ダイビル)
TEL : 03-3798-6402
E-Mail : info@embedded.jp.nec.co

サンプル販売中！

1グラムからサンプルをご用意しています。
詳しくは、ホームページを御覧ください。

カーボンナノホーン サンプル販売ホームページ

<http://www.nec.co.jp/embedded/products/cnh/>



これが、新しいラマンのかたち。



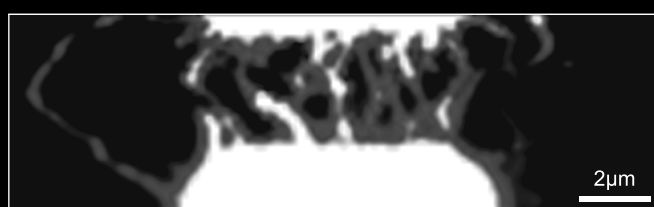
レーザーラマン顕微鏡

RAMANtouch

世界最高の空間分解能と超高速ラマンイメージング

- 回折限界に迫る 350nmの空間分解能
- ライン照明による超高速ラマンイメージング
- **[NEW]** グラフェン解析に便利な新ツールを今春リリース予定！

CNTの高分解能ラマンイメージング

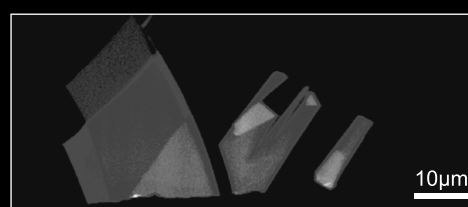


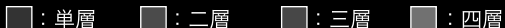
Gバンド強度： 強  弱

CNT-FET（電界効果トランジスタ）のラマンイメージです。電極間に合成されたCNTの分布を、回折限界に迫る空間分解能で捉えています。（532nm、100倍、13,200画素、16分）

※このサンプルは、東京大学の丸山茂夫教授よりご提供頂きました。

グラフェンの層数分布イメージング



 : 単層  : 二層  : 三層  : 四層

熱酸化したシリコン基板上に分布するグラフェン薄膜をラマンイメージングした画像です。単層および多層グラフェンの分布を、5分で測定できます。（532nm、100倍、67,600画素、5分）

※このサンプルは、物質・材料研究機構の津谷大樹様よりご提供頂きました。

溶液中の粒子のナノレベル微細化・分散に

BRANSON 超音波ホモジナイザー

ホーン先端部の振幅の安定性を、より高めた Advance タイプ になりました。

近年のナノテクノロジーの発展及び粉体関連技術の向上により、より微細な粒子に対する乳化分散処理の要望が増えてまいりました。

超音波ホモジナイザーを使用し、均質な乳化分散処理を行い、安定させることにより製品の機能は向上します。

ブランソン社では 20kHz 機と、40kHz 機の 2 タイプを用意しております。

1 次粒子の凝集力にも拠りますが、20kHz 機では 100nm 程度までの分散力があります。40kHz 機は、さらに細かいレベルで分散ができる可能性があります。



20KHz 超音波ホモジナイザー
BRANSON SONIFIER シリーズ

高周波 40KHz 超音波ホモジナイザー
BRANSON SLPe シリーズ



ブランソン社の製品は、ホーン先端部の振幅の安定性が高く、強力なキャビテーションが得られ、効率良く、再現性の高い分散処理が行えます。

主なアプリケーション

分散

カーボンナノチューブ 有機顔料 無機顔料 セラミック セメント 感光体 記録材料
磁性粉 粉末冶金 酸化鉄 金属酸化物 シリカ アルミナ カーボンブラック
ポリマー ラテックス 製紙 ファンデーション

研磨剤 電池 フィラー 光触媒 触媒 ワクチン 体外診断薬 歯磨き粉 シャンプー
半導体 電子基盤 液晶 貴金属 金属 宝石 タイヤ 発酵菌類 その他

乳化

エマルジョン製剤 農薬 トナー ラテックス 界面活性剤 クリーム 乳液 クリーム 等

SC 株式会社 **セントラル** 科学貿易

本社：111-0052 東京都台東区柳橋 1-8-1
Tel 03-5820-1500 Fax 03-5820-1515
URL <http://www.cscjp.co.jp/>

大阪支店：Tel 06-6325-3171 Fax 06-6325-5180
福岡営業所：Tel 092-482-4000 Fax 092-482-3797
札幌出張所：Tel 011-764-3611 Fax 011-764-3612

ナノラプター NANORUPTOR[®] サンプル密閉式超音波分散装置

—— バイオの技術をナノテクへ ——

本装置はカーボンナノチューブ・グラフェンや燃料電池用触媒を始めとする
各種ナノ粒子を分散させる事を目的に開発いたしました。

実施例：カーボンナノチューブ・グラフェンの分散、燃料電池触媒評価
納入実績：各大学、自動車メーカー、光学機器メーカー、電子部品メーカー



デモ機をご用意
しております。
どうぞお気軽に
問い合わせ
ください。



回転機構付破碎槽



標準50mlチューブ



高効率新型破碎槽



15mlチューブ



ネット・収束装置付破碎槽



1.5mlチューブ

対象試料 / 特長

- カーボンナノチューブ、フラーレン、グラフェン等ナノ粒子
- 密閉処理（ナノリスク低減）：溶媒の蒸発・揮散やコンタミがありません。
- 多検体同時処理（100μl～20ml）：試料チューブの選択により、複数試料を同時に処理できます。
- 再現性良好：回転機構の採用により均一な超音波照射が可能です。
- 低騒音：高性能防音箱の採用により、超音波特有の騒音を防止。
- 温度制御が容易：バスタブ式なので低温から40℃まで任意に設定可能（オプション）。

NR-350仕様（予告無く変更する場合があります）

品番	NR-350
品名	密閉式超音波分散装置 Nanoruptor
超音波周波数	20 kHz
超音波出力	380,300,250,130 W (切替式)
電源	100 V、50/60 Hz、5.5 A
最低設置スペース概寸	400 (W) × 350 (D) × 680 (H) mm
発振ユニット概寸	400 (W) × 280 (D) × 160 (H) mm
処理ユニット概寸	250 (W) × 200 (D) × 300 (H) mm
消音箱概寸	400 (W) × 350 (D) × 520 (H) mm
NR-350 全体重量	36 Kg
ランタイム	599 サイクル
インターバルタイマー (ON)	0 ~ 59 秒、デジタル
インターバルタイマー (OFF)	0 ~ 59 秒、デジタル
処理本数	1 本 (50 mL チューブ) ~ 各種
付属品	高性能消音箱、電源ケーブル 接続ケーブル、排水ポンプ 取り扱い説明書、ユーザー登録カード
備考	NR-350 は機器のみです。別途処理量に応じたアクセサリ（ギヤ - 板 + チップ）をお買い求め下さい。

品名	品番	包装	希望販売価格
超音波密閉式分散装置	NR-350	1 UNIT	¥1,950,000-
50 mL チューブ用チップ	MM-50WS	1 SET	¥54,000-
使用可能チューブ：マルエム社製 50 mL ねじ口試験管			
ギヤ板	NG350-50	1 PC	¥9,000-
冷水循環器	CP80-R	1 UNIT	¥264,000-
冷水循環器接続チューブ	TU-100	1 PC	¥15,000

販売



人と科学のステキな未来へ

コスモ・バイオ株式会社

〒135-0016 東京都江東区東陽2-2-20 東陽駅前ビル
URL: <http://www.cosmobio.co.jp>
TEL (03) 5632-9610 FAX (03) 5632-9619
販売支援部 栗原 mkurihar@cosmobio.co.jp
開発部 笹原 ksasahar@cosmobio.co.jp

製造



東湘電機株式会社

〒232-0027 神奈川県横浜市南区新川町5-29-2 新井ビル2F
TEL (045) 261-8388 FAX (045) 252-8935
技術部長 伊藤
e-mail: k-ito@bioruptor.jp

分取 HPLC のスタンダード 好評の NEXT シリーズ

JAI のリサイクル分取 HPLC は発売以来40年
特に国内外の有機合成研究室で活躍しています。

高性能

使いやすさ

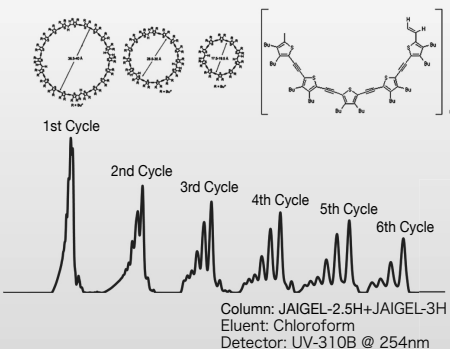
メンテナンス性能

3つの要素を徹底的に追求したNEXTシリーズが
あなたのラボの作業効率を飛躍的に向上。

コンパクト&スマート
次の時代へ
NEXTシリーズ

JAI

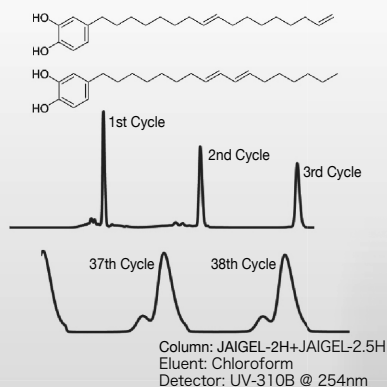
GPCリサイクルによる
Macrocylic Oligothiophenesの分離



Feature

- ・液晶タッチパネルインターフェイス
- ・溶媒置換に便利な自動洗浄機能
- ・PCコントロールで遠隔操作
- ・同一試料の重ね打ち注入
- ・全自動で繰返し注入&分取が可能
- ・独自のリサイクル(特許)を標準装備

GPCリサイクルによる位置異性体の分離



最大流量

- ・LC-9110NEXT 10ml/min MAX
- ・LC-9130NEXT 30ml/min MAX



LC-9110NEXT / LC-9130NEXT

JAI 日本分析工業株式会社

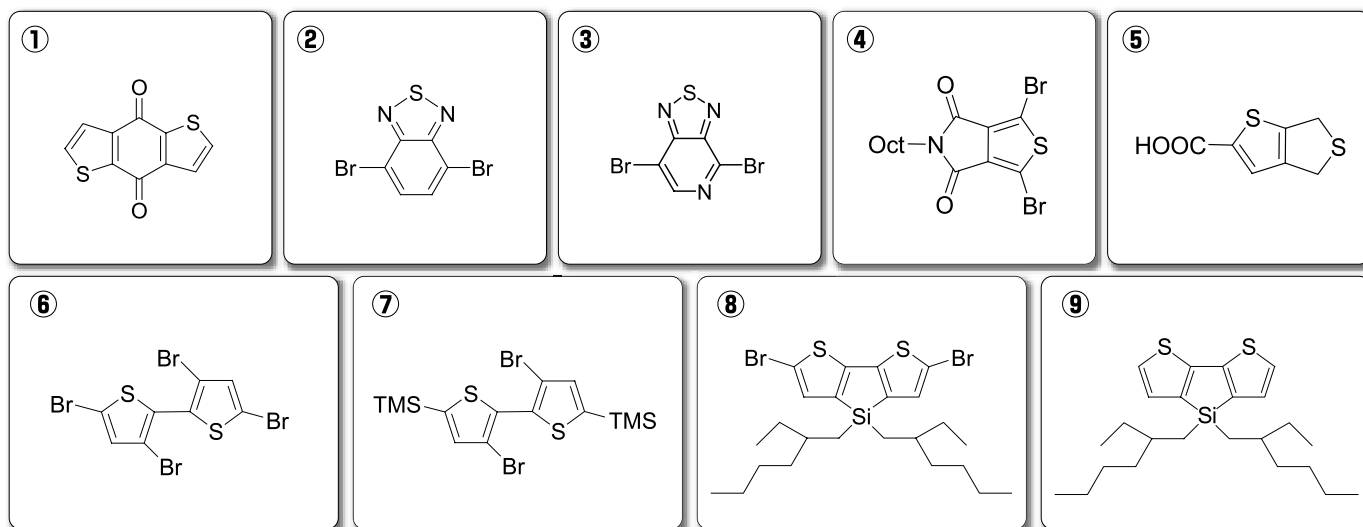
URL <http://www.jai.co.jp/> ISO9001/14001 取得

■本社・工場：〒190-1213 東京都西多摩郡瑞穂町武蔵 208 TEL 042-557-2331 FAX 042-557-1892
 ■大阪営業所：〒532-0002 大阪市淀川区東三国 5-13-8-303 TEL 06-6393-8511 FAX 06-6393-8525
 ■名古屋営業所：〒465-0025 愛知県名古屋市名東区上社 3-609-3D TEL 052-709-5400 FAX 052-709-5403

JAI Japan Analytical Industry Co., Ltd.

有機薄膜太陽電池材料合成用 ビルディングブロック

次世代の太陽電池として期待される有機薄膜太陽電池の研究用試薬です。
誘導化に利用しやすいよう様々なタイプの中間体をラインアップしました。
材料合成にご利用下さい。



番号	コードNo.	品名	規格	容量
①	025-17321	Benzo[1,2- <i>b</i> :4,5- <i>b'</i>]dithiophene-4,8-dione	有機合成用	1g
	021-17323			5g
②	045-31961	4,7-Dibromo-2,1,3-benzothiadiazole	有機合成用	1g
	041-31963			5g
	043-31962			25g
③	043-32121	4,7-Dibromo-[1,2,5]thiadiazolo[3,4- <i>c</i>]pyridine	有機合成用	250mg
	049-32123			1g
④	042-31971	1,3-Dibromo-5-octyl-4 <i>H</i> -thieno[3,4- <i>c</i>]pyrrole-4,6(5 <i>H</i>)-dione	有機合成用	1g
	048-31973			5g
⑤	049-31981	4,6-Dihydrothieno[3,4- <i>b</i>]thiophene-2-carboxylic Acid	有機合成用	1g
	045-31983			5g
⑥	208-18851	3,3',5,5'-Tetrabromo-2,2'-bithiophene	有機合成用	1g
	204-18853			5g
	206-18852			25g
⑦	040-32131	3,3'-Dibromo-5,5'-bis(trimethylsilyl)-2,2'-bithiophene	有機合成用	1g
	046-32133			5g
⑧	047-32141	2,6-Dibromo-4,4'-bis(2-ethylhexyl)-4 <i>H</i> -silolo[3,2- <i>b</i> :4,5- <i>b'</i>]dithiophene	有機合成用	1g
⑨	024-17651	4,4'-bis(2-ethylhexyl)-4 <i>H</i> -silolo[3,2- <i>b</i> :4,5- <i>b'</i>]dithiophene	有機合成用	1g
	020-17653			5g

ご購入に際し製品情報（適用法規・保管条件など）のご確認は、当社総合カタログおよび検索サイト（siyaku.com）をご参照ください。

和光純薬工業株式会社

本社：〒540-8605 大阪市中央区道修町三丁目1番2号
 東京支店：〒103-0023 東京都中央区日本橋本町四丁目5番13号
 営業所：北海道・東北・筑波・東海・中国・九州

問い合わせ先
 フリーダイヤル：0120-052-099 フリーファックス：0120-052-806
 URL：http://www.wako-chem.co.jp
 E-mail：labchem-tec@wako-chem.co.jp



COSMOSIL

誘導体化フラーレン用HPLCカラム

COSMOSIL[®] Buckyprep-D

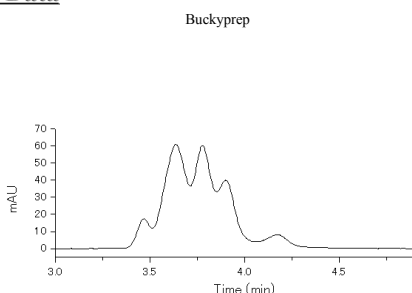
- 誘導体化フラーレン用HPLCカラム
- トルエン移動相中で誘導体化フラーレンが分離可能

■ C₆₀インデン付加体の分析例

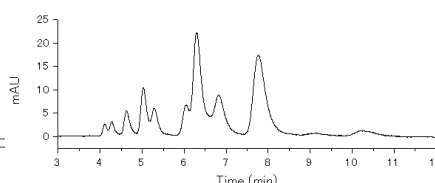
C₆₀インデンは誘導体化フラーレンの一種であり、有機薄膜太陽電池のn型半導体材料として注目されている化合物です。コスモシール Buckyprep-Dを用いることにより高い分離性能が得られます。

COSMOSIL Application Data

Column: Buckyprep
 Column size: 4.6mm I.D.-250mm
 Mobile phase: Toluene
 Flow rate: 1.0 ml/min
 Temperature: 30°C
 Detection: UV 325nm
 Sample: C₆₀ [Indene]₂ (1.0mg/ml)
 Inj. Vol.: 1.0μl



Buckyprep-D



Data courtesy of Yusuke Tajima, Dr. Sci. Organic Optoelectronics Laboratory, RIKEN (Institute of Physics and Chemistry)

NACALAI TESQUE, INC

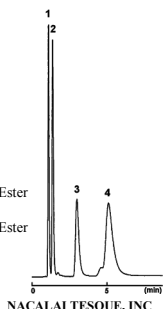
■ Buckyprepシリーズの用途

- フラーレン分離のスタンダードカラム → COSMOSIL Buckyprep
- 誘導体化フラーレンの分離 → COSMOSIL Buckyprep-D
- 金属内包フラーレンの分離 → COSMOSIL Buckyprep-M

・ 誘導体化フラーレン (Buckyprep-D)

COSMOSIL Application Data

Column: Buckyprep-D
 Column size: 4.6mm I.D.-50mm
 Mobile phase: Toluene
 Flow rate: 1.0 ml/min
 Temperature: 30°C
 Detection: UV325nm
 Sample: 1; C₆₀ (0.125mg/ml)
 2; C₇₀ (0.250mg/ml)
 3; [6,6]-Phenyl-C₆₁ Butyric Acid Methyl Ester [PCBM] (0.125mg/ml)
 4; [6,6]-Phenyl-C₇₁ Butyric Acid Methyl Ester [[70]PCBM] (0.375mg/ml)
 Inj. Vol. 1.0μl

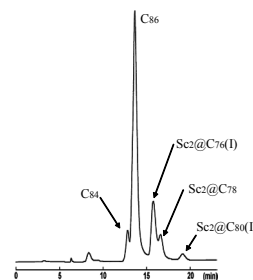


NACALAI TESQUE, INC

・ 金属内包フラーレン (Buckyprep-M)

COSMOSIL Application Data

Column: Buckyprep-M
 Column size: 4.6mm I.D.-250mm
 Mobile phase: Toluene
 Flow rate: 1.0 ml/min
 Temperature: 30°C
 Detection: UV312nm
 Sample: Sc₂@C₇₆(I)
 Sc₂@C₇₈
 Sc₂@C₈₀(I)
 C₈₆



NACALAI TESQUE, INC

Sample courtesy of Prof. H. Shinohara, Department of chemistry, Nagoya University

詳しい情報はWeb siteをご覧ください。

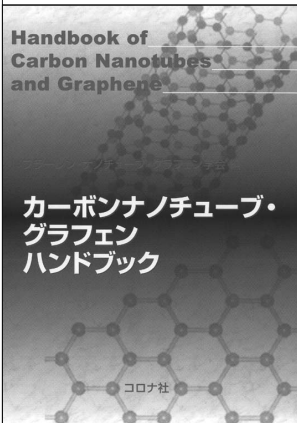
ナカライテスク株式会社

〒604-0855 京都市中京区二条通烏丸西入東玉屋町498

価格・納期のご照会 フリーダイヤル 0120-489-552
 製品に関するご照会 TEL:075-211-2746 FAX:075-211-2710
 Web site :<http://www.nacalai.co.jp>

書籍のご案内

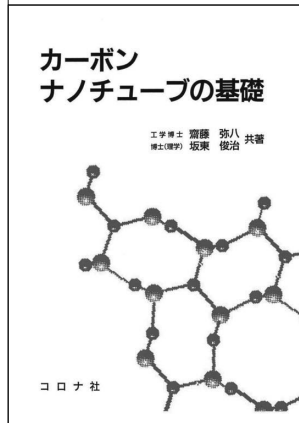
カーボンナノチューブ・ グラフェンハンドブック



フラーレン・ナノチューブ・
グラフェン学会 編
B5判/368頁
定価10,500円

本ハンドブックでは、カーボンナノチューブの基本的事項を解説しながら、エレクトロニクスへの応用、近赤外発光と吸収によるナノチューブの評価と光通信への応用の可能性を概観。最近囁目のグラフェンやナノリスクについても触れた。

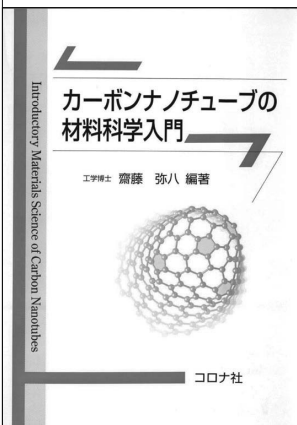
カーボンナノチューブの基礎



齋藤弥八・坂東俊治
共著
A5判/220頁
定価2,940円

カーボンナノチューブはC₆₀ フラーレンに次ぐ新しい炭素材料であり、エレクトロニクスやエネルギー分野への応用が注目されている。本書は、ナノチューブとその関連物質の作製法、構造、物性および応用を平易に述べた入門書である。

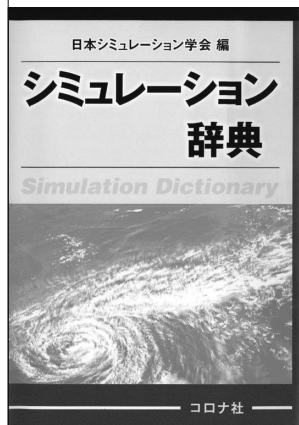
カーボンナノチューブの 材料科学入門



齋藤弥八 編著
坂東俊治・中山喜萬・
春山純志・久保佳実
共著
A5判/250頁
定価3,570円

材料科学に新分野を創出し、エレクトロニクスからエネルギー分野まで広範囲な応用が期待されるナノテクノロジー材料の典型物質「カーボンナノチューブ」について、その製法から物性、実用の可能性までを解説した。

シミュレーション辞典



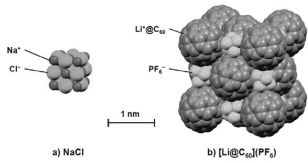
日本シミュレーション学会 編
A5判/452頁
定価9,450円

シミュレーションの内容を共通基礎、電気・電子、機械、環境、生命、社会、可視化、通信の八つに区分し、シミュレーションの学理と技術に関する広範囲の内容について、1ページを1項目として約380項目をまとめた。

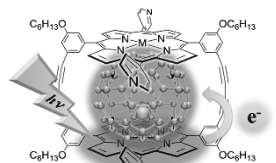


リチウム内包フラーレンは $\text{Li}^+@C_{60}$

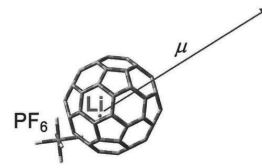
Li^+ イオンを殻内に偏在させた C_{60} を使って
 応用上興味深い性質を備えた新しい”分子”が次々と産み出されています。



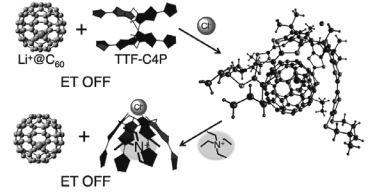
$[\text{Li}^+@C_{60}] \cdot \text{PF}_6^-$
 S.Aoyagi, H.Shinohara et al.,
 Angew.Chem.Int.Ed. 2012,51,3377-3381



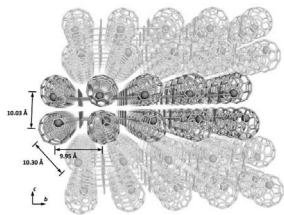
$\tau(\text{CS}) = 0.50 \text{ ms (M = H}_2), 0.67 \text{ ms (M = Ni)}$
 超分子錯体の長寿命光電荷分離状態
 Fukuzumi, S. and Tani, F. et al., Chem.
 Sci. 2013, 5, in press



巨大な電気双極子モーメントを持つ
 $\text{Li}^+@C_{60} \cdot \text{PF}_6^-$ イオン対
 一東北大学大学院理学研究科
 権根相先生一

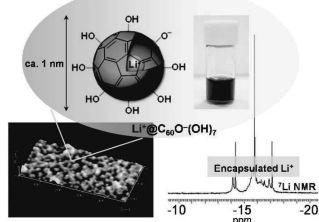


イオンによる電子移動 ON/OFF 制御
 Fukuzumi, S. et al. J. Am. Chem. Soc.
 2011, 133, 15938

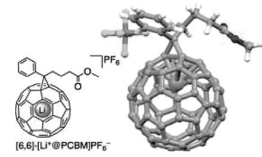


初めてリチウムイオンの内包化を
 証明した $[\text{Li}^+@C_{60}](\text{SbCl}_6)$ 単結晶
 S. Aoyagi, H.Sawa, H.Tobita et al.,
 Nature Chemistry, 2, 678 (2010).

“Cation Encapsulated Anion Nanoparticle”



H. Ueno, K. Kokubo, T. Oshima et al. Nanoscale,
 2013, 5, in press.



$[\text{Li}^+@PCBM]\text{PF}_6$
 Y.Matsuo, H.Okada et al., Org.Lett
 2012,14,3784.



001B01 リチウム内包フラーレンクラスター

$\text{Li}^+@C_{60}$ を中心に据えてその周囲を十数個の C_{60} が取り囲むように凝集した粉末	1,000 mg	500,000 円
	500 mg	250,000 円

001D04 リチウム内包フラーレン PF

化学式： $[\text{Li}^+@C_{60}](\text{PF}_6^-)$ $\text{Li}^+@C_{60}$ と PF_6^- が 1:1 で対を成す 微結晶の粉末	10 mg	210,000 円
	20 mg	390,000 円
	30 mg	570,000 円
	40 mg	747,000 円
	50 mg	930,000 円
	50mg 以上の mg 当たりの単価	18,600 円

TS001 リチウム内包フラーレンクラスター特別試作品

$\text{Li}^+@C_{60}$, Li , C_{60} , の混成粉末を Ar 雰囲気中で梱包したもの	1,000 mg	400,000 円
	500 mg	200,000 円

Li@C60 の製造・販売

イデア・インターナショナル株式会社

<http://www.lic60.jp>

e-mail : info@idea-i.jp

仙台支店・仙台開発センター

〒981-0922 宮城県仙台市青葉区鷹森1-15-35

Tel:022-342-8410

共同研究室

〒980-8579 宮城県仙台市青葉区荒巻字青葉6-6-04

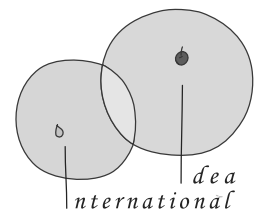
東北大学未来科学技術共同研究センターハッチェリースクエア高橋研究室

Tel:022-795-3164

本社

〒802-0005 福岡県北九州市小倉北区堺町2-1-1 ライズ小倉ビル

Tel : 093-383-6577 Fax : 093-383-6271



Idea International Co., Ltd.

Sendai Office and R&D center

1-15-35 Sagigamori, Aobaku, Sendai, Miyagi, 981-0922 Japan
 +81-22-342-8410

Joint Research Center

Takahashi-Lab. Hatchery Square, Tohoku-University, 6-6-04
 Aramaki Aza Aoba, Aoba-ku, Sendai, Miyagi 980-8579 Japan
 +81-22-795-3164

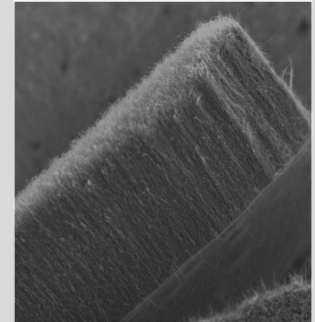
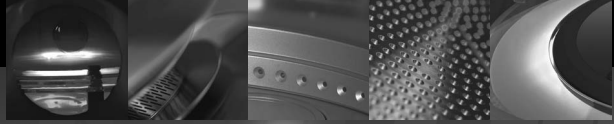
Head Office

Rise Kokura Bldg. 2-1-1 Sakai-cho, Kokurakita-ku, Kitakyushu,
 Fukuoka, 802-0005 Japan
 +81-93-383-6577 Fax: +81-93-383-6271

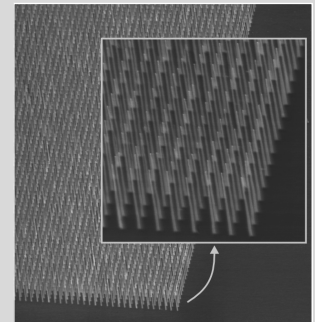
AIXTRON

アイクストロン社の

カーボンナノチューブ&グラフェン成長用CVD装置 **BM Series**



Dense CNT



Horizontal SWCNT



Graphene

- 多様な基板サイズに対応
BM II System(2インチ基板用)、BM Pro System(4、6インチ基板用)、BM 300(300mm基板用)
- 1台の装置で、再現性の高いCNT及びグラフェン成長可能(最大8種類のガス系を搭載)
熱CVD、プラズマCVD、トップヒータによる熱輻射CVD等、多様な成長モード
- オリジナルの成長レシピ付
(シングルCNT用、ダブルCNT用、マルチCNT用、横方向CNT用、低圧カプロセスCNT用、高速成長CNT用、モノレイヤーグラフェン用、マルチレイヤーグラフェン用etc.)
- プラズマエッチングによる簡単クリーニング

アイクストロン株式会社

<http://www.aixtron.com>

E-mail: JAPANINFO@aixtron.com

〒140-0001 東京都品川区北品川 1-8-11 Daiwa 品川 North ビル 9F TEL: 03-5781-0931 FAX: 03-5781-0940



微小物分析用顕微レーザーラマン

DXR Raman Microscope

微小物をかんたん確実に分析、新しい顕微ラマンシステム

- 前処理不要、1 μm の微小物を分析
- 特許の自動光軸調整、微小物の確実な分析
- 内包物の非破壊分析、深さ方向分析
- 分析に最適な条件を、全て自動で設定
- 豊富なライブラリによるラマンスペクトル検索



サーモフィッシャーサイエンティフィック株式会社

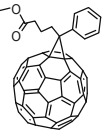
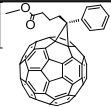
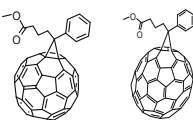
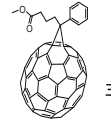
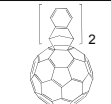
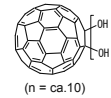
〒221-0022 神奈川県横浜市神奈川区守屋町3-9 C棟2F ☎ 0120-753-670

E-mail: info-jp@thermofisher.com www.thermoscientific.jp

Part of Thermo Fisher Scientific

Thermo
SCIENTIFIC

nanom フロンティアカーボンのフラーレン製品

銘柄	分子構造	純度(HPLC面積%、代表値) 内容他	最低数量 (g)	
nanom purple フラーレンC60		ST	99	10
		TL	99.5	2
		SU	99.5/昇華精製品	2
		SUH	99.9/昇華精製品	1
		SC	99.9/昇華精製/単結晶品	1
nanom orange フラーレンC70		ST	97	1
		SU	98/昇華精製品	0.5
nanom mix 混合フラーレン		C60,C70,その他高次 フラーレンの混合物 ※微粒化品(ST-F)もあります	50	
nanom spectra [60]PCBM (phenyl C61-butylric acid methyl ester)		E100	99	1
		E100H	99.5	1
		E102	99.9	0.5
nanom spectra E400 bis[60]PCBM (bis-phenyl C61-butylric acid methyl ester)		98/異性体トータル ※位置異性体の混合物	1	
nanom spectra E123 [60,70]PCBM		[60]PCBM、[70]PCBMの混合物	1	
nanom spectra [70]PCBM (phenyl C71-butylric acid methyl ester)		E110	99/異性体トータル ※位置異性体の混合物	0.5
		E112	99.5/異性体トータル ※位置異性体の混合物	0.5
nanom spectra Q100 [60]インデン付加体		99	0.5	
nanom spectra Q400 [60]インデン2付加体		99/異性体トータル ※位置異性体の混合物	1	
nanom spectra D100 水酸化フラーレン		C ₆₀ OH _n n=10を主成分とする混合物	1	
nanom spectra A100 水素化フラーレン		C ₆₀ H _n n=30を主成分とする混合物	1	

銘柄、取扱数量等は予告無く変更する場合がございます。予めご了承下さい。

2013年1月8日現在

当社製品は、下記2社から購入いただけます。直接お問い合わせください。

・関東化学株式会社 試薬事業本部

〒103-0022 東京都中央区日本橋室町2-2-1 TEL:03-6214-1090 FAX:03-3241-1047

<http://www.kanto.co.jp> E-mail:reag-info@gms.kanto.co.jp

・第一実業株式会社 新事業推進室【担当:鎰広(カギヒロ)】 E-mail:masaru.kagihiro@djk.co.jp

〒102-0084 東京都千代田区二番町11-19 TEL:03-5214-8579 FAX:03-5214-8503

<本資料に関するお問い合わせ先>

フロンティアカーボン株式会社【担当:梶原】

〒100-8086 東京都千代田区丸の内2-6-1丸の内パークビルディング24階

TEL:03-3210-2620 FAX:03-3210-4606 <http://www.f-carbon.com>

※弊社へのお問い合わせはHPよりお願いいたします。